AN INVESTIGATION OF SCALING PARAMETERS

GOVERNING FILM-COOLING.

C.J. PATRICK FORTH

KEBLE COLLEGE

JUNE 1985.

A thesis submitted for the degree of Doctor of Philosophy,

Oxford University.

Dept. Engineering Science,

Osney Laboratory,

Oxford.

to de king

ABSTRACT.

AN INVESTIGATION OF SCALING PARAMETERS GOVERNING FILM-COOLING.
A thesis submitted for the degree of Doctor of Philosophy, by C.J.P. FORTH, Keble College, Oxford.

The thesis describes an investigation into the fundamental scaling parameters which govern the process of film-cooling. This method of cooling has wide applicability in the hot portion of gas turbine engines. Well-designed cooling configurations and accurate prediction of heat transfer loads are essential in this extremely hostile environment. However, a great deal of the design data used has been acquired in constant properties experiments which are unrepresentative of engine conditions. At present, there is no consensus on how best to scale this data to the turbine environment.

In particular, the effect of varying the ratio of coolant-to-freestream density has been studied. Experimentally, this variation has been produced, as in the engine, by varying the the injection-to-freestream temperature ratio. For the three geometries tested (a single and double row of 30^{o} holes and a 30^{o} slot), the effect of this parameter was found to be very significant. The widely used mass flux ratio does not take this dependence into account, so that other scaling parameters need to be determined.

For injection rates where the coolant flow remains close to the surface, good scaling is achieved with the momentum flux ratio. All injection rates for the slot and double row occurred in this largely unseparated, "weak" injection regime. However, for the single row, the injection jets penetrated into the freestream at a critical value of the momentum flux ratio. At higher injection rates, in the "strong" injection regime, fluid mechanic scaling was best with velocity ratio.

A simple model is proposed, based on theoretical and experimental considerations, suggesting scaling parameters which successfully collapse all the data in each regime for different injection rates and distances downstream from injection. Alternative scaling parameters based on pressure and temperature measurements are also found to be highly successful.

The effect on heat transfer of the variation of properties through the injection layer at the wall-to-freestream temperature ratios encountered in gas turbines was also found to be significant. This has been quantified.

Experiments were performed using an Isentropic Light Piston Tunnel, a transient facility which enables conditions representative of those in engines to be attained. The results were interpreted using a superposition model, which is shown to be a valuable and concise method of characterising the effects of injection.

ACKNOWLEDGEMENTS.

I am indebted to several people who have helped with the work presented in this thesis. I am particularly grateful to my supervisor, Dr. T.V. Jones, who has been a continual source of inspiration and encouragement. My thanks are due in general to the turbomachinery group at Osney, headed by Professor D.L. Schultz. It is a pleasure and a privilege to be part of the team. Trevor Godfrey helped to run and maintain the rig during the course of this research, and his cheerful support has been invaluable.

I would also like to thank the following people who have made contributions to this work : Alistair Fitt provided much useful information on the mathematical modelling ; Beverley Robertson performed the computational work on turbulent boundary layers ; Peter Loftus was of great assistance in acquainting me with the rig and software; Peter Wray carried out the film-cooling computing at Rolls Royce.

The work was funded by the S.E.R.C., whose support is acknowledged. I am also grateful to the Rhodes Trust and Rolls Royce for their financial support.

I would also like to thank my parents, family and friends, and in particular, Jules and Graham, who have made it all worthwhile.

CONTENTS.

NOMENCLATURE

a	Speed of sound, m/s
b	Height of injection layer, m
c	Capacitance per unit length, F/m
c_p	Specific heat capacity at constant pressure, kJ/kg K
D	Diffusion constant, m^2/s
d	Injection hole diameter, m
e	Internal energy, kJ/kg
h	Heat transfer coefficient, W/m^2K
i	Current, A
k	Thermal conductivity, W/m K
m	Mass transfer rate kg/m^2s
$\dot{m}$	Mass flow rate, kg/s
p	Pressure, Pa
q	Heat transfer rate, W/m^2
R	Gas constant, kJ/kg K
	Resistance, Ω
r	Resistance per unit length, Ω/m
s	Slot width, m
T	Temperature, K
t	Time, s
u	Velocity (in x direction unless otherwise stated), m/s
V	Voltage, V
v	Velocity in y direction, m/s
x	Co-ordinate, measured downstream from injection, m
y	Co-ordinate, measured upwards from surface, m
z	Co-ordinate, measured in cross stream direction, m

Non-dimensional Parameters.

A	Mixing parameter in superposition model, Eqn.(2.12)
B	Coolant temperature parameter in superposition model, Eqn.(2.12)
c	Mass fraction of foreign gas
G	Mass Flux Ratio or Blowing Rate $\frac{\rho_i u_i}{\rho_\infty u_\infty}$
I	Momentum Flux Ratio $\frac{\rho_i u_i^2}{\rho_\infty u_\infty^2}$
M	Mach Number u/a
Nu	Nusselt Number $\frac{q\ x}{k_{t\infty}(T_{t\infty} - T_w)}$
Pr	Prandtl Number $\frac{\mu_{t\infty}\ c_p}{k_{t\infty}}$
Re	Reynolds Number $\frac{\rho_\infty u_\infty x}{\mu_\infty}$
Sh	Sherwood Number $mx/D\rho_w$
Sc	Schmidt Number $\frac{\mu}{\rho_\infty D}$
SIP	Strong Injection Parameter, Eqn.(4.29)
WIP	Weak Injection Parameter, Eqn.(4.32)
ϵ	Mean cooling system effectiveness, Eqn.(1.1)
γ	Ratio of specific heats
η	Film cooling effectiveness
Θ	Temperature Parameter $\frac{T_{t\infty} - T_{ti}}{T_{t\infty} - T_w}$
ξ	Energy balance correlating parameter, Eqn.(4.12)

Greek Symbols.

α	injection angle, in Eqn.(4.20)
	coefficient of resistivity, K^{-1}
	thermal diffusivity, m^2/s, in Eqn.(8.10)
δ	boundary layer thickness, m
ϵ	Turbulent diffusivity, m^2/s
	A small parameter, Eqn.(7.8)
μ	coefficient of viscosity, kg/m s
ν	coefficient of kinematic viscosity, m^2/s
ρ	density, kg/m^3
ζ	vorticity, s^{-1}

Subscripts.

aw	adiabatic wall
awis	isothermal, adiabatic wall
b	blade
cp	constant properties
dump	conditions in dump tank
eff	effective
exit	conditions at injection exit
f	film
I	iso-energetic
i	injection
iaw	iso-energetic, adiabatic wall
iso	isothermal
o	without injection
r	recovery
ref	reference
t	total
w	wall
∞	freestream
*	reference, in Eqn.(4.13)

CHAPTER 1.

Introduction.

1.1 Object of Investigation.

The aim of this study is to provide an insight into the parameters which govern the process of film-cooling. This technique has been the subject of a great deal of research during the past two decades. Much of the experimental data has been acquired in essentially constant properties situations, where the temperature ratios and hence density ratios are close to unity. However, a major application of film-cooling is in the protection of turbine blades from hot combustor exit gas, where the injection-to-freestream and wall-to-freestream temperature ratios are considerably less than unity. It is essential, therefore, to conduct experiments as far as possible at conditions which encompass those which are representative of the gas turbine environment . Experimental data of this nature can then be used to reach conclusions concerning the vital issue of the scaling of the injection process. There is still no consensus in the literature as to whether, for example, the injection-to-freestream mass flux, momentum flux or velocity ratio is the dominant parameter.

Questions and comments from a workshop on fundamental heat transfer research for gas turbines [1.1] illustrate the requirement for a definitive statement on this issue :

"Where do we stand on the accurate prediction of effects ... of discrete hole cooling on heat transfer under the extreme variable property environments characteristic of actual gas turbine conditions ? Much of the experimental data which have guided the development of turbulence models for these effects has been taken under nearly constant property conditions. Have these models been adequately evaluated for the much higher temperatures and heat fluxes of actual engines ?"

"There is a need for better correlations [in film-cooling] to unify the wide variety of data with its many parameters."

"Do we really understand the basic problem of mixing of two streams of different temperature and different velocity ?"

This thesis describes experimental data obtained from three typical film-cooling geometries. The merits of several existing correlating parameters are discussed ; successful scaling is achieved using two relatively new parameters based on pressure and temperature measurements. This will enable experimental data to be successfully extrapolated to engine conditions.

1.2 Trends in Gas Turbine Design.

The optimum design solution for many engineering problems is one which results in a product which exhibits a high efficiency whilst at the same time being reliable for a reasonable service life time. These general objectives are particularly challenging for the designer of the hot portion of gas turbine engines. Two key design variables are the cycle pressure ratio and the gas temperature at entry to the turbine. For real cycles, the thermal efficiency is increased by an increase in turbine entry temperature. This has a beneficial effect on two performance characteristics, the specific thrust and the thrust specific fuel consumption (at a given propulsive efficiency). Fuel efficiency has become a major consideration since the tripling of aviation kerosene prices in the 1970's; more than 50% of the direct operating cost of a civil aircraft is now due to fuel charges [1.2].

As a consequence of this, turbine entry temperatures have risen from about 1100 K to as high as 1800 K in high performance jet engines over the last thirty years. These gas temperatures are in excess of the melting points of the high temperature alloys employed, and hence components exposed to the hot flow must be cooled. About half of this temperature rise has been due to improvements in materials technology. However, Fig.1.1 shows the substantial contribution made by improvements in cooling techniques.

The designer also has to take account of the requirement for greater component reliability and longer component life. Greater emphasis has been placed on these aspects due to the stabilising of fuel prices and cost effectiveness constraints on military engines in peace time. A large portion of engine maintenance and repair costs is accounted for by the hot section.

The environment in which these hot end turbine components operate, meanwhile, becomes increasingly hostile. For example, the first stage nozzle guide vanes, immediately downstream of the combustor, experience very turbulent combustor exit gases which are also grossly non-uniform in temperature [1.3]. Off-design conditions can be still more severe, and large temperature fluctuations during engine transients such as start up also have to be considered. In addition, blades should be sturdy enough to withstand the impact of foreign matter such as carbon. Indeed, if alternative fuels with higher aromatic contents are employed in the future, corrosion problems will worsen, whilst increased gas radiation will add to the heat load [1.4]. In such environments, typical modes of failure of turbine blades are creep, based on average blade section stress and temperature, thermal fatigue and failure due to oxidation and corrosion. These are examined in some detail by FULLAGAR [1.5].

1.3 Turbine Cooling Systems.

It is essential, then, that cooling systems should be devised for the turbine. In the blades, relatively cool air bled from the compressor is employed. The main requirements of such a cooling system are:

(1) To establish allowable temperature levels in metal components, and to achieve uniform blade temperature distributions in order to reduce thermal stresses.

(2) To minimise the amount of cooling air required, because of its detrimental effect on engine performance.

(3) Low cost and ease of manufacture.

Cooling techniques can be classified into the following groups:

a) Internal cooling, where air is fed through the blade root into radially aligned passages, typically in the thicker mid-chord region. In the thinner trailing edge, the heat transfer coefficient of this internal flow can be enhanced by the presence of roughness elements and pin fins. The flow might then exit through trailing edge slots or through film-cooling holes where it might perform active cooling. The development of ceramic thermal barrier coatings has increased the emphasis on internal cooling to remove the heat flux efficiently. In addition, new manufacturing techniques such as diffusion bonding allow more complex, three-dimensional internal cooling geometries to be realised.

b) Impingement cooling, where jets of internal coolant flow exit from a perforated shell within the aerofoil and impinge against the inside of the blade shell.

c) Transpiration cooling, in which the coolant passes through to the external surface through a porous material. This provides effective use of coolant, but has yet to be applied to a production engine [1.4]. There are several reasons for this: the porous materials tend to be weak, and have to extend over large areas in order to provide sufficient cooling ; variations in coolant injection rates around the blade would be difficult to achieve, and the probability of hole clogging would decrease reliability.

d) Film-cooling, in which coolant ejection to the external surface is through discrete holes or slots. In contrast to transpiration cooling, this method produces a cooling effect downstream from the injection location. The flow can be thought of either as a heat sink for the mainstream gas, or as an insulating layer between the mainstream and the wall. Even with the advent of ceramic coated blades, it is still thought that film-cooling will remain an important cooling mechanism. This is because by reducing the surface heat flux, thermal stresses through the blade section are reduced.

Fig.1.2 shows a typical high pressure rotor blade and nozzle guide vane, illustrating these types of cooling. Film-cooling is most usually employed in the high heat transfer region of the leading edge stagnation point, but is also used on both the suction and pressure surfaces.

Blade cooling has a parasitic effect on overall engine performance. Firstly, cooling air bled from the compressor reduces the mass flow through the turbine, so that for every per cent of compressor air used, the increase in specific fuel consumption is about 0.75% for a typical high bypass, high pressure ratio turbofan engine [1.6]. Secondly, this cooling air removes heat from the hot gas stream over the turbine blades, decreasing the work output and the turbine efficiency by around one per cent. In addition, film-cooling has an adverse effect on turbine aerodynamic efficiency, as discussed later. These are, however, arguments in favour of designing to maximise the cooling efficiency rather than arguments against the use of cooling. The benefits to be gained from cooling are enormous : for example, by lowering the mean blade temperature by fifteen degrees, the service life can be doubled.

Because of the strong influence that cooling systems can have on engine performance, the blade cooling engineer is now involved with new engine design alongside the aerodynamicist from the beginning. His task is to balance the heat flux to the external surface with that transferred from the inner surface to the internal cooling air, so that the surface temperature is maintained below that set by metallurgical constraints.

The external heat load will be largely determined by the design turbine entry temperature and the blade heat transfer coefficient distribution. The heat flux will typically be high at the leading edge, where the boundary layer is thin. Generally, heat loads are high on the pressure surface where the accelerating flow preserves a thin boundary layer. A normally well-defined transition to a turbulent boundary layer increases heat transfer on the suction surface. Reynolds Number effects, shock-boundary layer interactions, wakes, surface roughness effects, freestream turbulence and secondary flow effects all add to the complexity of the external heat transfer distribution. The application of film-cooling, either as a "pepper-pot" configuration at the leading edge, in single rows or as multi-hole full coverage film-cooling, will modify this distribution.

Internal heat transfer must then be tailored, for example by changing the wetted area, the geometry or the coolant flow rate , so that the resulting metal temperatures are acceptable. The use of thermal barrier coatings will permit higher turbine entry temperatures or a reduction in cooling flow, but it seems likely that film-cooling will still be a necessity.

Careful consideration must be given to the pressures of the coolant flows. This is to ensure that there is no mainstream ingestion, and that the required internal and film-cooling injection rates are set. A high pressure supply is required, for example, for leading edge film-cooling where the external static pressure is high. However, at other locations, the compressor air is expanded through pre-swirl vanes, thus reducing the coolant temperature.

A parameter can be defined as

$$\epsilon = \frac{T_\infty - T_b}{T_\infty - T_i} \qquad (1.1)$$

where T_b is the mean blade temperature ; its variation with the different combinations of cooling techniques is shown in Fig.1.3.

It follows, then, that the designer must have some procedure for estimating the performance of a given cooling system design at a given coolant flow rate. With respect to film-cooling, analytical models are rather crude, and a great deal of work is still to be done on numerical codes. At present, these tend to be very cumbersome and expensive. In addition, they suffer from an incomplete knowledge of the physics of the turbine flowfield and usually require a substantial empirical input. It is clear that there is still a requirement for experimental data which can promote a greater understanding of the fundamental aspects of cooling techniques, as well as to provide a coherent data base for numerical models. This thesis aims to make a contribution of this nature with respect to film-cooling.

1.4 Factors Influencing Film-Cooling.

HENNECKE [1.4] remarks that despite the vast amount of research which has taken place on film-cooling, the designer still lacks correlated data. Further, it is stated in [1.1] that "Work is needed in film-cooling, in terms of better organisation of existing data and more work on basic analyses. Prediction of film-cooling is at present a weak point." This is due to the complexity of the flowfield and the large number of variables. As an introduction to the technique, some factors affecting its performance are listed below ; a more detailed survey has been carried out by LOFTUS [1.7].

1) The injection rate, characterised for example by injection-to-freestream density and velocity ratios. For a single row of holes, cooling efficiency tends to increase with injection rate close to injection up to a maximum, above which increased injection rate causes a decrease in efficiency. This is attributed to separation of the injection jets from the downstream surface.

2) Injection geometry. Two-dimensional or slot geometries are generally more efficient than three-dimensional or hole geometries, since they

provide a more uniform insulating layer and generate less mixing. These are feasible configurations on nozzle guide vanes ; however, structural considerations preclude their use on rotating blades. GOLDSTEIN et al [1.8] note that increasing the angle of injection from the horizontal for hole injection increases jet penetration into the mainstream and therefore reduces cooling effectiveness at low injection rates. However, the lateral spread of the jets is increased. The effect of lateral injection can be beneficial, in that the lateral spread of each jet is increased and the separation of the jets from the surface is supressed. SMITH [1.9] and GOLDSTEIN et al [1.10] show that cooling advantages result from shaping the exit of the injection hole to a "fishtail" section. With two rows of holes, separation is less noticeable [1.11] and a staggered rather than in-line configuration is superior [1.12].

3) Pressure gradients. Both the effectiveness [1.13] and heat transfer coefficient [1.14] are decreased significantly by the presence of a favourable pressure gradient at low injection rates. An adverse pressure gradient has little effect.

4) Curvature. The effect of concave surface curvature is to reduce the cooling effectiveness at low jet momentum flux ratios and to increase it at high values. The reverse is the case for a convex surface ([1.15] and [1.16]).

5) Radial flows, due to three-dimensional and secondary flows in a cascade. These can cause substantial displacement of the trajectory of film-cooling jets, particularly on the pressure surface [1.17].

6) Compressibility. This appears to have very little effect on film-cooling performance [1.13]

7) Freestream Reynolds Number. An investigation of this parameter by the author revealed that for a given injection-to-freestream mass flux ratio and density ratio, increasing the freestream Reynolds Number increases the film-cooled Nusselt Number.

8) Freestream turbulence. CARLSON & TALMOR [1.18] show that increasing the freestream turbulence intensity decreases the film-cooling effectiveness.

9) Surface roughness. Roughness typical of that found on gas turbine blades can significantly affect film-cooling [1.19]. At injection rates which do not cause gross jet separation from the surface, a decrease in effectiveness of up to twenty per cent can result.

10) Upstream boundary layer. This appears to have little effect on the film-cooled heat transfer coefficient [1.14].

11) Unsteady effects, such as wake passing and shock interactions.

In addition, film-cooling can have the following side effects on engine performance, most of which are detrimental. It can cause laminar boundary layers to undergo transition, and may give rise to shock waves at the injection location. There will be mixing losses in the boundary layer downstream of injection, and possibly an increased wake, which will increase aerodynamic losses. This mechanism has been modelled by HARTSEL [1.20] and has been the subject of several experimental studies. For example, HORTON [1.21] concludes that cooling geometries on the suction surface produce more loss per unit mass flow than those on the pressure surface, and that the losses were associated with the flowfield close to injection. He also points out that the loss generation mechanism is sensitive to the injection-to-freestream temperature ratio, which is a parameter of major interest in the present study. Finally, the effect of the nozzle guide vane film-cooling flow on the rotor must be considered.

Clearly, then, the process of film-cooling in gas turbine engines is highly complex.

1.5 Outline of Thesis.

Chapter 2 describes how the film-cooling process can be defined , and shows how the concept of superposition of temperature fields can be used as a means of interpretation. Chapter 3 reviews some of the experimental techniques which have been employed in investigating film-cooling, and highlights their relevance to gas turbine conditions. Chapter 4 gives an outline of the analytical and numerical models for film-cooling which have been proposed. The suggested correlating parameters are compared with those which have resulted from experimental studies. Two scaling parameters resulting from dimensional analysis arguments are also proposed. The test facility is described in Chapter 5, with particular emphasis on recent modifications. Chapters 6-8 contain experimental results. In Chapter 6, the effect of variable gas properties on heat transfer to a turbulent flat plate boundary layer is reported and compared with numerical results. In Chapter 7, the aerodynamic effects of coolant injection are examined and experimental results are discussed with reference to a new analytical prediction for injection flowfields. Chapter 8 gives the experimental heat transfer results for injection through three geometries ; a single row of holes, a slot and a double row of holes. Data is obtained at three or more injection-to-freestream temperature ratios over a range of wall-to-freestream temperature ratios and injection mass flows. The success of the various scaling parameters at collapsing this data is examined. Conclusions drawn from this investigation, and recommendations for modifications to turbine cooling design procedures, are presented in Chapter 9.

CHAPTER 2.

Description of the Film-Cooled Heat Transfer Process.

2.1 Introduction.

Convective heat transfer is traditionally described using a heat transfer coefficient which relates the surface heat flux to a temperature potential difference

$$q = h\,(T_w - T_{ref}) \tag{2.1}$$

Then for constant property flows, h is independent of the temperature field and is a fluid mechanic property of the system.

In the film - cooled environment, the choice of reference temperature has led to two approaches in the precise definition of a heat transfer coefficient. These are described and compared in this Chapter.

2.2 Adiabatic Wall Temperature Definition.

In this approach, described in detail by GOLDSTEIN [2.1], the local wall temperature is referenced to the local temperature assumed by an adiabatic wall downstream from the injection location.

$$q = h_{aw}\,(T_w - T_{aw}) \tag{2.2}$$

T_{aw} typically has the form shown in Fig.2.1. An adiabatic wall effectiveness is then defined as

$$\eta_{aw} = \frac{T_{aw} - T_\infty}{T_i - T_\infty} \tag{2.3}$$

This parameter will partially quantify the degree of cooling, varying with distance and injection rate, typically being close to unity at the injection location (where $T_{aw} \approx T_i$) and zero far downstream (where $T_{aw} \approx T_\infty$). Early work (for example GOLDSTEIN et al.[2.2]) then made the assumption that h_{aw} was approximately equal to the heat transfer coefficient in the absence of injection, defined as

$$q_o = h_o\,(T_w - T_\infty) \tag{2.4}$$

thus allowing η_{aw} to completely characterise the cooling performance. This assumption is most valid far downstream from injection, where the flow has essentially reverted to behaving like a turbulent boundary layer. However, close to injection, the severe disruption of the flowfield makes this assumption invalid. Thus, an accurate prediction of heat transfer requires the determination of two parameters, η_{aw} and h_{aw}, which are functions of the flowfield with injection.

2.3 Superposition Model.

This approach, first suggested by METZGER et al.[2.3], references the wall temperature to the freestream temperature, so that the effect of injection can be contained wholly within a heat transfer coefficient :

$$q = h\,(T_w - T_\infty) \tag{2.5}$$

The method utilises the form of the energy equation for the boundary layer, assuming a constant property, incompressible flow

$$\bar{u}\,\frac{\partial \bar{T}}{\partial x} + \bar{v}\,\frac{\partial \bar{T}}{\partial y} = \frac{k_{eff}}{\rho\, c_p}\,\frac{\partial^2 \bar{T}}{\partial y^2} \tag{2.6}$$

(from Appendix 1, for a turbulent boundary layer).

This equation is linear and homogeneous in temperature and so a sum of solutions with different sets of boundary conditions will also be a solution for the boundary condition which is the sum of those sets.

For the film-cooling situation, the relevant temperature boundary conditions are shown in Fig.2.2 (from LOFTUS & JONES [2.4]). All temperatures are referenced to the freestream value, allowing wall temperatures to be superimposed conveniently. It can be seen that the temperature field in the presence of film-cooling resulting from the top set of boundary conditions may be interpreted as the sum of those obtained from sets (1) & (2). Representing this by the temperature field for a unit temperature difference multiplied by the relevant temperature difference,

$$T(x,y,z) = T_1(x,y,z)[T_w - T_\infty] + T_2(x,y,z)[T_i - T_w] \qquad (2.7)$$

(T_1 is the field for a unit temperature difference between wall and freestream, with the coolant at the wall temperature, and T_2 is the field for a unit temperature difference between coolant and wall, with the wall at the freestream temperature). Differentiating with respect to y , setting y = 0 and averaging across the span gives

$$q(x) = h_1(x)[T_w - T_\infty] + h_2(x)[T_i - T_w] \qquad (2.8)$$

where the suffices refer to the conditions above. Dividing this by the heat transfer rate without injection ,Eqn.(2.4),

$$\frac{q}{q_o}(x) = \frac{h_1}{h_o}(x) + \frac{h_2}{h_o}(x)\frac{(T_i - T_w)}{(T_w - T_\infty)} \qquad (2.9)$$

This may be rearranged in terms of the non-dimensional temperature parameter Θ to give

$$\frac{q}{q_o}(x) = \frac{(h_1 - h_2)}{h_o}(x) + \frac{h_2}{h_o}(x)\,\Theta \qquad (2.10)$$

or

$$\frac{q}{q_o}(x) = A(x) + B(x)\Theta \qquad (2.11)$$

and thus the effects of injection are contained within the definition of the heat transfer coefficient. A(x) and B(x) are dependent on the freestream and injection conditions, and will be constants for a given geometry and flowfield.

The above analysis holds for incompressible, constant property flows. In order to incorporate different mainstream temperatures, Eqn.(2.11) may be written in terms of the Nusselt Number, for a given Reynolds Number :

$$\frac{Nu}{Nu_o} = A(x) + B(x)\Theta \qquad (2.12)$$

This assumes that there is no effect of gas-to-wall temperature ratio, the validity of which is discussed in Chapter 6.

Both A and B have a concise physical interpretation : for small temperature differences, when the coolant is at the freestream temperature, Θ is zero and A quantifies the change in heat transfer produced by the mixing of the two flows. B quantifies the change in heat transfer produced by the injection temperature being different from the mainstream temperature. For injection-to-freestream temperature ratios and corresponding density ratios greater or less than unity, this must be modified. A is the relative enhancement of heat transfer produced by the interaction of these two streams at the same value of Θ, and B is a measure of the change in the Nusselt Number produced by the variation in wall temperature for a given primary and secondary flow. Thus, once again, two parameters which depend on the flowfield must be determined in order to find the heat transfer rate.

2.4 Comparison of Definitions of Heat Transfer Coefficient in Film-Cooling.

The relative merits of these two approaches can now be considered. ECKERT [2.5] shows how the adiabatic wall temperature definition can be constructed by superposition of the following boundary conditions :

(1) An adiabatic wall temperature distribution, or zero heat flux at the wall, and

(2) Finite heat flux along the wall for the case of isoenergetic temperature injection, when the coolant temperature is equal to the freestream temperature for the same flowfield.

This description has the advantage of defining a continuously varying heat transfer coefficient, since the driving temperature and the heat flux approach zero together. In comparison, the heat transfer coefficient defined by Eqn.(2.5) becomes very large in magnitude as the wall temperature approaches the freestream temperature. However, this is catered for by the fact that theta also becomes very large, so that the parameters A and B are well behaved. In addition, ECKERT points out that this situation does not arise in gas turbine film cooling.

However, inherent in the formulation of the adiabatic wall temperature description is an adiabatic wall temperature distribution. In a film-cooled gas turbine environment, the surface more closely approximates to an isothermal temperature boundary condition, as mentioned by LOUIS [2.6]. This results from longitudinal conduction in the cooled component, and from a design requirement to reduce thermal gradients on the surface. Far from behaving like an insulated surface, there is considerable transfer of heat, which is removed by internal cooling. It is therefore important that experimental investigations should preserve this boundary condition. This leads to the major objection of the adiabatic wall effectiveness description of film cooling over an isothermal surface. The adiabatic wall temperature T_{aw} measured at a given position downstream of injection will be different from the isothermal temperature T_{awis} to which the whole surface must be raised in order to produce zero heat transfer at that point. Thus, in Fig.2.1, when the isothermal wall temperature T_w has the value $T_{aw}(x^*)$, then for this position the wall heat flux will not be zero, as Eqn.(2.2) would predict. There will in fact be heat transfer to the wall due to the relatively hotter upstream boundary layer in the isothermal case (for $T_i < T_\infty$). The correct reference temperature for the adiabatic wall effectiveness description should therefore be T_{awis} , which is greater than $T_{aw}(x)$, so that

$$q = h_{awis}(T_w - T_{awis}) \tag{2.13}$$

and

$$\eta_{awis} = \frac{(T_{awis} - T_\infty)}{(T_i - T_\infty)} \tag{2.14}$$

With these definitions, it can be seen that h_{awis} and η_{awis} can be related directly to A and B. From the revised adiabatic description,

$$\frac{q}{q_o} = \frac{h_{awis}}{h_o} \frac{(T_w - T_{awis})}{(T_w - T_\infty)} . \tag{2.15}$$

Combining this with the definition of η_{awis} gives

$$\frac{q}{q_o} = \frac{h_{awis}}{h_o} - \frac{h_{awis}}{h_o} \eta_{awis} \Theta \tag{2.16}$$

Equating heat transfers gives the relations

$$A = \frac{h_{awis}}{h_o} \tag{2.17}$$

$$B = -\frac{h_{awis}}{h_o}\,\eta_{awis} \tag{2.18}$$

$$B/A = -\,\eta_{awis} \tag{2.19}$$

In order to compare the large body of adiabatic wall effectiveness data with the more rigorously modelled isothermal wall data, the assumption $T_{aw} = T_{awis}$ must be made. This assumption appears to have been made by CHOE et al [2.7] who make similar comparisons between the two schemes. LOUIS [2.6] states the relationship

$$\eta_{iso} = 1 - \frac{h_{aw}}{h_o}\,(1 - \eta_{aw}\Theta) \tag{2.20}$$

where $$\eta_{iso} = 1 - h/h_o. \tag{2.21}$$

This is equivalent to Eqn.(2.16) and, as noted by VILLE et al [2.8] should strictly only be applied when the adiabatic wall temperature is evaluated under isothermal conditions. ECKERT [2.5] makes the point that the upstream temperature history within a boundary layer does not affect the turbulent heat transfer strongly as long as temperature gradients are not too large near the region under consideration. For the unblown turbulent boundary layer, the effect of a non-uniform wall temperature distribution was shown to be significant by LOFTUS & JONES [2.4]. In the special case where $T_i = T_\infty$, the adiabatic boundary condition would also be isothermal, so that

$$A = h_{aw}/\,h_o$$

without restriction.

It should also be noted that even if the thermal boundary condition is isothermal, Eqns.(2.17) - (2.19) relate local values of heat transfer parameters. If spanwise averaged values of η_{awis} and h_{aw}/h_o, for example, are measured, their product will not in general be equal in magnitude to a spanwise averaged value of B.

2.5 Parameters in Film-Cooling.

The advantages of both descriptions of the film cooling process, and the complications associated with the application of data obtained under adiabatic conditions to the case of an essentially isothermal surface, have been debated. It is now pertinent to generalise the discussion to include all the criteria necessary to simulate the temperature and velocity fields in a film-cooled engine environment. Dimensional analysis is particularly useful in enabling the conditions for the preservation of dynamic similarity to be determined. Since the incompressible, constant properties situation has been assumed in order to use superposition, the corresponding non-dimensional parameters should be considered. For a flat plate with zero pressure gradient, the relevant independent variables may be listed as

$$\rho, (T_\infty - T_i), (T_\infty - T_w), (p_{t\infty} - p_\infty), (p_{ti} - p_\infty), x, d, q, \mu, k \qquad (2.22)$$

With five reference dimensions mass, length, time, temperature and heat transfer, this yields the dimensionless groups

$$\frac{q\ x}{k(T_\infty - T_w)}, \quad \frac{T_\infty - T_i}{T_\infty - T_w}, \quad \frac{\rho^{1/2}(p_{t\infty} - p_\infty)^{1/2} x}{\mu}, \quad \frac{p_{ti} - p_\infty}{p_{t\infty} - p_\infty}, \quad \frac{x}{d} \qquad (2.23)$$

The first three parameters are the Nusselt Number, Theta and the Reynolds Number. Thus, for a fixed position, freestream Reynolds Number and Theta, the Nusselt Number will vary with pressure difference ratio. This will vary monotonically with blowing parameters such as mass flux or momentum flux ratio.

In compressible, variable properties conditions, the relevant independent variables become

$$p_{t\infty}, p_{ti}, u_\infty, T_{t\infty}, T_{ti}, \mu_{t\infty}, k_{t\infty}, R, c_p, d, x, q, T_w \qquad (2.24)$$

Using the four reference dimensions mass, length, time and temperature, the system may be described by the non-dimensional parameters

$$\frac{x}{d}\ ,\ \frac{T_{ti}}{T_{t\infty}}\ ,\ \frac{T_w}{T_{t\infty}}\ ,\ \frac{p_{ti}}{p_{t\infty}}\ ,\ \frac{c_p}{R}\ ,\ \frac{\mu_{t\infty} c_p}{k_{t\infty}}\ ,\ \frac{p_{t\infty}\, u_\infty\, x}{R\, T_{t\infty} \mu_{t\infty}}\ ,\ \frac{u_\infty}{\sqrt{(RT_{t\infty})}}\ ,\ \frac{q\ x}{k_{t\infty} T_{t\infty}} \qquad (2.25)$$

The last five parameters represent γ , Pr , Re , M and Nu respectively. (It is assumed that the wall-to-gas temperature ratio governs the effect of viscosity and conductivity variations with temperature). In order to follow the incompressible, constant properties approach as far as possible, this may be rearranged as

$$\frac{x}{d}\ ,\ \Theta\ ,\ \frac{T_w}{T_{t\infty}}\ ,\ \frac{p_{ti} - p_\infty}{p_{t\infty} - p_\infty}\ ,\ \gamma\ ,\ Pr\ ,\ Re\ ,\ M\ ,\ Nu \qquad (2.26)$$

Blowing parameters will be affected by changing either the injection-to-freestream total pressure ratio or total temperature ratio. Thus, there is an additional parameter to consider ; correct scaling would take account of the variation of both these groups. The wall-to-freestream temperature ratio can still be interpreted as the parameter governing property variations, but a change in this ratio will cause a change in theta. Theta will also be influenced by changes in the injection-to-freestream temperature ratio. However, when expressed in this manner, the extension of the principle of superposition to the compressible, variable properties situation can be postulated.

Typical values of some of these parameters in film-cooled gas turbine conditions might be

Freestream Mach Number	0.1 - 1.0
Freestream Reynolds Number	$0.5 - 2.0 \times 10^7$ per metre
Injection-to-freestream total temperature ratio	± 0.60

Wall-to-freestream total temperature ratio	± 0.80
Ratio of specific heats	1.3
Prandtl Number	± 0.70

Engine representative experiments should therefore be conducted at the same conditions as far as possible. Consideration might also be given to correct scaling of surface roughness and the scale and intensity of the freestream turbulence. Surface curvature, pressure gradients and rotational effects will also be present in the engine, but are outside the scope of the present study.

CHAPTER 3.

A Summary of Previous Experimental Methods.

3.1 Introduction.

Various experimental techniques reported in the literature are now described, and their applicability to the engine environment and to blade cooling is evaluated in the light of the previous chapter. For a more detailed summary of the geometries investigated and a description of the results, the reader is referred to GOLDSTEIN's extensive review [3.1] or LOFTUS [3.2]. HAY [3.3] has reviewed some of the more recent heat transfer measurement techniques which are relevant to film-cooling. This chapter concentrates on assessing the success of different methods in attaining the correct boundary conditions and values of dimensionless parameters. For example, in many experiments, air, with a ratio of specific heats of 1.4 is used, whereas the combusted gases in the turbine have a value of about 1.3, so this parameter is not completely correctly modelled.

3.2 Steady State Techniques.

3.2.1 Film Heating.

A common technique used to determine a film-cooling effectiveness is to measure the adiabatic wall temperature downstream of a heated injection flow in a steady state facility. This method was employed by WIEGHARDT's pioneering study [3.4], and subsequently by several investigators, e.g. GOLDSTEIN, ECKERT & RAMSEY [3.5], LIESS [3.6] and PAPELL [3.7]. Thermocouples are usually used to determine the adiabatic wall temperature, although other methods have been employed. BROWN & SALUJA [3.8] use cholesteric liquid crystals, and SASAKI et al.[3.9] scan the film-cooled region with an infra-red camera.

Film heating has the advantage of being more economical than heating the mainstream flow. For small temperature differences, the flow is assumed to have constant properties, so that the results will be applicable to film cooling. However, this necessarily means that if the injection and mainstream fluids are the same, the density ratio will have an upper limit of unity. GOLDSTEIN, ECKERT & BURGGRAF [3.10] simulate the effect of injection-to-freestream density ratio resulting from the injection-to-freestream temperature ratio by using Freon vapour as an injection fluid. This was a highly successful extension of the technique, but introduces an unknown dependence on the ratios of injection-to-freestream transport properties.

3.2.2 Mainstream heating.

Several successful, if more expensive, experiments of this nature have been performed. PAPELL & TROUT [3.11] achieve conditions over the range $0.36 < T_{ti}/T_{t\infty} < 1.83$ for compressible flow by combusting the mainstream gas in a steady state tunnel. PARADIS [3.12] obtains representative coolant-to-freestream temperature ratios by locating a test section between a combustion chamber and a turbine. ARTT et al [3.13] and KRUSE [3.14], by electrically heating the mainstream gas, perform tests at an injection-to-freestream temperature ratio of 0.80. In these cases, film cooling effectiveness results were evaluated from measurements of adiabatic wall temperatures.

3.2.3 Mass Transfer Analogy - Foreign gas injection.

The adiabatic wall boundary condition, requiring zero heat flux from the surface and no local heat conduction, is difficult to achieve, particularly close to the injection position, where temperature gradients can be large, particularly for engine representative injection-to-freestream temperatures. The use of the mass transfer analogy enables the effects of large injection-to-freestream density ratios to be studied without resorting to large temperature differences.

Typically, the injected flow contains a trace of foreign gas, and its mass fraction at an impermeable wall downstream is measured. This is analagous to the adiabatic wall temperature, yielding a film cooling effectiveness equivalent to a mass fraction difference ratio :

$$\eta_{aw} = \frac{c_{iw} - c_{\infty}}{c_i - c_{\infty}} \qquad (3.1)$$

The analogy will only be exact if the corresponding dimensionless parameters of the flow are equal. This requires that the molecular and turbulent Schmidt Numbers for the mass transfer process should be equal to the corresponding Prandtl Numbers for the heat transfer process. PEDERSEN et al [3.15] show that for a porous plate, the effectiveness is insensitive to a variation in Schmidt Number between 0.226 and 1.54, suggesting that the viscous sub-layer only has a small effect on the overall flow. LAUNDER & YORK [3.16] state that it is generally acknowledged that the turbulent values are equal ; this is reinforced by

NICOLAS & LE MEUR [3.17] who report that mass transfer experiments give the same value of effectiveness as adiabatic wall temperature measurements. BURNS & STOLLERY [3.18] point out that the mass concentration is in fact analagous to the adiabatic wall effectiveness based on enthalpy, and that it is the mole fraction which is analagous to effectiveness based on temperature.

Despite these uncertainties, which make it difficult to apply the experimental data directly to a situation where density ratios are largely temperature induced, and heat transfer occurs from an isothermal surface, this method does highlight the effect of density ratio on cooling performance. For example, BURNS & STOLLERY and PAI & WHITELAW [3.19], achieve a variation in injection-to-freestream density ratio of between 0.1 and 4.17 for slot injection. PEDERSEN et al [3.15] performed experiments over the range $0.75 < \rho_i/\rho_\infty < 4.17$ for a single row of holes.

3.2.4 Constant Heat Flux Experiments.

All the techniques mentioned so far only result in the evaluation of the one parameter, adiabatic wall effectiveness. However, concern over the validity of assuming that the second parameter, h_{aw}, could be equated to the unblown value led to experiments designed to evaluate film-cooled heat transfer coefficients.

HARTNETT et al [3.20] and SEBAN & BACK [3.21] use heater pads downstream of injection to supply a known heat flux to the flow. A constant heat flux boundary condition is chosen, and measurements of the heat flux and the wall temperature, together with previously measured values of T_{aw}, enable h_{aw} to be determined. ERIKSEN & GOLDSTEIN [3.22] use a similar technique, but make the freestream and injection temperatures equal, referencing the wall temperature to the freestream temperature and thus obviating the necessity for two sets of measurements. Since this latter boundary condition is isothermal, the resulting value will be the same as the value of A (from the superposition definition) for an incompressible, constant properties flow. CRAWFORD et al [3.23] establish an isothermal wall boundary condition with surface heaters in order to measure heat transfer coefficients.

Although SEBAN & BACK [3.21] and ERIKSEN & GOLDSTEIN [3.22] indicate a dependence of the heat transfer coefficient on the injection process, particularly close to injection, significant errors are incurred due to wall conduction. This is particularly evident in the important region immediately downstream of injection. In addition, this method is only used for injection-to-freestream density ratios close to unity. It should also be noted that measurements taken with a constant heat flux boundary condition may be somewhat different from those on an isothermal surface.

3.2.5 Mass Transfer Analogy - Sublimation Experiments.

GOLDSTEIN & TAYLOR [3.24] overcame the conduction problem by resorting to another application of the mass transfer analogy. In this technique, a naphthalene surface is cast with the desired geometry. In the presence of flow, mass will be lost due to diffusion and convection in a manner equivalent to heat transfer. In the analogy, the driving temperature difference is replaced by a vapour pressure difference ; this varies from the saturated value at the isothermal surface to zero in the freestream. After a run, which typically lasts for an hour, corresponding changes of height at the surface are measured. Together with the known density or concentration, these are used to calculate a local mass transfer rate. The resulting Sherwood Number $mx/D\rho_w$ is equivalent to the Nusselt Number if the Schmidt and Prandtl Numbers are equal. If the latter two numbers are constant, the Sherwood Number can be considered to be proportional to the Nusselt Number, so that values of h/h_o can be inferred. This method has the advantage that an isothermal surface would give a constant naphthalene saturated vapour pressure, analagous to the preferred isothermal boundary condition in heat transfer. One assumption that has to be made is that the finite normal component of velocity at the wall does not affect the analogy. HAY et al [3.25] employ a similar technique, measuring by holographic interferometry the change in thickness of a swollen polymer surface due to evaporation of the swelling agent in the presence of forced convection. Although time consuming, the technique provides detailed , three-dimensional distributions of the heat transfer coefficient.

3.3 Transient Techniques.

All of the above techniques utilise steady state wind tunnels, often with low flow velocities and unit Reynolds Numbers. However, transient facilities have become more widely used in recent years for three main reasons : they offer advantages in the measurement of heat transfer ; they facilitate a more complete modelling of the engine environment, and they are capable of producing data quickly and relatively cheaply.

3.3.1 Transient measurements in steady state facilities.

LIESS [3.6] used a blowdown wind tunnel, attaining representative Mach Numbers and Reynolds Numbers. Heat transfer coefficients were obtained by heating the injection flow, suddenly inserting the instrumented portion into the working section and measuring the rise in surface temperature with time. METZGER et al.[3.26] heat the surface downstream of injection to a constant temperature, once the mainstream and heated injection flows are established. When the wall heating is removed, the transient cooling of the surface is recorded. Excellent agreement was reported between results from this method and the more time consuming measurements of steady state heat flux from an isothermal wall. FERRI et al [3.27] also take transient measurements of wall temperature rise on an initially isothermal surface downstream of a slot in compressible flow. From these, values of q/q_o are found.

3.3.2 Shock Tunnels.

Shock tunnels have been successfully used to measure film-cooled heat transfer, for example by JONES & SCHULTZ [3.28], SMITH [3.29] and LOUIS et al [3.30]. In addition to correct simulation of Reynolds Number, Mach Number and gas-to-wall temperature ratio, the surface boundary condition is isothermal as required. In the reflected shock mode, the duration of the run is about 10 ms, with the subsonic Mach Number set by a downstream throat. Thin film heat transfer gauges are used with analogue circuits to give heat transfer rates. When non-dimensionalised with respect to unblown values, the isothermal film-cooling effectiveness η_{iso} can be evaluated.

3.3.3 Isentropic Light Piston Tunnel.

This type of tunnel, referred to in detail in Chapter 5, was developed in order to model as fully as possible the conditions in a gas turbine engine. In addition to Reynolds Number and Mach Number scaling, the injection-to-freestream density ratio can be simulated. This is achieved, as in the engine, by changing the temperatures of the mainstream and injection gases and therefore does not invoke any analogies, with their associated uncertainties. Running times of about 0.5 second result in greater measurement accuracy than with the shock tunnel, whilst the running cost is very low compared to continuous running facilities. The relatively small temperature rises during a tunnel run do not necessitate the use of expensive, high temperature resistant materials or cooled instrumentation. The initial surface temperature boundary condition is isothermal as desired. Further, it is possible to independently raise or lower the whole wall temperature prior to a run. This is particularly advantageous, since the value of Θ in Eqn.(2.12) can be changed without having to alter the mainstream or injection flows. This enables values of A and B, the two parameters necessary to predict heat transfer on an isothermal, film-cooled surface, to be evaluated in addition to values of q/q_o. Thus, results from this facility will be directly relevant in the prediction of heat transfer loads in the engine environment.

CHAPTER 4.

Correlating Parameters in Film Cooling.

4.1 Introduction.

This chapter contains a review of both theoretical and empirical attempts to determine correlating parameters in film cooling. Many theoretical models have been proposed, which can be compared with experimental data. This heat transfer data may be presented in several forms, for example as η_{aw}, h_{aw}/h_o, q/q_o, or A and B, depending upon the experimental facility used and its associated thermal boundary condition. For each geometry, collapse of such data is sought over a range of velocity ratios, density ratios and positions. Variations due to compressibility effects, the state of the approach boundary layer, changes in the unit Reynolds Number and different values of the ratio of specific heats are also important. Relations might also be sought between the cooling proficiency for different injection angles and geometries.

4.2 Analytical Models.

Prediction of film cooling effectiveness downstream of injection has usually been approached in either of two ways: by using heat sink models, or by performing an energy balance in the injection layer.

4.2.1. Heat Sink Models.

This approach, first given by TRIBUS & KLEIN [4.1], represented the effect of slot coolant injection by a line source of heat in a turbulent boundary layer. The strength of the source is determined by the net enthalpy flow of the injection fluid,

$$q = \rho_i u_i s \, c_p (T_i - T_\infty) \qquad \text{at } x = 0, \text{ per unit span.} \quad (4.1)$$

No attempt is made to incorporate the altered flowfield; velocity and initial temperature profiles are assumed to obey the 1/7th power law. Using an integration kernel developed from a solution for heat transfer rate from a turbulent boundary layer with a step change in wall temperature, the variation of adiabatic wall temperature along the plate was calculated. This gave

$$\eta_{aw} = 5.76 \, Pr^{2/3} Re^{0.2} \left[\frac{\mu_i}{\mu_\infty} \right]^{0.2} \frac{c_{pi}}{c_{p\infty}} \left[\frac{x}{G\,s} \right]^{-0.8} \qquad (4.2)$$

If $c_{pi} / c_{p\infty} = 1$ and $Pr = 0.72$, this reduces to

$$\eta_{aw} = 4.62 \left[\frac{x}{s} \right]^{-0.8} Re_\infty^{\,0.2} \, G \qquad (4.3)$$

This suggests that for a given position and unit Reynolds Number, the adiabatic film cooling heat transfer rate depends only on the mass flux ratio. Close to the hole and at large blowing rates, the experimentally observed lower values of effectiveness are attributed to the effects of interaction of the two flowfields.

More sophisticated heat sink models have been proposed, such as that by ECKERT [4.2]. This models the mainstream as a homogeneous semi-infinite medium, and gives the line heat sink a velocity u_∞ relative to the mainstream in the opposite direction. The adiabatic wall effectiveness would then have the form

$$\eta_{aw} = \frac{\rho_i u_i s\, c_{pi}}{\pi\, \rho_\infty c_{p\infty} \epsilon_\infty}\, e^{(u_\infty x/2\epsilon_\infty)}\, K_o \left[\frac{u_\infty x}{2\epsilon_\infty}\right] \tag{4.4}$$

where K_o is a Bessel function of the second kind of order zero. Empirical input is required for the value of the effective average turbulent diffusivity ϵ_∞, which will vary with distance and blowing. In addition, the theory still does not take account of the aerodynamic effects of mass injection.

In the case of injection through rows of holes, the line sink may be replaced by rows of point or line sinks. The resulting expression for the spanwise averaged effectiveness is identical to Eqn.(4.4), if the hole area per unit width is used instead of the slot height.

A generalisation of this method by ERIKSEN et al [4.3] attempts to account for the penetration of the jets into the mainstream by positioning the sinks above the surface. In this case, the adiabatic wall boundary condition is preserved by placing equal sinks at the same distance beneath the surface. Reasonable predictions of heat transfer rate can be obtained with appropriate empirical input, but this requirement is a restriction on the model's usefulness.

4.2.2 Energy Balance Models.

Another model used to predict values of slot effectiveness, and the fluid mechanic parameters on which it depends, is based on an energy balance in the boundary layer with coolant injection. This has been developed, for example, by KUTATELADZE & LEONT'EV [4.4] and STOLLERY & EL-EHWANY [4.5]. It assumes a well-mixed and constant temperature boundary layer comprised of injected gas and gas entrained from the mainstream, see Fig.(4.1).

Continuity of mass gives

$$\dot{m} = \dot{m}_i + \dot{m}_\infty = \int_0^\delta \rho u \,\partial y \tag{4.5}$$

and the steady flow energy equation gives

$$(\dot{m}_i + \dot{m}_\infty)\bar{c}_p\bar{T} = \dot{m}_i c_{pi} T_i + \dot{m}_\infty c_{p\infty} T_\infty \tag{4.6}$$

where $\bar{T}$ is the mean temperature in the boundary layer and

$$\bar{c}_p = \frac{(\dot{m}_i c_{pi} + \dot{m}_\infty c_{p\infty})}{\dot{m}_i + \dot{m}_\infty} \tag{4.7}$$

If $\bar{T}$ is assumed equal to the adiabatic wall temperature,

$$\eta_{aw} = \frac{1}{1 + \dfrac{\dot{m}_\infty c_{p\infty}}{\dot{m}_i c_{pi}}} \tag{4.8}$$

An estimate of the entrained mass flow is made by assuming a 1/7th power law turbulent velocity profile

$$\frac{u}{u_\infty} = \left[\frac{y}{\delta}\right]^{1/7} \tag{4.9}$$

and a boundary layer thickness given by

$$\delta/x' = 0.37\ Re_{x'}^{-0.2} \tag{4.10}$$

where x' is the distance from the assumed beginning of the turbulent boundary layer. STOLLERY & EL-EHWANY [4.5], for example, assume that the boundary layer starts at injection, at which position there is zero mass flow in the boundary layer. Inserting Eqn.(4.9) into Eqn.(4.5) gives

$$\dot{m} = 7/8 \; \rho_\infty u_\infty \delta \tag{4.11}$$

Since $\dot{m}_i = \rho_i u_i s$, Eqn.(4.8) becomes

$$\eta_{aw} = 3.09 \left[\frac{x}{G\ s}\right]^{-0.8} \left[Re_i \frac{\mu_i}{\mu_\infty}\right]^{0.2}$$

or
$$\eta_{aw} = 3.09 \; \xi^{-0.8} \tag{4.12}$$

where
$$\xi = \left[\frac{x}{G\ s}\right] \left[(\mu_i/\mu_\infty)\ Re_i\right]^{-0.25}$$

Improvements to the analysis can result from estimating δ at the point of injection by equating the mass flow in a fictitious upstream boundary layer to that in the slot.

For compressible flows, GOLDSTEIN, ECKERT & WILSON [4.6] recommend the evaluation of properties at a reference temperature

$$T_* = T_\infty + 0.72(T_r - T_\infty) \tag{4.13}$$

giving

$$\xi_* = \left[\frac{x}{G\ s}\right] \left[(\mu_i/\mu_*)\ Re_i\right]^{-0.25} (\rho_*/\ \rho_\infty) \tag{4.14}$$

This may be written as

$$\xi_* = \left[\frac{x}{s}\right]^{1.25} G^{-1.25} \left[(\mu_\infty/\mu_*)\ Re_\infty\right]^{-0.25} (\rho_*/\rho_\infty) \tag{4.15}$$

Thus, at constant freestream Mach Numbers and unit Reynolds Numbers, the effectiveness would still only vary with mass flux ratio in this scheme.

For high speed flows, GOLDSTEIN et al. [4.6] then propose an alternative definition for the effectiveness based on an isoenergetic-injection wall temperature distribution,

$$\eta_{iaw} = \frac{T_{aw} - T_{iaw}}{T_{ti} - T_{iti}} \qquad (4.15)$$

T_{ti} is the injection stagnation temperature ; T_{iti} is the injection stagnation temperature for isoenergetic conditions when, at a given flow rate, the mainstream and injection flows have equal stagnation temperatures; T_{iaw} is the isoenergetic adiabatic temperature, and will be a function of position. If constant properties are assumed, the velocity field will be the same for the film-cooling case as for the corresponding isoenergetic case. Thus, if the solutions are subtracted, as in the definition of η_{iaw}, the viscous dissipation term disappears. Better correlations are reported between low and high speed flows with this parameter. However, it does not address the question of varying the injection-to-freestream density ratio.

The main objections to the energy balance model are that the adiabatic wall temperature will be lower than the corresponding average boundary layer temperature, and that once again, the aerodynamic effects of injection are ignored. As with the heat sink approach, the model suggests that for a given unit mainstream Reynolds Number, the most important parameter governing the fluid mechanics is the mass flux ratio.

SEBAN & BACK [4.7] and STOLLERY & EL-EHWANY identify three regions in the case of injection from a tangential slot: an initial potential core region in which the wall temperature remains near the injection temperature; a wall jet region, beginning when the velocity profile of the free shear layer merges with the wall shear layer; and a final region in which velocity and temperature profiles resemble those in a turbulent boundary layer (see Fig.(4.2)). Region 1 has unity effectiveness, and regions 2 and 3 are assumed to have the properties of a turbulent boundary layer so that they would be amenable to an energy balance analysis. Clearly, the boundary layer model will be most successful for low injection rates, where the wall-jet region would be non-existent, and at large values of x/s. STOLLERY & EL-EHWANY report successful correlation of slot injection data from the literature for $G < 1.5$. They also note the inadequacies of the model for dealing with large density differences between the coolant and the mainstream.

4.3 Numerical Models.

SPALDING [4.8] first investigated the possibility of a numerical solution of the differential equations applicable to film-cooling. These equations are parabolic and therefore forward marching procedures can be employed. He postulates that velocity and temperature profiles can be described by formulae which contain both "boundary layer" and "wall jet" components. Mainstream entrainment would then occur in the same manner as into a turbulent jet, although it would be difficult to predict the effect of large density differences between the two fluids on this process. PATANKAR & SPALDING [4.9] outlined a numerical scheme for solution of the turbulent boundary layer equations.

KACKER, PAI & WHITELAW [4.10] and PAI & WHITELAW [4.11] utilised this, with the added empirical input of mixing length and effective Prandtl Number distributions, to predict the film cooling effectiveness of a wall jet. This procedure was successful in producing a dependence on injection-to-freestream density ratio which was similar to the experimental results of [4.21].

Similar numerical schemes have been extended to three-dimensional flows. BERGELES et al [4.12] consider angled injection from a row of holes in laminar flow. The upstream pressure effects introduce an element of ellipticity which necessitates storage of the complete three-dimensional pressure field. In addition, there is now a significant velocity normal to the wall, so care is needed in applying boundary layer assumptions. The method however is successful in predicting the existence of counter-rotating vortices downstream from each hole.

CRAWFORD, KAYS and MOFFAT [4.13] developed a two-dimensional boundary layer program to predict spanwise-averaged heat transfer for full coverage film cooling. The injection process and entrainment diffusion was modelled by assuming that drag forces "tear off" strips of the emerging jet. Thus the injection gas is shed into boundary layer stream tubes, according to an empirically derived mass shed ratio which is a function of mass flux rate, hole spacing and injection angle. The turbulence model takes account of jet induced turbulence by locally enhancing the value of the eddy viscosity. Results show good agreement with experiment, but because of the empirical input required, this model cannot predict the dependence of the film cooling process on velocity and density ratios. The results from a numerical procedure based on this model are briefly described in Chapter 8.

RAMETTE and LOUIS [4.14], recognising the limitations of the boundary layer assumptions, provide a model for three-dimensional cooling which describes the trajectory and mixing of the jets, and then determines the growth of the mixed layer. Since contra-rotating vortices are known to exist in the jets, they are included in the modelling. This is the only reported model other than those reporting purely numerical solutions which incorporates this very noticeable feature of three-dimensional injection. Entrainment of the mainstream flow is then due to both the action of the vortices and to turbulent diffusion. Predictions compare reasonably well with experimental results, except close to injection where the discrepancy is attributed to the assumption of constant jet velocity profile.

The models described above have proved moderately successful in predicting film cooling performance in particular circumstances, for example at low blowing rates, for unity density ratios and for specific geometries. They might also be used as a means of interpolating between experimental data points. However, it is apparent that a great deal of progress is still required in developing a satisfactory model to simulate the complex flow patterns associated with this problem. In particular, the models only reveal limited information on the fluid mechanic parameters most likely to scale the injection process for a given geometry.

This situation highlights the importance of relevant experimental work to the engine designer. This would provide firstly a data base for the present generation of prediction programmes, and secondly an insight into the correct scaling.

4.4 Experimental Correlations.

4.4.1 Slot Geometries.

There have been numerous suggestions for correlating parameters based on experimental data. WIEGHARDT [4.15] produced good collapse of data from a tangential slot with the parameter $\left[\frac{x}{s}\frac{\rho_\infty u_\infty}{\rho_i u_i}\right]^{-0.8}$ for x/s > 100 and G < 1.0. This result is similar to predictions from the heat sink and energy balance models. This agreement would be expected if the flowfield resembled a turbulent boundary layer, which would be the case far downstream from injection.

PAPELL and TROUT [4.16] correlated η_{aw} data for a tangential slot over a range of blowing rates, Mach Numbers, and for injection to freestream temperature ratios between 0.36 and 1.83, using

$$\eta_{aw} = 12.6 \left[\frac{\rho_i\ u_i}{\rho_\infty\ u_\infty}\right] \left[\frac{s}{x}\right]^{0.72} \left[\frac{T_i}{T_\infty}\right]^{0.5} \qquad (4.17)$$

for values of $\eta_{aw} < 0.70$, and distances greater than about ten slot heights downstream. This is the first mention of a temperature ratio effect on the performance of film cooling . Results at higher injection-to-freestream temperature ratios yielded higher cooling effectiveness values. The experimenters attribute about half of the effect to property variations, and the balance to increased mixing due to increased turbulence at higher mainstream temperatures. With the assumption that $T_i/T_\infty \approx \rho_\infty/\rho_i$, this corresponds roughly to a correlation of η_{aw} with the parameter $\rho_i u_i^2/\rho_\infty u_\infty^2$. Close to injection, and for $\eta_{aw} > 0.70$, the temperature ratio dependence is not observed; this is attributed to the preservation of the cooling film by its initial momentum.

CHIN et al [4.17] obtained an empirical correlation for slot injection:

$$\eta = 12.7\ A^{-0.65} \qquad \text{for } A > 72$$

where

$$A = \left[\frac{\rho_i}{\rho_\infty}\right]^{-1.5} \left[\frac{u_i}{u_\infty}\right]^{-1.0} \left[\frac{\rho_i u_i s}{\mu_i}\right]^{-0.3} \left[\frac{\rho_\infty u_\infty l}{\mu_\infty}\right]^{0.19} \frac{x}{s} \qquad (4.18)$$

(l is the hydrodynamic starting length of the upstream boundary layer). The density ratio was varied over the range $0.83 < \rho_i/\rho_\infty < 1.17$, and evidently had a marked effect on the adiabatic wall effectiveness.

BROWN [4.18] uses an energy balance correlation for 30° slot results but includes an empirically derived dependence on the momentum flux ratio. This parameter is thought to govern the amount of cooling air lost to the mainstream in the initial mixing of the two flows. The resulting relationship is

$$\eta = 4.0 \left[\frac{\rho_i u_i^2}{\rho_\infty u_\infty^2}\right]^{-0.21} \left[\frac{\rho_i u_i}{\rho_\infty u_\infty}\right] \frac{s}{x}\ Re_x^{0.2} \left[1 - \frac{x_i}{x_o}\right]^{-1} \qquad (4.19)$$

where x_o is the distance from the leading edge and x_i is the distance from the leading edge to the injection location. This states that the dependence on the injection-to-freestream density ratio, relative to the dependence on velocity ratio, is stronger than that proposed by PAPELL & TROUT but weaker than that proposed by CHIN.

ARTT, BROWN & MILLER [4.19] found that for 15° and 30° slots, at a given position and blowing rate, the film cooling effectiveness increased with velocity ratio until a velocity ratio of unity, above which the effectiveness decreased. For a given unit Reynolds Number, the results for each geometry were correlated using a mass flux ratio multiplied by a momentum flux ratio raised to a power.

PAI & WHITELAW [4.20], investigating a tangential slot with foreign gas injection, observe a density ratio effect which is similar to the temperature ratio effect observed by PAPELL & TROUT [4.16].

BURNS & STOLLERY [4.21] also find that for a given mass flow rate, the lightest injection gases give the highest cooling efficiency. LOUIS et al [4.22] produced the following correlation for the isothermal efficiency downstream from angled slot injection;

$$\eta_{iso} = 1.55\ A^{-0.18} \qquad (4.20)$$

where $A = \left[\frac{\rho_i u_i}{\rho_\infty u_\infty}\right]^{-0.675} \left[\frac{T_i}{T_\infty}\right]^{-1.35} Re_i^{-0.25} (\cos^2 \alpha)^{-1.35} \frac{x}{d}$

This equation agrees with the result for tangential injection that for a constant mass flux and freestream Reynolds Number, increasing the injection to freestream density ratio decreases the cooling efficiency.

METZGER et al [4.23] employ a superposition approach and show the linearity of h/h_o with Θ for a given blowing rate, for angled slot injection. Data for other injection rates and positions can then be made to fall on a single line using the scaling parameter

$$\Theta \left[\frac{\rho_i u_i}{\rho_\infty u_\infty}\right]^{0.6} \left[\frac{s}{x}\right]^{0.5}$$

However, since the injection-to-freestream density ratio was unity in these experiments, the stated dependence on blowing rate was not wholly verified.

4.4.2 Hole Geometries.

Before experiments were devised whereby the injection-to-freestream density ratio could be varied independently from the mass flux ratio, the latter parameter was usually used to correlate data, (for example, GOLDSTEIN, ECKERT & RAMSEY [4.24]). This would give an indication of the relative amounts of hot mainstream and cold coolant gas present in the modified boundary layer. However, the results from foreign gas injection experiments revealed a marked dependence of the process on the density ratio.

GOLDSTEIN, ECKERT and BURGGRAF [4.25] found that for 35° holes, Freon injection produced higher cooling efficiencies than air injection at high mass flux ratios. The momentum flux ratio $\dfrac{\rho_i u_i^2}{\rho_\infty u_\infty^2}$ is suggested as a better correlating parameter, and brings the two maximum efficiency peaks into line. The explanation might be that the decrease in efficiency is caused by jet penetration into the mainstream, and that this process is governed by the relative momentum of the jet. SMITH [4.26] shows that this parameter is successful at correlating values of q/q_0 for a slot, a single row of holes and a double row of holes. SMITH also notes that an energy flux ratio $\dfrac{\rho_i u_i^3}{\rho_\infty u_\infty^3}$ is also successful at correlating his data in comparison with mass flux ratio.

PEDERSEN et al [4.27] produce data for a single row of 35° holes which correlates centre-line effectiveness (below the maximum value) with momentum flux ratio. Collapse of data is good at $x/d = 10.29$ although it is not as pronounced further downstream. At values of effectiveness above the maximum, for $x/d = 10.29$ and 39.26, the velocity ratio u_i/u_∞ is a good correlating parameter.

4.5 Dimensional Analysis.

JONES [4.28] reveals that scaling parameters for the injection process can be found using dimensional analysis. For the incompressible mass transfer experiments, the parameters describing the situation may be listed as

$$p_{t\infty}\ ,\ p_{ti}\ ,\ \rho_\infty\ ,\ \rho_i\ ,\ p_\infty\ ,\ x\ ,\ d\ ,\ \rho_w\ ,\ \mu\ ,\ D \tag{4.21}$$

Pressures may be referenced to the freestream static, giving the following non-dimensional parameters

$$\frac{\rho_w}{\rho_\infty}\ ,\ \frac{\rho_i}{\rho_\infty}\ ,\ \frac{p_{ti}-p_\infty}{p_{t\infty}-p_\infty}\ ,\ \frac{d\sqrt{\rho_\infty(p_{t\infty}-p_\infty)}}{\mu}\ ,\ \frac{\mu}{\rho_\infty D}\ ,\ \frac{x}{d} \tag{4.22}$$

The wall-to-injection mass fraction ratio is analagous to the adiabatic mass effectiveness in heat transfer, where

$$\eta_{aw} = \left[\frac{\rho_w-\rho_\infty}{\rho_i-\rho_\infty}\right]\frac{\rho_i}{\rho_w} \tag{4.23}$$

This can be formed from a combination of ρ_w/ρ_∞ and ρ_i/ρ_∞, so the non-dimensional parameters would be

$$\eta_{aw}\ ,\ \frac{\rho_i}{\rho_\infty}\ ,\ \frac{(p_{ti}-p_\infty)}{(p_{t\infty}-p_\infty)}\ ,\ Re\ ,\ Sc,\ \frac{x}{d} \tag{4.24}$$

PEDERSEN et al [4.27] produce data for a single row of 35° holes which correlates centre-line effectiveness (below the maximum value) with momentum flux ratio. Collapse of data is good at x/d = 10.29 although it is not as pronounced further downstream. At values of effectiveness above the maximum, for x/d = 10.29 and 39.26, the velocity ratio u_i/u_∞ is a good correlating parameter.

4.5 Dimensional Analysis.

JONES [4.28] reveals that scaling parameters for the injection process can be found using dimensional analysis. For the incompressible mass transfer experiments, the parameters describing the situation may be listed as

$$P_{t\infty} , P_{ti} , \rho_\infty , \rho_i , P_\infty , x , d , \rho_w , \mu , D \qquad (4.21)$$

Pressures may be referenced to the freestream static, giving the following non-dimensional parameters

$$\frac{\rho_w}{\rho_\infty} , \frac{\rho_i}{\rho_\infty} , \frac{P_{ti} - P_\infty}{P_{t\infty} - P_\infty} , \frac{d \sqrt{\rho_\infty (P_{t\infty} - P_\infty)}}{\mu} , \frac{\mu}{\rho_\infty D} , \frac{x}{d} \qquad (4.22)$$

The wall-to-injection mass fraction ratio is analagous to the adiabatic mass effectiveness in heat transfer, where

$$\eta_{aw} = \left[\frac{\rho_w - \rho_\infty}{\rho_i - \rho_\infty}\right] \frac{\rho_i}{\rho_w} \qquad (4.23)$$

This can be formed from a combination of ρ_w/ρ_∞ and ρ_i/ρ_∞, so the non-dimensional parameters would be

$$\eta_{aw} , \frac{\rho_i}{\rho_\infty} , \frac{(P_{ti} - P_\infty)}{(P_{t\infty} - P_\infty)} , Re , Sc, \frac{x}{d} \qquad (4.24)$$

A consideration of the flow configuration, together with empirical input, allows parameters to be derived for the cases of strong and weak injection (characterised by whether the film cooling performance has reached a maximum value or not).

4.5.1 Strong Injection.

In this regime, the coolant is assumed to emerge as a solid body. The freestream recovers pressure against the jet, so that the effective exit pressure is dependent on the dynamic head of the freestream. For incompressible flow

$$P_{ti} - P_{exit} = \frac{1}{2}\rho_i u_i^2 \tag{4.25}$$

where $P_{exit} = P_\infty + \beta \frac{1}{2} \rho_\infty u_\infty^2$, and β is a constant.

The third non-dimensional parameter in Eqn.(4.24) can then be given as

$$\frac{P_{ti} - P_\infty}{P_{t\infty} - P_\infty} = \frac{\rho_i u_i^2}{\rho_\infty u_\infty^2} + \beta \tag{4.26}$$

This suggests that for a given η_{aw}, a relationship should exist between the momentum flux ratio and the density ratio in this region. Plots of this form using data from [4.27] indicate that this relationship is in fact linear, of the form

$$\frac{\rho_i u_i^2}{\rho_\infty u_\infty^2} = - C + f\{\eta_{aw}\} \frac{\rho_i}{\rho_\infty} \tag{4.27}$$

Rearranging,

$$\eta_{aw} = F\{ \left[\frac{\rho_i u_i^2}{\rho_\infty u_\infty^2} + C\right] \frac{\rho_\infty}{\rho_i} \} \tag{4.28}$$

This includes a term of the form suggested by (4.26), so that η_{aw} may depend on a strong injection parameter SIP where

$$SIP = \left[\frac{P_{ti} - P_{\infty}}{P_{t\infty} - P_{\infty}}\right] \frac{P_{t\infty}}{P_{ti}} \frac{T_{ti}}{T_{t\infty}} \tag{4.29}$$

(The incompressible injection-to-mainstream density ratio has been replaced by the corresponding total density ratio for the compressible case.)

4.5.2 Weak Injection.

At lower injection rates, the exit injection flow is greatly influenced by the recovery of the freestream. BERGELES et al.[4.29] found that the pressure distribution around the hole scales with a dynamic head based on a product of the injected and freestream velocities. This suggests that if the coolant and freestream densities were different, the relationship could be expressed as

$$p_{exit} = p_{\infty} + \gamma \frac{1}{2} \left[\rho_i u_i^2 \rho_{\infty} u_{\infty}^2\right]^{1/2} \quad \text{, where } \gamma \text{ is a constant.} \tag{4.30}$$

The third group in Eqn.(4.24) now becomes

$$\frac{P_{ti} - P_{\infty}}{P_{t\infty} - P_{\infty}} = \frac{\rho_i u_i^2}{\rho_{\infty} u_{\infty}^2} + \gamma \left[\frac{\rho_i u_i^2}{\rho_{\infty} u_{\infty}^2}\right]^{1/2} \tag{4.31}$$

Again a relationship is sought between the momentum flux ratio and density ratio at a given effectiveness. For data from PEDERSEN [4.27] at injection rates below maximum cooling effectiveness, the momentum flux ratio is sensibly independent of density ratio. This indicates that a weak injection parameter WIP may be formed as

$$WIP = \frac{P_{ti} - P_{\infty}}{P_{t\infty} - P_{\infty}} \qquad (4.32)$$

Collapse of data from [4.27] and [4.30] is very convincing with these parameters. LOFTUS [4.31], using the superposition approach adopted by this study, achieved good correlation of 30° single row results at two injection-to-freestream temperature ratios, using JONES' parameters in the relevant regions.

The Strong and Weak Injection Parameters are different from the other correlating parameters considered since they do not depend on measurements of velocities and densities in the flowfield. The fact that they are based on pressures and temperatures which will be known to the designer makes them very convenient.

It is crucial to examine the results obtained in this investigation in the light of the correlating parameters suggested in this Chapter. The relative success of the parameters at collapsing data obtained at different injection-to-freestream velocity and density ratios will suggest how the engine designer might make best use of the experimental data available to him.

CHAPTER 5.

Description of Test Facility and Instrumentation.

5.1 Introduction - Design and Principle of Operation of Isentropic Light Piston Tunnel.

As mentioned in Chapters 2 & 3, it is important that film-cooling experiments should be carried out at conditions which simulate the gas turbine environment as fully as possible. In this regard, the ILPT is an excellent test rig. It is a transient facility in which the Reynolds Number and Mach Number can be varied independently. In addition, wall-to-freestream and injection-to-freestream temperature ratios typical of turbine blades can be attained, and the wall thermal boundary condition is isothermal as required.

The principle of operation can be explained with the use of a schematic diagram, Fig.5.1. Test gas in the pump tube is compressed and therefore heated isentropically by a piston which is driven by air from a high pressure reservoir. Thus, a wall-to-freestream temperature ratio from a turbine entry temperature of 1700 K and a blade temperature of 1100 K can be simulated by isentropic compression of the test gas to 465 K and an ambient wall. This is particularly advantageous, since at lower flow temperatures, the unit Reynolds Number is significantly increased and so rig pressure levels can be smaller.

When the test gas has been compressed to the required temperature and pressure, a slide valve is activated which allows flow into the working section, for a duration of about 0.5 s. If the volume flow rate of reservoir air into the tube equals that of the test gas out of the tube, the flow is matched and conditions will be steady.

The Mach Number is set in the present tests by a downstream throat, although supersonic flow can be achieved by placing the throat upstream. The dump tank can be evacuated to ensure choking at the throat. The Reynolds Number can then be set by the temperature and pressure levels resulting from compression.

The wall temperature in the working section can be raised or lowered over the range 260 K < T_w < 380 K prior to a run by convective heating or cooling. A liquid nitrogen heat exchanger allows the test gas to be pre-cooled if required, resulting in a range of mainstream total temperatures 270 K < $T_{t\infty}$ < 600 K. The injection can be heated or cooled as required, over the range 260 K < T_{ti} < 350 K.

The ILPT used has a tube of length 1.85m and diameter 0.154m. It is shown in Plate 5.1, and an operating map is given in Fig.5.2. The shaded area represents conditions over which the ranges of temperature ratios 0.43 < $T_w/T_{t\infty}$ < 1.40 and 0.43 < $T_{ti}/T_{t\infty}$ < 1.30 are possible. The maximum unit Reynolds Number is determined by the pressure level in the pump tube, which is stressed to 500 psi. The minimum unit Reynolds Number in subsonic flow is determined by the extent to which the dump tank can be evacuated to ensure choking in the working section throat at low pressure levels. The minimum value of $p_{dump}/p_{t\infty}$ also limits the maximum Mach Number which can be attained. The maximum total temperature is restricted to approximately 600 K by the shortening of the running time at high compression ratios. There is in fact an additional loss in useful running time caused by the formation of a relatively cold gas vortex which originates from the gas adjacent to the pump tube wall. This gas rolls up ahead of the piston as it moves down the tube, and is expelled through the test section at the end of the run.

The piston is made from molybdenum-loaded nylon and has a mass of approximately 350g. This is light enough to ensure that the working section pressure oscillations, as a result of piston velocity oscillations when the slide valve opens, are negligible.

A more complete theory of operation of the tunnel is given by JONES et al.[5.1].

5.2 Instrumentation.

5.2.1 Heat Transfer Measurement.

Spanwise-averaged heat transfer rates are measured using a transient technique employing thin film gauges. The technique is well established and ideally suited to a transient facility such as the ILPT, providing a major advantage over continuously running facilities.

A measurement of surface temperature with time is required, which can be obtained from a thin film platinum resistance thermometer operating on an electrically insulating substrate. They utilise a constant current supply, so that

$$\Delta T = \frac{1}{\alpha}\,\frac{1}{V_o}\,\Delta V \qquad (5.1)$$

where α is the gauge temperature coefficient of resistivity, V_o is the applied voltage at ambient temperature T_o and ΔV and ΔT are the changes in voltage and temperature respectively. In the present study, machinable glass ceramic was used as the substrate. A comprehensive account of thin film technology is provided by SCHULTZ & JONES [5.2], and the use of thin films to measure heat transfer rates on turbine blades is described by SCHULTZ et al.[5.3].

Over the time scale of a tunnel run, one-dimensional semi-infinite assumptions may be made about the substrate. The relevant heat conduction equation is therefore

$$\frac{\partial^2 T}{\partial y^2} = \frac{\rho c_p}{k} \frac{\partial T}{\partial t} \tag{5.2}$$

with boundary conditions

$$\begin{aligned} &T = 0 \text{ at } t = 0 \text{ for all } y \\ &T = 0 \text{ at } y = \infty \text{ for all } t \\ &q_{y=0} = -k \left[\frac{\partial T}{\partial y}\right]_{y=0} \end{aligned} \tag{5.3}$$

where y is positive into the substrate. The heat transfer rate is then given by

$$\bar{q} = \sqrt{(\rho c_p k)}\, \sqrt{s}\, \bar{T} \tag{5.4}$$

where barred symbols are Laplace transformed variables and s is the Laplace variable. If q varies with time, the solution is

$$q = \frac{\sqrt{(\rho c_p k)}}{\pi} \left[\frac{T(t)}{\sqrt{t}} + 1/2 \int_0^t \frac{T(t) - T(\tau)}{(t - \tau)^{3/2}}\, d\tau\right] \tag{5.5}$$

In practice, an electrical analogue is used in order to determine the surface heat flux. The one-dimensional heat conduction equation (5.2) is analagous to the equation for the variation of voltage along a transmission line with distributed resistance r and capacitance c per unit length,

$$\frac{\partial^2 v}{\partial y^2} = rc \frac{\partial v}{\partial t} \tag{5.6}$$

with boundary conditions

$$v = 0 \text{ at } t = 0 \text{ for all } y$$

$$v = 0 \text{ at } y = \infty \text{ for all } t \qquad (5.7)$$

$$i = \frac{1}{r}\left[\frac{\partial v}{\partial y}\right]$$

giving $\quad \bar{I} = \sqrt{(c/r)}\,\sqrt{s}\,\bar{V} \qquad (5.8)$

The spanwise-averaged surface heat flux is then related to the analogue input current i_{in} by

$$q = \sqrt{(\rho c_p k)}\,\sqrt{(r/c)}\,\frac{1}{V_o \alpha}\,i_{in} \qquad (5.9)$$

OLDFIELD et al.[5.4] have re-designed the analogue circuit using a logarithmic scaling of the resistive and capacitive elements. This has improved the accuracy and has increased the working bandwidth to approximately 0.1Hz - 100kHz. Typical heat transfer traces with time are shown in Figs.5.3 - 5.4. The heat transfer rate falls off with time as the surface temperature rises.

In the past, the following scheme was adopted in order to extract the heat transfer rate to the initially isothermal surface. The heat transfer rate was plotted against the corresponding temperature rise, which can be computationally reconstructed using Eqn.(5.4) and approximating the heat transfer rate by the summation of a series of ramps. The linear portion of this plot was then extrapolated back to zero surface temperature rise to obtain the heat transfer rate for the isothermal wall. Further details of this approach can be found in OLDFIELD et al. [5.5]. The method is entirely satisfactory, but at high mainstream temperatures and therefore short running times and less measuring points, a small error in the gradient of the extrapolated line can lead to a significant error in the initial heat transfer rate. For example, typical values of experimental scatter on flat plate Nusselt Numbers are 20% for Nu ≈ 3000 and 7% for Nu ≈ 1500, for mainstream temperatures of 500K and 365K respectively, and initially ambient wall temperatures. This scatter is reduced to 4% and 1% if the Nusselt Number is constructed from a point on the line fit through the measured data. An example of this processing method is shown in Fig.5.5.

This second approach implies that there will be a slight temperature distribution along the wall at the measuring time because of the change in heat transfer rate down the plate. This is reduced by choosing a measuring point as far forward in time as possible. Typical blown and unblown profiles are shown in Fig.5.6. In the unblown situation, the effect of this can be estimated in the manner described in Section 6.4, and introduces an error of approximately 1%. It is difficult to make a similar estimate for film-cooled results. However, it can be seen from Fig.5.7, which shows the variation of Nu/m with distance for a typical film-cooled run with initially ambient wall, that extrapolation introduces scatter into the results which is not present in results using values picked from the line-fit. (The difference in absolute level of Nu/m between the two methods is due to the increase in the value of theta as the wall temperature rises). For a series of runs presented as Nu/m against θ, as in Chapter 8, the results using measured point values generally lie within the scatter of those produced by extrapolation, so that no systematic error is introduced. This provides justification for adopting the second approach in this study, as it is felt that the measurements are used to better effect.

5.2.2 A Brief Description of Thin Film Gauges and their Construction.

Methods of depositing thin film gauges on insulating substrates have been developed at Oxford over several years. Vacuum deposition has been successfully performed, but adhesion of the film to the substrate is sometimes unsatisfactory, and it is difficult to predict the final gauge resistance.

The following method gives extremely good results. The ceramic substrate is first polished and cleaned. The thin films are then hand painted, using a suspension of platinum in a lacquer (Hanovia Liquid Bright 05-X) and a single hair paint brush. At the same time, a suspension of gold is used for the gauge tags which connect the gauges to the lead wires on the side of the liner, to ensure that their resistance is as low as possible. After painting each coat, the liner is fired in a furnace at 680 K for half an hour.

After about six or seven coats, the gauge resistances have dropped to the required value of about 40 ohms. The films are then about 0.5 mm wide and of the order of 1 micron thick. Fine copper wires are then soldered, using low melting point solder, to platinum tips at the end of the gold tags to form a strong connection of low electrical resistance. Solder is preferred to a conducting epoxy since the latter undergoes glass transition within the range of operating temperatures. This was found to be a problem when calibrating the gauges, which is done in water, since the epoxy absorbed moisture above the glass transition temperature and lost its adhesive strength. A silver loaded epoxy is, however, coated over the soldered joint to decrease the resistance of the joint. At this stage, a careful check is made to ensure that none of the gauges are electrically connected. The tag-to-wire connections are then smeared with silicon grease to lessen any joint stress caused by thermal expansion. They are then potted in a fast-setting putty which is chosen for having a very similar rate of thermal expansion to the glass ceramic. The putty is shaped so that it is flush with the side of the ceramic liner. The completed liner is shown in Plate 5.2 and Fig.5.8. Gauges manufactured in this manner are extremely durable and have a very low failure rate.

5.2.4 Surface Temperature Measurement.

This is achieved using the thin film gauges as resistance thermometers, as depicted by Eqn.(5.1). Since in general pre-run wall-heating or cooling takes place, the corresponding voltage change is required in addition to that associated with the run. Whilst the latter can be constructed from heat transfer data, the run initial gauge temperatures can only be found from monitoring the voltage across the gauges. An oscillatory instability, due to positive feedback of an earth loop, developed when the temperature amplifiers were placed at the input stage to the heat transfer analogues. This was reduced by placing resistors on the earth leads to the temperature amplifiers. A typical wall temperature trace during a run is included in Fig.5.3.

The following points should be born in mind when considering the accuracy of temperature measurement using thin film gauges.

(i) Calibration. The temperature coefficient of resistivity of the thin film gauges are determined by immersing the liner in de-ionised water and noting the increase in resistance as the water is uniformly heated. A specimen calibration is produced as Fig. 5.9 ; the resulting value of α is accurate to 0.5%. It has been noted in previous work at

Oxford, and by MILLER [5.6], that the exposure of new thin films to temperature cycles decreases their resistance, presumably as a result of annealing. However, whilst the absolute resistance of the gauges tends to increase over a long period of time (probably due to abrasion), the value of α remains very similar. The re-calibration of a liner two years after manufacture produced lower values of α which were nevertheless within 2% of the original values. MILLER quotes a variation of less than 3% in α between results from calibrations before and after a series of tests.

Care has to be taken to ensure that the copper wires connecting the gauges to the instrumentation do not introduce unacceptable errors. Since these leads will heat up to some extent when the liner is heated in the working section, there will be an additional voltage increase which should be kept to a minimum. Calibrations performed with "hot leads" and "cold leads" were found to differ by as much as 2%. The maximum error due to gauge tag and lead heating can be found by examining the resistances and coefficients of resistivity. In general,

$$R_T = R_o\ (\ 1 + \alpha_o \Delta T\ ) \qquad (5.10)$$

where R_o is the reference resistance, R_T is the resistance if the temperature is changed by ΔT, and α_o is the coefficient of resistivity of the gauge, tags and leads at the reference temperature. R_T is comprised as follows :

$$R_T = R_{fo}(1 + \alpha_{fo} \Delta T_f) + R_{lo}(1 + \alpha_{lo} \Delta T_l) \qquad (5.11)$$

where suffix f refers to the film, and l refers to the leads (the resistance of the tags is very small). For platinum gauges, $\alpha_f \approx 0.0025/K$, and for copper wire, $\alpha_l \approx 0.0050/K$. In order to ensure that α does not vary from α_f by more than ±1%, the condition to be satisfied is $R_{lo} < 0.01\ R_{fo}$.

Thus, for a gauge resistance of 40 ohms, the leads have a resistance of about 0.4 ohms, which allows sufficient length to make connections to the instrumentation. MILLER estimates a maximum lead heating error of 4% based on the leads accounting for 4% of the total resistance.

(ii) Ohmic heating. This is the heating effect of passing a current through the films, which will not be accounted for in their calibration. It has been investigated by AINSWORTH [5.7] by passing varying amounts of power through test gauges and measuring the gauge resistances. Similar tests undertaken in the present study show that the temperature rise associated with operating conditions is less than $0.5^{\circ}C$ (see Fig. 5.10).

5.2.5 Injection and Mainstream Temperature Measurement.

These were measured using fast-response micro-miniature thermocouples manufactured from 12 micron diameter chromel/alumel wires. The injection thermocouple is mounted in the injection plenum and therefore measures the injection total temperature. Careful measurements of the injection temperature by LOFTUS [5.8] revealed that the centre-line temperature at exit from the injection geometry was very close to the plenum temperature. Thus, active cooling in the holes could be ignored and the thermal boundary condition of Fig.2.2 was achieved. The most successful mounting for the mainstream thermocouple was found to be a forward-facing stagnation probe, the design of which was based on considerations outlined by MOFFAT [5.9]. Low probe velocities ensure negligible recovery effect, while the small junction bead and wires limit conduction error and decrease the response time. The junction was approximately 1mm from the mount to reduce conduction error and at the same time to preserve rigidity. The small temperature difference between thermocouple and shield would make radiation errors small.

At a total temperature of 365 K, corresponding to a test gas compression ratio of about two, the measured total temperature is less than two degrees smaller than the calculated isentropic temperature. This difference is about ten degrees at a total temperature of 500 K, corresponding to a compression ratio of about six. This agrees well with similar measurements by HENDLEY [5.10]. In addition, for a set of runs at constant mainstream temperature, where the wall temperature is varied, plots of heat transfer against driving temperature for gauges upstream of injection give straight lines which extrapolate through the origin within experimental error.

As can be seen from Figs.5.3 - 5.4, the response times of the thermocouples are very fast, of the order of 10 ms. Previously, the thermocouple reference junction had consisted of a water bath at the side of the working section. This was found to heat up by as much as 1.5°C after prolonged heating of the wall, and was replaced by an electrically balanced reference junction.

5.2.5 Pressure Measurement.

Measurement of the mainstream total and static pressures, and of the injection total pressure, were made using quartz piezo-electric Kistler pressure transducers. The transducers are grounded before the run so pressure changes are measured relative to either the initial pump tube or dump tank pressure. These are set using precision Wallace and Tiernan dial gauges. The pressure differences between mainstream total and static, and between injection total and mainstream static, are also measured using semi-conductor strain gauge differential pressure transducers. All the pressure transducers were calibrated in situ through their amplification equipment and data acquisition system. When calibrating the differential pressure transducers, their common mode response must be taken into account. The transducer output can be considered to have the form

$$V_{out} = K_d \left[(p_+ - p_-) + \alpha \frac{(p_+ + p_-)}{2} \right] \qquad (5.12)$$

where K_d is the differential gain, α is the reciprocal of the common mode rejection ratio and p_+ and p_- are the pressure changes at the positive and negative ports respectively. K_d and α are found by two separate calibrations. Firstly, the negative port is left at atmospheric whilst the positive port is varied over the operating pressure range. Secondly, both ports are connected and raised over the same pressure range.

5.2.6 Data Acquisition and Processing System.

Heat transfer, temperature and pressure signals are recorded for inspection on an 8" ultra-violet chart recorder, and for analysis on a tunnel-dedicated mini-computer.

The mini-computer is a Digital Equipment Corporation PDP 11/10 ; Fig. 5.11 shows how the instrumentation is linked to the computer.

A suite of programmes, described by OLDFIELD et al. [5.5], allows the data to be acquired, displayed and then processed. A number of modifications have been made to the processing programme in order to increase the measurement accuracy. The method of extracting a value of heat transfer at a corresponding wall temperature from a line fit through the data has already been described. However, it can be seen from

Eqn.(5.4) that the heat transfer rate is proportional to the property product $\sqrt{(\rho c_p k)}$ of the ceramic. This can be found by pulsing a constant current through the gauge and monitoring the change in voltage resulting from the increased resistance due to ohmic heating. Initially, the voltage is found to vary with the square root of time according to

$$\Delta v = \frac{1}{\sqrt{(\rho c_p k)}} \frac{2}{\sqrt{\pi}} \alpha_o \frac{R_{fo}}{A} R_f i^3 \sqrt{t} \tag{5.13}$$

where A is the film area, and subscripts f and o refer to the film and the reference temperature respectively. By repeating the test with the film covered by glycerine, whose thermal properties are well known, measurement of the film area can be eliminated so that

$$\sqrt{(\rho c_p k)} = \sqrt{(\rho c_p k)_g} \Big/ \left[\frac{\Delta v/\sqrt{t}}{\Delta v_g/\sqrt{t}} - 1\right] \tag{5.14}$$

where subscript g refers to the properties of glycerine and Δv_g is the associated voltage rise. In this manner, the value of $\sqrt{(\rho c_p k)}$ for machinable glass ceramic was found to be 2050 J $m^{-2}K^{-1}s^{-1/2}$ ±2%. However, this value may vary by about 4% for different ceramic batches, so it is recommended that each liner is tested individually.

Further, the value of $\sqrt{(\rho c_p k)}$ varies with temperature. By pulsing a liner over a range of steady temperatures in an oven, DOORLY [5.11] quantified this variation as

$$\sqrt{(\rho c_p k)} = \sqrt{(\rho c_p k)_{293}} \, (1 + 0.0012(T - 293)) \tag{5.15}$$

This enables the properties to be evaluated at the measured temperature.

It is realised that this does not completely account for the variation of $\sqrt{(\rho c_p k)}$ with time and distance into the substrate during the run. DRUMMOND et al. [5.12] recommend the use of an effective property product for a given material which would be found from numerically solving the heat conduction equation, with ρ, c_p and k varying with time and position. The effective property product would then vary only with surface temperature and is independent of heat flux. However, its variation would be less than the variation of the uniform temperature value given by Eqn.(5.15).

5.3 Tunnel Features.

The reader is referred to HENDLEY [5.10] or LOFTUS [5.8] for a comprehensive description of the standard components of the tunnel. In large part, only modifications which have increased the accuracy of measurements or which have extended the operating range of the tunnel are considered in detail here.

5.2.1 Working Section.

This is shown schematically in Fig.5.12. The cross section changes smoothly from circular to rectangular downstream of the slide valve. However, a new boundary layer is established at the front of the test flat plate, using a boundary layer bleed connecting with the dump tank in the run configuration. For pre-run wall heating or cooling, the dump tank is isolated and the bleed valve serves as an inlet for the hot or cold air.

The instrumented liner is machined from glass ceramic. This is an ideal material since it is electrically insulating, and also has a low thermal conductivity which increases the surface temperature rise and decreases the depth to which a heat pulse penetrates in a given time. In addition, the liner, including intricate injection geometries, can be manufactured from one piece of ceramic. This obviates the necessity for inserts, which can alter the temperature and velocity field in the boundary layer.

5.3.2 Slide Valve.

This communicates the pump tube with the working section. It is activated when a signal from a pressure transducer monitoring the test gas pressure reaches a pre-set level. A capacitor is then discharged across a solenoid, which strikes a plunger on the slide valve. This action breaks a seal and allows a high pressure air supply to open the shutter. The opening time is typically 30 ms, so that the flow is established across the working section in a uniform manner.

5.3.3 Shutter.

This is located between the working section and the dump tank, and is detailed in Fig.5.13. In the pre-run position, it seals the dump tank and allows wall-heating or cooling air to exhaust to atmosphere. Just prior to the run, the shutter is manually operated so that the working section communicates with the dump tank. The shutter is necessary for two reasons :

1. It allows the pre-run wall temperature to be varied at low total temperatures or Reynolds Numbers where the dump tank has to be evacuated in order for the throat to choke.
2. It prevents transient convective currents which can give rise to unsteady heat transfer rates before the run. These will then contribute to the output from the heat transfer analogues at the onset of the run.

This was first noticed before the shutter was installed when, for an uncooled flat plate, a non-zero intercept resulted from plotting heat transfer data against the driving temperature (see uncorrected results, Fig. 5.14). Examination of the processes occurring during heating of the wall, and over the time elapsing between turning off the heating system and initiating the run, indicates that there is significant heat transfer taking place before the run which causes a zero offset. This would increase as the wall temperature is raised. Fig. 5.15 gives a sketch of a typical surface temperature trace and heat transfer analogue output over this period.

It is relevant to examine the governing equations in this light to ensure that the electrical circuit used in determining the the heat transfer is still an analogue for the heat transfer process. With the wall at ambient temperature, Eqn.(5.2) describes the variation of temperature with distance and time. For the case of the wall at an elevated temperature, however, the temperature is the sum of the distribution caused by the steady state heating and any time dependent processes occurring,

$$T(y,t) = T_1(y) + T_2(y,t) \tag{5.16}$$

$T_1(y)$ will be linear in a one-dimensional steady state condition, so the corresponding heat transfer rate will be a constant, q_1, and $\dfrac{\partial^2 T_1}{\partial y^2} = 0.$

Thus, the one dimensional unsteady heat transfer equation can be written in terms of T_2 :

$$\frac{\partial^2 T_2}{\partial y^2} = \frac{\rho c_p}{k} \frac{\partial T_2}{\partial t} \tag{5.17}$$

This has boundary conditions $T_2 = 0$ for all y at t = 0

$$T_2 \quad 0 \text{ for all } t \text{ at } y = \infty \tag{5.18}$$

In addition, the surface boundary condition is

$$-k \left[\frac{\partial T_2}{\partial y} \right]_{y=0} = q_w(t) - q_1$$

Eqns.(5.17) and (5.18) in T_2, with the wall heat transfer modified to include the steady state term, are equivalent to the Eqns.(5.2) and (5.3) in T, so that the electrical analogue is still valid.

The various stages shown in Fig. 5.15 can now be analysed. An explanation can also be given for the form of the heat transfer trace reconstructed from the temperature trace (similar to a perfect analogue output) and this can be related to the output from a real analogue, whose time constant is such that it does not reproduce steady state heat transfer rates over the period in question.

In region 1, during heating, analogue output will be zero when there is no change in surface temperature. In region 2, where the heating has been switched off, the heat transfer will be the sum of the steady negative heat transfer q_1 and any unsteady pre-run convective heat transfer q_w. At the onset of the run, q_1 persists but $q_{w(t<t_r)}$ is taken off and replaced by $q_{w(t>t_r)}$, corresponding to the initial run heat transfer rate. Both perfect and real analogues will respond identically to this sudden change, so that for the case shown, the heat transfer "jump" recorded, zeroed at position X, will be overestimated by a zero error corresponding to the convective heat transfer before the run. The magnitude of this term was experimentally determined by estimating the value of q_1 and subtracting this from the values of heat transfer given by traces reconstructed computationally from temperature traces. It was found to vary approximately linearly with the difference between wall and ambient temperature. The results shown in Fig.5.14 are corrected firstly with this term and then for a non-isothermal wall temperature distribution. The corrected results show that the heat transfer and the driving temperature approach zero together as expected.

In order to make this correction unnecessary, the shutter was installed so that before the run is initiated, the working section can be abruptly brought down to sub-atmospheric conditions, resulting in a perfect analogue as shown in Fig.5.15.

5.3.4 Pre-run wall heating and cooling.

This is achieved by passing air from a throttled 400 psi supply line into the working section via the boundary layer bleed and out to atmosphere through the shutter. The air is heated using two banks of 3 x 0.75 kW electrical heaters whose heating can be controlled by a rheostat. Cooling is achieved using a heat exchanger where the air passes through about 3m of 12mm diameter coiled copper tubing immersed in liquid nitrogen. This air can be mixed with ambient air in order to increase the mass flow rate and provide a more uniform wall temperature profile. In this way, the start-of-run wall temperatures are reasonably isothermal, and the temperature range is about 100^{o}C, which represents a significant increase over the tunnel's previous operating range.

5.3.5 Tube cooling.

The liquid nitrogen heat exchanger can also be used to feed cool air through a jacket surrounding the piston tube. With no test gas compression, this allows an extremely uniform gas temperature of 280 K to be attained. It is equally conceivable to pre-heat the tube and raise either the maximum value of the total temperature or the running time at a given total temperature. However, this was not pursued since the test gas compression caused the temperature non-uniformities in the tube to give unsteady values of total temperature in the working section.

5.3.6 Injection Mechanism.

Injection flow is introduced into the injection plenum via a calibrated orifice, so that the injection mass flow can be determined from the injection temperature and the injection reservoir pressure. This flow is initiated by a solenoid-activated shuttle valve which is timed to open when the mainstream flow enters the working section. In this arrangement, however, the pressure in the injection plenum would initially be less than the working section static pressure, so that ingestion of mainstream gas would occur. To prevent this, another injection reservoir has been fitted. Just before the run, air from this tank fills the injection plenum to a pressure slightly above the anticipated working section static pressure. When the run is initiated, the shutter which turns on the calibrated (constant mass flow) injection flow also turns off this pre-run plenum filling flow, thus preventing ingestion.

A lagged copper jacket surrounds both injection supply lines and the injection shutters. For injection heating, air heated by electric heaters is passed through this jacket; for injection cooling, cool air from the liquid nitrogen heat exchanger is passed through the jacket. In this way, the injection temperature can be varied from 260 K to 350 K. Outside this range, the following problems are encountered :

1. Temperature gradients are set up in the injection air supply so that the injection temperature is not constant over the period of the run.

2. The mass surrounding the injection plenum tends to act as a heat source or sink. This affects both the establishment of an isothermal wall temperature distribution along the liner, and the range of wall temperatures which can be attained.

3. Severe injection cooling causes leaks as the rubber 'O' rings lose their flexibility.

Within these temperatures, however, the system is extremely reliable and the injection temperature profiles are good (see Figs.5.3 - 5.4). Another advantage is that the amount of heating or cooling can be varied to ensure that the injection temperature is not affected significantly from run to run due to prolonged wall heating. This is very important, since in order to find values of A and B (from Eqn.(2.12)), theta must be varied by varying the wall temperature for a fixed injection and freestream temperature.

CHAPTER 6.

The Effect of Wall-to-Gas Temperature Ratio on Heat Transfer.

6.1 Introduction.

This chapter describes theoretical and experimental investigations undertaken in order to quantify the effect of the wall-to-gas temperature ratio on the Nusselt Number on an unblown flat plate with a turbulent boundary layer in compressible flow. Since this temperature ratio is one of the parameters on which film-cooling may depend, as shown in (2.26), it is important to determine its influence. Before conclusions can be drawn about the film-cooled situation, however, the unblown boundary layer must be studied. The effect of the temperature ratio would arise because of variations in density and transport properties through the boundary layer.

Dimensional analysis is used to describe the situation, and the case of a laminar boundary layer is studied analytically in order to provide some physical insight into the mechanism of the effect. Experimental results from the ILPT are then compared with results from a numerical solution of the turbulent boundary layer. The literature, which is rather sparse on this topic, is reviewed, and finally the implications of the effect of property variations in the film-cooling situation are discussed.

6.2 Dimensional Analysis.

This allows the non-dimensional parameters governing the physical situation to be found. These parameters will in general be different depending upon the assumptions made about the flow. The following cases are considered :

1. Incompressible, constant-properties, without viscous dissipation.

The relevant independent variables can be chosen as

$$\rho \;,\; u_\infty \;,\; k \;,\; \mu \;,\; c_p \;,\; x \;,\; (T_w - T_\infty) \;,\; q \qquad (6.1)$$

where temperatures are referenced to the freestream value since the governing differential equations are linear in temperature. These variables form three non-dimensional parameters,

$$\frac{q\;x}{k(T_\infty - T_w)} \;,\; \frac{\mu\, c_p}{k} \;,\; \frac{\rho\, u_\infty\, x}{\mu} \qquad (6.2)$$

2. Compressible, constant properties.

In this case, the equation of state is employed and density becomes a non-linear function of temperature. This implies that absolute, rather than reference temperatures, must be used, so that the relevant independent variables become

$$\rho_\infty \;,\; u_\infty \;,\; k \;,\; \mu \;,\; c_p \;,\; R \;,\; x \;,\; T_w \;,\; T_{t\infty} \;,\; q \qquad (6.3)$$

giving non-dimensional parameters

$$qx/kT_{t\infty} \;,\; T_w/\,T_{t\infty} \;,\; \frac{\rho_\infty u_\infty x}{\mu} \;,\; c_p/R \;,\; \frac{\mu\, c_p}{k} \;,\; \frac{u_\infty^2}{c_p T_{t\infty}} \qquad (6.4)$$

The first two parameters can be rearranged to give $Nu(T_w/T_{t\infty} - 1)$ and $T_w/T_{t\infty}$ and may be combined to give the conventional parameters

$$Nu \;,\; T_w/T_{t\infty} \;,\; Re \;,\; \gamma \;,\; Pr \;,\; M \qquad (6.5)$$

3. Compressible, variable properties.

This may introduce more non-dimensional parameters, depending on the assumed form of the property variations.

(a) If c_p, μ and k are represented by linear functions of temperature, for example

$$\mu = \mu_{t\infty}(1 + \alpha_1(T_{t\infty} - T)) \tag{6.6}$$

then in addition to the non-dimensional parameters in (6.5) the solutions would also depend on $\alpha_1 T_{t\infty}$, etc. Thus the Nusselt Number may be influenced by absolute temperatures as well as the wall-to-gas temperature ratio. This would also be the case for more complicated viscosity-temperature relationships, such as Sutherland's law.

(b) A common assumption for gases is to treat c_p and Pr as constants, and to represent the viscosity (and therefore conductivity) variation with temperature as a power law

$$\mu = \mu_{t\infty} (T/T_{t\infty})^m \tag{6.7}$$

In this case, the non-dimensional parameters remain as in (6.5). If these assumptions are made with respect to the experiments performed, then since M, γ and the unit Reynolds Number were constant, for a given position

$$\frac{q}{k_{t\infty}(T_{t\infty} - T_w)} = \text{constant } f(T_w/T_{t\infty}) \tag{6.8}$$

If there was no wall-to-gas temperature ratio effect, the functional dependence on the temperature ratio would be unity and the Nusselt Number would assume its fixed, incompressible, constant properties value, so that the general expression is

$$Nu = Nu_{cp} f(T_w/T_{t\infty}) \tag{6.9}$$

As shown above, this can be expressed as

$$q/k_{t\infty}T_{t\infty} = \text{constant } (1 - T_w/T_{t\infty}) f(T_w/T_{t\infty}) \tag{6.10}$$

This is a convenient form in which to plot the data, since at small temperature differences, uncertainties arise in the evaluation of the Nusselt Number. If $f(T_w/T_{t\infty}) = 1$, $q/k_{t\infty}T_{t\infty}$ would vary linearly with $T_w/T_{t\infty}$; if not, any curvature could be approximated by a power law

$$f(T_w/T_{t\infty}) = (T_w/T_{t\infty})^n \tag{6.11}$$

so that

$$Nu/Nu_{cp} = (T_w/T_{t\infty})^n \tag{6.12}$$

6.3 The Laminar, Compressible Boundary Layer - an Analytical Analysis.

A valuable insight into the manner in which the wall-to-gas temperature ratio should affect the Nusselt Number can be gained by studying the equations for a laminar, compressible boundary layer. With the use of the Howarth-Dorodnitsyn transformation, the momentum and energy equations can be written as follows :

$$ff'' + (Cf'')' = 0$$

$$((C/Pr)T')' + fT' + (\gamma-1)M_\infty^2 CT_\infty f''^2 = 0 \tag{6.13}$$

with boundary conditions

$$f(0) = f'(0) = 0\ ,\quad T(0) = T_w\ ,\quad f'(\infty) = 1\ ,\quad T(\infty) = T_\infty$$

where

$$' = \frac{d}{ds}\ ,\quad T = T(s)\ ,\quad \Psi = \surd(2\mu_\infty u_\infty x/\rho_\infty) f(s)\ ,\quad C = \rho\mu/\rho_\infty\mu_\infty$$

and the similarity variable s is defined by

$$s = \surd(\rho_\infty u_\infty/(2x\mu_\infty)) \int_0^Y \frac{\rho}{\rho_\infty}\, dy$$

Following FITT et al.[6.1], the Nusselt Number for a Prandtl Number of unity can be written as

$$Nu = C_w \sqrt{(Re/2)}\, f''(0) \tag{6.14}$$

Two approximations to the variation of viscosity with temperature are now considered :

(a) If $\mu \propto T$, the value of C_w is unity. The momentum equation then reduces to the Blasius Equation, uncoupled to the energy equation, so that $f''(0)$ and hence the Nusselt Number cannot be affected by the wall-to-gas temperature ratio.

(b) If $\mu \propto T^m$, then both C_w and hence $f''(0)$ will depend on m. An expression for C from the energy equation can be inserted into the momentum equation ; solving for $f''(0)$, with a Prandtl Number of unity, reveals that

$$Nu/Nu_{cp} = (T_w/T_{t\infty})^{0\cdot 2411(m - 1)} \tag{6.15}$$

A reasonable estimate of m for air is 0.7, so that

$$Nu/Nu_{cp} = (T_w/T_{t\infty})^{-0\cdot 07} \tag{6.16}$$

6.4 Experimental Investigation.

Results were obtained on a flat plate turbulent boundary layer, using an ILPT, at the following conditions :

$Re/m = 2.7 \times 10^7/m$

$M_\infty = 0.55$

$T_{t\infty} = 280$ K, 365 K and 500 K

$300\ K < T_w < 365\ K$, approximately.

This provided an overall temperature ratio variation $0.60 < T_w/T_{t\infty} < 1.30$. The boundary layer was tripped at $Re = 5.4 \times 10^5$.

The data is plotted in the form suggested by Eqn.(6.10) in Fig.6.1 (a)-(d) for four locations. There was inevitably some deviation from an isothermal wall temperature distribution due to uneven pre-run forced convective heating, and to the difference in the temperature rise at different locations during the run prior to the measurement time. The changes in heat transfer rate due to these temperature distributions were evaluated using a superposition method described by LOFTUS [6.2] after KAYS & CRAWFORD [6.3]. Typical variations due to this effect were of the order of 1% for the wall temperature distributions achieved.

It can clearly be seen that for all four positions, the results lie on a curve rather than a straight line, indicating that there is a discernable effect of the wall-to-gas temperature ratio. This can be represented as a power law, as in Eqn.(6.11); the experimental value of n depends upon the manner in which properties are chosen to vary with temperature. Three sets of relationships were employed , the following two relationships are common to all of them :

$$c_p = 1005 \text{ kJ/kgK}$$

$$\mu = 1.4528 \times 10^{-6}\, T^{3/2}/(T + 110.33), \text{ from Sutherland.}$$

Case 1. $Pr = 0.6834$

This gave an average value of the exponent n of -0.36.

Case 2. $Pr = 0.72(1 - 2.92 \times 10^{-4}(T-250))$; this variation is obtained from a linefit from data in [6.4]. The resulting values of n varied between -0.21 and -0.28. There was no systematic variation of the exponent with distance.

Case 3. $k = 0.0047 + 7 \times 10^{5}T$; this expression is obtained from a linefit through data over the appropriate temperature range from [6.3]. This is the relationship used in reducing the film-cooled data, and is used in Fig.6.1. The resulting values of n are as in Case 2.

The conclusion of the experimental investigation is that the following turbulent boundary layer relation should be used for air in the range $0.6 < T_w/T_{t\infty} < 1.3$:

$$Nu/Nu_{cp} = (T_w/T_{t\infty})^{-0.25} \qquad (6.17)$$

6.5 Numerical Investigation.

A numerical solution to the turbulent, compressible boundary layer on a flat plate was carried out by ROBERTSON [6.5] so that comparisons could be made with the experimental data. The code is based on the programmes of CEBICI & SMITH [6.6] and BLOTTNER [6.7]. The turbulence model was based on a mixing length theory and employed the concept of a turbulent Prandtl Number to relate the eddy viscosity to the eddy conductivity. Different types of turbulent Prandtl Number models were found to have little effect. Provision was made to alter the form in which transport properties vary with temperature.

If c_p and Pr are constant, and the variation of viscosity and therefore conductivity with temperature is represented as a power law, then the exponent m can be related to the exponent n governing the wall-to-gas temperature ratio effect on the Nusselt Number. This is shown in Fig.6.2 for a laminar and turbulent boundary layer and is compared with the laminar analytical solution from Section 6.3, Eqn.(6.15). It can be seen that the dependence on the wall-to-gas temperature ratio is more pronounced for a turbulent boundary layer.

If the dependence of properties on temperature is that given in Case 2 of Section 6.4, the numerical calculations produce an exponent n varying from −0.13 to −0.18 for the same Mach Number, freestream Reynolds Number and positions as those in the experimental investigation. These results are included in Fig. 6.1 ; they compare very well with the experimental data, although the numerical results exhibit slightly less curvature, and n is found to increase with distance.

6.6 Comparisons with the Literature.

There is a lack of experimental data in the literature, but reported analytical work for air tends to suggest a decrease in Nusselt Number with increasing wall-to-gas temperature ratio. KAYS & CRAWFORD [6.3], for example, give a value of n of −0.4 for $T_w/T_{t\infty} > 1$. ECKERT [6.8] proposes the use of a reference temperature at which gas properties can be evaluated ; this corresponds to an exponent n = −0.19. BROWN's computations of flat plate heat transfer [6.9] also show a decrease of Nusselt Number with wall-to-gas temperature ratio, as do the turbulent heat transfer charts presented by NEAL & BERTRAM [6.10]. Previous work at Oxford by LOFTUS & JONES [6.11] suggested that the effect was small. BOSE [6.12] solves the turbulent boundary layer equations numerically for $T_w/T_{t\infty}$ = 0.1, 0.5 and 0.9 and lists different correlations of Stanton Number with Reynolds Number for each temperature ratio considered. These results, which are included on Fig. 6.1, again imply a negative value of the exponent n.

HERWIG [6.13] analyses laminar, fully developed pipe flow using asymptotic theory, expanding physical properties as Taylor series. The resulting equation for the Nusselt Number is

$$Nu/Nu_{cp} = (\rho_w/\rho_b)^{0\cdot 340 - 0\cdot 128/Pr}(\mu_w/\mu_b)^{-0\cdot 107}(k_w/k_b)^{0\cdot 245}(c_{pw}/c_{pb})^{0\cdot 255} \quad (6.18)$$

where subscipt b refers to bulk conditions. Thus, as with FITT et al [6.1], the influence of the physical properties can be identified separately. It is left to the user to make appropriate approximations as to how each property varies with temperature , for a given fluid and temperature range. For example, for a Prandtl Number of unity, constant specific heat capacity and a power law variation of viscosity $\mu \propto T^m$,

$$Nu/Nu_{cp} = (T_w/T_{t\infty})^{-0\cdot 212 + 0\cdot 138\, m} \quad (6.19)$$

This is included in Fig.6.2 and can be compared with Eqn.(6.15). The trends are similar, with the difference in slopes probably resulting from the different velocity profiles in the flow.

VILEMAS & SIMONIS [6.14] carry out an experimental investigation into heat transfer from an annular surface to air over the range $1.0 < T_w/T_\infty < 2.8$. For a smooth surface, the value of n was found to be -0.32, and independent of Reynolds Number.

6.7 Application to the Film-Cooled Environment.

The question remains as to how to incorporate this effect in the situation where property variations through the injection layer may depend on the wall, freestream and injection temperatures.

One approach would be to assume that the corresponding temperature ratio in this case is the wall-to-adiabatic wall temperature ratio. This is plausible since the form of the temperature profile close to the surface relates to T_{aw} in the same way that it does to T_{∞} in the unblown, incompressible case, as shown in Fig.6.3. This is where the variation of properties might be expected to be most important.

The assumption might then be made that the power law governing this effect would be the same in both cases. Thus, Eqn.(2.12) could be modified as

$$\frac{Nu}{Nu_{o,cp}} \left(T_w/T_{aw}\right)^{0 \cdot 25} = A + B\,\theta \qquad (6.20)$$

Another approach might be to assume that the effect of property variations can be accounted for simply by normalising with respect to the unblown Nusselt Number at the correct wall-to-gas temperature ratio, giving

$$\frac{Nu}{Nu_{o,cp}} \left(T_w/T_{t\infty}\right)^{0 \cdot 25} = A + B\,\theta \qquad (6.21)$$

It can be seen that far downstream from injection, where the adiabatic wall approaches the mainstream total temperature, these two corrections have the same effect. The manner in which this effect influences the heat transfer data is shown in Chapter 8, where it is concluded that a correction of the form of Eqn.(6.21) is most successful. Unless otherwise stated, this correction has been applied to all the heat transfer data presented. It should be noted that whilst both proposed corrections would alter the magnitudes of A and B, the parameter -B/A would be unaffected.

CHAPTER 7.

Aerodynamic Results.

7.1 Introduction.

This chapter is concerned with the manner in which the secondary flow emerges into the mainstream. If a designer's film-cooling data-base is in terms of flow characteristics such as the blowing rate or momentum flux ratio, it is vital that this information can be related to the total pressure in the coolant manifold. However, the flowfield for discrete, non-tangential injection is highly complicated. This is mainly because the velocities normal to the cooled surface make boundary layer assumptions inappropriate. Viscous effects also have to be considered.

In the following, the main features of fluid injection into a crossflow from slot and hole geometries are described. Dimensional analysis and potential flow theory are then used to make certain predictions about the flow configurations. Finally, experimental results from the Isentropic Light Piston Tunnel and a low-speed tunnel are presented and compared where possible with theoretical predictions.

7.2 Qualitative Description of the Injection Process.

7.2.1 Slot Geometry.

This flow is shown schematically in Fig.7.1 for a flow where the total mainstream pressure is greater than the total injection pressure. A shear layer is present due to the difference between injection and mainstream velocities at the dividing streamline. As noted by PITT et al. [7.1], this streamline will tend to separate from the leading edge parallel to the x-axis for $p_{ti} < p_{t\infty}$. This can be thought of as a "lid" across the front of the slot opening, and results in the formation of a sink-like flow at the rear vertex, where most of the injection mass flow emerges. The shear layer will degenerate into a turbulent vortex sheet where mixing of the two flows will occur. The upstream boundary layer may generate viscous interaction ahead of the slot, and there may be a separated region downstream of injection. The form of the static pressure distribution is as follows : upstream of the slot, the pressure rises to a value close to the slot pressure, as the mainstream recovers against the emerging flow. The pressure is then almost uniform across the slot, until the rear vertex where there is a large suction peak corresponding to the sink. LEE & CLARK [7.2] identify an inner mixing layer between the injected flow and the separated region. The outer mixing layer, however, rolls up to form large, coherent, transverse vortex tubes. Further downstream, these break down into small scale turbulence and the velocity profiles begin to exhibit similarity.

7.2.2 Hole geometry.

This is shown schematically in Fig.7.2 for low and high injection rates. Once again, there is an increase of pressure upstream of each hole, with a low pressure region downstream. This tends to distort the injection velocity profile, so that a larger proportion of the injection mass flow emerges from the rear of the hole. These injection profiles were measured by BERGELES et al. [7.3]. FOSS [7.4] has undertaken an extremely detailed investigation of the non-uniformity of hole exit conditions, and refers to a "partial cover" over the front of the hole at blowing rates of less than unity. ANDREOPOULOS [7.5] also concludes that for small injection rates, large distortions of the jet approach flow occur close to the exit plane.

The force resulting from the pressure distribution deflects the injected jets in a streamwise direction. A shear layer develops around the periphery of each jet, and the jet cross-section is deformed to a characteristic kidney shape. ABRAMOVICH [7.6] attributes this to greater deflection of the particles at the edge of the jets, which possess less momentum than those at the jet centres.

A pair of large, contra-rotating vortices is known to exist within this structure. This vortex structure was generated numerically, for low blowing rates, using a three-dimensional finite difference procedure, by BERGELES et al.[7.7] (for laminar jets) and [7.8] (for turbulent jets). The vortices are regarded as being a manifestation of vorticity introduced into the flow by the fluid injection. They were also observed from measurements of mean velocity distributions by KADOTANI & GOLDSTEIN [7.9], and from streakline flow visualisation carried out by COLLADAY & RUSSELL [7.10]. The literature is by no means agreed on the origins and early development of these vortices. Following ANDREOPOULOS & RODI [7.11], there appear to be three broad mechanisms for the generation of vorticity (shown in Fig.7.3) :

(i) Vorticity issuing from the pipe. Vorticity is generated in the injection pipe flow due to boundary layer growth, Fig.7.3(a). Initially, the vorticity will be in the cross-sectional plane of the pipe and normal to the radial direction. MOUSSA et al [7.12] state ESKINAZI's result for a thermal plume in cross-flow [7.13] : the bending of the jet introduces an asymmetric component of acceleration equal to ($\underline{U}_{-\infty}$ x $\underline{\zeta}$). The convective acceleration vector is

$$\underline{a} = (\underline{u}.\nabla)u = 1/2\ \nabla\ u^2 - \underline{u} \times \underline{\zeta} \qquad (7.1)$$

where $\underline{u}$ is a general velocity vector. In this case, taking co-ordinates relative to an injection vortex ring,

$$\underline{u} = \underline{U}_{-\infty} - \underline{u}_{-i}. \qquad (7.2)$$

The interaction of the freestream velocity with the vorticity in the z-direction (see Fig.7.2) will provide an asymmetric component of acceleration of the vortex ring. This will have its maximum negative value on the windward side of the ring and positive values on the leeward side. As a result, the vortex ring will decelerate on the windward side and accelerate on the leeward side relative to the centre (see Fig.7.2). This re-orientation of vorticity concentrates the vortex rings into two bound vortex tubes in the streamwise direction. They can be thought of as being joined at infinity, and are similar, though in the opposite direction, to aeroplane wing-tip vortices. ANDREOPOULOS & RODI [7.11] state that this is the dominant mechanism at velocity ratios less than 0.6, whereafter the following mechanism becomes more important.

(ii) Vorticity generated at the interface of the two streams. For example, Fig.7.3(b) shows that streamwise vorticity will be generated at the sides of the jet because of the shear forces resulting from the normal velocity gradients in the z-direction. Vorticity will also be generated in the y-direction, Fig.7.3(c), because of the shear forces set up by the flow around each cross-section of the injection flow. This mechanism was studied in 1942 by LU [7.14] who developed a potential flow solution to the cross-flow around a deforming circular jet. It is argued that since the pressure distribution acts around a section perpendicular to the jet axis, the magnitude of the jet velocity does not affect the solution. The problem was reduced to two dimensions by examining how the form of the cross-section normal to the deflected jet axis deforms with time. LU also approached the problem by approximating the vortex sheet between the two streams by sixteen point vortices of differing strengths in the y-direction, varying from zero at the upstream and downstream stagnation points to maximum values at the positions of maximum cross-flow velocity. The deformation of the vortex sheet due to the velocities induced by the vortices and to the influence of the mainstream is similar to that found by experiment ; the evolution of the jet cross-section into the familiar kidney shape is clear.

HIGDON & POZRIKIDIS [7.15] study the self-induced motion of a circular vortex sheet with a sinusoidal circulation distribution, which would be similar to the distribution around a jet in cross-flow caused by interaction between the jet and the mainstream. The vortex sheet is represented by a collection of circular arcs, and the circulation by trigonometric polynomials. Because of this, more marker points can be added during the calculation in order to resolve detail. Again, the kidney-shaped cross-section is formed, and the vorticity is found to concentrate in two positions corresponding to the leeside vortex tubes mentioned in (i). Eventually, singularities appear in the circulation distribution at these two locations.

Thus, the vorticity generated by this mechanism bends over with the jet and rolls up into two concentrations of opposite signs aft of the jet, contributing to the streamwise bound vortex. At large injection rates, where the jet has penetrated well into the mainstream, some of this vorticity is shed in the same manner as a Karman vortex street behind a cylinder in crossflow. This was observed by KEFFER & BAINES [7.16], KAMOTANI & GREBER [7.17], RAMSEY & GOLDSTEIN [7.18] and by MOUSSA et al [7.12].

(iii) Vorticity generated by the approach mainstream boundary layer, Fig.7.3(d). This will produce vorticity in the z-direction. The vortex lines will then be bent around the emerging jet to form a horseshoe vortex in the streamwise direction. This structure, observed from surface flow visualisation patterns by BERGELES et al [7.3] is of opposite sign to the kidney-shaped vortices, and is generally much weaker.

The structure of the flowfield undergoes considerable change at an increased value of injection rate. For a unity injection-to-freestream density ratio, FOSS [7.4] reports that this occurs at a velocity ratio between 0.4 and 0.6. This corresponds closely with the velocity ratios at which RAMSEY & GOLDSTEIN [7.18] notice changes in trends in the temperature profiles downstream of injection.

FOSS is able to characterise this transition using both injected dyes and kerosine and lampblack surface streakline flow visualisation. Whilst at low blowing rates, the hole trailing edge streamline separates from the surface (for 90°injection), the injected fluid is quickly deflected and remains close to the surface. At high injection rates, the jet acts more like a solid body and is able to penetrate further into the mainstream.

A topological interpretation of the surface shear stress lines enables further distinguishing features to be found in the two flow regimes. Points of zero surface shear stress can be classified into saddle points, at which two oppositely directed, orthoganal surface stress lines intersect, and nodal points, where an infinite number of surface stress lines intersect. HUNT et al [7.19] show that for a surface mounted obstacle, represented by the emerging jet, the number of saddles exceeds the number of nodes by one. FOSS shows that for small injection rates, this saddle is upstream of the hole. As the injection rate is increased, there is a discontinuous change in the number and distribution of these singular points, so that at large injection rates, the net saddle point is positioned downstream. Examples of these flow patterns are shown in Fig.7.4.

The vortex patterns discussed above dominate the flow pattern for this geometry. They are formed very close to the hole exit [7.12],[7.20] and are known to persist far downstream (FEARN & WESTON [7.20] note that vortices are easily detectable 45 hole diameters downstream). RAMETTE & LOUIS [7.21] state that the decay of vortex strength is found to be negligible over the film-cooled surface. They carry out an analysis which considers mixing between the injection and mainstream due to turbulent diffusion and vortex entrainment. The vortices are responsible for a substantial amount of the entrainment of mainstream fluid, and this mixing must be expected to have a deleterious effect on film-cooling efficiency.

7.3 Dimensional Analysis.

This can be used to predict the parameters governing the injection of a jet into a crossflow. In particular, it is of interest to relate the injection mass flow rate to the pressure difference causing the flow. For incompressible viscous fluids where injection and mainstream densities are not equal, the independent variables can be listed as

$$(p_{t\infty} - p_{\infty}) \;,\; (p_{ti} - p_{\infty}) \;,\; u_{\infty} \;,\; u_i \;,\; \rho_i \;,\; \mu \;,\; d \tag{7.3}$$

where pressures are referenced to the freestream static since they only occur as differences in the governing equations. (It is assumed that the freestream density can be found by Bernoulli's Equation). These variables can be arranged into the non-dimensional groups

$$\frac{(p_{ti} - p_{\infty})}{(p_{t\infty} - p_{\infty})} \;,\; \frac{u_i}{u_{\infty}} \;,\; \frac{\rho_i u_i^{2}}{(p_{t\infty} - p_{\infty})} \;,\; \frac{(p_{t\infty} - p_{\infty})\, d}{u_{\infty}\, \mu} \tag{7.4}$$

so that at constant freestream Reynolds Number, the pressure difference ratio can be expressed as a function of the velocity ratio and the density ratio. This could equally be written in terms of the discharge coefficient ; the independent variables are then

$$(p_{t\infty} - p_{\infty}) \;,\; (p_{ti} - p_{\infty}) \;,\; u_i \;,\; \rho_i \;,\; \rho_{\infty} \;,\; \mu \;,\; d \tag{7.5}$$

giving non-dimensional parameters

$$\frac{(p_{ti}-p_\infty)}{(p_{t\infty}-p_\infty)}\ ,\ \frac{\rho_i}{\rho_\infty}\ ,\ \frac{\rho_i u_i^2}{(p_{ti}-p_\infty)}\ ,\ \frac{\rho_\infty (p_{t\infty}-p_\infty)\, d^2}{\mu^2} \qquad (7.6)$$

At constant freestream Reynolds Number, the pressure difference ratio would then be a function of the density ratio and the discharge coefficient (the third parameter in (7.6)). In compressible flow, there would also be a dependence on the Mach Number and the ratio of specific heats. However, these were constant in the experiments performed in this investigation.

The groups in (7.4) can be rearranged to provide the relation, at constant freestream Reynolds Number,

$$\frac{(p_{ti}-p_\infty)}{(p_{t\infty}-p_\infty)} = F\left[\frac{\rho_i u_i^2}{\rho_\infty u_\infty^2}\ ,\ \frac{\rho_i}{\rho_\infty}\right] \qquad (7.7)$$

Empirical evidence is now invoked to provide the form of this functional relationship. Eqn.(4.30), derived from BERGELES et al [7.3],leads to the expression (4.31) in which the pressure difference ratio is solely a function of the momentum flux ratio for weak blowing. Similarly for strong blowing, Eqn.(4.26) suggests that the effect of density ratio and velocity ratio variation can be fully described using the ratio of dynamic heads. If this is so then it follows that the discharge coefficient can be expressed as a function of the pressure difference ratio only. ABRAMOVICH [7.6] refers to an empirical equation, proposed by Shandorov, which correlates the angle of deflection of the jet axis with the ratio of freestream-to-injection dynamic heads over a range of velocity and temperature ratios. This scaling is also mentioned by FEARN & WESTON [7.20]. HORTON [7.22] obtains results for hole geometries at injection-to-freestream temperature ratios of 0.67 and

0.77, and concludes that there is no effect of this temperature ratio variation on the discharge coefficient.

7.4 Experimental Results.

Figs.7.5(a) - 7.8(a) show the momentum flux ratio plotted against the pressure difference ratio for all three geometries tested. It is concluded that there is no discernable effect of the density ratio over this range. Similarly, Figs.7.5(b) - 7.8(b) show the discharge coefficient plotted against the total injection-to-mainstream static pressure ratio (which is similar to the pressure difference ratio for a constant mainstream Mach Number) for the three geometries. Once again, within experimental scatter, there is no dependence on the density ratio.

Lines representing data from discharge into still air are included on these figures so that the effect of cross-flow can be studied. For all three geometries, the effect of the mainstream recovering pressure against the emerging jets and locally raising the exit pressure can be seen for values of p_{ti}/ p_{∞} less than 1.25, above which the cross-flow does not appear to affect the discharge coefficient significantly. For a mainstream Mach Number of 0.55, this value corresponds very closely to an injection-to-mainstream total pressure ratio of unity, so that at larger total injection pressures, the upstream separation streamline would initially be perpendicular rather than parallel to the surface. Thus the "lid" effect would no longer impede the emerging jet.

ANDREWS & MKPADI [7.23] conclude that there is no influence of cross-flow on discharge coefficients for hole Reynolds Numbers above

5000, whilst DEWEY [7.24] states that the criterion is an injection-to-freestream velocity ratio of above 0.70. Approximate corresponding values from the present study are a hole Reynolds Number of 8000 and a velocity ratio of 0.6, so that these conclusions are not contradictory.

Moreover, the results are in agreement with HAY et al [7.25], who report that for a 30^{o} single row of holes, the final (large blowing) value of the discharge coefficient is about 0.72, and is only very weakly affected by mainstream cross-flow. Comparison with HAY et al's results in Fig.7.5(b) shows good agreement on the level of the discharge coefficient. The present results are also within the scatter of SMITH's results [7.26].

A comparison between the geometries reveals that the slot discharge coefficients are considerably smaller than the hole results, particularly at low injection-to-freestream pressure ratios and in the presence of cross-flow. This is partly due to the greater recovery of the freestream since the emerging slot flow presents a greater or more "solid" obstacle to the flow. Results from [7.27] also reveal slot discharge coefficients considerably smaller than those from a double row of holes.

7.5 An Analytical Method for Predicting Injection Flowfields.

It is of great importance to be able to predict the precise manner in which injection flows emerge into a cross-flow. FITT et al [7.1] have made substantial progress in quantifying the interaction between slot injection flow and a mainstream. A two-dimensional, irrotational, inviscid model, sketched in Fig.7.9, is proposed, with no separated regions. The aim is to establish how the influence of the mainstream affects the mass flow from the slot. The flow regime considered is where the total injection pressure is only slightly greater than the freestream static pressure, so that perturbations to the freestream can be examined. However, this pressure difference is large enough to ensure that the injection layer is thick in comparison with a typical viscous boundary layer.

Dimensionless asymptotic expansions are then formed in terms of the velocity potential in the freestream, slot and film regions. Matching pressures across these regions results in the formation of a non-linear integral equation, relating the velocity potential to the mass flow rate and the form of the dividing streamline.

The orders of magnitude arguments will be given here for the case considered by FITT [7.28] where the injection density is different from the freestream density. The injection total pressure can be given by

$$p_{ti} = p_{\infty} + 1/2\ \rho_{\infty} u_{\infty}^{2} \epsilon^{2} \tag{7.8}$$

where ϵ is a small parameter. The pressure in the injected film would then be

$$p_{f} = p_{\infty} + O(\rho_{\infty} u_{\infty}^{2} \epsilon^{2}) \tag{7.9}$$

so that

$$\rho_{i} u_{f}^{2} = O(\rho_{\infty} u_{\infty}^{2} \epsilon^{2}) \tag{7.10}$$

Thus the film momentum flux ratio is of order ϵ^{2}. From thin aerofoil theory, where an aerofoil of thickness-to-chord ratio δ produces freestream pressure variations of $O(\delta \rho_{\infty} u_{\infty}^{2})$, it follows that the injection layer height can be given by

$$\frac{b}{s} = O(\epsilon^2). \tag{7.11}$$

Continuity gives $$\rho_i u_i s = \rho_i u_f b \tag{7.12}$$

so that $$\frac{u_i}{u_f} = O(\epsilon^2) \tag{7.13}$$

Using Eqn.(7.10), the height of the injection layer can now be related to the jet momentum flux by

$$\frac{b}{s} = O\left\{\left[\frac{\rho_i u_i^2}{\rho_\infty u_\infty^2}\right]^{1/3}\right\} \tag{7.14}$$

This important result implies that the height of the injection layer scales with the momentum flux ratio for unseparated slot flow. This is different ,for example, from the energy balance model assumption that the initial height of the injection layer can be given by a boundary layer equation such as Eqn.(4.10).

Similarly, the momentum flux ratio and the pressure difference ratio are related by

$$\frac{\rho_i u_i^2}{\rho_\infty u_\infty^2} = O\left\{\left[\frac{P_{ti} - P_\infty}{P_{t\infty} - P_\infty}\right]^3\right\} \tag{7.15}$$

This implies that the momentum flux ratio and hence the discharge coefficient are only functions of the pressure difference ratio. This is in agreement with the present experimental results, Fig. 7.6.

A solution of the integral equation for a 90° slot gives

$$\frac{\rho_i u_i^2}{\rho_\infty u_\infty^2} = 1.25 \left[\frac{P_{ti} - P_\infty}{P_{t\infty} - P_\infty}\right]^3 \tag{7.16}$$

For angled injection, this would be expected to scale with the sine of the angle so that for 30° injection, the constant would be 5.02. This prediction is plotted in Fig.7.8 , along with predictions resulting from the assumptions firstly that the slot exit pressure is the freestream static pressure, and secondly that the slot exit pressure is the average of the freestream static and total pressures. Experimental points from a 30° slot in an incompressible flow, open circuit wind tunnel, and from the 30° slot results in the ILPT, are plotted for comparison.

The difference between the two sets of experimental points is attributed largely to the difference in geometries at entrance to the injection pipe; this is via a smooth bellmouth in the incompressible experiments, whereas in the ILPT, the entrance from the injection plenum is sharp-edged. This would undoubtedly produce separation and a vena contracta, lowering the mass flow for a given pressure difference ratio. Agreement, however, between the incompressible results and the theory is good over an important range of injection rates. At higher injection rates, as separation effects become noticeable, the theory overestimates the mass flow. At very low injection rates, the theory under-predicts the mass flow rate; this is because the boundary layer thickness is significant compared to the injection layer thickness, so that viscous forces in the mainstream flow become important.

The conclusions which can be drawn from this theory are very illuminating. Firstly, it confirms that the injection velocity profile is distorted by the mainstream which acts as a lid over the slot, with the injection mass flow emerging close to the rear vertex. Secondly, it provides a good prediction to relate the injection rate to the pressure difference ratio. This can therefore provide the starting point for establishing how the flowfield and ultimately the heat transfer will scale with injection.

CHAPTER 8.

Film-Cooled Results.

8.1 Presentation of Results.

The superposition model discussed in Chapter 2 predicts a linear variation of Nusselt Number at a given position with theta for a given injection rate as shown in Fig.8.1. The parameters A and B are the intercept and slope respectively, non-dimensionalised by the unblown level of Nusselt Number at that position. This relationship is only predicted if the injection and freestream flows are constant, and the variation in theta is effected by changing the isothermal wall temperature. The linearity of heat transfer coefficient with theta has been experimentally verified in the constant property situation for a single row of holes and slot injection by METZGER & FLETCHER [8.1]. CHOE et al.[8.2] (for full coverage film cooling) and VILLE et al.[8.3] (for a double row of holes) also show this linearity, but the latter vary both the injection and the wall temperature, so that the injection-to-freestream temperature ratio varies between 0.72 and 0.90. However, the results of LOFTUS [8.4] (for a single row of holes), where the wall temperature is varied at at a constant freestream temperature for two injection temperatures so that $0.80 < T_{ti} / T_{t\infty} < 1.00$, clearly show that

(i) the heat transfer coefficient varies linearly with theta for a given gas temperature, injection temperature, and blowing rate, and

(ii) different lines, characterised by different values of A and B, result from changing the injection-to-freestream temperature ratio.

Present results are analysed by examining the variation of the following heat transfer parameters with distance and strength of injection :

(a) A and B

(b) Linear combinations of A and B ; for example, (A + B), with $\theta = 1$, which corresponds to q/q_o if the freestream conductivity is constant.

(c) $-B/A$, the adiabatic wall effectiveness occurring when the wall temperature is isothermal at the local adiabatic wall temperature. This should be less sensitive to the effects of property variations since the levels of Nusselt Number characterised by A and B should be similarly influenced when corrected for property variations in the manner indicated in Chapter 6.

Unless otherwise indicated, all results are normalised with respect to the unblown Nusselt Number at the corresponding wall to freestream temperature ratio.

8.2 SINGLE ROW RESULTS.

INJECTION GEOMETRY : single row of 30° holes,

spacing-to-diameter ratio = 2.5

length-to-diameter ratio = 5.0

Results were obtained for the following four sets of injection and mainstream total temperatures :

T_{ti} = 270 K	$T_{t\infty}$ = 540 K	$T_{ti}/T_{t\infty}$ = 0.50	SYMBOL : ⊡
T_{ti} = 300 K	$T_{t\infty}$ = 500 K	$T_{ti}/T_{t\infty}$ = 0.60	SYMBOL : ×
T_{ti} = 300 K	$T_{t\infty}$ = 365 K	$T_{ti}/T_{t\infty}$ = 0.82	SYMBOL : ⦶
T_{ti} = 345 K	$T_{t\infty}$ = 280 K	$T_{ti}/T_{t\infty}$ = 1.23	SYMBOL : +

TABLE 8.1

This key should be used for Figs.8.2 - 8.25, unless otherwise stated.

8.2.1 General Description of Results.

Figs.8.2(a)-(d) show typical data sets at specified conditions where theta is varied by varying T_w. For all positions, injection-to-freestream temperature ratios and injection rates considered, the variation of Nusselt Number per metre with theta appeared to be linear, justifying the superposition model. Values of A and B are obtained from a least square line fit through the data. However, Fig.8.3 demonstrates that for a given position and blowing rate, a different line is obtained if the fluid mechanics are altered by changing the injection or mainstream temperature. This result is in agreement with LOFTUS [8.4] but is more convincing as similar theta ranges are covered for each value of $T_{ti}/T_{t\infty}$. Thus, for this geometry, it is crucial to be able to predict how A and B vary with not only blowing rate, but also with injection-to freestream temperature ratio.

The general effects of injection can be seen by examining the variation of (A+B), or Nu/Nu_o at Theta = 1, with x/d for different blowing rates, Figs.8.4-8.7. Fig.8.4 shows this variation for $T_{ti}/T_{t\infty} = 1.23$. In order to facilitate comparison with other injection-to-freestream temperature ratios, a decrease in the magnitude of the Nusselt Number at a given position will be referred to as "cooling effect", despite the fact that this temperature ratio represents film heating. For a blowing rate G = 0.13, there is good cooling close to the holes, decreasing gradually with increasing x/d. Harder blowing increases the cooling at all positions, with a maximum reduction in Nusselt Number per metre of 42% at x/d = 2, G = 0.26.

By G = 0.35, the film-cooled level of heat transfer has begun to increase close to the holes. This could be attributed to the phenomenon of "lift off", discussed in Chapter 7, when the injected jets penetrate into the freestream, separating from the wall and permitting the freestream to flow around and under the jets. This situation can be inferred from flowfield temperature contours by RAMSEY & GOLDSTEIN [8.5] and KRUSE [8.6]. Streakline flow visualisation by COLLADAY & RUSSELL [8.7] and COLLADAY et al. [8.8] using helium bubbles show that the injection jets separate from the surface for 30^{o} hole injection at "velocity ratios of 0.5 and greater." Schlieren photographs by LOFTUS [8.4] reinforce this interpretation.

Another possible explanation entails assuming that increasing the injection rate has two main effects : it causes a thickening of the boundary layer, reducing the heat transfer, and increases the turbulent mixing, which enhances the heat transfer. It would then be argued that at the position and blowing rate under discussion, the latter effect begins to exert a stronger influence.

Examination of other experimental results, for example those of GOLDSTEIN, ECKERT & BURGGRAF [8.9], suggests that the dramatic decrease in cooling performance close to the holes is best explained by lift off. Thus, when the holes are shaped in order to prevent penetration, the decrease in centre-line effectiveness is only very slight at high blowing rates. This would presumably be due to increased turbulent mixing. By G = 0.59, the level of heat transfer is higher than the unblown value, and rises further for higher blowing rates, where more downstream positions become affected.

Far downstream,the jets will have merged and the flow will more closely resemble a turbulent boundary layer. However, differences are still noticeable : at low blowing rates, the level of Nusselt Number is slightly greater than the unblown level, presumably due to the persistence of the vortex structure and the associated mixing. It has been reported, for example by FEARN & WESTON [8.10], that coherent vortices are still detectable at these large values of x/d. As the injection rate increases, however, the mass of coolant gradually changes the bulk temperature in the layer, improving the cooling.

Fig.8.5, at $T_{ti}/ T_{t\infty} = 0.82$, display similar trends in that for low blowing rates, the best cooling is at small x/d's, although at an equivalent blowing rate, cooling is not as good as for $T_{ti}/ T_{t\infty} = 1.23$. Blowing at $G = 0.12$ has only a small effect (from -2% to +13%) on heat transfer down the plate. By $G = 0.25$, there is a 32% reduction at $x/d = 2$, the effect decreasing monotonically with distance downstream to $x/d = 98$ where it is enhanced by 13%. The blowing rate $G = 0.40$ gives best close-to-hole cooling, a 43% reduction at $x/d = 2$, with little effect at $x/d = 98$. The decline in cooling performance associated with lift off has occurred by $G = 0.59$, but cooling is still greatest at small x/d's. At $G = 0.76$, however, the effect of jet penetration is apparent further downstream, and the decrease in heat transfer has become about 10% over the whole plate. At the highest blowing rate, the level of heat transfer is significantly higher at low x/d's and is greater than the unblown level. Results by LOFTUS [8.4] at this temperature ratio are very similar in character and in level.

The same pattern is again evident in Fig.8.6, at $T_{ti}/ T_{t\infty} = 0.60$. The heat transfer is within 9% of the unblown value at the lowest blowing rate. An increase in cooling takes place at low x/d's with increasing blowing rate, until $G = 0.59$, after which increasing the blowing rate causes a decrease in close-to-hole cooling. In general, the cooling behaviour is equivalent to that at a slightly lower blowing rate for $T_{ti}/ T_{t\infty} = 0.80$.

The results from $T_{ti}/ T_{t\infty} = 0.50$, Fig.8.7, exhibit the same characteristics. At $G = 0.25$, the value of q/q_o down the plate varies between 0.91 and 1.09. Cooling increases close to the hole with increasing blowing rate up to $G = 0.59$. For higher blowing rates, this cooling then decreases. The level of film-cooled heat transfer drops gradually at large x/d's as the blowing increases, due to the greater mass flux of coolant flow.

Fig.8.8 compares a sample of the present data with that in the literature for similar geometries and conditions. Effectiveness data is converted to q/q_o data using Eqn.(2.20) and assuming $h_{aw}= h_o$. All the results shown are qualitatively similar. Absolute differences can be explained by the different injection rates, geometries and measuring techniques.

More insight into the effect of the film cooling process can be gained from employing the superposition model to study the variation of the two components of the ratio of Nusselt Numbers, A and B. In this way, the effect of the mixing of the two flows, and the effect of the coolant being at a different temperature from the freestream can be isolated.

Figs.8.9–8.11(b) show the values of B along the flat plate at different blowing rates, for three temperature ratios. It can be seen that the variations in this parameter are sizeable and in fact dominate the Nusselt Number variation. For example, Fig.8.9(b) shows that at G = 0.13, the fact that the coolant is at a different temperature from the mainstream has a marked effect on the heat transfer coefficient close to the holes, diminishing as x/d increases. This is because turbulent mixing causes the jets to become diluted by the mainstream, which weakens the effect of a change in injection temperature at these positions.

As the blowing is increased, the coolant temperature effect increase for all x/d's until G = 0.35, when the effect begins to decrease close to the holes whilst still gradually increasing further downstream. An interpretation of this is that if the injection jets lift off,their effectiveness as a relatively cool insulating layer would be reduced. Further downstream, where the jets are likely to have reattached, the increased coolant mass flow produces a significant coolant–temperature effect, since dilution by the mainstream will be relatively less at a given x/d position. At larger blowing rates, these trends become more pronounced until at G = 0.77, the effect of the difference in coolant temperature is smallest close to the holes, and is very noticeable at all x/d's. Figs. 8.10–8.11(b) can be similarly explained, although the values of B may be less accurate since for the same wall temperature range, the variation in theta is less at the higher freestream temperatures, decreasing confidence in the line fit of the Nusselt Number versus theta data.

Figs.8.9-11(a) show the corresponding variations in A, which quantifies the mixing effect of the two flows at the same temperature. In the majority of cases, the extrapolation of the linefit through the data provides a value of A which is greater than unity, suggesting that if injection were at the freestream temperature, the interaction of the two flows would increase the level of heat transfer. In general (for example, see Fig.8.9(a)) A tends to be higher at low x/d's, where the velocity gradient between injection and freestream will be largest, promoting greater mixing . Enhancement of the heat transfer coefficient is about 15% at x/d = 2 for G = 0.13, but the level drops to the unblown value by about eight hole diameters.

In addition, the level increases in general with increasing blowing rate, as the interaction becomes more severe. Enhancement of the heat transfer coefficient rises to 57% above its unblown value at x/d = 2 for G = 1.24, and at x/d = 20 is still over 25%. The gradual but noticeable increase in the value of A even at large x/d values may be attributed to the extra mixing generated by the contra-rotating vortices from each hole, which persist well after the jets have merged. Figs.8.9-8.11(a) show that 20% increases in A moderately far downstream are not uncommon. This calls into question the validity of the assumption that $h_o = h_{aw}$, even at large x/d's. Again, there are larger uncertainties in the value of A as the injection-to-freestream temperature ratio decreases, since it is derived from the extrapolation of a fitted line through data covering a smaller theta range.

Several recent experimental works have concentrated on quantifying the mixing effect A (or h_{aw}/ h_o in the adiabatic wall temperature approach) in addition to B (or ,say, η_{aw}) in order to accurately predict heat transfer rates in the presence of injection. Some comparisons between the present data and that reported in the literature for single-row hole configurations are shown in Fig.8.12. There is reasonable agreement with the transient heat transfer data from LIESS [8.11], whilst results from GOLDSTEIN & TAYLOR [8.12] and HAY et al [8.13], obtained using mass transfer techniques, suggest less enhancement for both injection rates considered. It should be noted that the present results are for a slightly lower injection angle and a smaller spacing-to-diameter ratio. According to HAY et al [8.13], increasing the injection angle increases h/h_o close to injection and decreases h/h_o far downstream. KRUSE [8.14] reports that increasing the spacing-to-diameter ratio decreases h/h_o.

The levels of A and B and the manner in which they vary with blowing rate and downstream position are consistent with those from the two injection-to-freestream density ratios investigated by LOFTUS [8.4].

8.2.2 Correlation with Fluid Mechanic Parameters.

It is of great importance to establish the parameters which scale the injection process most effectively, both with distance and with strength of blowing, for a given geometry. Initially, the merits of various fluid mechanic parameters will be examined at fixed downstream positions . At small x/d's, the variation of B and the isothermal adiabatic wall effectiveness -B/A will be considered rather than A which is less sensitive to the injection process.

Figs.8.13(a) & (b) show how these vary at the first measuring position with blowing rate, which is a widely used parameter. Quite clearly, there is a large dependence on the injection-to-freestream temperature ratios. For example, a blowing rate of 0.5 has often in the past been regarded as the most efficient for a single row of holes, and yet Fig.8.13(a) shows that this efficiency can be incorrect by a factor of two over the temperature ratio range considered. This highlights the inadequacies of using a test rig where $T_{ti}/\ T_{t\infty}$ = 1.0 to predict the film-cooling efficiency of a turbine blade operating at the same blowing rate but with $T_{ti}/\ T_{t\infty}$ = 0.60.

Whilst blowing rate does not appear to correlate the low injection results very well, the variation with temperature ratio is most pronounced at larger blowing rates above those which gave maximum cooling performance. As the injection-to-freestream temperature ratio decreases, the blowing rate at which this maximum occurs increases. This may be because the lift off phenomenon depends on the momentum flux of the injection flow relative to the freestream, which is higher for larger values of $T_{ti}/\ T_{t\infty}$ at a given blowing rate. Figs.8.14(a) & (b) show similar trends at the next measured position, x/d = 8.

A method of displaying the effect of changing the injection-to-freestream density ratio without incorporating the uncertainties due to line extrapolations is to examine the data at Θ = 1.3. Results were obtained at this value for all injection-to-freestream temperature ratios ; in addition, this value of theta is a typical engine value. This is done in Fig.8.15. At x/d = 2, Fig.8.15 shows that in the normal film cooling situation $T_{ti} < T_w < T_{t\infty}$, the reduction in Nusselt Number is most at a given blowing rate for high values of $T_{ti}/\ T_{t\infty}$ before "lift off", the reverse being the case for higher blowing rates. Further downstream, the jet penetration has a progressively smaller effect, possibly due to the resulting mixing of the two flows, and any subsequent reattachment.

It is thus concluded that the mass flux ratio is not an effective correlating parameter for heat transfer data downstream from a single row of film cooling holes. This applies equally to weak blowing (i.e. before maximum cooling efficiency) and to strong blowing. This is in agreement with similarly acquired data by LOFTUS [8.4] for the same geometry, and two injection-to-freestream temperature ratios, 0.80 and 1.00. Mass transfer results by FOSTER & LAMPARD [8.15] for the centre-line effectiveness downstream from 90° injection holes, and by PEDERSEN et al.[8.16] for 35° holes, show that the variation in injection-to-freestream density ratio produces qualitatively similar effects to those reported in the present investigation. CAMCI & ARTTS [8.17], investigating leading edge film-cooling on a turbine blade, also note that an increase in the injection-to-freestream temperature ratio at a blowing rate of 0.60 increases the film-cooled heat transfer rate. This can be attributed to an increase in the severity of the jet separation and displays the same trend as the present data.

Figs.8.16(a) & (b) show the present data plotted against momentum flux ratio for x/d = 2. This parameter correlates the data well at low injection rates and brings the peaks in effectiveness closer together for each injection-to-freestream temperature ratio. At injection rates above maximum cooling, the data separates and can be considered to fall off along lines of constant mass flux ratio. This trend is consistent with the data from LOFTUS [8.4], PEDERSEN et al.[8.16] and FOSTER & LAMPARD [8.15].

The results of Chapter 7, along with Eqn.(4.31), indicate that the Weak Injection Parameter will scale the results in the same manner as the momentum flux ratio. This is shown in Fig.8.16(c) for x/d = 2, where the same low injection data is correlated.

Fig.8.17 shows the corresponding correlations for x/d = 8 and x/d = 14, which again are reasonable for low blowing. The conclusion may therefore be drawn that for this geometry, the momentum flux ratio and the Weak Injection Parameter are good parameters with which to scale experimental results at low injection rates, close to the holes. It is noted that at these positions, correlation is improved with the momentum flux ratio even at higher injection rates. Further, its success at scaling the close-to-hole values of peak effectiveness, Fig.8.16(a), indicate that it governs the mechanism of jet lift off.

The Strong Injection Parameter is used to correlate the same data in Figs.8.18 & 8.19. This parameter is derived to be applicable for injection rates where the jet penetration into the freestream is significant. It is very successful, particularly at x/d = 2, at collapsing this data. Fig. 8.18 can be compared with JONES' correlations [8.18] of the data from FOSTER & LAMPARD [8.15] and PEDERSEN et al. [8.16], Fig.8.20. Spanwise-averaged effectiveness data from PEDERSEN et al. also correlates in the same way. In addition, LOFTUS [8.4] reports good collapse of data close to the holes with this parameter.

PEDERSEN et al. also achieve an approximate correlation by plotting spanwise-averaged effectiveness, divided by blowing rate, against momentum flux ratio. This relation is suggested by a heat sink model in which a row of heat sinks are placed above the surface and the boundary layer turbulence is described by a Reynolds Number in which the viscosity is replaced by an average turbulent viscosity. Collapse of the present results in this manner, presented in Fig.8.21, is good.

An inspection of this scaling parameter reveals that it has similar implications to the Strong Injection Parameter. If at a given position,

$$\eta/G = \text{function } (I) \qquad (8.1)$$

then at a given value of the momentum flux ratio, the effectiveness will be proportional to the mass flux ratio, which can now only be varied by varying the density ratio. Eqn.(8.1) may therefore be re-written as

$$\eta = \left[\frac{\rho_i}{\rho_\infty}\right]^{1/2} \text{function } (I) \qquad (8.2)$$

This compares with the Strong Injection Parameter model which suggests that

$$\eta = \text{function } \left\{ \left[\frac{\rho_i u_i^2}{\rho_\infty u_\infty^2} + C\right] \frac{\rho_\infty}{\rho_i} \right\} \qquad (8.3)$$

If this functional dependence is approximated by a power law,

$$\eta = \text{constant} \left[\frac{\rho_i}{\rho_\infty}\right]^n \left[\frac{\rho_i u_i^2}{\rho_\infty u_\infty^2} + C\right]^{-n} \tag{8.4}$$

which is similar in form to Eqn.(8.2) for $n = 1/2$.

In addition, PEDERSEN et al. collapse their strong injection results with velocity ratio. Fig.8.22(a) shows that this parameter is also successful with the present data. Further, the velocity ratio achieves correlation of the condition of minimum Nusselt Number associated with jet lift off, for a given downstream position, as shown in Fig.8.22(b).

The relationship between velocity ratio and the Strong Injection Parameter is in fact fairly insensitive to variation in injection-to-freestream temperature ratio over the range of conditions employed, so that either parameter is recommended for scaling.

However, the two parameters have slightly different implications for the designer. Whilst the velocity ratio depends on a flowfield measurement and is thus dependent on the mechanism by which the secondary flow exits from the holes, the strong injection parameter would only require a knowledge of stagnation conditions and a static pressure. Thus, its incorporation into a design procedure would be very convenient.

An industrial prediction programme based on the method of CRAWFORD et al.[8.19] has been run for this geometry, for conditions similar to those in the experiment. Plots of Nusselt Number against theta were constructed, as in the experiments, by varying the wall temperature for a constant mainstream temperature, injection temperature and injection rate. The relationship was found to be roughly linear over the range of theta used in the experiments, and linefits through each set of data gave values of A and B.

Results at $x/d = 2$ are shown in Fig.8.23. It can be seen that the programme predicts a maximum in the cooling performance for each injection-to-freestream temperature ratio, which is in agreement with experimental results. Since there is no mechanism for jet lift off in the programme, the maxima result from the increase of the film-induced turbulence with injection rate. The programme also simulates the effect of injection-to-freestream density ratio in a manner qualitatively similar to the experimental results. The reason for this is that the empirically prescribed mass shed ratio which distributes the injection flow within the streamtubes of the mainstream, has been chosen to scale with velocity ratio rather than blowing rate. Thus the programme is successful in generating heat transfer data which compares well with the present experimental results, but the empirical input required restricts its useful ness in terms of extracting scaling parameters.

Overall, the conclusion drawn from the experimental data is that for strong blowing, data is well scaled close to the holes using the strong injection parameter. The further dependence of injection-to-freestream density ratio implicit in this parameter may result from a gross change in the flowfield immediately behind the holes if lift off has occurred. However, as x/d increases, and the jet reattaches, this effect has less influence on the scaling. As a result, the choice between momentum flux ratio and strong injection parameter or velocity ratio is more difficult over the injection conditions investigated.

It should also be noted that the effect of the variation of transport properties through the injection layer, due to the temperature variations between the freestream and the wall, has considerable impact on the level of film cooled heat transfer. This is in fact the major influence far downstream over the test range of injection rates and injection-to-freestream temperature ratios. Fig.8.24 shows a comparison between data non-dimensionalised with respect to a constant properties level of Nusselt Number, and the same data non-dimensionalised with respect to the Nusselt Number at the relevant wall-to-freestream temperature ratio (as discussed in Chapter 6). This has a definite influence on the form of the results. If the data was corrected using the wall-to-adiabatic wall temperature ratio, the modification would be very similar, particularly far downstream where the adiabatic wall temperature approaches the freestream temperature. The former appears to bring the data closer together and is recommended.

It is of interest to search for a physical explanation for the success of these scaling parameters. ABRAMOVICH [8.20] states that the trajectory and penetration of the jets is primarily dependent on the relative dynamic pressures of the two streams. It is reasonable to assume that whilst the jet remains attached to the surface, this parameter would also govern the heat transfer rate. Cooling effectiveness would increase as the momentum flux ratio increased until a critical value was attained at which, for this geometry, lift off occurs.

LE BROCQ, LAUNDER & PRIDDIN [8.21], using air and Freon injection, take velocity profile measurements in the injection region and conclude that a maximum value of film cooling effectiveness occurs at an injection rate just less than that at which a velocity maximum appears in the near wall profile. The explanation given is that the rate of shear will be least for this condition, so that entrainment of mainstream fluid will be a minimum. They also point out that this effect may be complicated by the fact that the effectiveness of points midway between holes increases with increasing injection rates.

The performance of the conventional correlating parameter ξ (defined in Eqn.(4.15)), resulting from energy balance models, is now assessed. Data for each position at injection rates below that giving a minimum Nusselt Number is plotted against this parameter for two injection-to-freestream temperature ratio in Figs.8.25. The collapse with respect to downstream distance is good, suggesting that for low blowing rates, the heat transfer scales with $(x/d)^{1.25}$ for a given injection-to-freestream temperature ratio. As x/d decreases or the blowing rate increases, the data falls away from the region of correlation. It is clear, however, that the data for each injection-to-freestream temperature ratio tends to collapse on different lines, implying that correct fluid mechanic scaling is not achieved using

$$\left[\frac{\rho_i u_i}{\rho_\infty u_\infty}\right]^{1.25} .$$

8.2.3. Development of New Correlating Model.

A model is proposed which considers two-dimensional injection for the case where the injection density is different from the freestream density. It suggests that if the injection does not separate from the surface, the dominant fluid mechanic scaling parameter is the momentum flux ratio. This cannot be deduced from the energy balance model, which is for essentially constant property flows and therefore cannot separately identify the effect of the injection-to-freestream density ratio from the injection-to-freestream velocity ratio. Further, the proposed model does not resort to turbulent boundary layer assumptions for mass entrainment and velocity profiles in the injection layer. It has however, not been developed to the stage where heat transfer parameters can be predicted.

The flow is divided into two regimes : in the first, the coolant flow is injected inviscidly into the crossflow, and in the second, the viscous mixing and mainstream entrainment is considered.

1. The injection region. This is modelled as described in Section 7.5 after FITT [8.22]. This yields

$$\frac{b}{s} = 0\left[\frac{\rho_i u_i^2}{\rho_\infty u_\infty^2}\right]^{1/3} \tag{8.5}$$

This shows that the height of the injection layer at the end of the inviscid region is purely a function of the momentum flux ratio.

2. Mixing region. Once the coolant has emerged, the problem becomes one of the mixing and mainstream entrainment occurring in a wall jet. Empirical evidence is invoked to suggest the correct scaling for this process. NARAYAN & NARASHIMA [8.23] find that the jet momentum flux is a dominant quantity ;

they achieve scaling of the non-dimensionalised jet velocity maximum using the parameter

$$\frac{x}{b}\,\frac{u_\infty^2}{u_f^2} \tag{8.6}$$

for the constant density situation. This suggests that scaling would occur with

$$\frac{x}{b}\,\frac{\rho_\infty u_\infty^2}{\rho_i u_f^2} \tag{8.7}$$

for a wall jet of different initial density.

Thus the velocity field would depend on

$$\frac{x}{s}\,\frac{b}{s}\,\frac{\rho_\infty u_\infty^2}{\rho_i u_i^2} \tag{8.8}$$

Using Eqn.(8.5), this depends on

$$\frac{x}{s}\left[\frac{\rho_i}{\rho_\infty}\right]^{-2/3}\left[\frac{u_i}{u_\infty}\right]^{-4/3} \tag{8.9}$$

Thus, the velocity field in the wall jet region would be a function of position and initial jet-to-mainstream momentum flux ratio.

The assumption is now made that the temperature field will scale similarly. This would result from the similarity of the differential equations governing the injection layer, assumed here to be the boundary layer equations

$$\bar{u}\,\frac{\partial \bar{u}}{\partial x} + \bar{v}\,\frac{\partial \bar{u}}{\partial y} = \frac{\partial}{\partial y}\left[(\nu + \epsilon_m)\frac{\partial \bar{u}}{\partial y}\right] \tag{8.10}$$

$$\bar{u}\,\frac{\partial \bar{T}}{\partial x} + \bar{v}\,\frac{\partial \bar{T}}{\partial y} = \frac{\partial}{\partial y}\left[(\alpha + \epsilon_t)\frac{\partial \bar{T}}{\partial y}\right]$$

The Reynolds Analogy gives $\epsilon_m = \epsilon_t$, and for Pr = 1, $\nu = \alpha$. Complete equivalence would result if the boundary conditions were matched so that

$$\frac{u_f}{u_\infty} = \frac{T_f - T_w}{T_\infty - T_w} \tag{8.11}$$

but under different boundary conditions, the scaling should be similar so that heat transfer parameters would depend only on position and momentum flux ratio, at a given Reynolds Number.

This scaling might also be capable of extension to the case of injection through holes, if the flow remains attached to the wall. For data in the strong injection regime, however, successful scaling can be achieved if (8.9) is modified to

$$\frac{x}{d} \quad \left[\frac{u_i}{u_\infty}\right]^{-4/3} \qquad (8.12)$$

Collapse of all the single row data below the injection rates which give a minimum in Nusselt Number at a given position is good, Fig.8.25(b). Most of this data lies in the strong injection region.

8.3 SLOT RESULTS.

INJECTION GEOMETRY: 30° slot

length-to-slot width ratio 5.0

Results were obtained for the following three sets of injection-to-mainstream total temperatures :

T_{ti} = 260 K	$T_{t\infty}$ = 500 K	$T_{ti}/T_{t\infty}$ = 0.52	SYMBOL : ⊡
T_{ti} = 300 K	$T_{t\infty}$ = 365 K	$T_{ti}/T_{t\infty}$ = 0.82	SYMBOL : ⦶
T_{ti} = 345 K	$T_{t\infty}$ = 280 K	$T_{ti}/T_{t\infty}$ = 1.23	SYMBOL : +

TABLE 8.2

This key should be used for Figs.8.26 -8.37, unless otherwise stated.

8.3.1 General Description of Results.

Fig.8.26 (a)-(c) show that for this geometry, at a given injection-to-freestream temperature ratio, the Nusselt Number varies linearly with theta as the wall temperature is changed. This is in agreement with METZGER's results [8.24] for non-tangential slot injection. Thus the results can again be analysed by examining the dependence of the parameters A and B on distance, blowing rate and injection-to-freestream temperature ratio.

The variation in normalised Nusselt Number at a value of theta of unity, with downstream distance and blowing rate is shown in Fig.8.27 (a)-(b) for the two extreme temperature ratios. Two general observations can be made :

(1) the level of heat transfer increases with increasing x/s for each blowing rate ;

(2) the level of heat transfer decreases with increasing blowing rate at all x/s positions. This is most pronounced at low blowing rates, so that an increase in the blowing rate has a progressively smaller beneficial effect, particularly close to the slot.

Thus, the dramatic decrease in cooling performance above a given injection rate observed for the single row of holes is not a feature of this geometry. This may be because there is no mechanism whereby the mainstream gas can flow around and underneath the two-dimensional injection flow.

Further information on the cooling behaviour of this geometry can be obtained by studying the separate variations of A and B with distance and blowing rate in, for example, Figs.8.28 and 8.29. The following description applies equally to all three temperature ratios. As with the single row of holes, the value of A is highest close to injection for a given blowing rate, falling to a value close to unity far downstream for the lowest blowing rates. For x/s > 14, some values of A are less than unity at low blowing rates. This can be explained if the dominant effect of injection at these conditions is to increase the boundary layer thickness. This has been suggested by ERIKSEN & GOLDSTEIN [8.25] for a single row of holes, and VILLE et al [8.3] for a double row. As the blowing rate is increased, the value of A increases. This is most pronounced at $x/s = 2$, where at large blowing rates, A can be as much as four times its unblown value. It is concluded that close to injection, the mixing of the two flows has a large and deleterious effect on the heat transfer coefficient. However, this effect is also significant far downstream, for example at $x/s = 62$, where enhancements of 12% - 27% are recorded for the highest blowing rates.

HARTNETT et al [8.26] show that for a 20° slot, a blowing rate of 1.23 will cause a 90% increase in heat transfer coefficient at $x/s = 5$, decreasing to 10% at $x/s = 90$. METZGER & FLETCHER [8.27] report that for a 60° slot, values of h/h_o at $\Theta = 0$ are significantly larger than unity (as high as 1.6 at $G = 0.75$, $x/s = 5$) for the first thirty slot widths downstream, for $G > 0.25$. However, they also indicate that for a 20° slot, the values were close to unity with few exceptions.

The enhancement of the heat transfer coefficient is more than offset by the injection-temperature effect characterised by B. The magnitude of B is greatest close to the slot for a given blowing rate, falling off rapidly with increasing x. As the blowing rate is increased at a given injection-to-freestream temperature ratio, the magnitude of B increases, and again this variation is largest close to injection. Thus, in contrast to the single row results, the mixing effect and the coolant temperature effect increase monotonically with injection rate at a given position over the range tested.

8.3.2 Correlation With Fluid Mechanic Parameters

Clearly, the thirty degree slot results do not divide into strong and weak blowing regions, implying that film-cooling with this geometry will scale in a different manner.

The heat sink and energy balance models for the film-cooling process suggest that the mass flux ratio should scale the data. Plots of A and B against this parameter for $x/s = 2$ are shown in Fig.8.30. These results are corrected as suggested by Eqn.(6.21) for the effect of variation of properties through the boundary layer. Correlation of A and B with mass flux ratio appears to be reasonable.

The parameter -B/A is plotted against blowing rate for two positions in Fig.8.31. Since A might be expected to vary in the same way as B with these property variations, the isothermal adiabatic wall effectiveness should be insensitive to this effect. As such it should be a good indicator of the best correlating parameter. It can be seen that collapse of data with blowing rate is only partial. However, when plotted against the Weak Injection Parameter, the correlation is excellent for all injection rates and x/s positions, see Fig.8.32.

It is thus concluded that for this geometry, there is also an effect of injection-to-freestream density ratio which could not have been predicted from data at a single density ratio. Correct scaling will therefore have to be applied when using data from unity density ratio experiments to predict heat transfer in a gas turbine environment. It is recommended that for inclined slots, the momentum flux ratio or the Weak Injection Parameter should be used as correlating parameters.

In order to ascertain the effect of property variations through the injection layer, correlation of normalised levels of Nusselt Number can be examined, for example at Theta = 1.3, see Fig.8.33. It can be seen that when the slot-cooled data is normalised with respect to the unblown Nusselt Number at the corresponding wall-to-freestream temperature ratio, the collapse is significantly better than with data which has been normalised with respect to the Nusselt Number at unity temperature ratio. This implies, for example, that at a wall-to-freestream temperature ratio of 0.65, the level of Nusselt Number (assuming constant c_p, and using the variation of conductivity and viscosity with temperature given in Section 6.4, Case 3) will be of the order of 11% larger than that predicted by results from a wall-to-freestream temperature ratio close to unity at the same value of the Weak Injection Parameter.

A correction involving the wall-to-adiabatic wall temperature ratio would have a similarly beneficial effect far downstream. However, close to injection, where the local isothermal, adiabatic wall temperature approaches the injection temperature, a correction using this ratio would have a smaller effect on the data. In this case, the wall-to-freestream temperature ratio appears to bring the data into line more efficiently.

Using this correction, the parameters A and B can now be adequately scaled with the Weak Injection Parameter for each downstream position, as shown in Fig.8.34. SMITH [8.28] reports that for the same injection geometry, data from shock tube experiments is best correlated using either $p_{ti}/\ p_{t\infty}$ (which is equivalent to the Weak Injection Parameter for fixed Mach Number), or the momentum flux ratio. WYGNANSKI & NEWMAN [8.29] also use the momentum flux ratio in order to successfully collapse data on reattachment distances for an inclined two-dimensional jet in a cross flow.

The energy balance correlating parameter ξ achieves good scaling of the data with distance and blowing rate for a given injection-to-freestream temperature ratio, Fig.8.35. However, as has been shown, the mass flux is not as good as the momentum flux at scaling the data from different injection-to-freestream temperature ratios, so that changing this parameter causes the data to fall on a slightly different line.

A more complete correlation is achieved by the parameter proposed in Section 8.2.3. Fig.8.36 shows that this parameter convincingly scales the data from all positions, injection-to-freestream temperature ratios and injection rates.

It is interesting to compare this with other parameters discussed in Chapter 4. The dependence of the injection-to-freestream temperature ratio is very similar to that stated by PAPELL & TROUT [8.30],(Eqn.(4.16)) for tangential slot injection. Collapse of the present data with this parameter is consequently good, see Fig.8.37.

8.4 DOUBLE ROW RESULTS.

INJECTION GEOMETRY : double row of staggered 30° holes,
spacing-to-diameter ratio = 2.5
length-to-diameter ratio = 5.0
row spacing-to-diameter ratio = 2.0

Results were obtained for the following three sets of injection-to-freestream total temperatures :

T_{ti} = 260 K	$T_{t\infty}$ = 500 K	$T_{ti}/T_{t\infty}$ = 0.52	SYMBOL : ⊡
T_{ti} = 300 K	$T_{t\infty}$ = 365 K	$T_{ti}/T_{t\infty}$ = 0.82	SYMBOL : ⊙
T_{ti} = 345 K	$T_{t\infty}$ = 280 K	$T_{ti}/T_{t\infty}$ = 1.23	SYMBOL : +

TABLE 8.3.

This key should be used for Figs.8.38 – 8.48, unless otherwise stated.

8.4.1 General Description of results.

Fig.8.38 is an example of the data, and shows once again the linearity of the Nusselt Number with theta for a constant injection temperature, freestream temperature and blowing rate over the range tested.

The variation of the normalised Nusselt Number at θ = 1.0 with downstream distance and blowing rate for the two extreme temperature ratios, is shown in Fig.8.39(a) & (b). Normalisation is with respect to the unblown value at the corresponding wall-to-freestream temperature ratio. In general, cooling is best close to injection for a given blowing rate, and an increase in blowing rate causes a decrease in the Nusselt Number at all downstream positions. This becomes less pronounced close to injection at high blowing rates, where at a sufficiently high blowing rate, the Nusselt Number begins to increase.

The variation of the constituent parameters A and B, defined from superposition theory, is shown in Figs.8.40 & 8.41. The effect of the mixing of the two flows, characterised by A, tends to enhance the heat transfer, particularly close to injection where the increase can be over double the unblown value. Further downstream, the enhancement is less, but still significant (for example, 25% at $x/d = 20$ and 3% at $x/d = 98$, for $G = 1.055$, $T_{ti}/T_{t\infty} = 1.25$). This suggests that for this geometry too, considerable error can be introduced by making the assumption that the adiabatic wall heat transfer coefficient is equal to the unblown value, even at large x/d. For all blowing rates, the magnitude of B, which denotes the effect on the heat transfer coefficient of the injection temperature being different from the mainstream temperature, is greatest close to injection, decreasing with increasing distance. Except at very high blowing rates and small x/d, this cooling effect increases with increasing blowing rate for a given injection-to-freestream temperature ratio. With increasing distance downstream, the injection temperature effect has a relatively larger impact on the Nusselt Number than the mixing effect. For example, the cooling effect causes reductions in the Nusselt Number at $\Theta = 1.3$ of 93% at $x/d = 20$ and 70% at $x/d = 98$ at the conditions quoted above. Thus, whilst the variation of A is important, particularly close to injection, the variation of B is again the dominant effect for this geometry.

Qualitative agreement is found between the present results and those by KRUSE [8.14], JABBARI & GOLDSTEIN [8.31] and VILLE et al [8.3]. KRUSE [8.14] comments on the lack of a marked separation behind the double row, consistent with the present results, but notes that heat transfer increases between the holes at high blowing rates. The variation of heat transfer coefficient with blowing rate at $T_{ti}/T_{t\infty} = 0.82$ is compared with results from JABBARI & GOLDSTEIN and VILLE et al, Fig.8.42. The trends are similar in all cases, and quantitative agreement is good at x/d = 14.

8.4.2 Correlation with Fluid Mechanic Parameters.

Again, the parameter -B/A is scaled initially to reduce the effect of the property variations on the data . Collapse is reasonable with the mass flux ratio (Fig.8.43) but is clearly improved when plotted against the Weak Injection Parameter or the momentum flux ratio, Fig.8.44. This is equivalent to the correlation of the slot data, and the single row results at low injection rates.

Once this scaling is established, the effect of property variations through the boundary layer can be studied. Fig.8.45 shows the difference between normalising the data with respect to the constant properties value of the unblown Nusselt Number, and the unblown value at the relevant wall-to-gas temperature ratio. The latter has a beneficial effect on the collapse.

The parameters A and B, normalised in this manner, are scaled by the Weak Injection Parameter in Fig.8.46. Collapse of data is good, confirming the choice of correlating parameter. In Fig.8.47, reasonable scaling with distance and mass flux ratio is achieved with the energy balance parameter. The parameter proposed in Section 8.2.3 is successful at collapsing the data with distance, mass flux and injection-to-freestream temperature ratio, as shown in Fig.8.48.

8.5 Comparison of the Three Geometries.

It is interesting to briefly note the relative cooling merits of the three geometries by comparing their performance at equivalent injection mass flow rates at a given injection-to-freestream temperature ratio, Fig. 8.49. Close to the injection location, there is a large difference between the cooling behaviour, with the slot most efficient and the single row of holes least efficient. This is because of the even distribution of injection mass flux in the case of the slot, and is made more apparent by jet lift off in the case of the single row. However, at a non-dimensionalised downstream distance of 62, the performance of the slot and double row are very similar, with the single row remaining worse. This indicates that at this position, injection from the two-row geometry has mixed out to form a two-dimensional injection layer identical to that from the slot. With the single row geometry, there is more space between the holes where the mainstream can reach the surface and mix with the injection flow. There will also be a downstream effect of lift off.

Thus, slot cooling is most efficient close to injection, whilst two rows of closely spaced, staggered holes, where jet lift off does not occur, are equally efficient far downstream.

CHAPTER 9.

Conclusion.

A systematic investigation of the fluid mechanic parameters which govern the process of film-cooling has been undertaken. This has emphasised the inadequacies of using film-cooling data obtained in a constant properties environment to directly predict film-cooling performance in the engine. In order to use this data most effectively, it must be scaled to engine conditions using the most successful and convenient fluid mechanic correlating parameters. These can only be found by performing experiments such as those in this study, where a large degree of simulation of the engine environment is achieved.

In particular, the following conclusions have been reached :

1. For all geometries under investigation, there was found to be a significant effect of injection-to-freestream density ratio. This effect can neither be predicted by experiments performed with essentially constant properties, nor by analyses which assume constant properties, such as the conventional energy balance model. This implies that the mass flux ratio, a hitherto widely used parameter, should not be used to scale experimental data to engine conditions in the design process. Preferable scaling parameters depend upon the injection geometry and may alter according to the injection regime.

Two regimes can be identified : the weak injection regime describes injection rates below that at which gross separation of the injection flow occurs, with its associated decrease in film-cooling performance close-to-injection. The strong injection regime describes injection rates above this value.

For a single row of 30° holes, data in the weak injection region scales best with the momentum flux ratio or a pressure difference ratio known as the Weak Injection Parameter. Changes in the injection-to-freestream density ratio in this region would therefore be as important as changes in the square of the corresponding velocity ratio.

Once the jets lift off from the surface and penetrate well into the freestream, data at all downstream positions scales best with the injection-to-freestream velocity ratio or a Strong Injection Parameter. This parameter is also successful at correlating strong injection data from foreign gas experiments in the literature. Thus, at a given velocity ratio, the influence of the injection-to-freestream density ratio is small. Alternatively, at a given value of the Weak Injection Parameter or momentum flux ratio, film-cooling performance is a function of the injection-to-freestream density ratio in this regime. In fact, the experimental evidence reveals that at this condition, the resulting Nusselt Numbers are roughly proportional to the square root of the density ratio, as suggested by Eqn.(8.2).

Jet lift off for a given geometry can be adequately characterised by a critical value of the ratio of momentum flux of the jets to that of the freestream. For a single row of 30° holes, this occurred at a momentum flux ratio of about 0.1. At momentum flux ratios above this critical value, the gross structure of the injection process changes, and as a consequence the scaling of the heat transfer parameters is altered. For example, a minimum level of Nusselt Number resulting from jet lift off occurs at each downstream position, and this is found to scale best with velocity ratio.

At low injection rates and large x/d's, it is difficult to assess whether momentum flux or velocity ratio scales the data best. This is because the dependence on any blowing parameter is weak, and is masked by the effect of property variations.

For a double row of 30° holes and a 30° slot, no gross effect of lift off is observed. Consequently, the injection all occurs in the weak injection regime and heat transfer data scales with the momentum flux ratio or the Weak Injection Parameter.

2. In addition to the dependence of the heat transfer results on the injection-to-freestream density (or temperature) ratio, there was also a separate influence of the wall-to-freestream temperature ratio. This accounts for the variation of properties through the injection layer. This effect, described by Eqn.(6.17), has been observed experimentally for a flat plate turbulent boundary layer, and compares well with numerical solutions of the turbulent boundary layer.

In the film-cooling situation, the effect is similar in character. The implications of this are that there can be an increase of about 12% in the level of Nusselt Number at engine conditions compared with a similar experimental situation where the wall-to-freestream temperature ratio is close to unity.

3. The method of superposition of temperature fields has been shown to give a concise and physically meaningful interpretation of the film-cooling situation. Although devised from incompressible, constant properties equations, it has been shown experimentally to be capable of extension to the case of compressible, variable properties flow. The two heat transfer parameters A and B generated by the superposition approach can be considered to characterise aerodynamic effects and coolant temperature effects respectively. A and B are found to scale in a similar manner with injection rate. Generally, the variation of B with position and injection rate is more pronounced than that of A. However, ignoring the aerodynamic effects of injection can lead to a serious under-prediction of the heat transfer rate. This is most severe close to injection, but should also be considered at all downstream positions corresponding to a normal blade film-cooling geometry. For example, enhancement of A can be as much as 20% at positions twenty hole diameters downstream.

4. When comparing the three geometries tested, the major difference is that for the double row of 30° holes and the 30° slot, gross lift off of the injection flow is supressed. Lift off has a dramatic effect on cooling at all downstream positions; thus, at a given injection-to-freestream density ratio and mass flow rate per unit span, the amount of cooling far downstream is less for the single row of holes (in the strong injection regime) than it is for the double row and slot (both in the weak injection regime).

5. For all three geometries, the momentum flux ratio was found to be a function of the pressure difference ratio only, with no further effect due to the injection-to-freestream density ratio. This agrees well with recent theoretical advances made in modelling the flow of a two-dimensional jet emerging into a crossflow.

A simple model for the film-cooling process where the injection and freestream densities are different has been proposed. This uses theoretical and empirical evidence to conclude that the dominant fluid mechanic scaling parameter in situations where the injection flow remains close to the wall is the momentum flux ratio. The parameter

$$\frac{x}{d}\left[\frac{\rho_i u_i^2}{\rho_\infty u_\infty^2}\right]^{-2/3}$$

is successful at scaling this data. Clearly, when the injection flow lifts off into the mainstream, the flow pattern is radically altered. This affects the manner in which the two flows mix, resulting in the use of a different scaling parameter for heat transfer results:

$$\frac{x}{d}\left[\frac{u_i}{u_\infty}\right]^{-4/3}$$

The approach to the characterisation of film-cooling used in this study is eminently suitable for design purposes. A flow chart to illustrate how it could be employed in order to estimate a film-cooled heat transfer rate is given in Fig.9.1.

The fact that an isothermal surface boundary condition is attained under experimental conditions makes the data highly applicable to turbine components. Thus, a proposed film-cooling geometry can be experimentally characterised by evaluating the functional dependence of A and B with distance and injection rate at a convenient injection-to-freestream density ratio. These results can then be scaled to the engine values of injection-to-freestream temperature ratio and wall-to-freestream temperature ratio using the parameters and relations suggested in this study. The designer would have the freedom to choose whether to use average flowfield measurements such as velocities and densities, or to use flow pressure and temperature measurements to construct values of the weak and strong injection parameters. At the proposed injection rate, the correct values of A and B can be determined. The correlating parameters proposed also allow for the scaling of results to different positions. Knowledge of the injection, mainstream and desired wall temperature allow a value of theta and hence the hot side Nusselt Number to be found. An iterative technique can then be adopted to match the heat flux in the internal and external coolant flows for the required wall temperature.

Experimental data at engine-representative conditions will allow for the development of more sophisticated film-cooling models which will more accurately simulate the flowfield in these variable property flows. Once these models become established, the dependence on empirical data in the design procedure will be reduced. However, a great deal more experimentation remains to be done. The effects of variations in Mach Number, Reynolds Number, pressure gradients, surface curvature, and surface roughness all have to be incorporated. In addition, the effects of secondary flows, rotation and unsteady phenomena have to be considered, and all these must be expected to exhibit a dependence on the injection-to-freestream density ratio. Thus, experiments of the type reported here are essential if the external heat transfer rates on film-cooled turbine components are to be predicted with greater accuracy.

APPENDIX.

The Turbulent Boundary Layer Energy Equation.

The conservation of energy for a fluid element of unit mass may be expressed as

$$\rho\frac{D}{Dt}\left[e + \frac{u_i u_i}{2}\right] = \frac{\partial}{\partial x_i}\left[-q_i\right] + \rho u_i F_i + \frac{\partial}{\partial x_i}\left[\pi_{ij}u_j\right] \tag{A.1}$$

(a) (b) (c) (d)

using Cartesian tensor notation.

(a) represents the rate of increase of internal and kinetic energy. This results from

(b) the rate of change of energy due to heat conduction;

(c) the work done on the fluid by body forces;

(d) the work done on the fluid by stress components.

For a Newtonian Fluid, the stress components are given by

$$\pi_{ij} = \left[-p + \lambda\frac{\partial u_k}{\partial x_k}\right]\delta_{ij} + \mu\left[\frac{\partial u_i}{\partial u_j} + \frac{\partial u_j}{\partial u_i}\right] \tag{A.2}$$

where if $i=j$, $\delta_{ij} = 1$, and if $i \neq j$, $\delta_{ij} = 0$.

If the momentum equation

$$\rho\frac{Du_i}{Dt} = \rho F_i + \frac{\partial \pi_{ij}}{\partial x_j} \tag{A.3}$$

is multiplied by u_i and subtracted from (A.1), the result is

$$\rho\frac{De}{Dt} = \frac{\partial}{\partial x_i}\left[-q_i\right] + \pi_{ij}\frac{\partial u_j}{\partial x_i} \tag{A.4}$$

This can be expressed in terms of the enthalpy h where

$$h = e + p/\rho. \tag{A.5}$$

Using the continuity equation

$$\frac{D\rho}{Dt} + \rho\frac{\partial u_j}{\partial x_j} = 0 \ , \tag{A.6}$$

$$\frac{Dh}{Dt} = \frac{De}{Dt} + \frac{1}{\rho}\frac{Dp}{Dt} + \frac{p}{\rho}\frac{\partial u_k}{\partial x_k} \tag{A.7}$$

so that (A.4) becomes

$$\rho\frac{Dh}{Dt} = \frac{\partial}{\partial x_i}\left[k\frac{\partial T}{\partial x_i}\right] + \frac{Dp}{Dt} + \Phi \tag{A.8}$$

where Φ is the dissipation function given by

$$\Phi = p\frac{\partial u_k}{\partial x_k} + \pi_{ij}\frac{\partial u_j}{\partial x_i} \tag{A.9}$$

Boundary Layer Approximations.

Eqn.(A.8) can be simplified using the usual two-dimensional boundary layer approximations. In Cartesian co-ordinates,

$$\begin{aligned} & u \gg v \\ & \frac{\partial u}{\partial y} \gg \frac{\partial u}{\partial x}, \frac{\partial v}{\partial x}, \frac{\partial v}{\partial y} \\ & \frac{\partial p}{\partial y} \approx 0 \\ & \frac{\partial T}{\partial y} \gg \frac{\partial T}{\partial x} \\ & \pi_{xx} \approx -p \end{aligned} \tag{A.10}$$

If the pressure and conductivity are constant, (A.8) becomes

$$\rho u\frac{\partial T}{\partial x} + \rho v\frac{\partial T}{\partial y} = \frac{k}{c_p}\left[\frac{\partial^2 T}{\partial y^2} + \frac{Pr}{c_p}\left[\frac{\partial u}{\partial y}\right]^2\right] \tag{A.11}$$

This can be re-written in terms of a stagnation enthalpy H where

$$H = h + 1/2(u^2 + v^2) \tag{A.12}$$

By adding u times the momentum equation

$$u\frac{\partial u}{\partial x} + v\frac{\partial u}{\partial y} = \frac{\mu}{\rho}\frac{\partial^2 u}{\partial y^2} \tag{A.13}$$

to (A.11), the energy equation becomes

$$\rho u\frac{\partial H}{\partial x} + \rho v\frac{\partial H}{\partial y} = \frac{\partial}{\partial y}\left\{\frac{\mu}{Pr}\left[\frac{\partial H}{\partial y} + (Pr - 1)\frac{\partial}{\partial y}\left[\frac{u^2}{2}\right]\right]\right\} \tag{A.14}$$

For a turbulent boundary layer, quantities are expressed in terms of a mean value (barred) plus a fluctuating (dashed) component. The latter can be grouped with the transport properties so that

$$\rho\bar{u}\frac{\partial\bar{H}}{\partial x} + \rho\bar{v}\frac{\partial\bar{H}}{\partial y} = \frac{\partial}{\partial y}\left\{\frac{\mu_{eff}}{Pr_{eff}}\left[\frac{\partial\bar{H}}{\partial y} + (Pr_{eff} - 1)\frac{\partial}{\partial y}\left[\frac{\bar{u}^2}{2}\right]\right]\right\} \qquad (A.15)$$

where

$$\mu_{eff} = \mu + \mu' = \mu + \rho\epsilon_m$$

$$Pr_{eff} = \frac{c_p\,\mu_{eff}}{k_{eff}}$$

$$k_{eff} = k + k' = k + \rho c_p \epsilon_h$$

For $Pr_{eff} = 1$, the viscous dissipation term vanishes so that for a turbulent boundary layer, the constant properties, incompressible energy equation is

$$\bar{u}\,\frac{\partial\bar{T}}{\partial x} + \bar{v}\,\frac{\partial\bar{T}}{\partial y} = \frac{k_{eff}}{\rho\, c_p}\,\frac{\partial^2\bar{T}}{\partial y^2} \qquad (A.16)$$

This is linear in temperature, and is the equation to which the principle of superposition is applied. If, as in the injection layer in film-cooling, the boundary layer approximations cannot all be applied, the resulting equation will still be linear in temperature for a constant properties, incompressible flow.

REFERENCES.

CHAPTER 1.

[1.1] "Fundamental Heat Transfer Research for Gas Turbine Engines", NASA Lewis CP 2178, 1980.

[1.2] BENNETT,H.W., "Aero-engine Development for the Future", Proc. Inst. Mech. Eng. Power Division, 1983.

[1.3] METZGER,D.E. "Developments in Air Cooling of Gas Turbine Vanes and Blades", ASME Paper 83-GT-160, 1983.

[1.4] HENNECKE,D.K., "Turbine Blade Cooling in Aero Engines - Some New Results, Future Trends, of Research Requirements", unpublished report.

[1.5] FULLAGAR,K.P.L., "The Design of Air Cooled Rotor Blades", ARC 35684, 1974.

[1.6] ELOVIC,E. & KOFFEL,W.K., "Some Considerations in the Thermal Design of Turbine Airfoil Cooling Systems", Int.J. Turbo & Jet Eng., 1, 1., 1984.

[1.7] LOFTUS,P.J., D.Phil. Thesis, Oxford, 1982.

[1.8] GOLDSTEIN,R.J., ECKERT,E.R.G., ERIKSEN,V.L. & RAMSEY,J.W., "Film Cooling Following Injection Through Inclined Circular Tubes", NASA CR-72612, 1969.

[1.9] SMITH,M.R., D. Phil. Thesis, Oxford, 1974.

[1.10] GOLDSTEIN,R.J., ECKERT,E.R.G. & BURGGRAF,F., "Effects of Hole Geometry and Density on Three-Dimensional Film Cooling", Int. J. Heat Mass Transfer, 17, 1974.

[1.11] KRUSE,H., "Film Cooling Measurements", DFVLR Int. Rep.352-74/9, 1974.

[1.12] AFEJUKU,W.O., HAY,N. & LAMPARD,D., "Measured Coolant Distribution Downstream of Single & Double Rows of Film Cooling Holes", ASME Paper 82-GT-144, 1982.

[1.13] LIESS,C., "Experimental Investigation of Film Cooling with Ejection from a Row of Holes for the Application to Gas Turbine Blades", J. Eng. Power, 97, 1975.

[1.14] HAY,N., LAMPARD,D. & SALUJA,C.L., "Effects of the Condition of the Approach Boundary Layer & of Mainstream Pressure Gradients on the Heat Transfer Coefficient on Film-Cooled Surfaces", J. Eng. G.T. & Power, 107, 1985.

[1.15] NICOLAS,J. & LE MEUR,A., "Curvature Effects on a Turbine Blade Cooling Film", ASME Paper 74-GT-156, 1974.

[1.16] ITO,S., GOLDSTEIN,R.J. & ECKERT,E.R.G., "Film Cooling of a Gas Turbine Blade", J. Eng. Power, 100, 1978.

[1.17] DRING,R.P., BLAIR,M.F. & JOSLYN,H.D., "An Experimental Investigation of Film Cooling on a Turbine Rotor Blade", J. Eng. Power, 102, 1980.

[1.18] CARLSON.L.W. & TALMOR,E., "Gaseous Film Cooling at Various Degrees of Hot-Gas Acceleration and Turbulence Levels", Int. J. Heat Mass Transfer, 11, 1968.

[1.19] GOLDSTEIN,R.J., ECKERT,E.R.G., CHIANG,H.D. & ELOVIC,E., "Effect of Surface Roughness on Film Cooling Performance", J. Eng. G.T. & Power, 107, 1985.

[1.20] HARTSEL,J.E., "Prediction of Effects of Mass Transfer Cooling on the Blade Row Efficiency of Turbine Aerfoils", ASME Paper 72-11, 1972.

[1.21] HORTON,F.G., D.Phil. Thesis, Oxford, 1985.

CHAPTER 2.

[2.1] GOLDSTEIN,R.J., "Film Cooling", in Advances in Heat Transfer, 7, Academic Press, 1971.
[2.2] GOLDSTEIN,R.J., ECKERT,E.R.G. & RAMSEY,J.W., "Film Cooling with Injection through a Circular Hole", NASA CR-54604, 1968.
[2.3] METZGER,D.E., CARPER,H.J. & SWANK,L.R., "Heat Transfer with Film Cooling Near Nontangential Injection Slots", J. Eng. Power,90, 1968.
[2.4] LOFTUS,P.J. & JONES,T.V.,"The Effect of Temperature Ratios on the Film Cooling Process", ASME Paper 82-GT-305, 1982.
[2.5] ECKERT,E.R.G., "Transpiration and Film Cooling", Presented at Symposium on Heat Transfer at Univ. Michigan, 1952.
[2.6] LOUIS,J.F., "Systematic Studies of Heat Transfer and Film Cooling Effectiveness", AGARD, Conference: 'High Temprature Problems in Gas Turbine Engines', Turkey, 1977.
[2.7] CHOE,H., KAYS,W.M. & MOFFAT,R.J., "The Superposition Approach to Film-Cooling", ASME Paper 74-WA/HR-27, 1974.
[2.8] VILLE,J-P, CUNAT,D. & RICHARDS,B.E., "The Measurement of Film Cooling Effectiveness in Short Duration Wind Tunnels", VKI TN127, 1978.

CHAPTER 3.

[3.1] GOLDSTEIN,R.J., "Film Cooling", in Advances in Heat Transfer, 7, Academic Press, 1971.
[3.2] LOFTUS,P.J., D. Phil. Thesis, Oxford, 1982.
[3.3] HAY,N., "Heat Transfer Measurement in Steady State Facilities",in VKI Lecture Series "Measurement Techniques in Turbomachines", 1985.
[3.4] WIEGHARDT,K., "On the Blowing of Warm Air for De-Icing-Devices", AAF Trans No F-TS-919-RE Wright Field, Ohio, 1946.
[3.5] GOLDSTEIN,R.J., ECKERT,E.R.G., ERIKSEN,V.L. & RAMSEY,J.W., "Film Cooling Following Injection through Inclined Circular Tubes", NASA CR-72612, 1969.
[3.6] LIESS,C., "Experimental Investigation of Film Cooling with Ejection from a Row of Holes for the Application to Gas Turbine Blades", J. Eng. Power, 97, 1975.
[3.7] PAPELL,S.S, "Effect on Gaseous Film Cooling of Coolant Injection Through Angled Slots and Normal Holes", NASA TN D-299, 1960.
[3.8] BROWN,A. & SALUJA,C.L., "The Use of Cholesteric Liquid Crystals for Surface-Temperature Visualisation of Film Cooling Processes", J. Phys. E. Sci. Instrum. 11, 1978.
[3.9] SASAKI,M., TAKAHARA,K., KUMAGAI,T. & HAMANO,M., "Film Cooling Effectiveness for Injections from Multirow Holes", J. Eng. Power,101, 1979.
[3.10] GOLDSTEIN,R.J., ECKERT,E.R.G. & BURGGRAF,F.,"Effect of Hole Geometry and Density on Three Dimensional Slot Geometries", Int. J. Heat Mass Transfer,17, 1974.
[3.11] PAPELL,S.S. & TROUT,A.M., "Experimental Investigation of Air Film Cooling Applied to an Adiabatic Wall by Means of an Axially Discharging Slot", NASA TN D-9, 1959.
[3.12] PARADIS,M.A., "Film Cooling of Gas Turbine Blades: A Study of the Effect of Large Temperature Differences on Film Cooling Effectiveness", J. Eng. Power, 99, 1977.

[3.13] ARTT,D.W., BROWN,A. & MILLER,P.P.,"An Experimental Investigation into Film Cooling with Particular Application to Cooled Turbine Blades", Proc. 4th Int. Heat Transfer Conf., Paris 1970.
[3.14] KRUSE,H., "Film Cooling Measurements", DFVLR Int. Rep.352-74/9, 1974.
[3.15] PEDERSEN,D.R., ECKERT,E.R.G. & GOLDSTEIN,R.J., "Film Cooling with Large Density Differences Between the Mainstream and Secondary Fluid Measured by the Heat-Mass Transfer Analogy", J. Heat Transfer, 99, 1977.
[3.16] LAUNDER,B.E. & YORK,J., "Discrete-Hole Cooling in the Presence of Free Stream Turbulence and Strong Favourable Pressure Gradient", Int. J. Heat Mass Transfer, 17, 1974.
[3.17] NICOLAS,J. & LE MEUR,A., "Curvature Effects on a Turbine Blade Cooling Film", ASME Paper 74-GT-156, 1974.
[3.18] BURNS,W.K. & STOLLERY,J.L., "The Influence of Foreign Gas Injection and Slot Geometry on Film Cooling Effectiveness", Int. J. Heat Mass Transfer, 12, 1969.
[3.19] PAI,B.R. & WHITELAW,J.H., "The Influence of Density Gradients on the Effectiveness of Film Cooling", ARC CP No. 1013, 1968.
[3.20] HARTNETT,J.P., BIRKEBACK,R.C. & ECKERT,E.R.G., "Velocity Distributions, Temperature Distributions, Effectiveness and Heat Transfer in Cooling of a Surface with a Pressure Gradient", ASME International Developments in Heat Transfer V, 1961.
[3.21] SEBAN,R.A. & BACK,L.H., "Effectiveness and Heat Transfer for a Turbulent Boundary Layer with Tangential Injection and Variable Free-Stream Velocity", J. Heat Transfer, 84, 1962.
[3.22] ERIKSEN,V.L. & GOLDSTEIN,R.J., "Heat Transfer and Film Cooling Following Injection through Inclined Circular Tubes", J. Heat Transfer, 1974.
[3.23] CRAWFORD,M.E., KAYS,W.M. & MOFFAT,R.J., "Full-Coverage Film Cooling on Flat, Isothermal Surfaces: A Summary Report on Data and Predictions", NASA CR 3219, 1980.
[3.24] GOLDSTEIN,R.J. & TAYLOR,J.R., "Mass Transfer in the Neighborhood of Jets Entering a Crossflow", ASME Paper 82-HT-62, 1982.
[3.25] HAY,N., LAMPARD,D. & SALUJA,C.L., "Effects of Cooling Films on the Heat Transfer Coefficient on a Flat Plate with Zero Mainstream Pressure Gradient", J. Eng. Power, 107 , 1985.
[3.26] METZGER,D.E., CARPER,H.J. & SWANK,L.R., "Heat Transfer with Film Cooling Near Nontangential Injection Slots", J. Eng. Power, 90, 1968.
[3.27] FERRI,A., MAHRER,A. & HEFNER,J.N., "Investigation of slot Cooling at High Subsonic Speeds", AIAA Journal 14, 1975.
[3.28] JONES,T.V. & SCHULTZ,D.L., "Film Cooling Studies in Subsonic and Supersonic Flows Using a Shock Tunnel", ARC 32420, 1970.
[3.29] SMITH,M.R., D. Phil. Thesis, Oxford, 1974.
[3.30] LOUIS,J.F., GOULIOS,G.N., DEMIRJIAN,A.M., TOPPING,R.F. & WIEDHOPF,J.M., "Short Duration Studies of Turbine Heat Transfer and Film Cooling Effectiveness", ASME Paper 74-GT-131, 1974.

CHAPTER 4.

[4.1] TRIBUS,M. & KLEIN,J., "Forced Convection From Non-Isothermal Surfaces", Heat Transfer Symposium, Univ. Michigan, 1953.

[4.2] ECKERT,E.R.G., "Film cooling with Injection through Holes", AGARD CP-73-71, 1971.

[4.3] ERIKSEN,V.L., ECKERT,E.R.G. & GOLDSTEIN,R.J., "A Model for the Analysis of the Temperature Field Downstream of a Heated Jet Injected into an Isothermal Crossflow at an Angle of 90 Degrees", NASA CR-72990, 1971.

[4.4] KUTATELADZE,S.S. & LEONT'EV,A.K., "Film Cooling With a Turbulent Gaseous Boundary Layer", J. Thermal Physics High Temp., 1, 1963.

[4.5] STOLLERY,J.L. & EL-EHWANY,A.A.M., "A Note on the Use of a Boundary-Layer Model for Correlating Film-Cooling Data", Int. J. Heat Mass Transfer, 8, 1965.

[4.6] GOLDSTEIN,R.J., ECKERT,E.R.G. & WILSON,D.J., "Film Cooling with Normal Injection Into a Supersonic Flow", J. Eng. Industry, 90, 1968.

[4.7] SEBAN,R.A. & BACK,L.J., "Velocity and Temperature Profiles in Turbulent Boundary Layer with Tangential Injection", ASME Paper 61-SA-24, 1962.

[4.8] SPALDING,D.B., "A Unified Theory of Friction, Heat Transfer and Mass Transfer in the Turbulent Boundary Layer and Wall Jet", ARC CP 829, 1965.

[4.9] PATANKAR,S.V. & SPALDING,D.B., "A Finite-Difference Procedure for Solving the Equations of the Two-Dimensional Boundary Layer", Int. J. Heat Mass Transfer, 10, 1967.

[4.10] KACKER,S.C., PAI,B.R. & WHITELAW,J.H., "The Prediction of Wall Jet Flows with Particular Reference to Film Cooling", in "Progress in Heat and Mass Transfer" ,2, p163, Pergammon Press, 1969.

[4.11] PAI,B.R. & WHITELAW,J.H., "The Prediction of Wall Temperature in the Presence of Film Cooling", Int. J. Heat Mass Transfer, 14, 1971.

[4.12] BERGELES,G., GOSMAN,A.D. & LAUNDER,B.E., "The Prediction of Three-Dimensional Discrete-Hole Cooling Processes", J. Heat Transfer, 98, 1976.

[4.13] CRAWFORD,M.E., KAYS,W.M. & MOFFAT,R.J., "Full-Coverage Film Cooling on Flat, Isothermal Surfaces: A Summary Report on Data and Predictions", NASA CR 3219, 1980.

[4.14] RAMETTE,P.H. & LOUIS,J.F., "Analytical Study of the Thermal and Fluid Mechanical Evolution of a Cooling Film Injected from a Single Line of Inclined Round Holes", M.I.T. Int. Rep., 1978.

[4.15] WIEGHARDT,K., "On the Blowing of Warm Air for De-Icing-Devices", AAF Trans No F-TS-919-RE Wright Field, Ohio, November 1946.

[4.16] PAPELL,S.S. & TROUT,A.M., "Experimental Investigation of Air Film Cooling Applied to an Adiabatic Wall by Means of an Axially Discharging Slot", NASA TN D-9, 1959.

[4.17] CHIN,J.H., SKIRVIN,S.C, HAYES,L.E. & SILVER,A.H., "Adiabatic Wall Temperature Downstream of a Single, Tangential Injection Slot", ASME Paper 58-A-107, 1958.

[4.18] BROWN,A., "A Theoretical and Experimental Investigation into Film Cooling", JSME, Semi-International Symposium, Tokyo, 1967.

[4.19] ARTT,D.W., BROWN,A. & MILLER,P.P., "An Experimental Investigation into Film Cooling with Particular Application to Cooled Turbine Blades", Proc. 4th Int. Heat Transfer Conf., Paris, 1970.

[4.20] PAI,B.R. & WHITELAW,J.H., "The Influence of Density Gradients on the Effectiveness of Film Cooling", ARC CP 1013, 1968.

[4.21] BURNS,W.K. & STOLLERY,J.L., "The Influence of Foreign Gas Injection and Slot Geometry on Film Cooling Effectiveness", Int. J. Heat Mass Transfer, 12, 1969.

[4.22] LOUIS,J.F., GOULIOS,G.N., DEMIRJIAN,A.M., TOPPING,R.F. & WIEDHOPF,J.M., "Short Duration Studies of Turbine Heat Transfer and Film Cooling Effectiveness", ASME 74-GT-131, 1974.

[4.23] METZGER,D.E., CARPER,H.J. & SWANK,L.R., "Heat Transfer with Film Cooling Near Nontangential Injection Slots", J. Eng. Power, 90, 1968.

[4.24] GOLDSTEIN,R.J., ECKERT,E.R.G. & RAMSEY,J.W., "Film Cooling with Injection through a Circular Hole", NASA CR-54604, 1968.

[4.25] GOLDSTEIN,R.J., ECKERT,E.R.G. & BURGGRAF,F., "Effects of Hole Geometry and Density on Three Dimensional Film Cooling", Int. J. Heat Mass Transfer, 17, 1974.

[4.26] SMITH,M.R., D. Phil. Thesis, Oxford, 1974.

[4.27] PEDERSEN,D.R., ECKERT,E.R.G. & GOLDSTEIN,R.J., "Film Cooling with Large Density Differences Between the Mainstream and Secondary Fluid Measured by the Heat-Mass Transfer Analogy", J. Heat Transfer, 99, 1977.

[4.28] JONES,T.V., "The Superposition Model of Film Cooling and Fluid Dynamic Scaling", VKI Lecture Series, 1978.

[4.29] BERGELES,G., GOSMAN,A.D. & LAUNDER,B.E., "The Near-Field Character of a Jet Discharged Normal to a Main Stream", J. Heat Transfer, 98, 1976.

[4.30] FOSTER,N.W. & LAMPARD,D., "Effects of Density and Velocity Ratios on Discrete Hole Film Cooling", AIAA Journal 13, 1975.

[4.31] LOFTUS,P.J., D. Phil. Thesis, Oxford, 1982.

CHAPTER 5.

[5.1] JONES,T.V., SCHULTZ,D.L. & HENDLEY,A.D., "On the Flow in an Isentropic Light Piston Tunnel", ARC 34217, 1973.

[5.2] SCHULTZ,D.L. & JONES,T.V., "Heat Transfer Measurements in Short Duration Hypersonic Facilities", AGARD AG-165, 1973.

[5.3] SCHULTZ,D.L, JONES,T.V., OLDFIELD,M.L.G., AINSWORTH,R.N. & DANIELS,L.C., "The Measurement of Heat Transfer Rates to Film Cooled External Surfaces and the Internal Passages of Turbomachine Components under Transient Conditions using Thin Film Gauges", OUEL Rep. 1152/76, 1976.

[5.4] OLDFIELD,M.L.G., BURD,H.J. & DOE,N.G., "Design of Wide Band-Width Analogue Circuits for Heat Transfer Instrumentation in Transient Tunnels", Proc. 14th/CHMT Symposium on Heat & Mass Transfer in Rotating Machinery, Dubrovnik, 1982.

[5.5] OLDFIELD,M.L.G., JONES,T.V. & SCHULTZ,D.L., "On-Line Computer for Transient Turbine Cascade Instrumentation", IEEE Trans. Aerospace and Electronic Systems, AES -14,No 5, 1978.

[5.6] MILLER,C.G., "Comparison of Thin-Film Resistance Heat-Transfer Gauges With Thin-Skin Transient Calorimeter Gauges in Conventional Hypersonic Wind Tunnels, NASA TM-83197, 1981.

[5.7] AINSWORTH,R.N., D. Phil. Thesis, Oxford, 1976.

[5.8] LOFTUS,P.J., D. Phil. Thesis, Oxford, 1982.

[5.9] MOFFAT,R.J., "Gas Temperature Measurement", Univ. of Stanford, Unpublished Rep. SF-97-13.
[5.10] HENDLEY,A.D., M.Sc. Thesis, Oxford, 1973.
[5.11] DOORLY,J.E., D. Phil. Thesis, Oxford, 1985.
[5.12] DRUMMOND,J.P., JONES,R.A. & ASH,R.L., "Effective Thermal Property Improves Phase Change Paint Data", AIAA Journal 14, No 10, 1976.

CHAPTER 6.

[6.1] FITT,A.D., FORTH,C.J.P., JONES,T.V. & ROBERTSON,B.A., "Temperature Ratio Effects in Compressible Turbulent Boundary Layers", Int. J. Heat Mass Transfer, to be published.
[6.2] LOFTUS,P.J., D. Phil. Thesis, Oxford, 1982.
[6.3] KAYS,W.M. & CRAWFORD,M.E., "Convective Heat and Mass Transfer", McGraw-Hill, 1980.
[6.4] "CRC handbook of Tables for Applied Engineering Science", CRC Press, 1976.
[6.5] ROBERTSON,B.A., M.Sc. Thesis, Oxford, 1985.
[6.6] CEBICI,T. & SMITH,A.M.O., "Analysis of Turbulent Boundary Layers", Academic Press, 1974.
[6.7] BLOTTNER,F.G., "Computational Methods for Inviscid and Viscous Two-and-Three-Dimensional Flow Fields", AGARD LS-73, 1975.
[6.8] ECKERT,E.R.G., "Engineering Relations for Friction and Heat Transfer to Surfaces in High Velocity Flow", J. Aero. Sci., 1955.
[6.9] BROWN,L.W.B., Private Communication, 1980.
[6.10] NEAL,L. & BERTRAM,M.H., NASA TN-3969, 1967.
[6.11] LOFTUS,P.J. & JONES,T.V., "The Effect of Temperature Ratios on the Film Cooling Process", J. Eng. Power, 105, 1983.
[6.12] BOSE,T.K., "Some Numerical Results for Compressible Turbulent Boundary-Layer Heat Transfer at Large Free-Stream/Wall Temperature Ratios", in "Studies in Heat Transfer - a Festschrift for E.R.G. Eckert", Hemisphere Press, 1979.
[6.13] HERWIG,H., "The Effect of Variable Properties on Momentum and Heat Transfer in a Tube with Constant Heat Flux across the Wall", Int. J. Heat Mass Transfer, 28, 1985.
[6.14] VILEMAS,J.V. & SIMONIS,V.M., "Heat Transfer and Friction of Rough Ducts Carrying Gas Flow with Variable Physical Properties", Int. J. Heat Mass Transfer, 28, 1985.

CHAPTER 7.

[7.1] FITT,A.D., OCKENDON,J.R. & JONES,T.V., "Aerodynamics of Slot Film Cooling, Theory and Experiment", J. Fluid Mech., to be published.
[7.2] LEE,L.H.Y. & CLARK, J.A., "Angled Injection of Jets into a Turbulent Boundary Layer", ASME Paper 80-FE-2, 1980.
[7.3] BERGELES,G., GOSMAN,A.D. & LAUNDER,B.E., "The Near-Field Character of a Jet Discharged Normal to a Main Stream", J. Heat Transfer, 98, 1976.
[7.4] FOSS,J.F., "Interaction Region Phenomena for the Jet in a Cross-Flow Problem", SFB 80/E/161, Univ. Karlsruhe, 1980.
[7.5] ANDREOPOULOS,J., "Measurements in a Pipe Flow Issuing Perpendicularly into a Cross Stream", SFB 80, Univ. Karlsruhe, 1980.

[7.6] ABRAMOVICH,G.N., "The Theory of Turbulent Jets", M.I.T. Press, 1963.
[7.7] BERGELES,G., GOSMAN,A.D. & LAUNDER,B.E., "The Prediction of Three-Dimensional Discrete-Hole Cooling Processes", J. Heat Transfer, 98, 1976.
[7.8] BERGELES,G., GOSMAN,A.D. & LAUNDER,B.E., "The Turbulent Jet in a Cross Stream at Low Injection Rates: A Three-Dimensional Numerical Treatment", Numerical Heat Transfer, 1, 1978.
[7.9] KADOTANI,K. & GOLDSTEIN,R.J., "On the Nature of Jets Entering a Turbulent Flow; Part A-Jet-Mainstream Interaction & Part B-Film Cooling Performance", J. Eng. Power, 101, 1979.
[7.10] COLLADAY,R.S., RUSSELL,L.M. & LANE,J.M., "Streakline Flow Visualization of Discrete Hole Film Cooling with Holes Inclined 30 Degrees to Surface", NASA TN D-8175, 1976.
[7.11] ANDREOPOULOS,J. & RODI,W., "Experimental Investigation of Jets in a Crossflow", J. Fluid Mech., 1984.
[7.12] MOUSSA,Z.M., TRISCHKA,J.W. & ESKINAZI,S., "The Near Field in the Mixing of a Round Jet with a Cross-Stream", J. Fluid Mech., 80, 1977.
[7.13] ESKINAZI,S., "Fluid Mechanics and Thermodynamics of our Environment", Academic Press, 1975.
[7.14] LU, HSIH-CHIA, "On the Surface of Discontinuity Between 2 Flows Perpendicular to each other", Int. Rep. National Tsing Hua University, 1942.
[7.15] HIGDON,J.J.L. & POZRIKIDIS,C., "The Self-Induced Motion of Vortex Sheets", J. Fluid Mech., 150, 1985.
[7.16] KEFFER,J.F & BAINES,W.D., "The Round Turbulent Jet in a Cross-Wind", J. Fluid Mech., 15 No 4, 1963.
[7.17] KAMOTANI,Y. & GREBER,I., "Experiments on a Turbulent Jet in a Cross Flow, AIAA Journal, 10, 1972.
[7.18] RAMSEY,J.W. & GOLDSTEIN,R.J., "Interaction of a Heated Jet with a Deflecting Stream", J. Heat Transfer, 93, 1971.
[7.19] HUNT,J.C.R., ABEL,C.J., PETERKA,J.A. & WOO,H., "Kinematical Studies of the Flows around Free or Surface-Mounted Obstacles; Applying Topology to Flow Visualization", J. Fluid Mech., 86, No 1, 1978.
[7.20] FEARN,R. & WESTON,R.P., "Vorticity Associated with a Jet in a Cross Flow", AIAA Journal, 12, 1974.
[7.21] RAMETTE,P.H. & LOUIS,J.F., "Analytical Study of the Thermal and Fluid Mechanical Evolution of a Cooling Film Injected from a Single Line of Inclined Round Holes", M.I.T. Internal Report, 1978.
[7.22] HORTON,F.G., D. Phil. Thesis, Oxford, 1985.
[7.23] ANDREWS,G.E. & MKPADI,M.C., "Full Coverage Discrete Hole Wall Cooling: Discharge Coefficients", ASME Paper 83-GT-79, 1983.
[7.24] DEWEY,P.E., "A Preliminary Investigation of Small Inclined Air Outlets at Transonic Mach Numbers", NASA TN 3442, 1955.
[7.25] HAY,N., LAMPARD,D. & BENMANSOUR, "Effect of Crossflows on the Discharge Coefficient of Film Cooling Holes", J. Eng. Power, 105, 1983.
[7.26] SMITH,M.R., D. Phil. Thesis, 1974.
[7.27] Rolls-Royce Bristol, Private Communication, 1973.
[7.28] FITT,A.D., D. Phil. Thesis, Oxford, 1984.

CHAPTER 8.

[8.1] METZGER,D.E. & FLETCHER,D.D., "Evaluation of Heat Transfer for Film-Cooled Turbine Components", J. Aircraft, 8, No 1, 1971.

[8.2] CHOE,H., KAYS,W.M. & MOFFAT,R.J., "The Superposition Approach to Film-Cooling", ASME Paper 74-WA/HR-27, 1974.

[8.3] VILLE,J-P, CUNAT,D.& RICHARDS,B.E., "The Measurement of Film Cooling Effectiveness in Short Duration Wind Tunnels", VKI TN127, 1978.

[8.4] LOFTUS,P.J., D. Phil. Thesis, Oxford, 1982.

[8.5] RAMSEY,J.W. & GOLDSTEIN,R.J., "Interaction of a Heated Jet with a Deflecting Flow", J. Heat Transfer, 93, 1971.

[8.6] KRUSE,H., "Film Cooling Measurements", DFVLR Int. Rep.352-74/9, 1974.

[8.7] COLLADAY,R.S. & RUSSELL,L.M., "Streakline Flow Visualization of Discrete-Hole Film Cooling with Normal, Slanted, and Compound Angle Injection", NASA TN D-8248, 1976.

[8.8] COLLADAY,R.S., RUSSELL,L.M. & LANE,J.M., "Streakline Flow Visualization of Discrete Hole Film Cooling with Holes Inclined 30 Degrees to Surface", NASA TN D-8175, 1976.

[8.9] GOLDSTEIN,R.J., ECKERT,E.R.G. & BURGGRAF,F., "Effects of Hole Geometry and Density on Three-Dimensional Film Cooling", Int. J. Heat Mass Transfer ,17, 1974.

[8.10] FEARN,R. & WESTON,R.P., "Vorticity Associated with a Jet in a Cross Flow", AIAA Journal, 12, 1974.

[8.11] LIESS,C., "Experimental Investigation of Film Cooling with Ejection from a Row of Holes for the Application to Gas Turbine Blades", J. Eng. Power, 97, 1975.

[8.12] GOLDSTEIN,R.J. & TAYLOR,J.R., "Mass Transfer in the Neighborhood of Jets Entering a Crossflow", ASME Paper 82-HT-62, 1982.

[8.13] HAY,N., LAMPARD,D. & SALUJA,C.L., "Effects of Cooling Films on the Heat Transfer Coefficient on a Flat Plate with Zero Mainstream Pressure Gradient", J. Eng. G.T. & Power, 107, 1985.

[8.14] KRUSE,H., "Effects of Hole Geometry, Wall Curvature and Pressure Gradient on Film Cooling Downstream of a Single Row", AGARD CPP-390, 1985.

[8.15] FOSTER,N.W. & LAMPARD,D., "Effects of Density and Velocity Ratios on Discrete Hole Film Cooling", AIAA Journal, 13, 1974.

[8.16] PEDERSEN,D.R., ECKERT,E.R.G. & GOLDSTEIN,R.J., "Film Cooling with Large Density Differences Between the Mainstream and Secondary Fluid Measured by the Heat-Mass Transfer Analogy", J. Heat Transfer, 99, 1977.

[8.17] CAMCI,C. & ARTS,T., "Experimental Heat Transfer Investigation Around the Film-Cooled Leading Edge of a High Pressure Gas Turbine Rotor Blade", ASME Paper 85-GT-114, 1985.

[8.18] JONES,T.V., "The Superposition Model of Film Cooling and Fluid Dynamic Scaling", VKI Lecture Series, 1978.

[8.19] CRAWFORD,M.E., KAYS,W.M. & MOFFAT,R.J., "Full-Coverage Film Cooling on Flat, Isothermal Surfaces: A Summary Report on Data and Predictions", NASA CR 3219, 1980.

[8.20] ABRAMOVICH,G.N., "The Theory of Turbulent Jets", M.I.T. Press, 1963.

[8.21] LE BROCQ,P.V., LAUNDER,B.E. & PRIDDIN,C.H., "Discrete Hole Injection as a Means of Transpiration Cooling - an Experimental Study", Proc. I. Mech. Eng., 187, 1973.

[8.22] FITT,A.D., D. Phil. Thesis, Oxford, 1984.

[8.23] NARAYAN,K.Y. & NARASHIMHA,R., "Parametric Analysis of Turbulent Wall Jets", Aero. Quarterly, 1973.
[8.24] METZGER,D.E., CARPER,H.J. & SWANK,L.R., "Heat Transfer with Film Cooling Near Nontangential Injection Slots", J. Eng. Power, 90, 1968.
[8.25] ERIKSEN,V.L. & GOLDSTEIN,R.J., "Heat Transfer and Film Cooling Following Injection through Inclined Circular Tubes", J. Heat Transfer, 96, 1974.
[8.26] HARTNETT,J.P., BIRKEBACK,R.C. & ECKERT,E.R.G., "Velocity Distributions, Temperature Distributions, Effectiveness and Heat Transfer in Cooling of a Surface with a Pressure Gradient", ASME International Developments in Heat Transfer V, 1961.
[8.27] METZGER,D.E. & FLETCHER,D.D., "Evaluation of Heat Transfer for Film-Cooled Turbine Components", J. Aircraft, 8, No 1, 1971.
[8.28] SMITH,M.R., D. Phil. Thesis, 1974.
[8.29] WYGNANSKI,I. & NEWMAN,B.G., "The Reattachment of an Inclined Two-Dimensional Jet to a Flat Surface in Streaming Flow", CASI Transactions, 1, 1968.
[8.30] PAPELL,S.S. & TROUT,A.M., "Experimental Investigation of Air Film Cooling Applied to an Adiabatic Wall by Means of an Axially Discharging Slot", NASA TN D-9, 1959.
[8.31] JABBARI,M.Y. & GOLDSTEIN,R.J., "Adiabatic Wall Temperature and Heat Transfer Downstream of Injection through Two Rows of Holes", J. Eng. Power, 100, 1978.

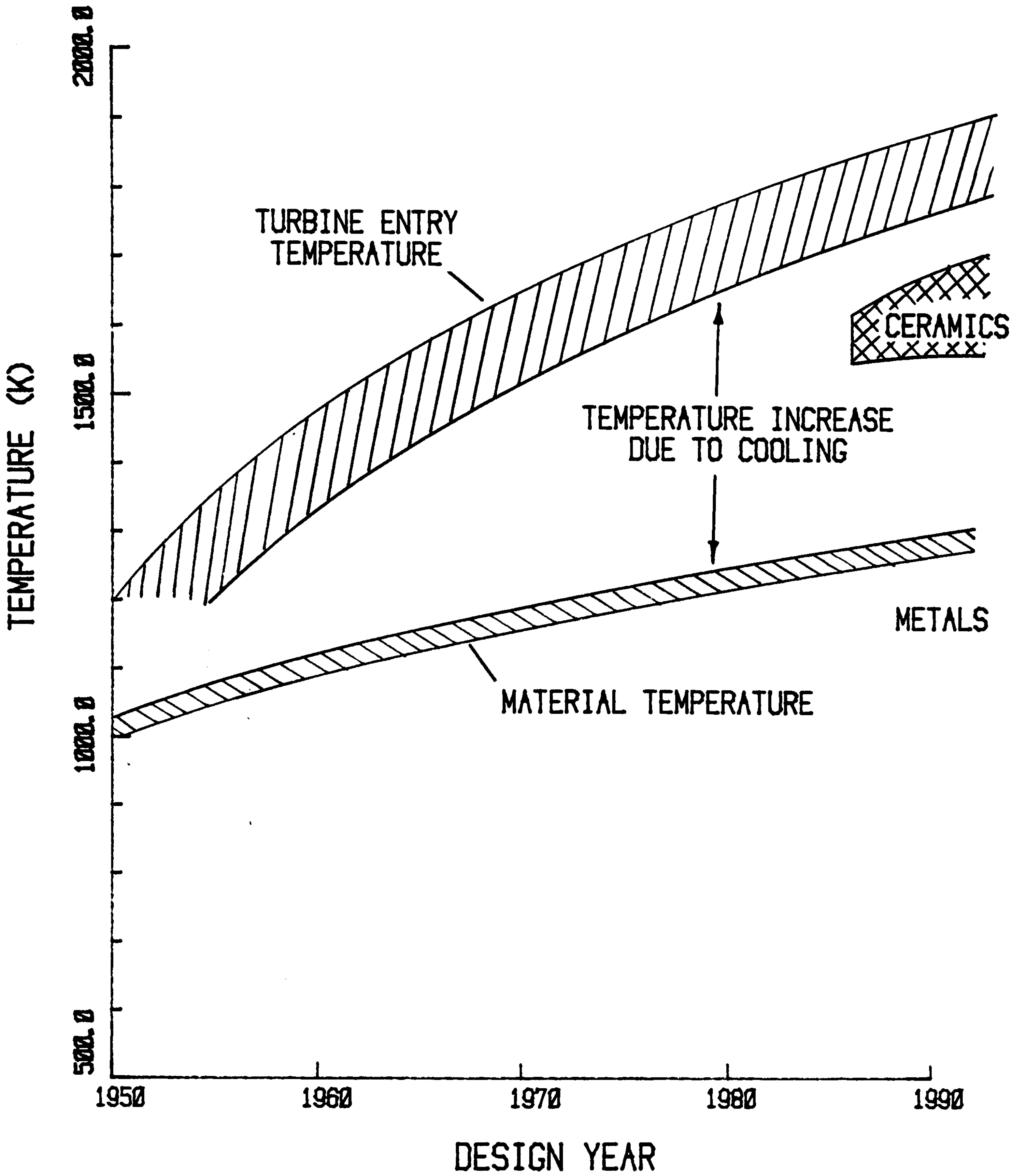

FIG. 1.1 Increase of Turbine Entry Temperature with Design Year.

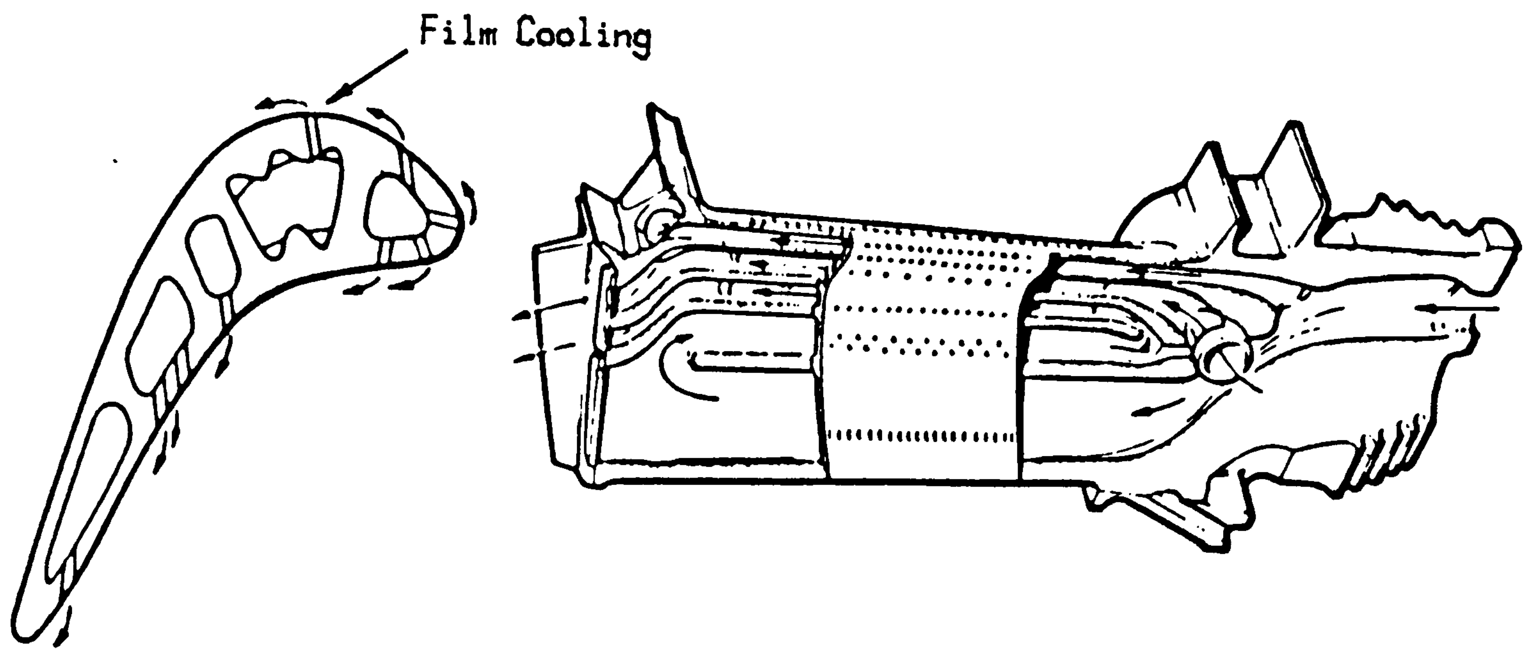

FIG. 1.2(a) Typical HP Rotor Cooling Configuration
(from Rolls Royce)

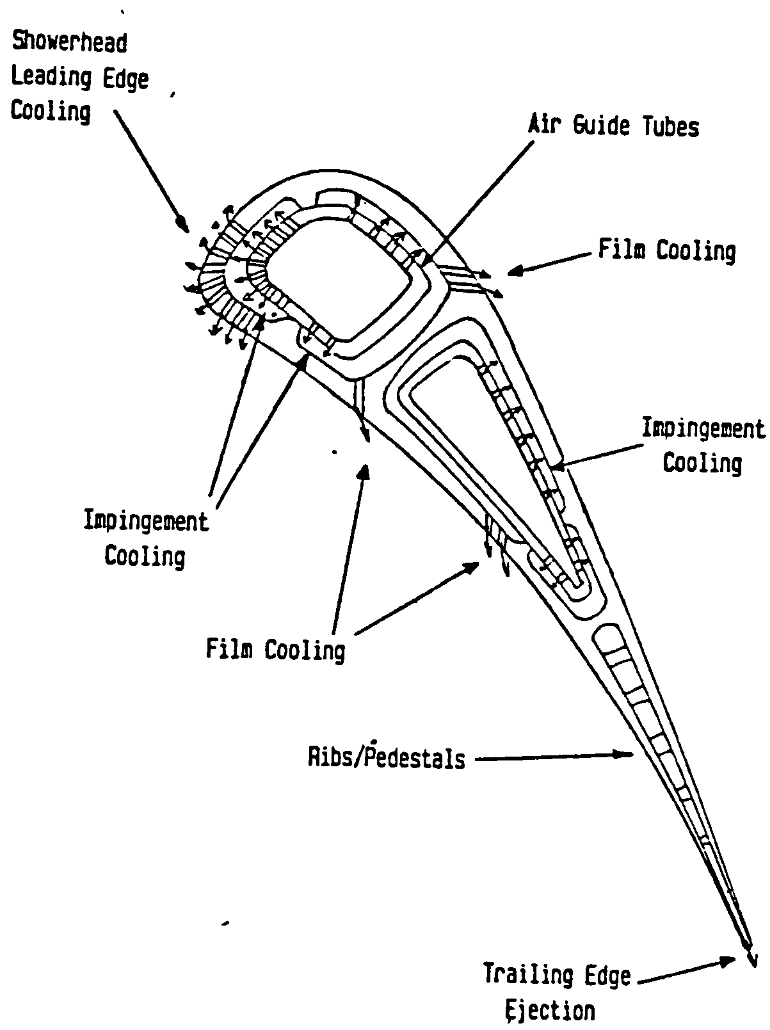

FIG. 1.2(b) Typical NGV Cooling Configuration
(from [3.2])

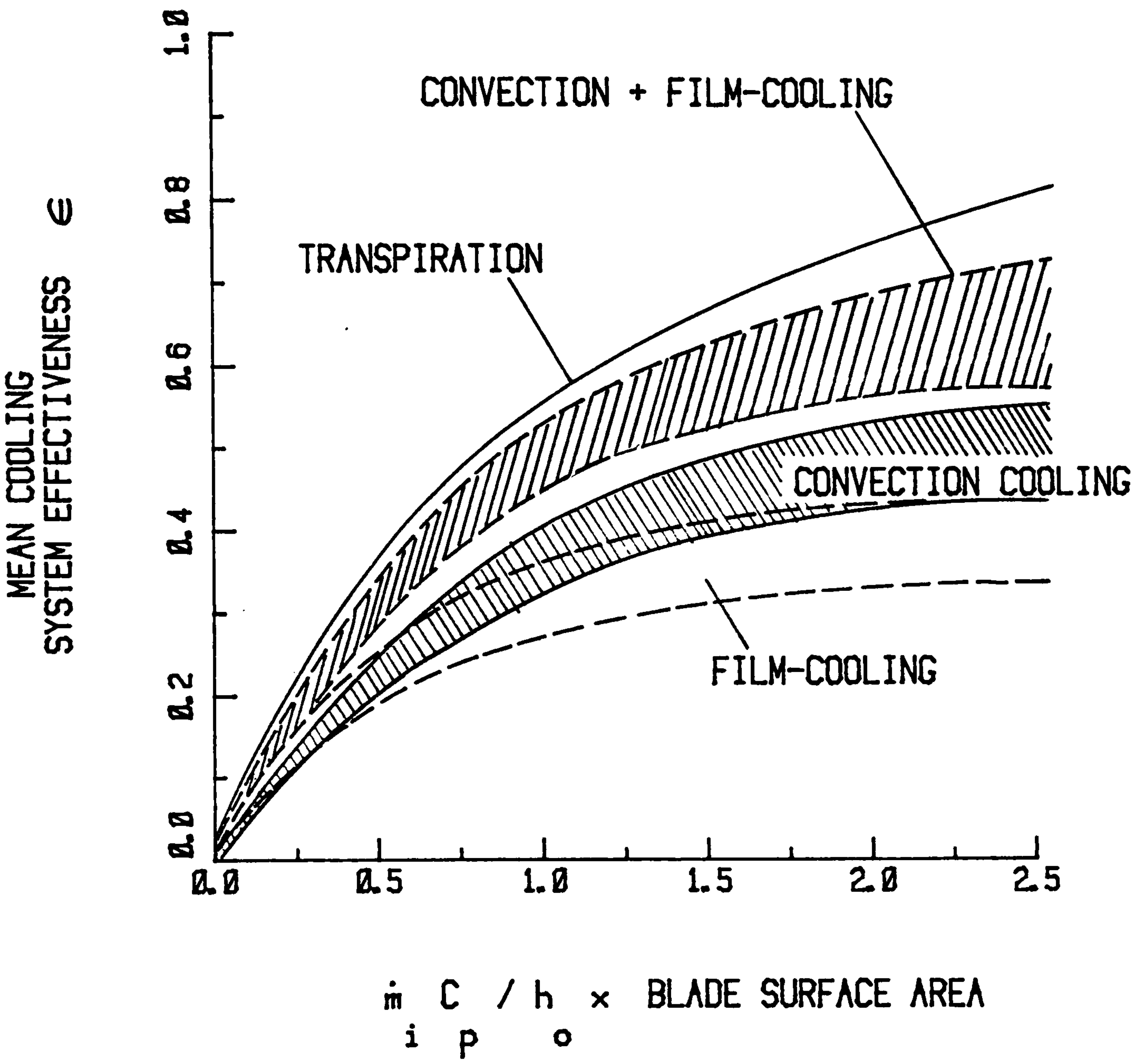

FIG. 1.3 Variation of Cooling System Effectiveness with Different Cooling Techniques (from [1.5])

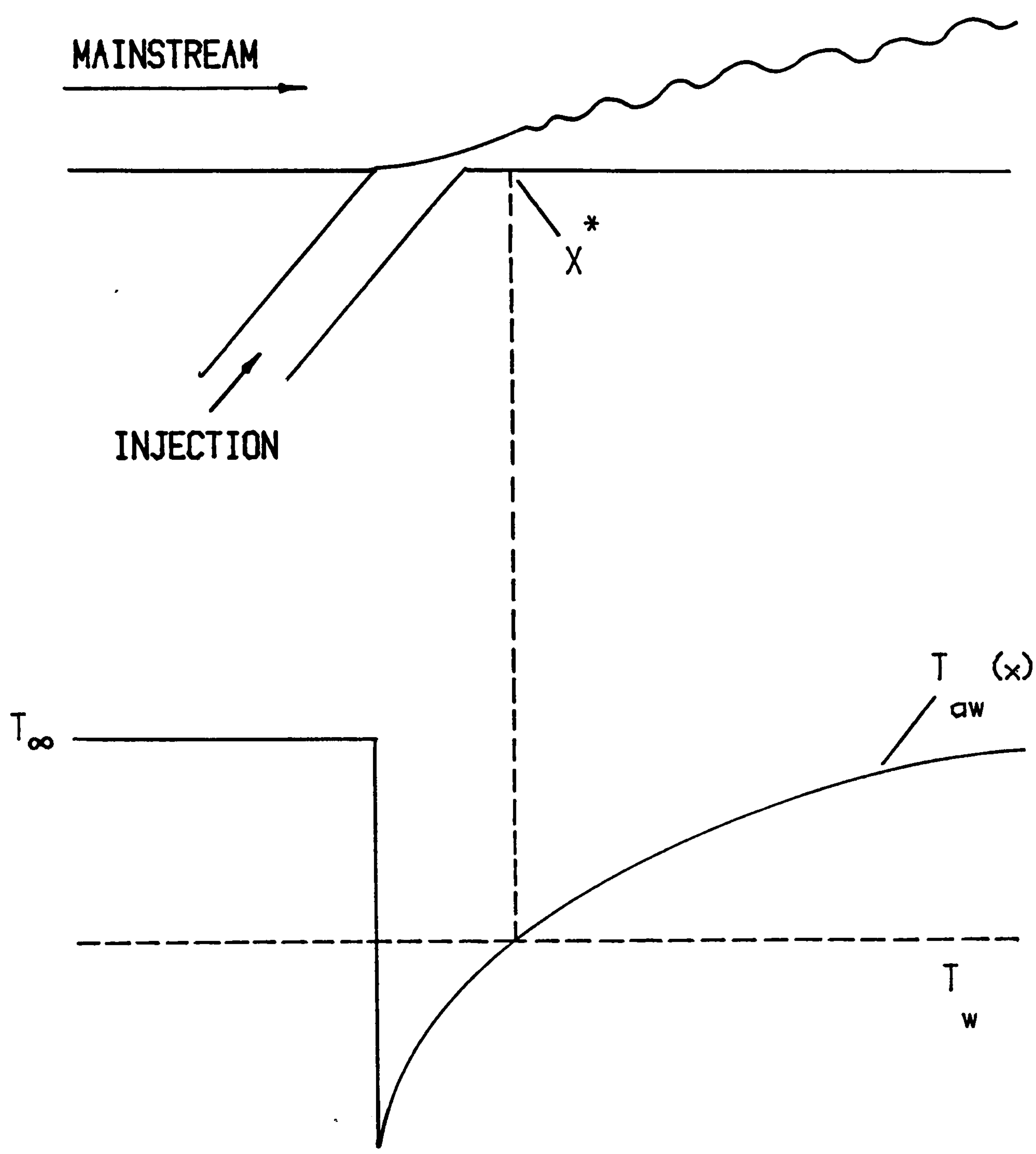

FIG. 2.1 Variation of Adiabatic Wall Temperature with Distance in Film Cooling.

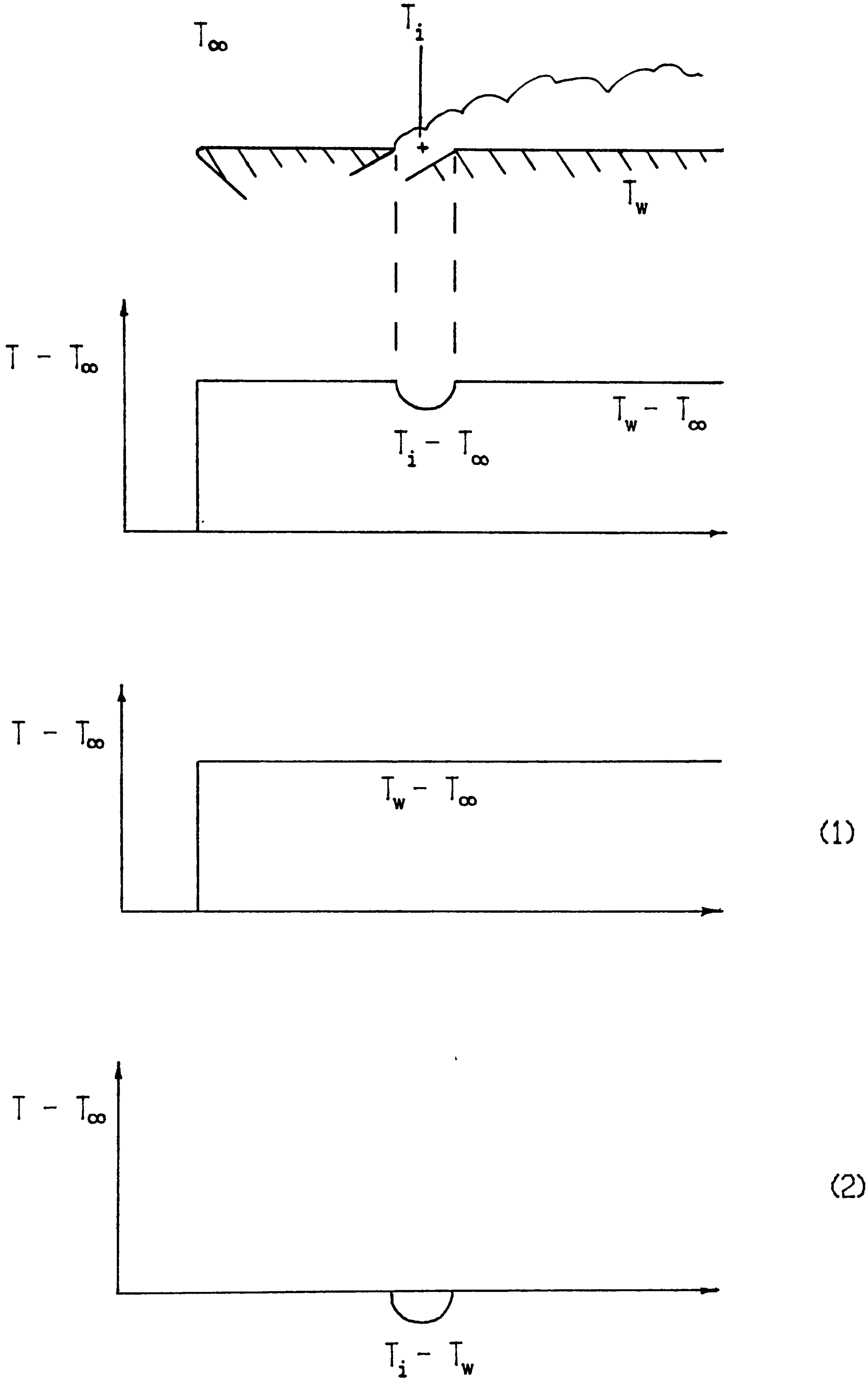

FIG. 2.2 Temperature Boundary Conditions for Film-Cooling.

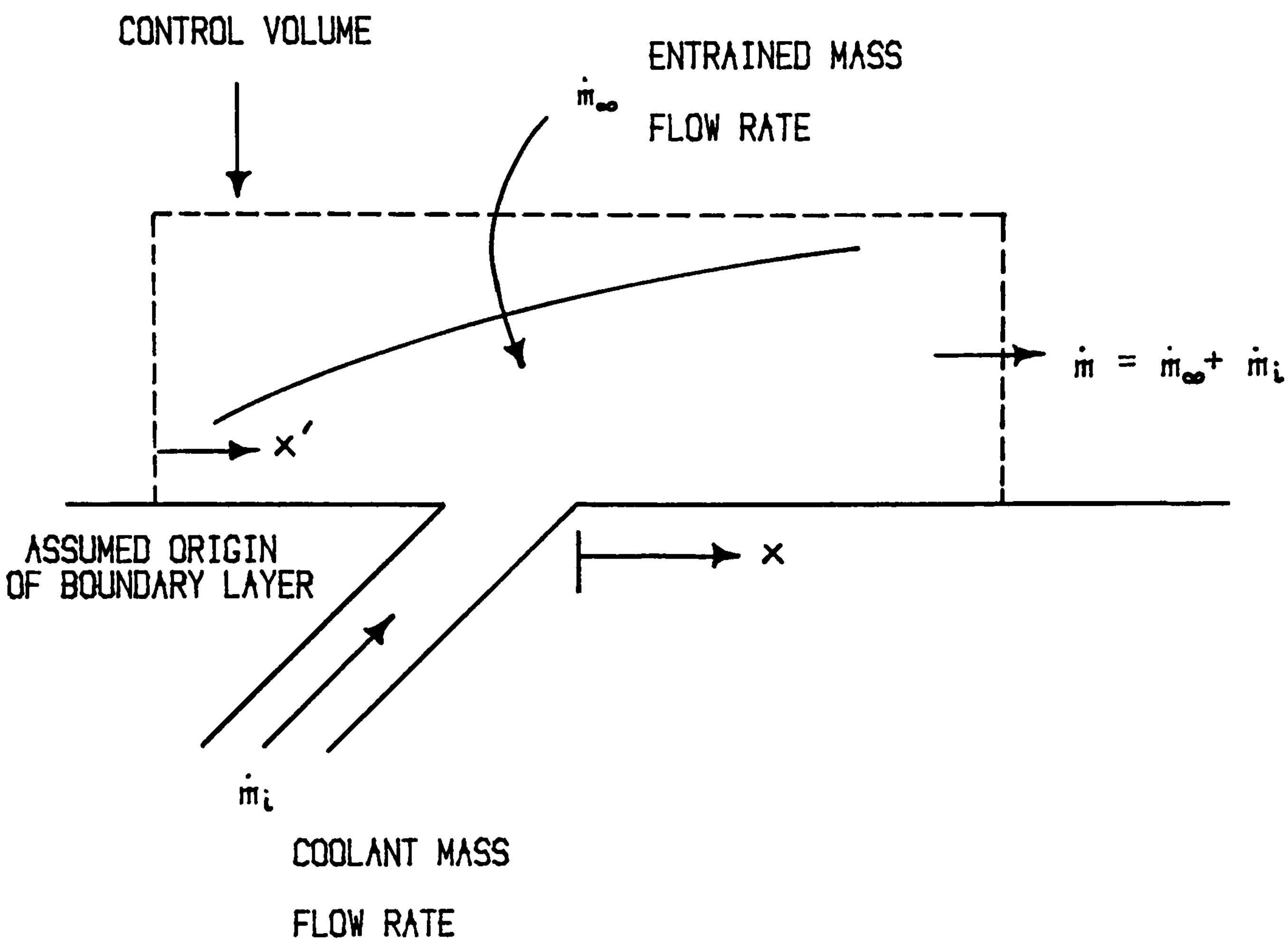

FIG. 4.1 Control Volume for Energy Balance Model.

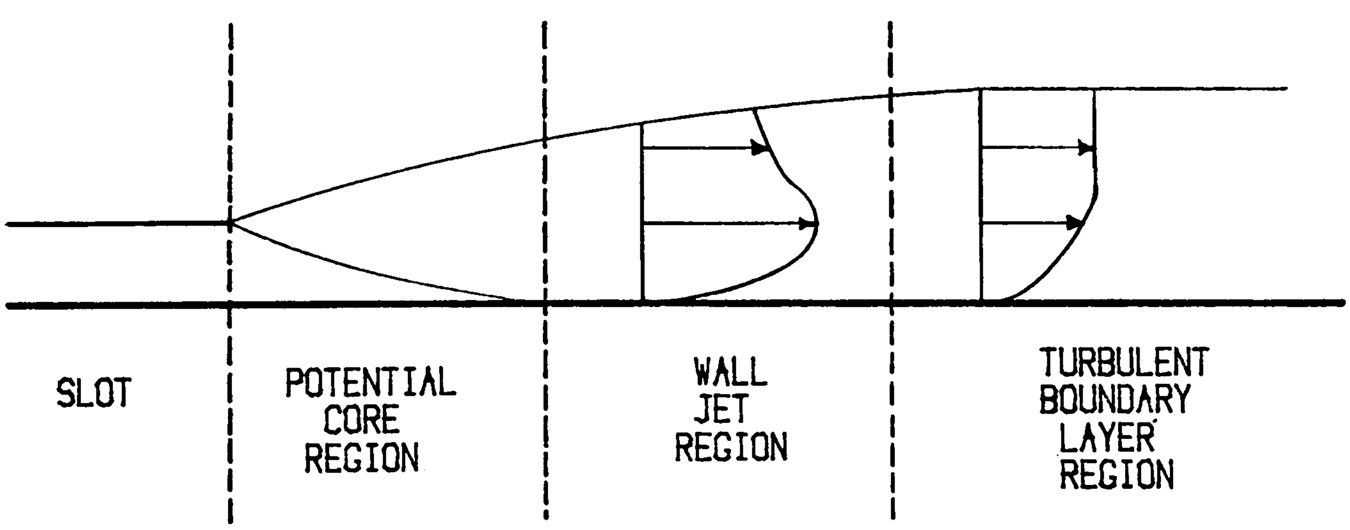

FIG. 4.2 Regions Downstream from a Tangential Slot (from [4.5]).

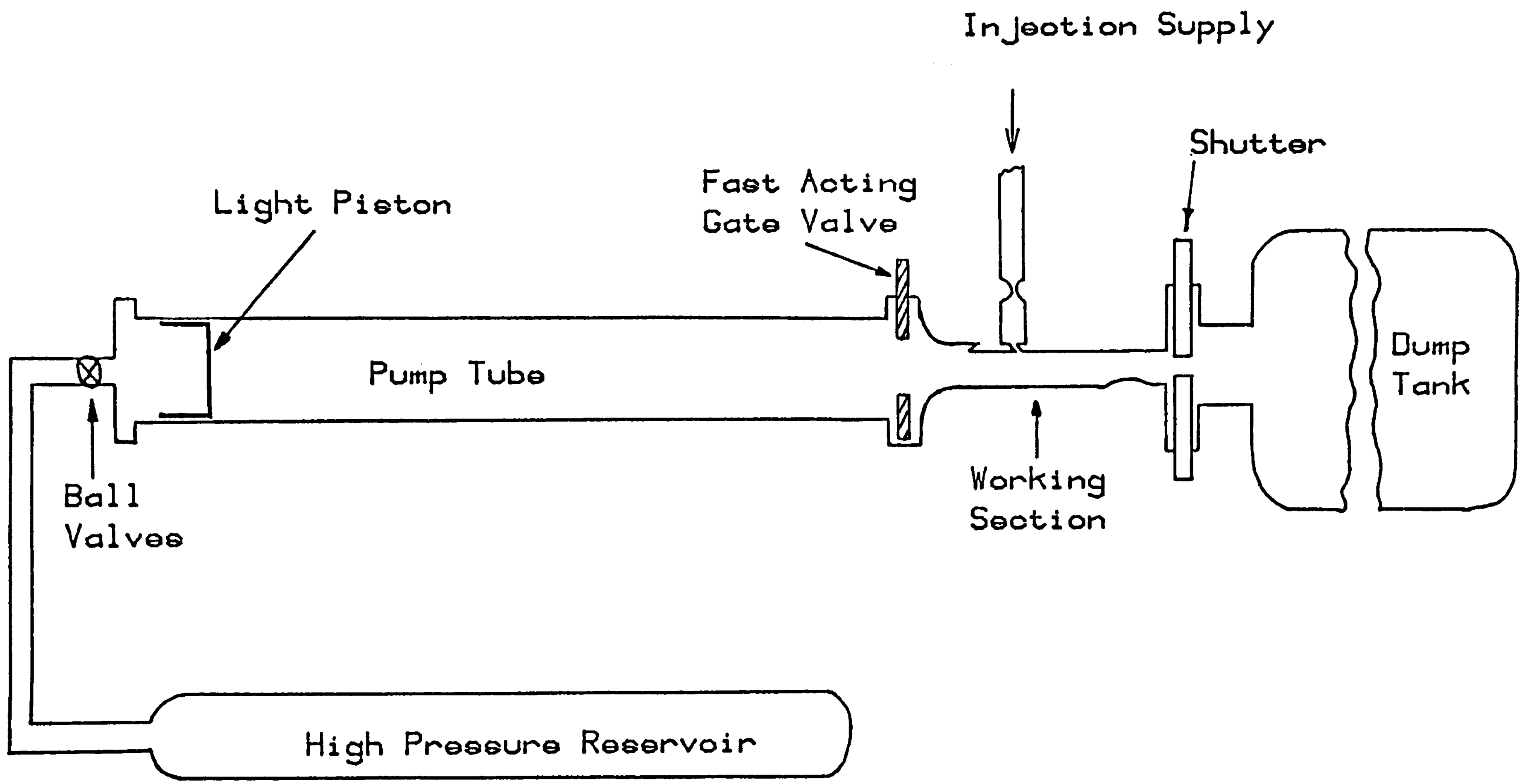

FIG. 5.1 Schematic Diagram of Isentropic Light Piston Tunnel.

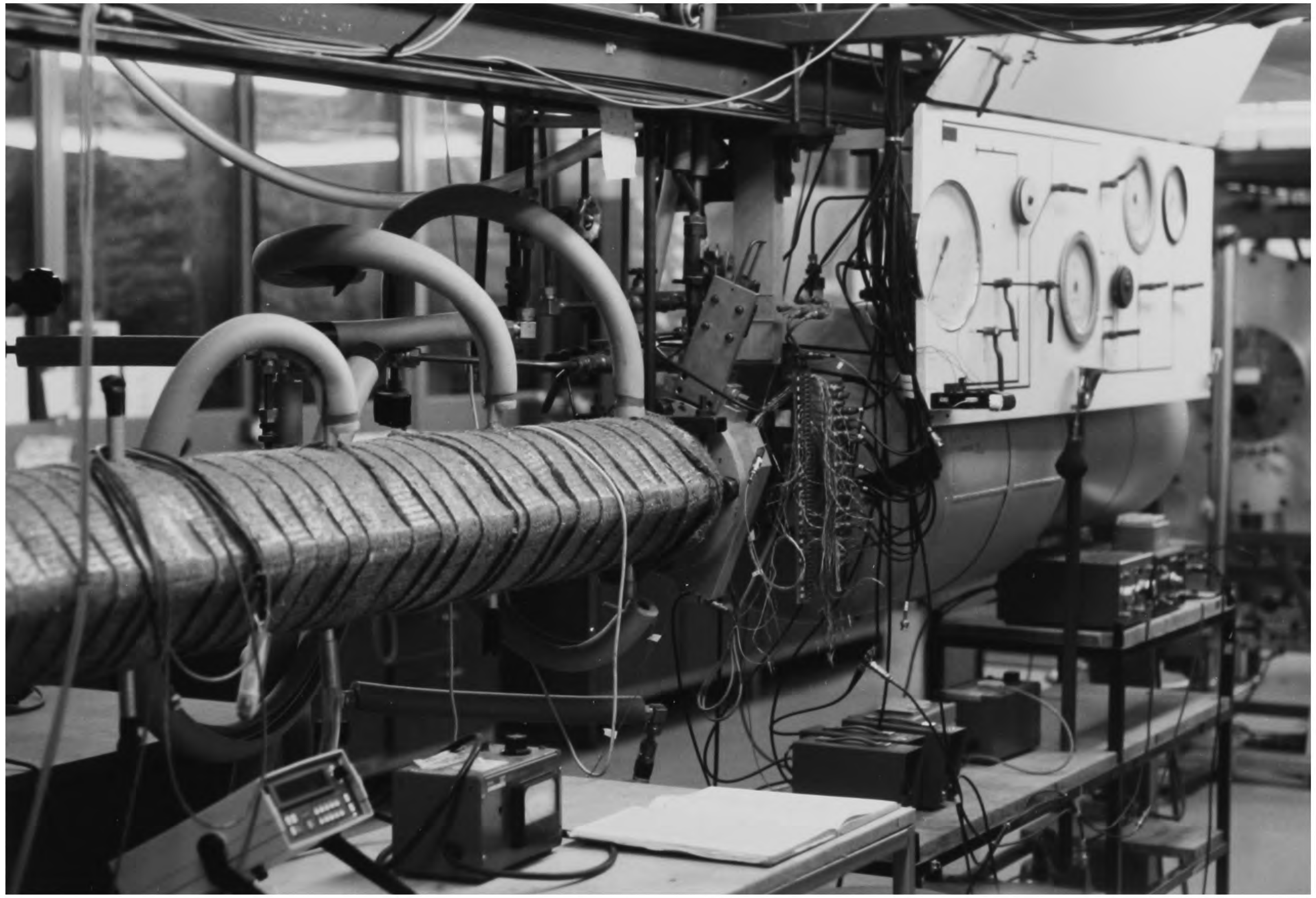

Plate 5.1 View of the 6 Inch Isentropic Light Piston Tunnel.

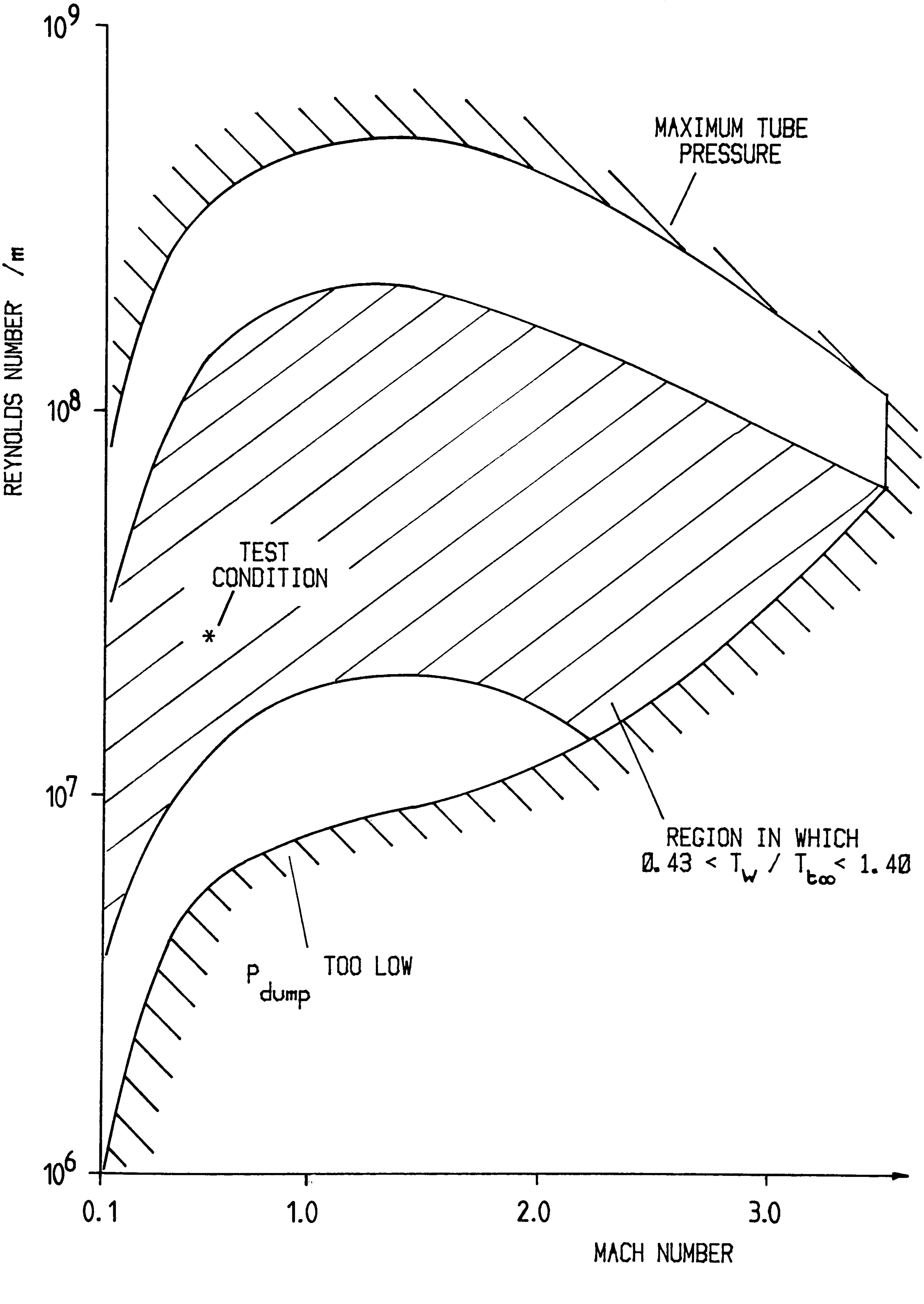

FIG. 5.2 Tunnel Operating Map.

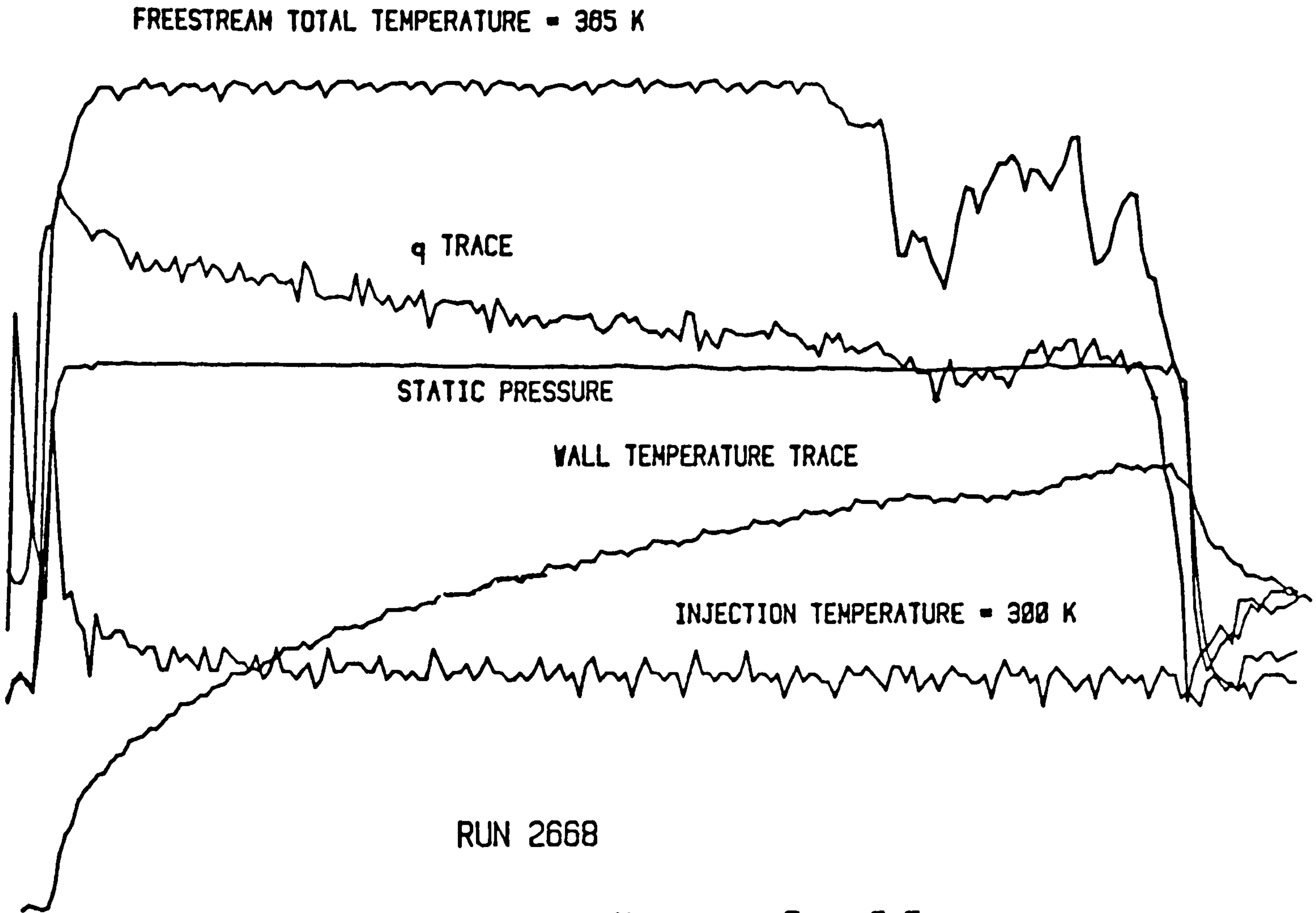

FIG. 5.3 Typical Run Traces - Measuring Time 0.5s

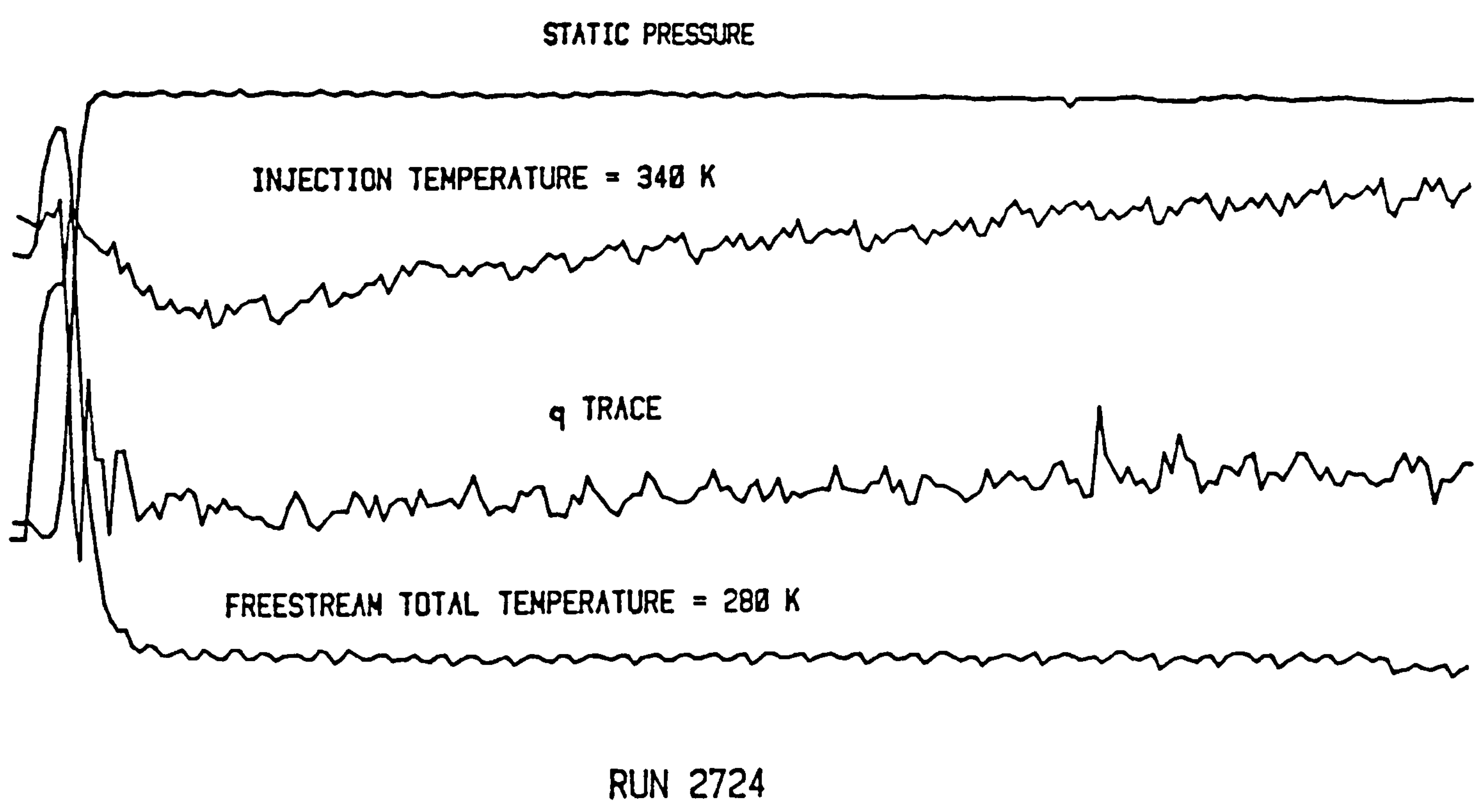

FIG. 5.4 Typical Run Traces - Measuring Time 0.5s

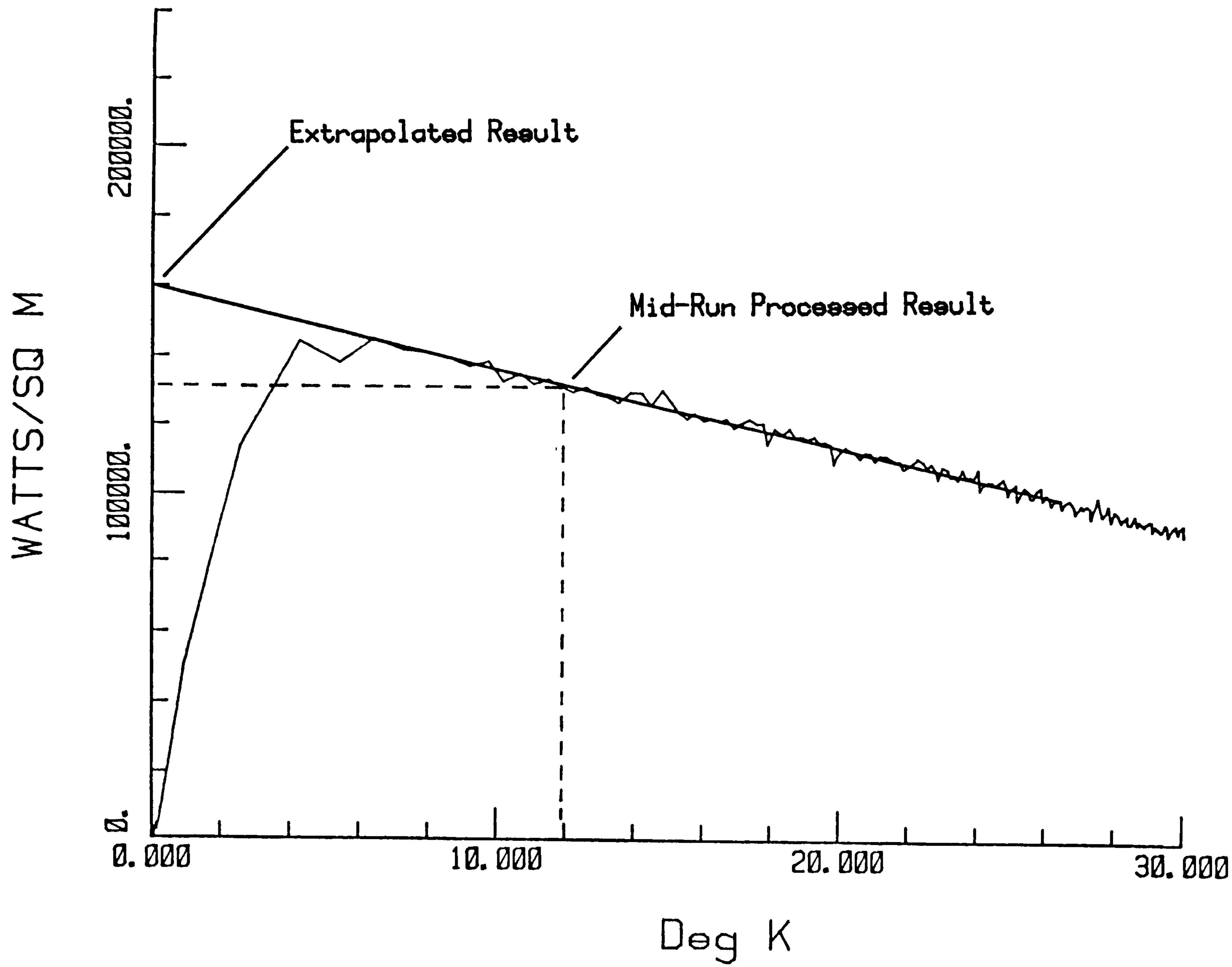

FIG. 5.5 Diagram to Illustrate Different Methods of processing heat transfer data.

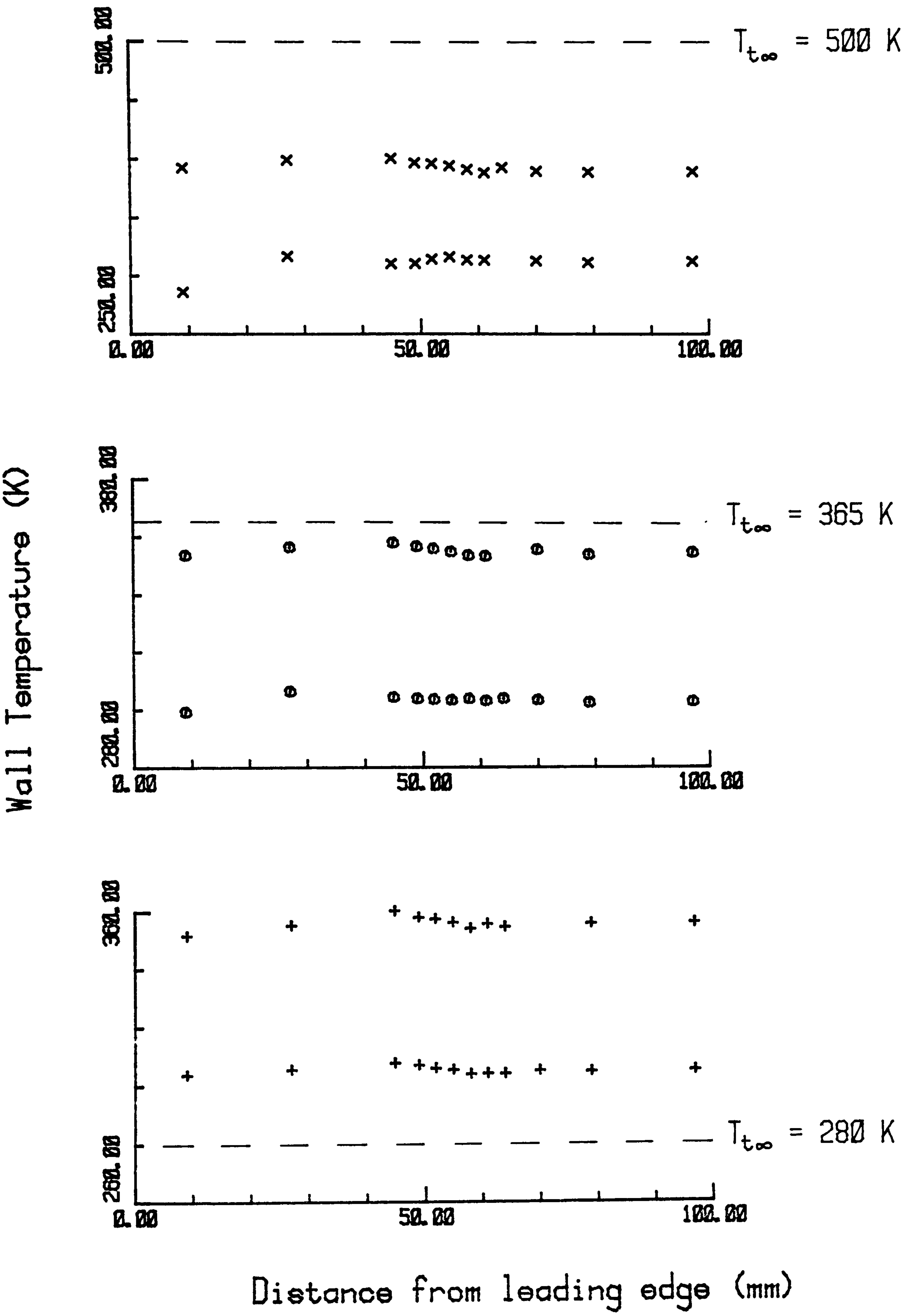

FIG. 5.6(a) Typical wall Temperature Distribution at Measurement time - without Film-Cooling.

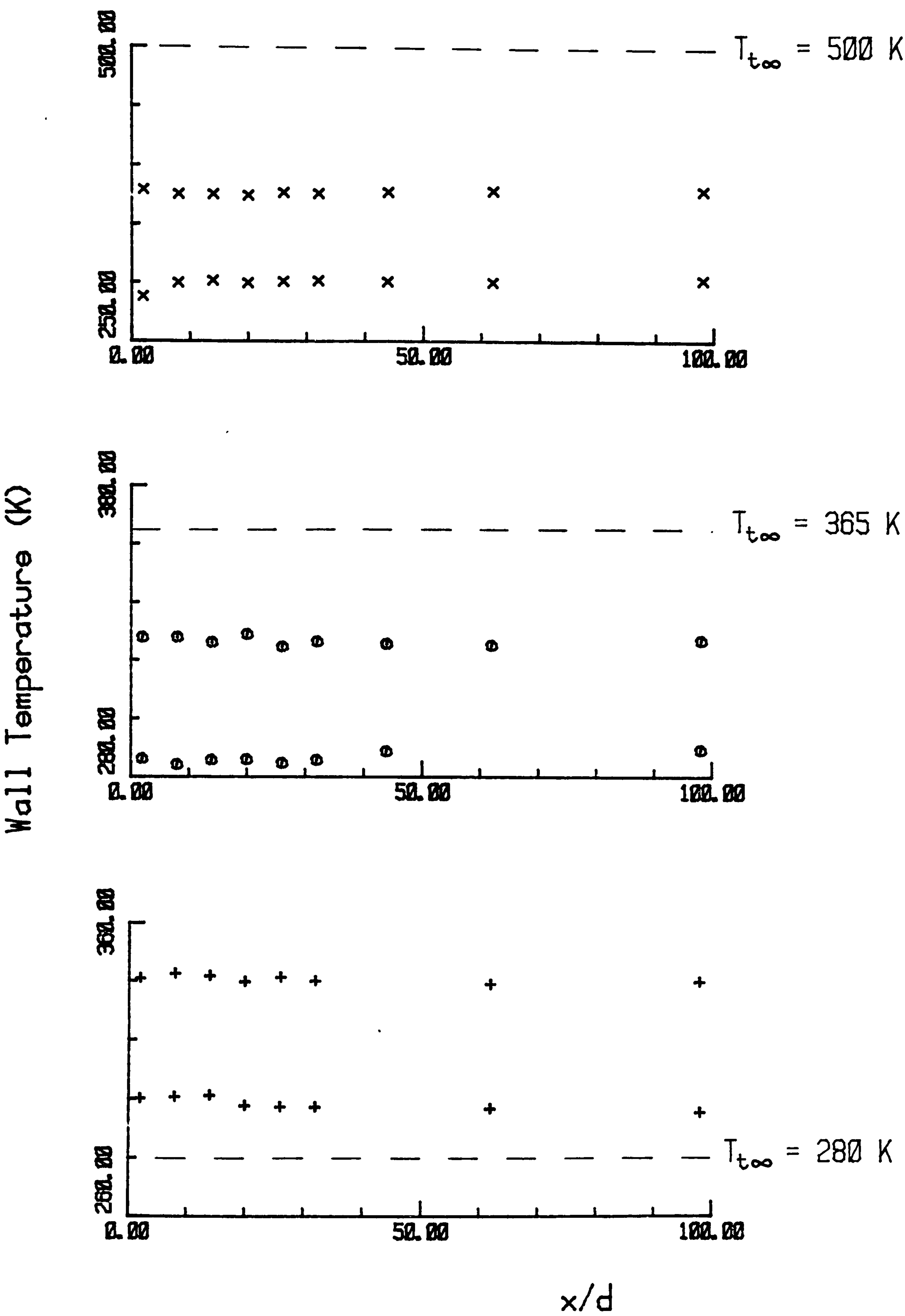

FIG. 5.6(b) Typical wall Temperature Distribution at Measurement time - Film-Cooled.

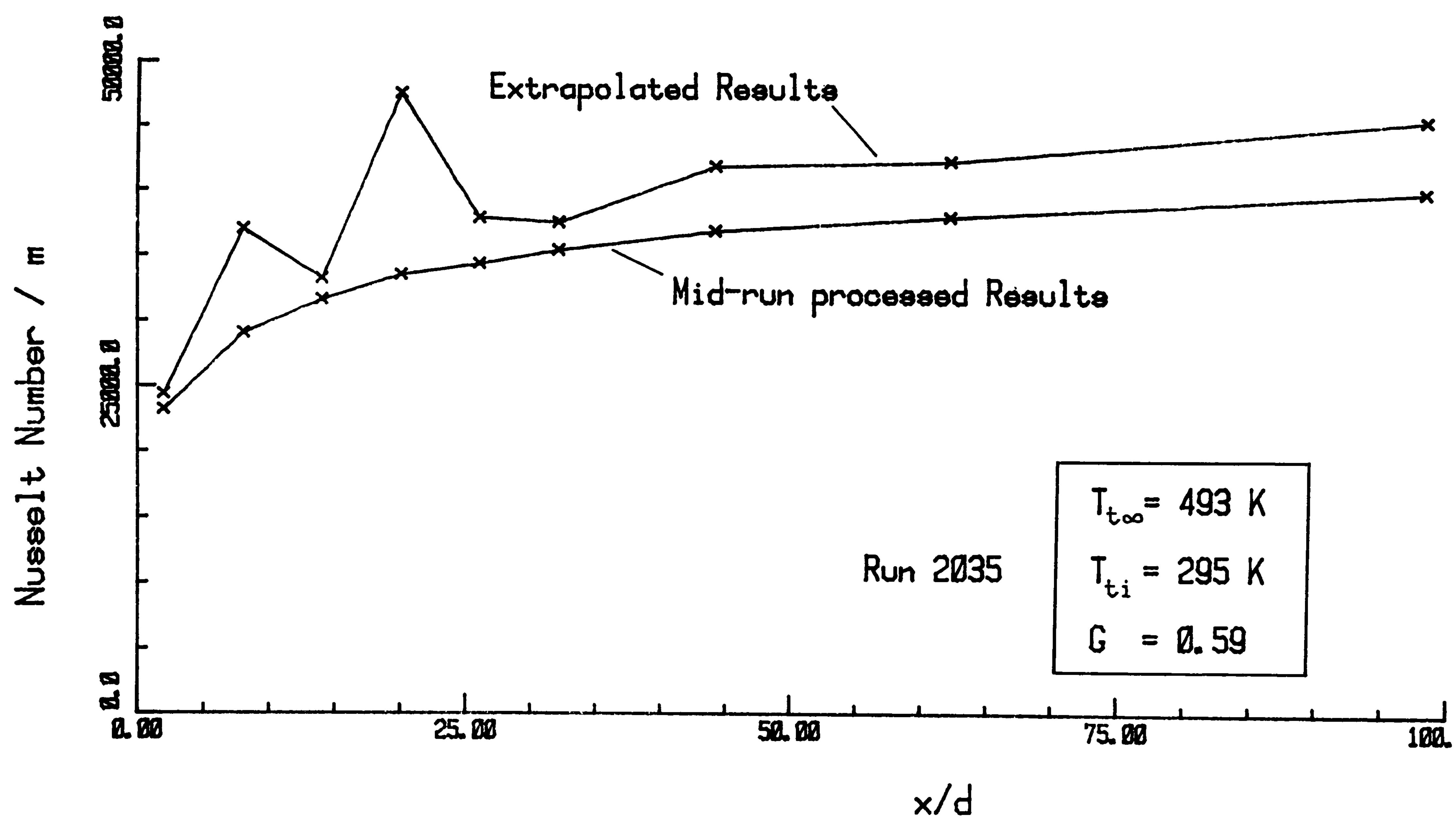

FIG. 5.7 Comparison Between Extrapolated and Mid-run processed results.

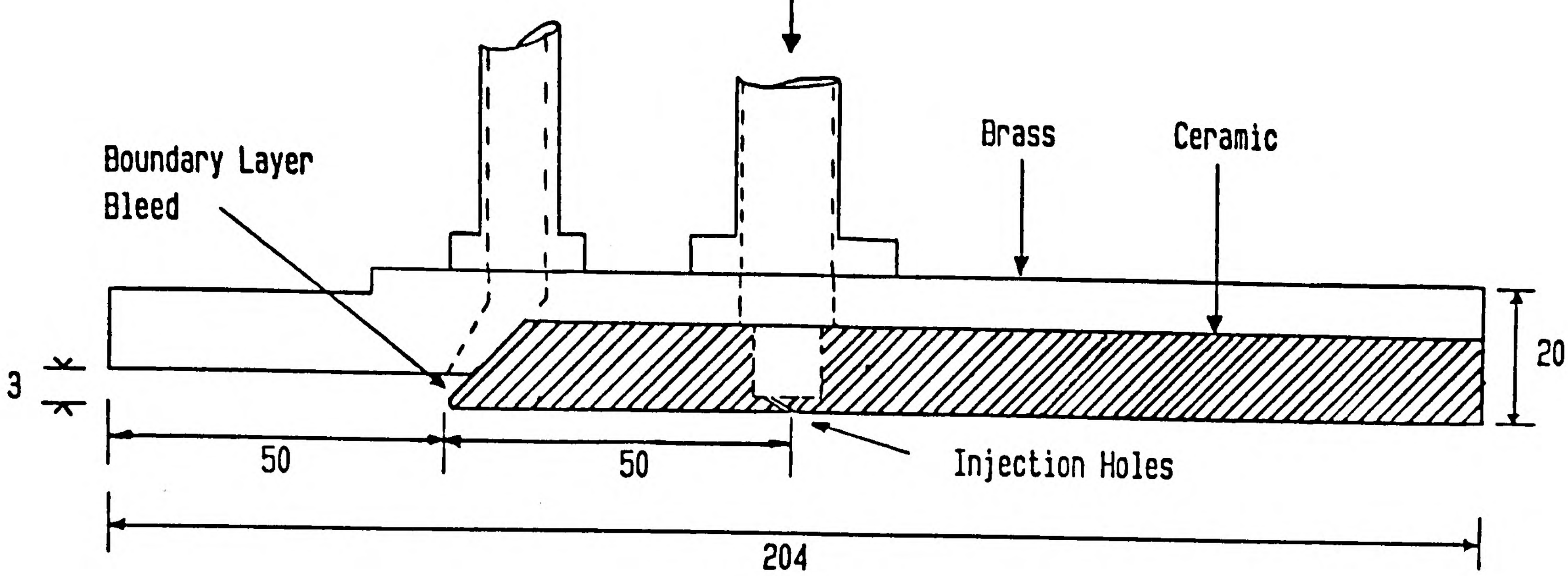

(Dimensions in mm)

Fig. 5.8 Diagram of Working Section Liner.

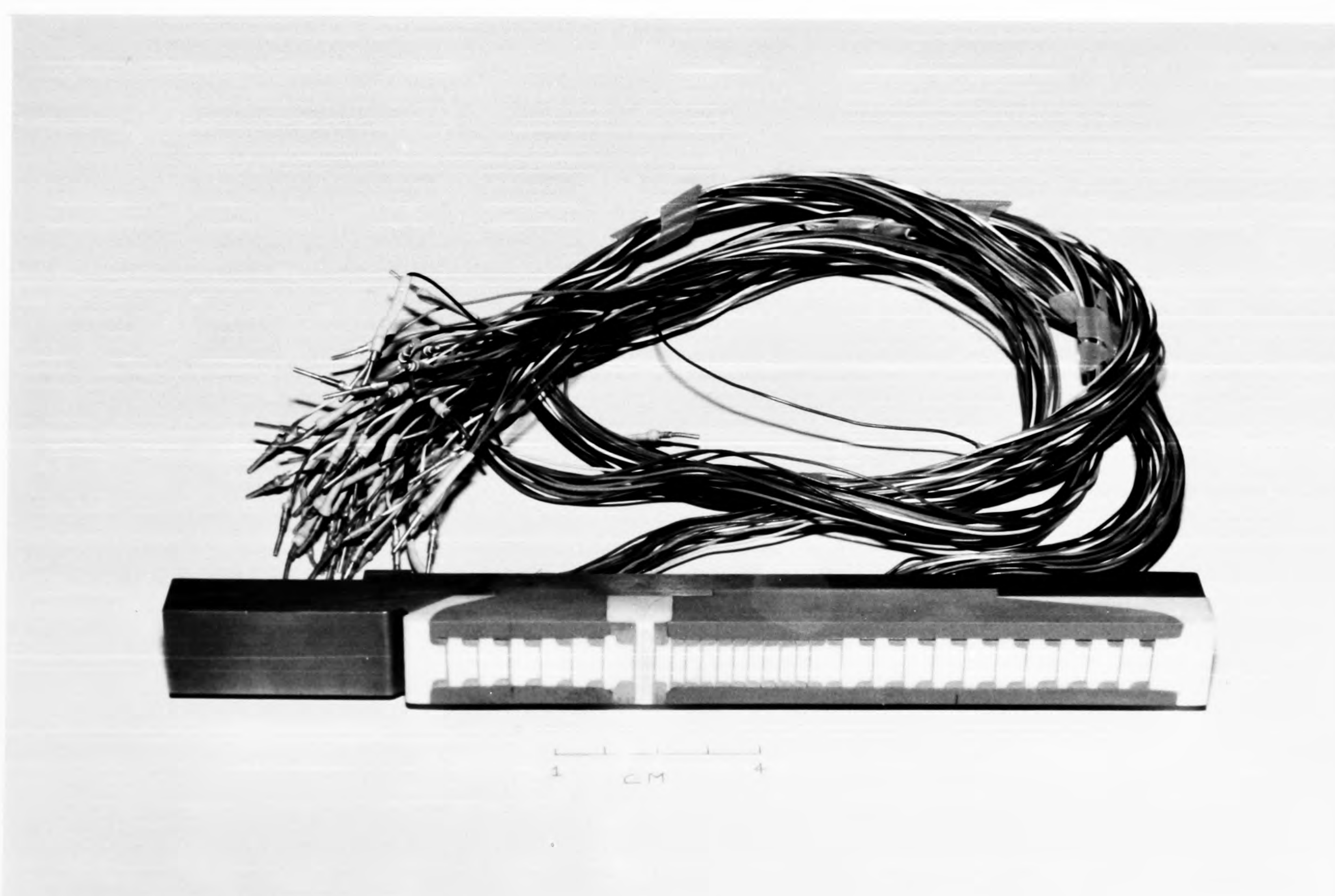

Plate 5.2 Completed, Instrumented, Ceramic Liner.

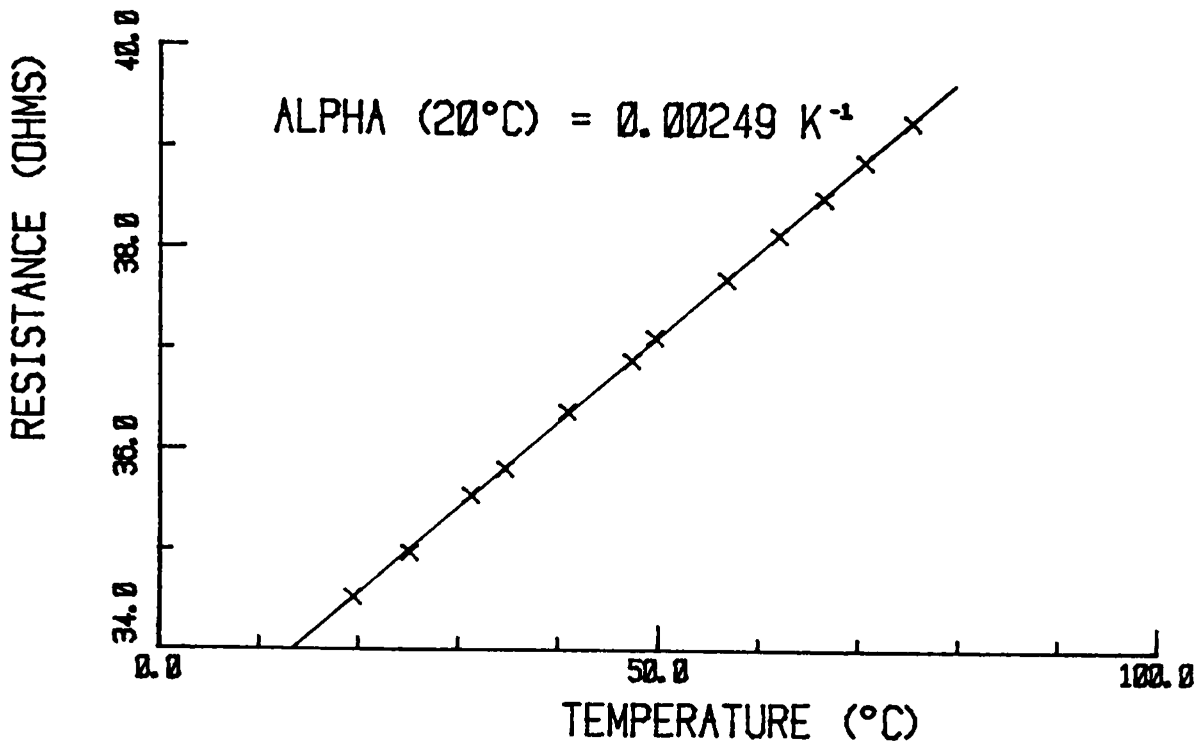

FIG. 5.9 Specimen Calibration of Thin Film Gauge.

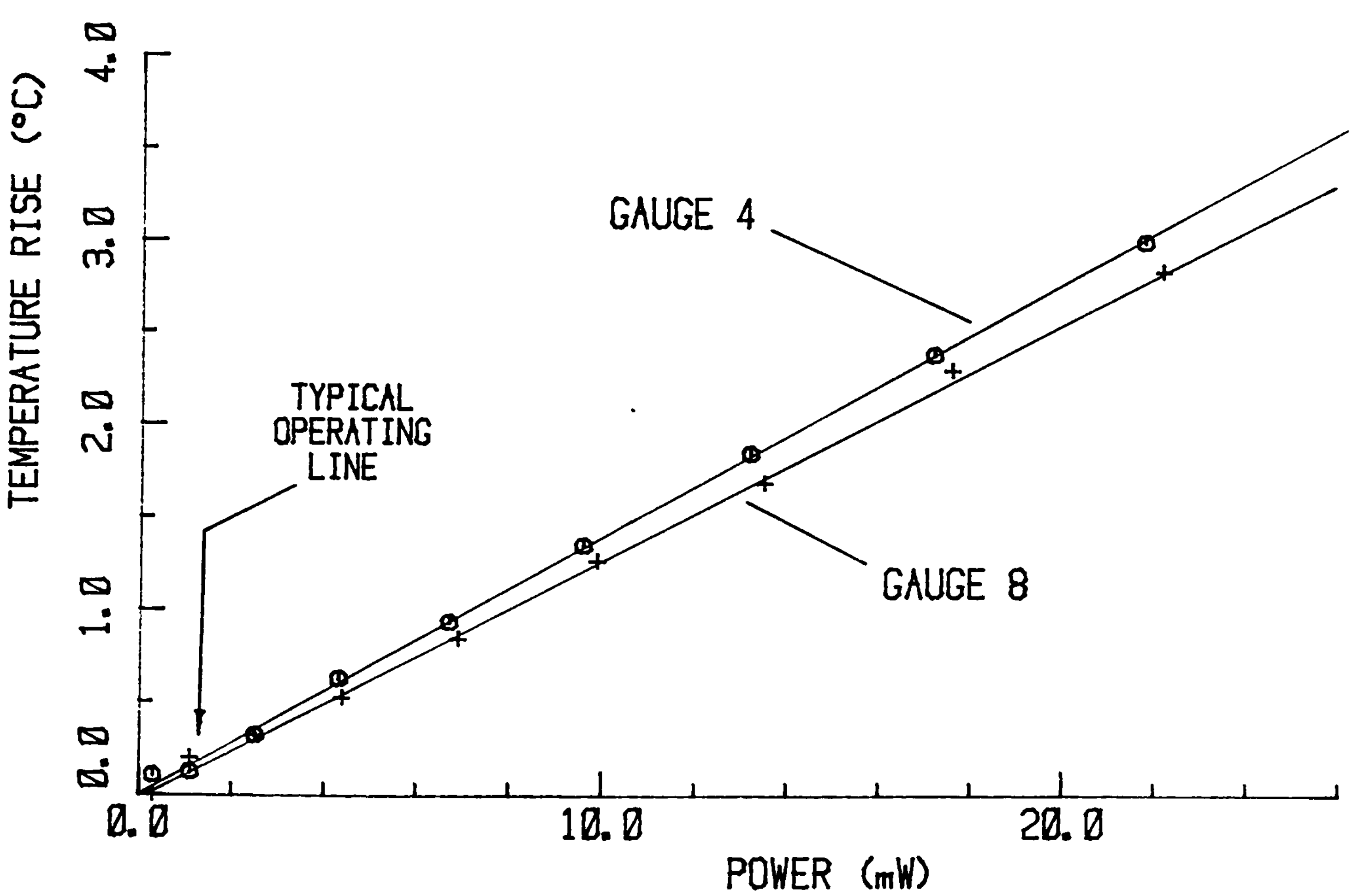

FIG. 5.10 Effect of Ohmic Heating on Gauge Temperature.

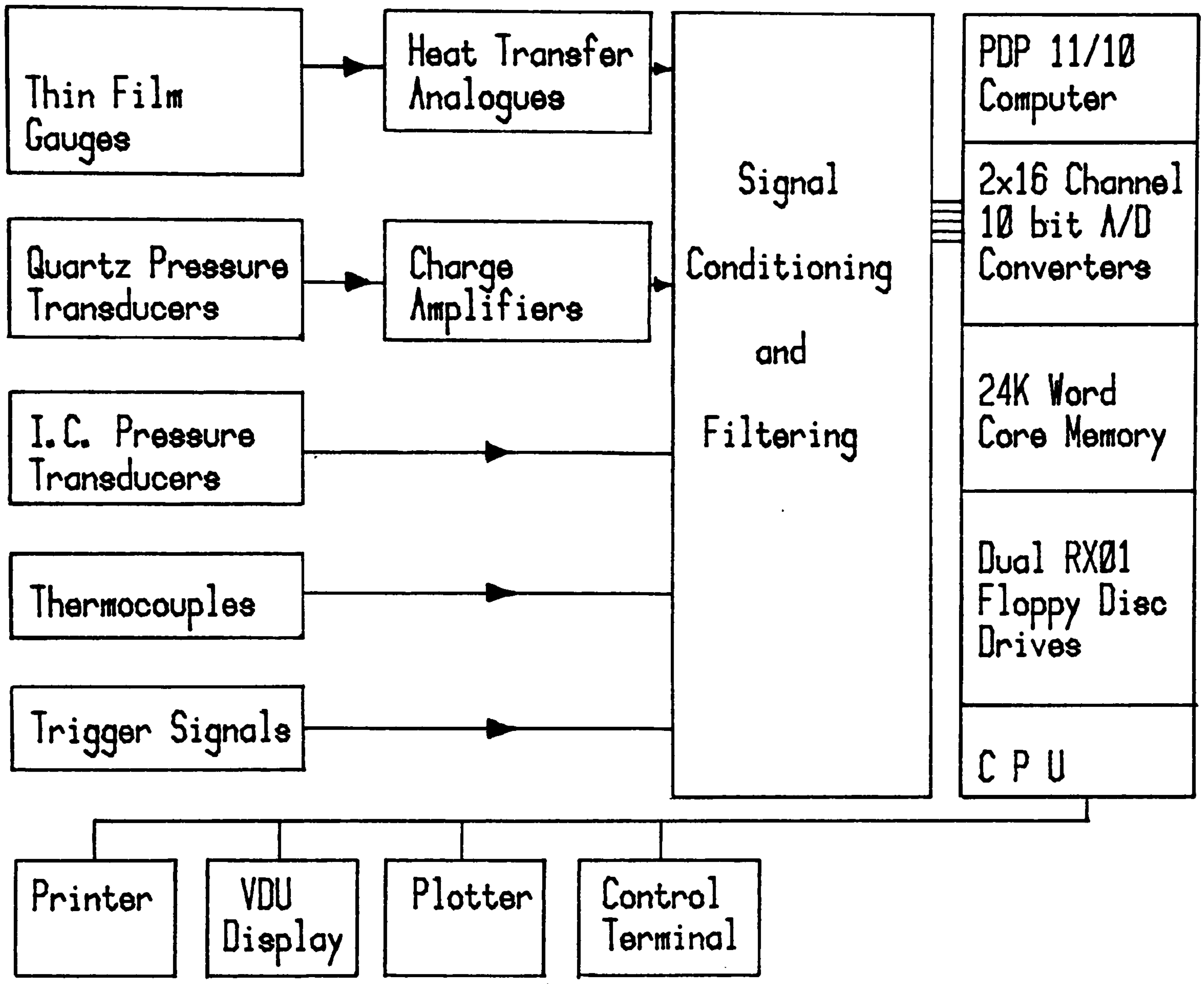

Analogue to Digital Conversion:

2 DEC 10 bit AR11's, each 16 ch A/D, 2 ch D/A with programmable clock. Maximum conversion rate 15 kHz. Input voltage range -2.5 V - +2.5 V.

Each run : 200 samples per channel on 32 channels, in 0.5 s.

FIG. 5.11 Computer Data Acquisition and Processing System.

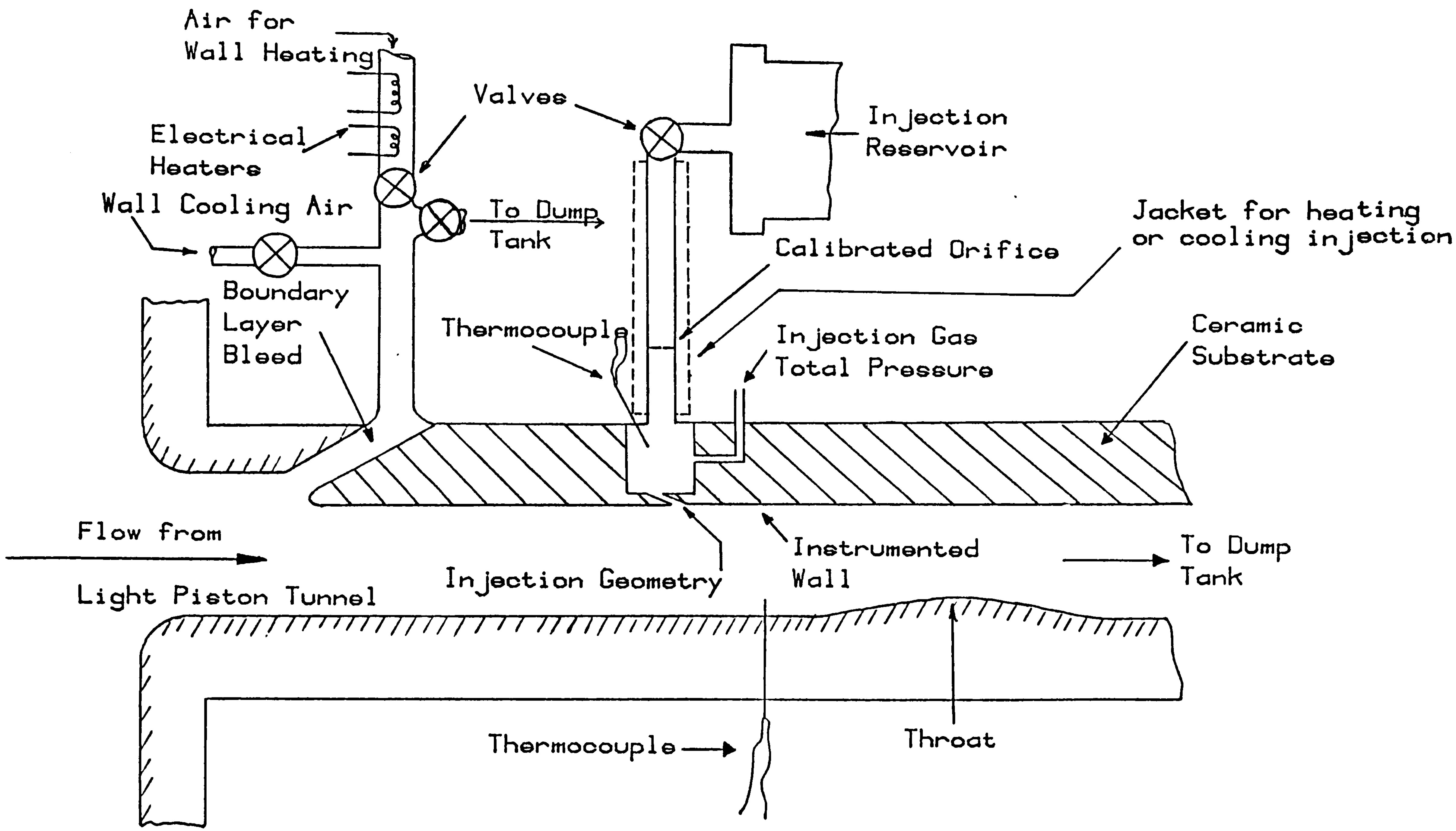

FIG. 5.12 Schematic Diagram of Working Section.

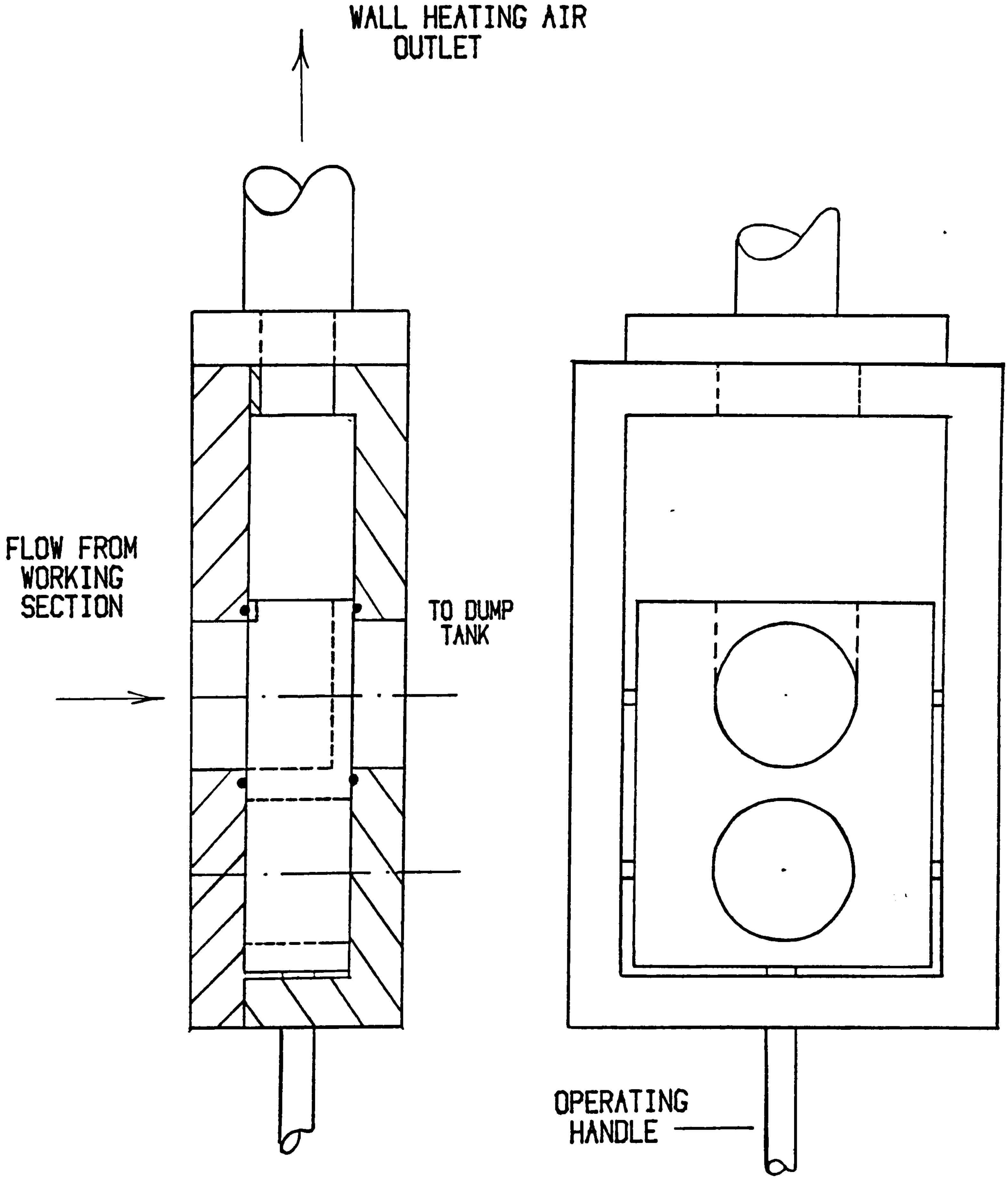

FIG. 5.13 Shutter for isolating the Dump Tank during pre-run wall heating.

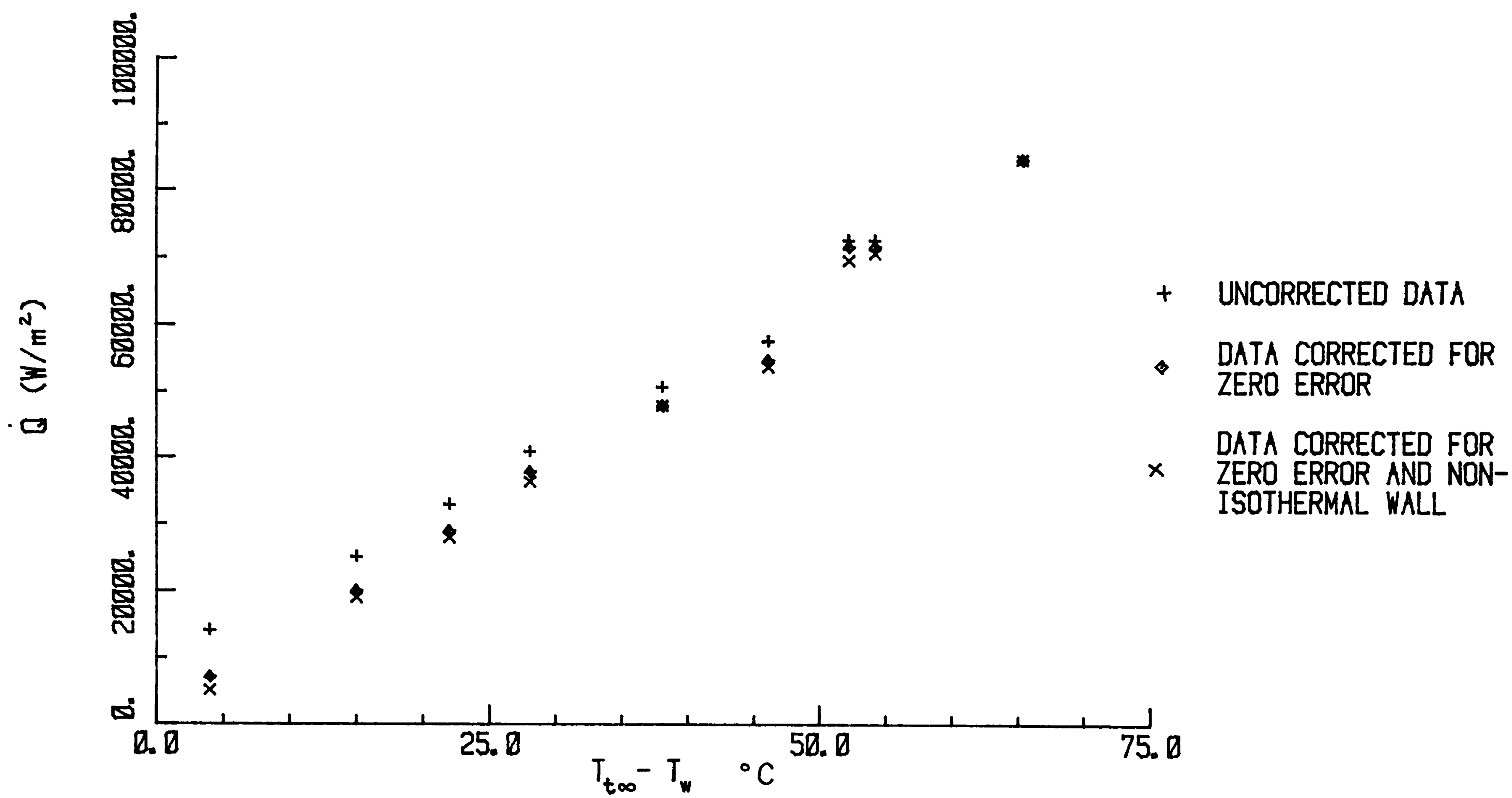

FIG. 5.14 Uncooled Flat Plate Heat Transfer Results - Effect of pre-run Convection before Installing the Shutter.

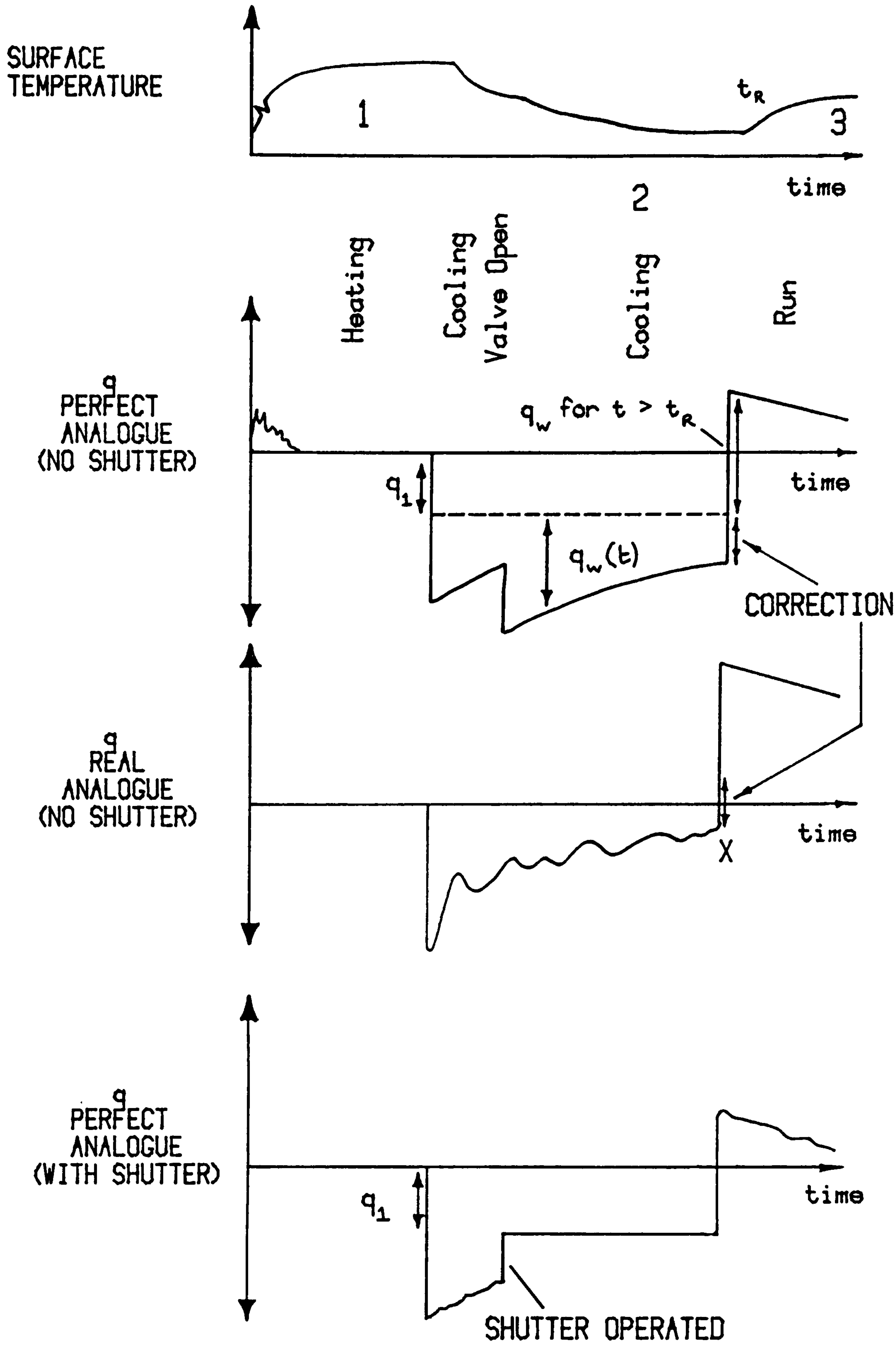

FIG. 5.15 Sketch of temperature, real analogue and perfect analogue traces covering pre-run heating, the cooling period and a run.

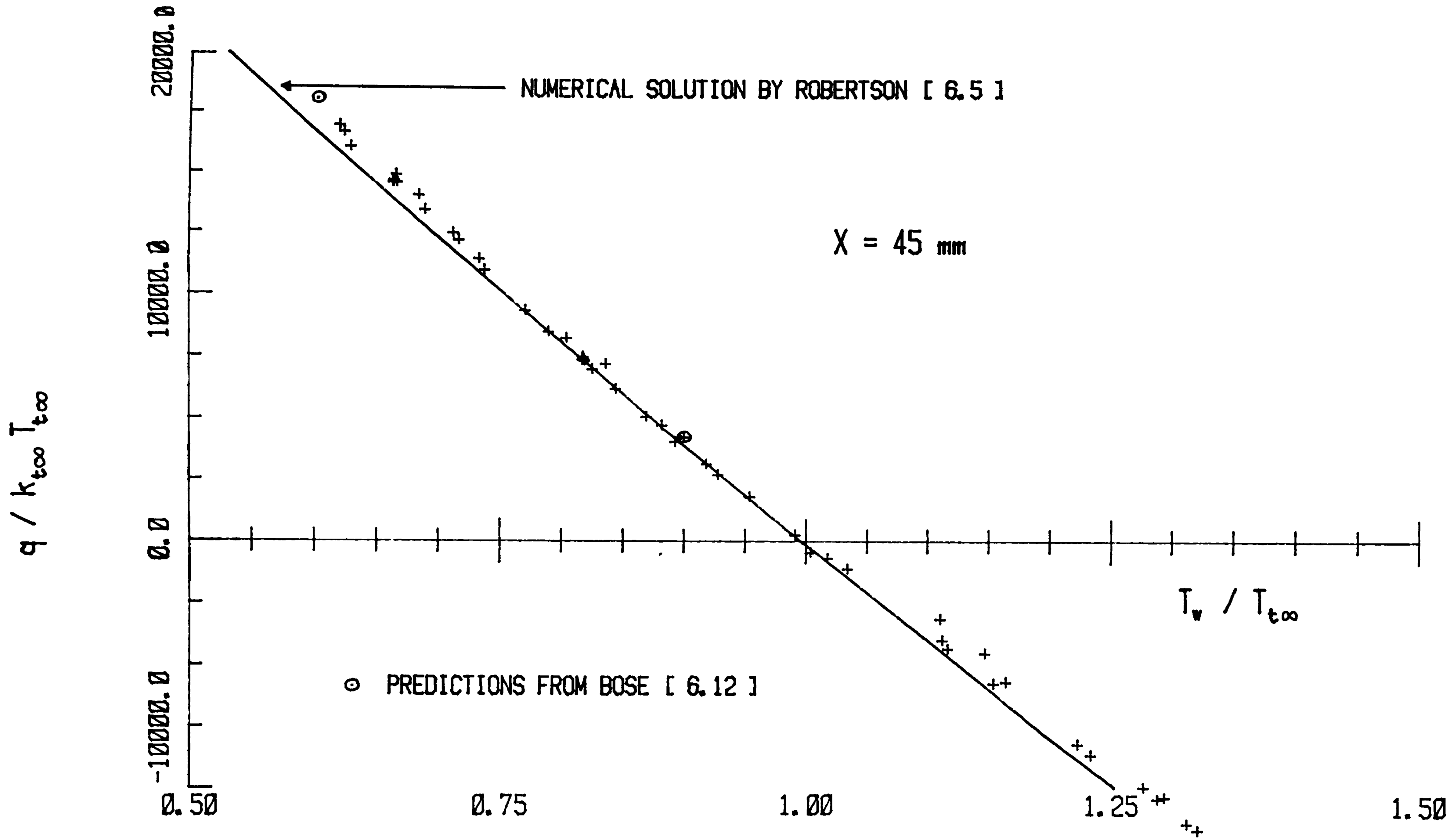

FIG. 6.1(a) Experimental Data Showing Effect of Property Variations on a Turbulent Boundary Layer.

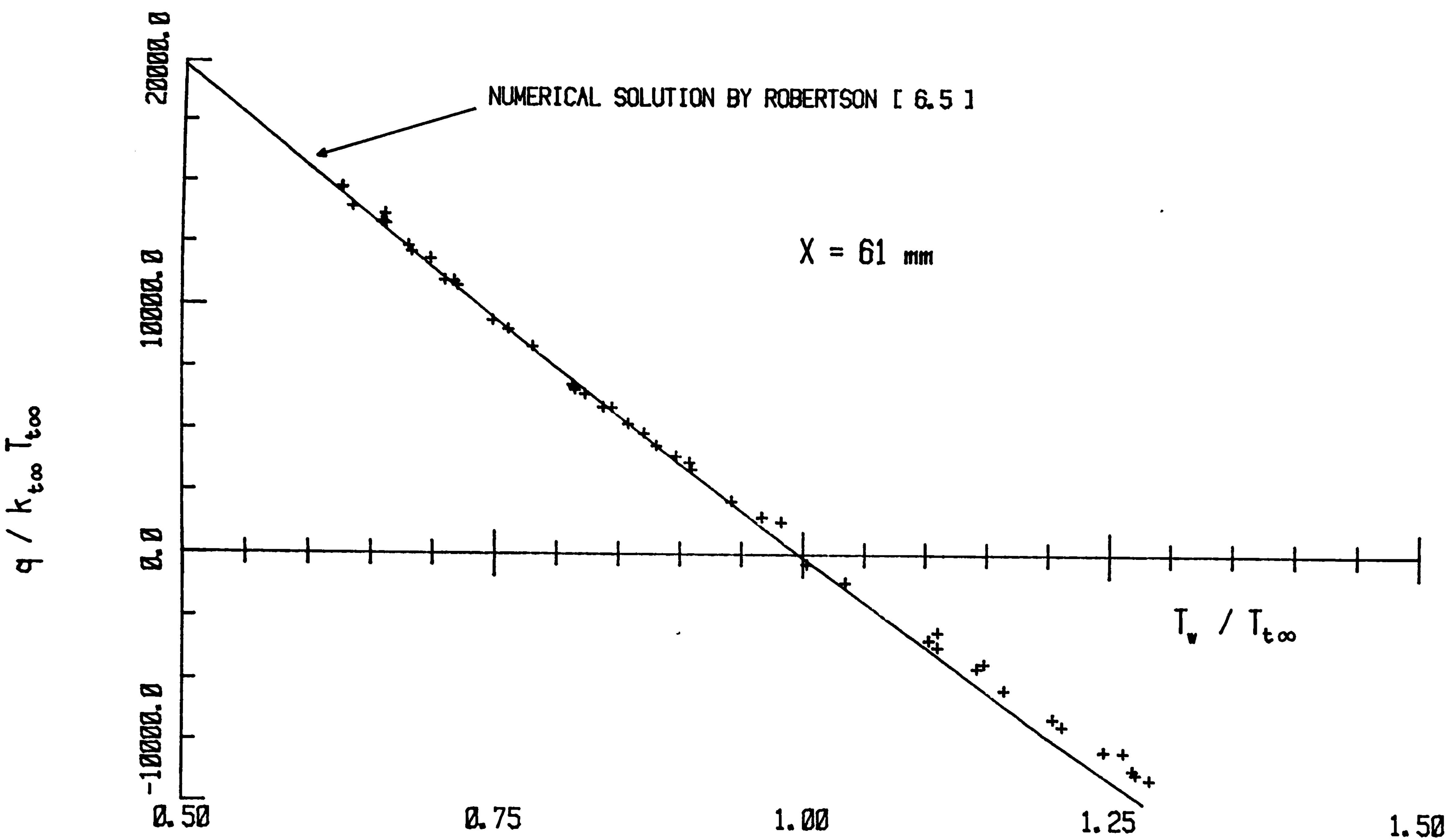

FIG. 6.1(b) Experimental Data Showing Effect of Property Variations on a Turbulent Boundary Layer.

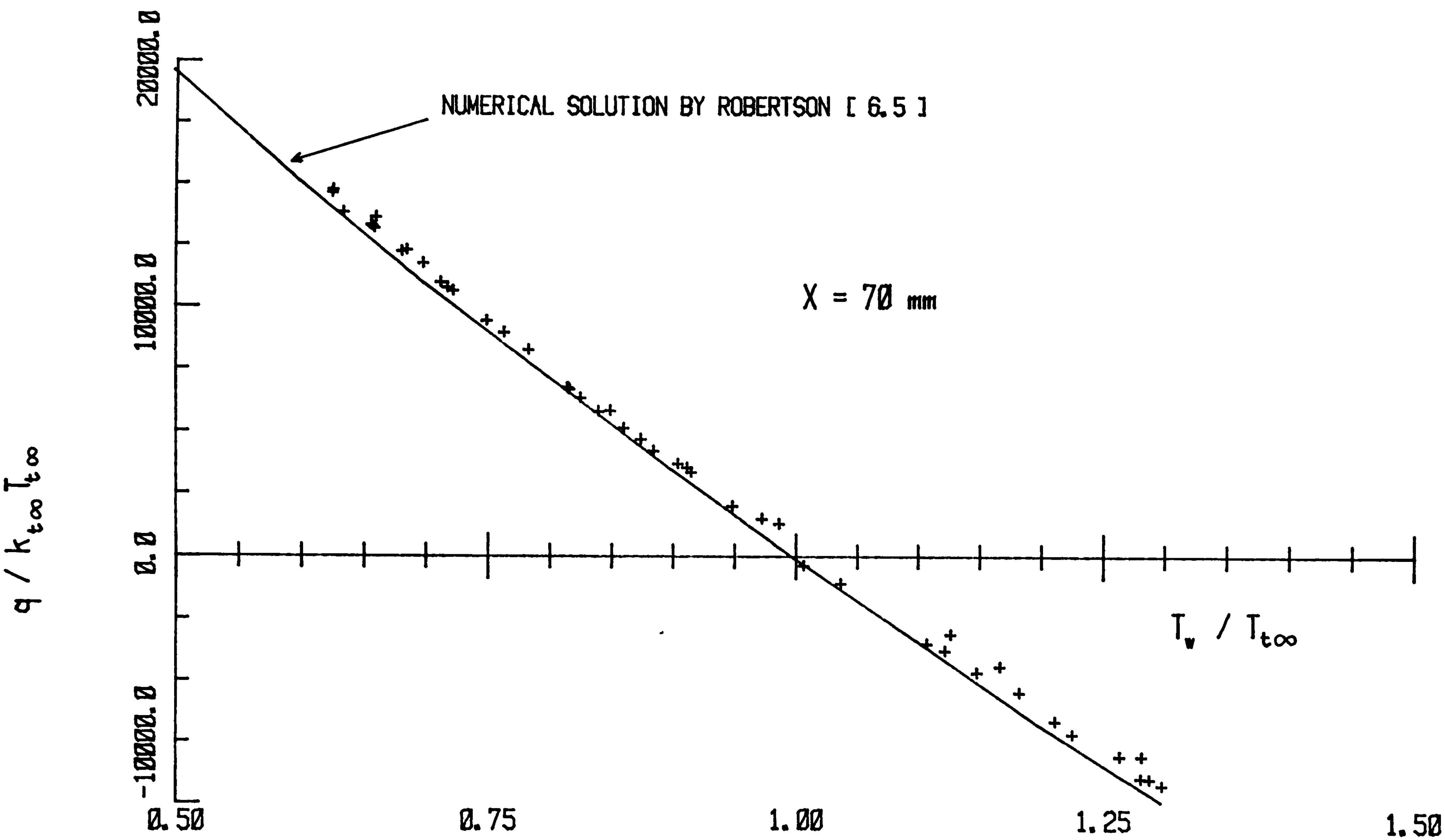

FIG. 6.1(c) Experimental Data Showing Effect of Property Variations on a Turbulent Boundary Layer.

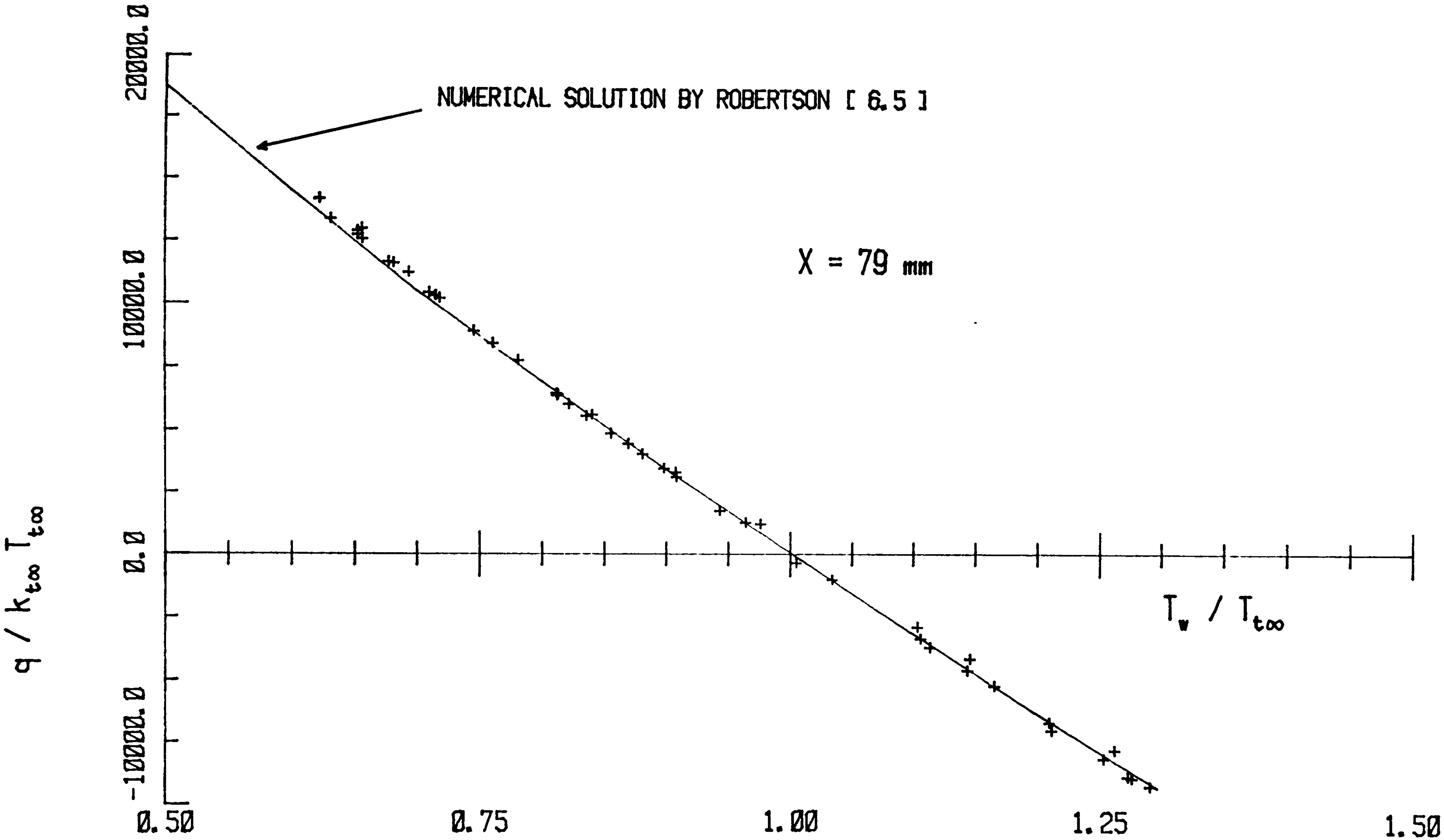

FIG. 6.1(d) Experimental Data Showing Effect of Property Variations on a Turbulent Boundary Layer.

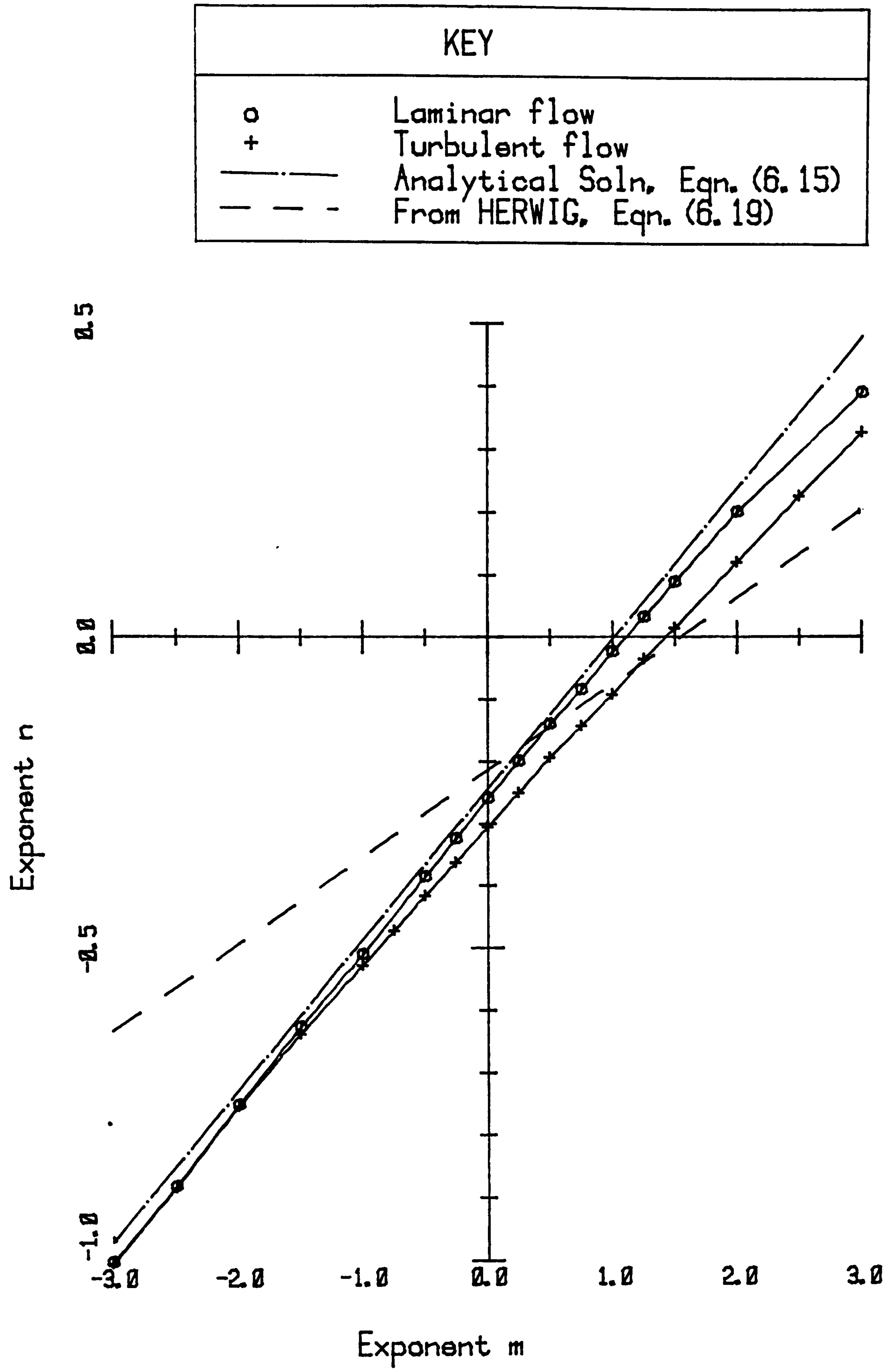

FIG. 6.2 Relationship Between Viscosity-Temperature Ratio Exponent and Nusselt Number-Temperature Ratio Exponent

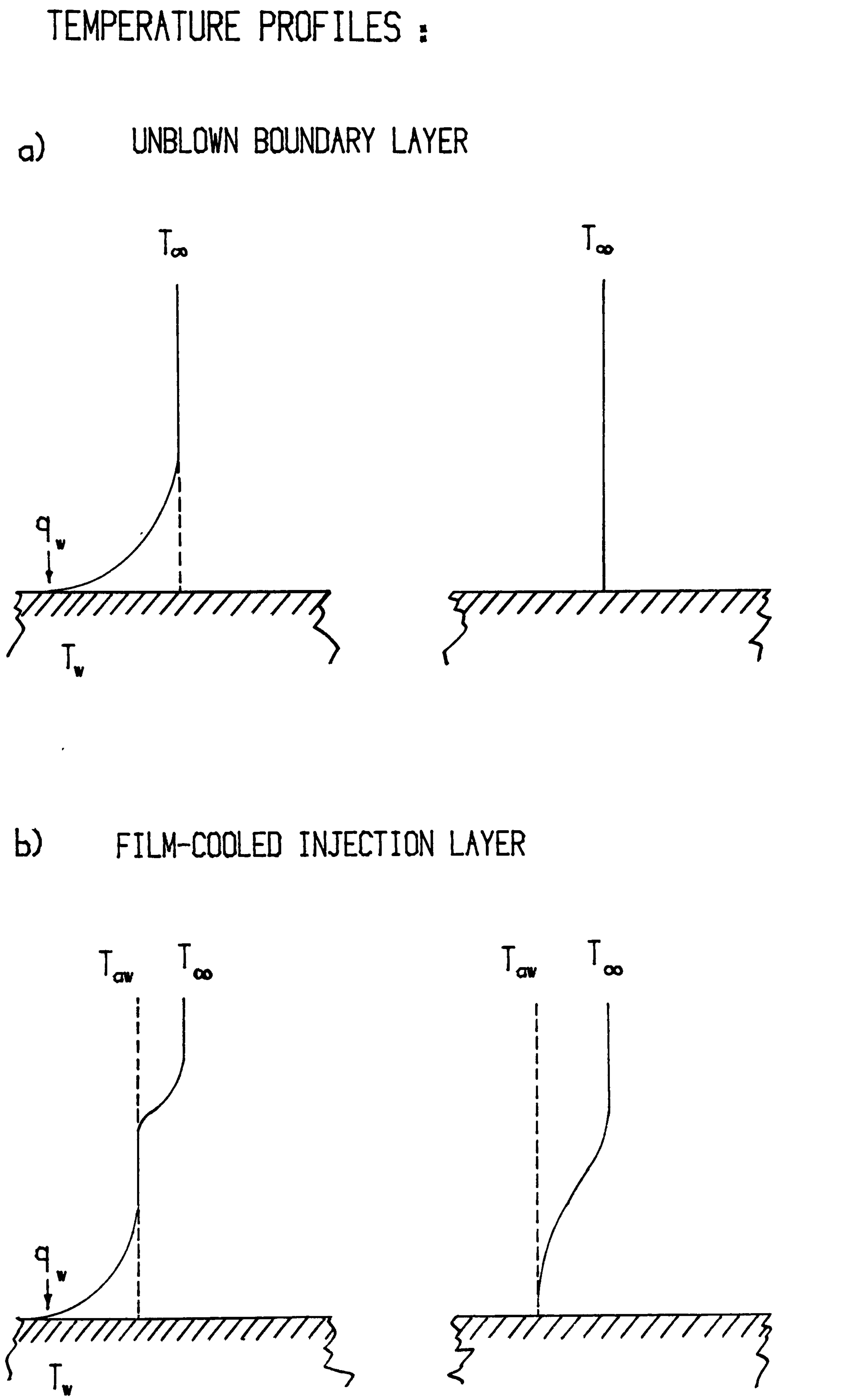

FIG. 6.3 Similarity Between T_{aw} in the Film-Cooled Situation and T_∞ in the Unblown Situation, with Reference to Property Ratio Corrections.

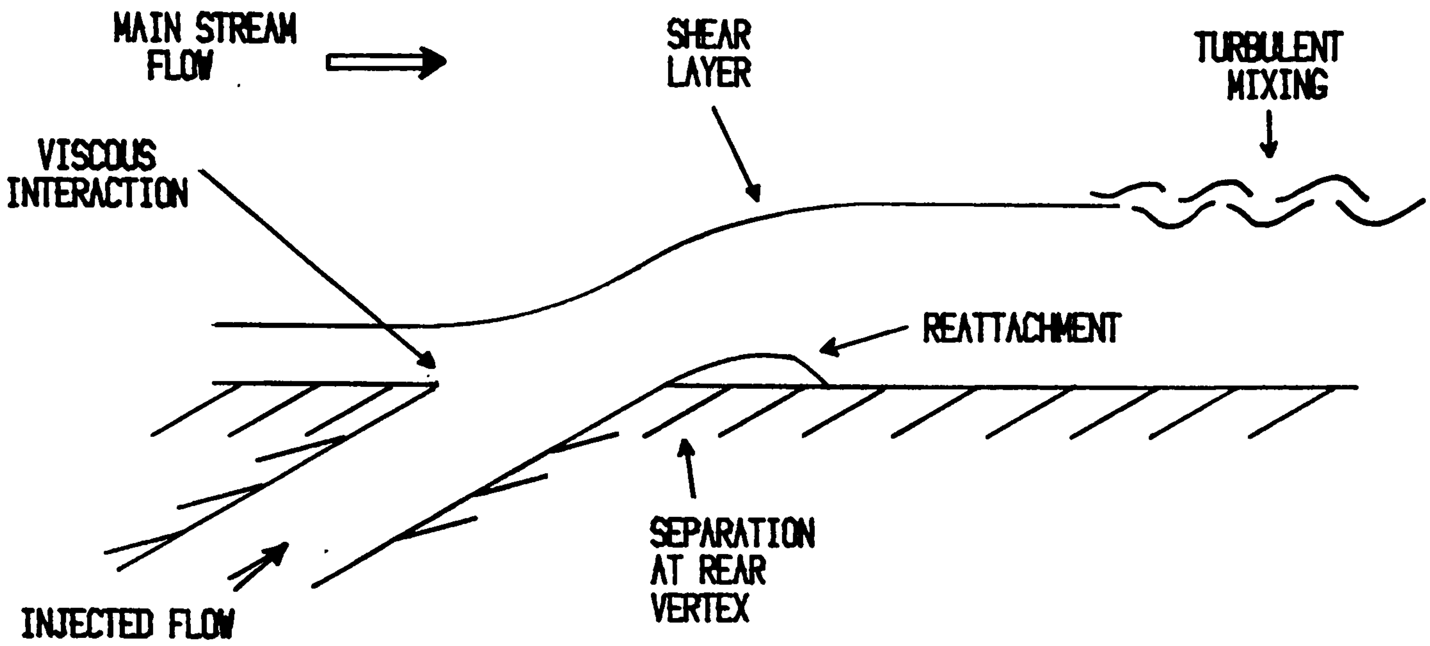

FIG 7.1(a) Schematic Representation of Slot Injection Flow.

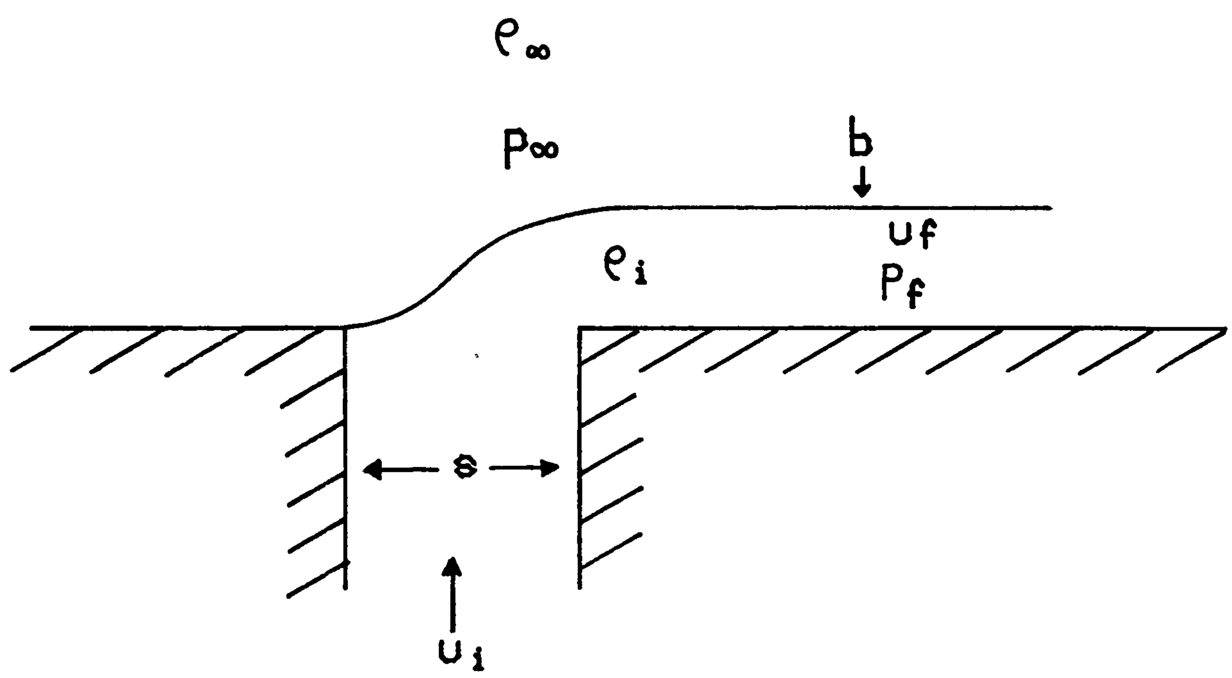

FIG. 7.1(b) Inviscid Model of Slot Injection Flow
(after Fitt et al. [7.1])

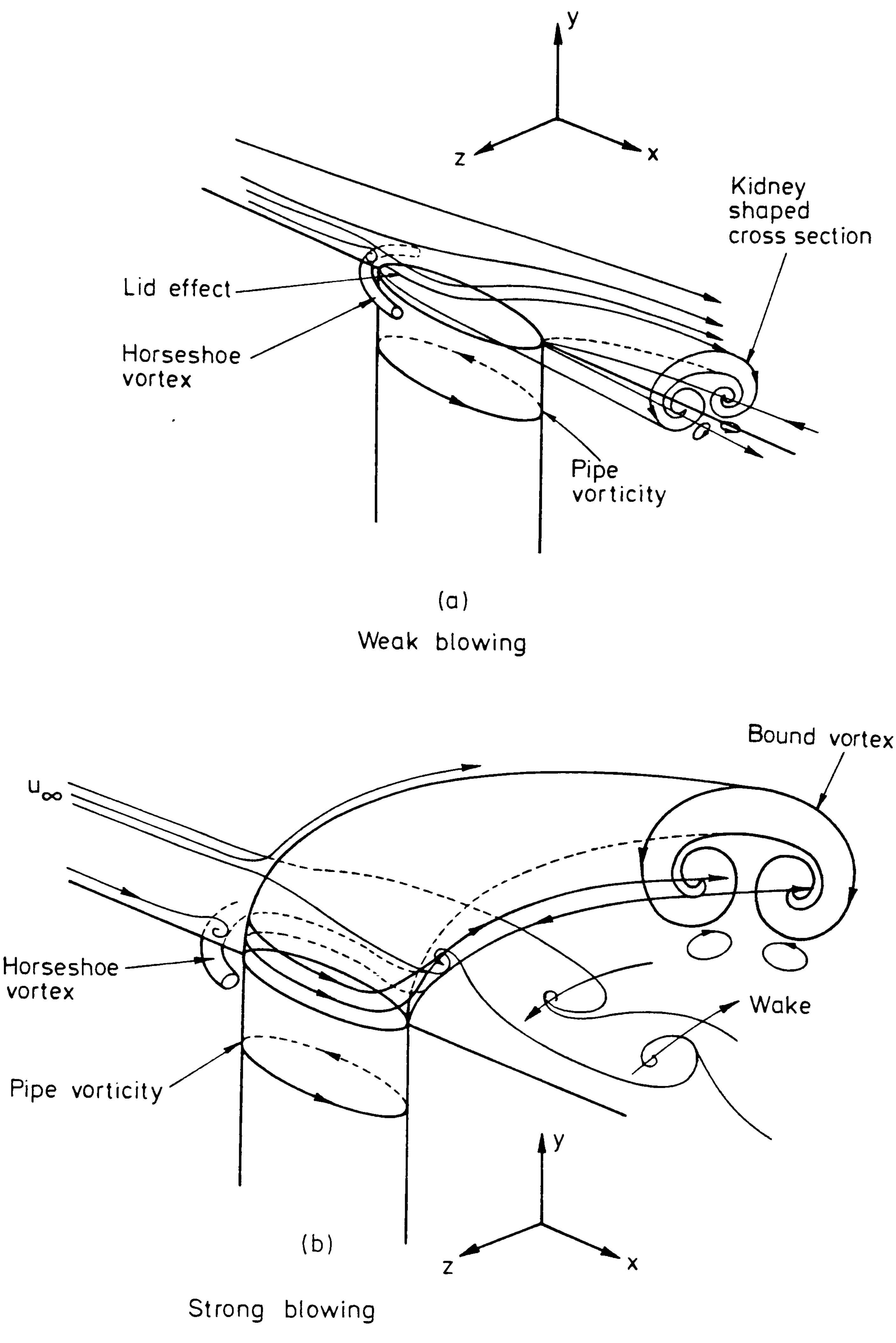

FIG. 7.2 Schematic Representation of Injection Through a Hole at Strong and Weak Injection Rates.

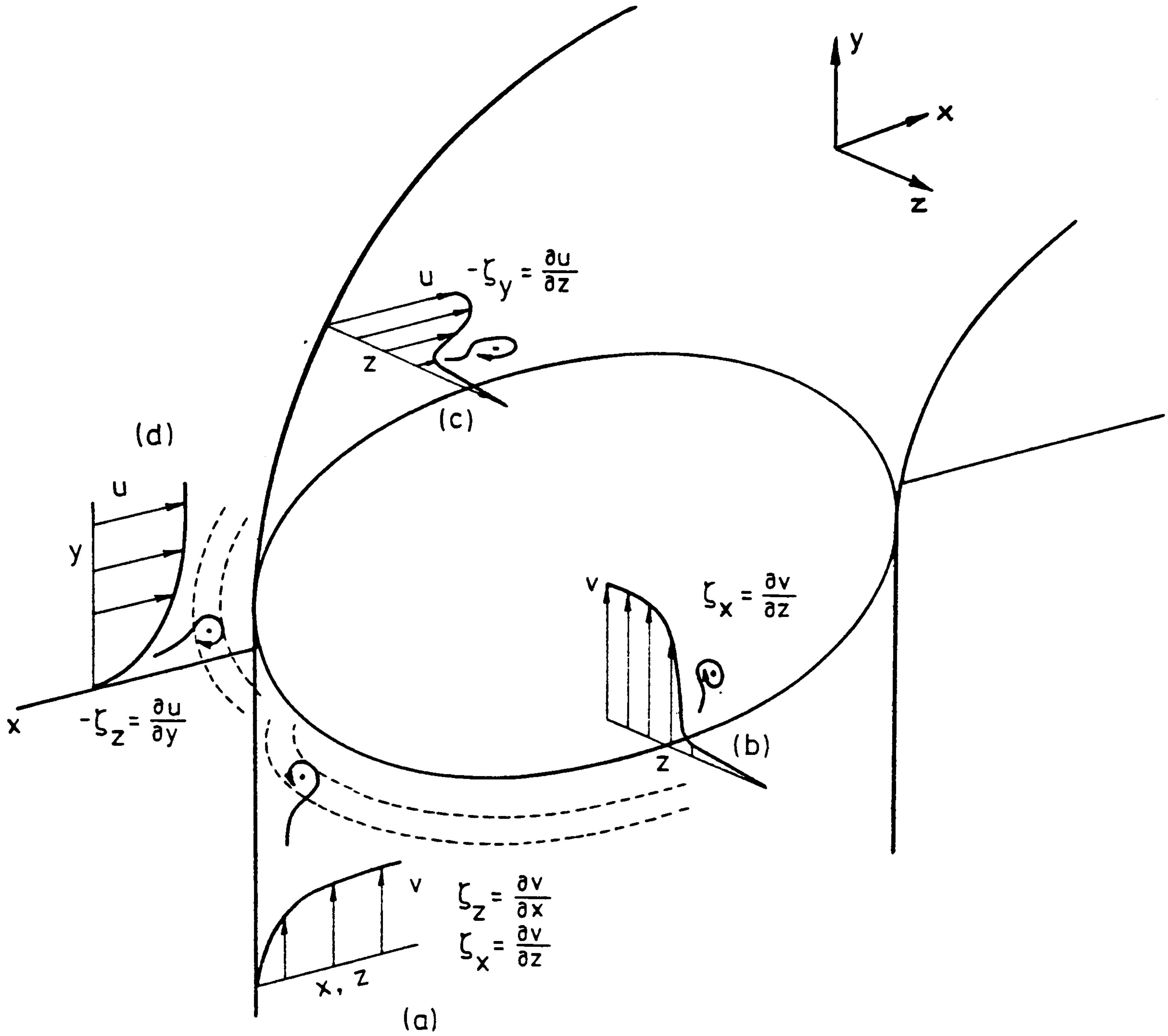

FIG. 7.3 Sketch Showing Mechanisms of Generation of Vorticity in Injection Through a Hole.

VELOCITY RATIO = Ø.3   NETT SADDLE UPSTREAM

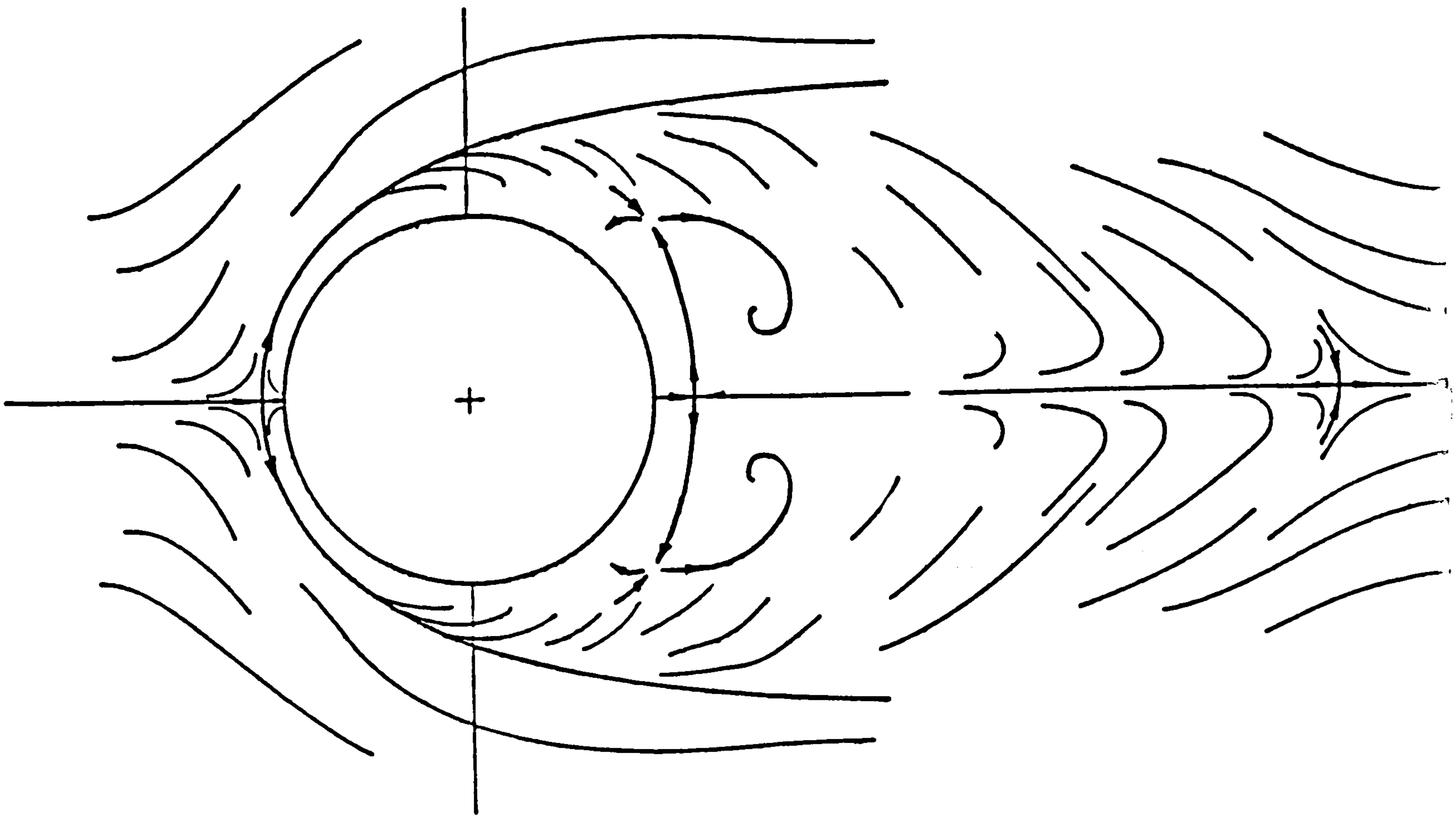

VELOCITY RATIO = Ø.9   NETT SADDLE DOWNSTREAM

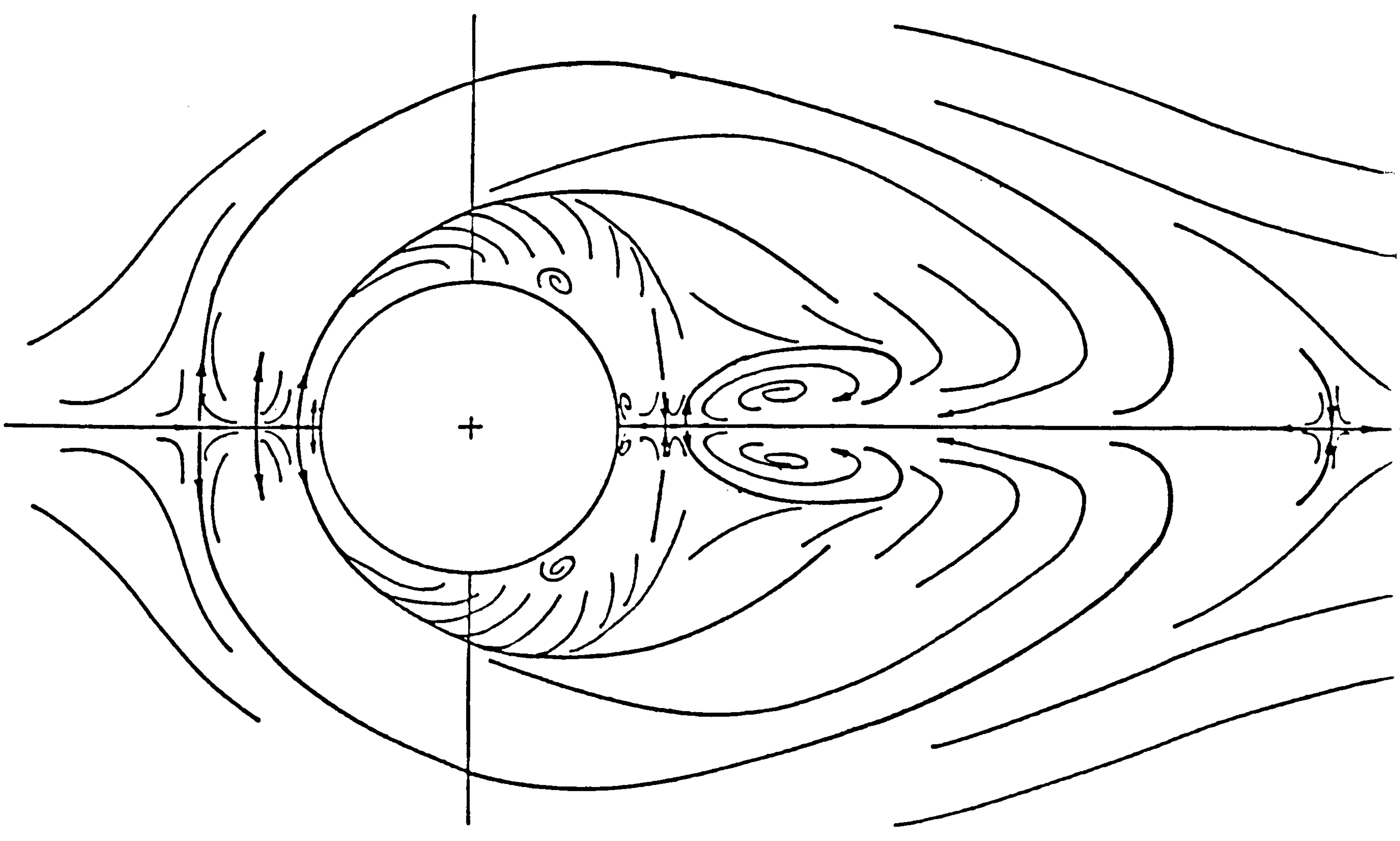

FIG. 7.4 Surface Stress Lines Indicating Transition Between Weak and Strong Blowing Regimes (after FOSS [7.4])

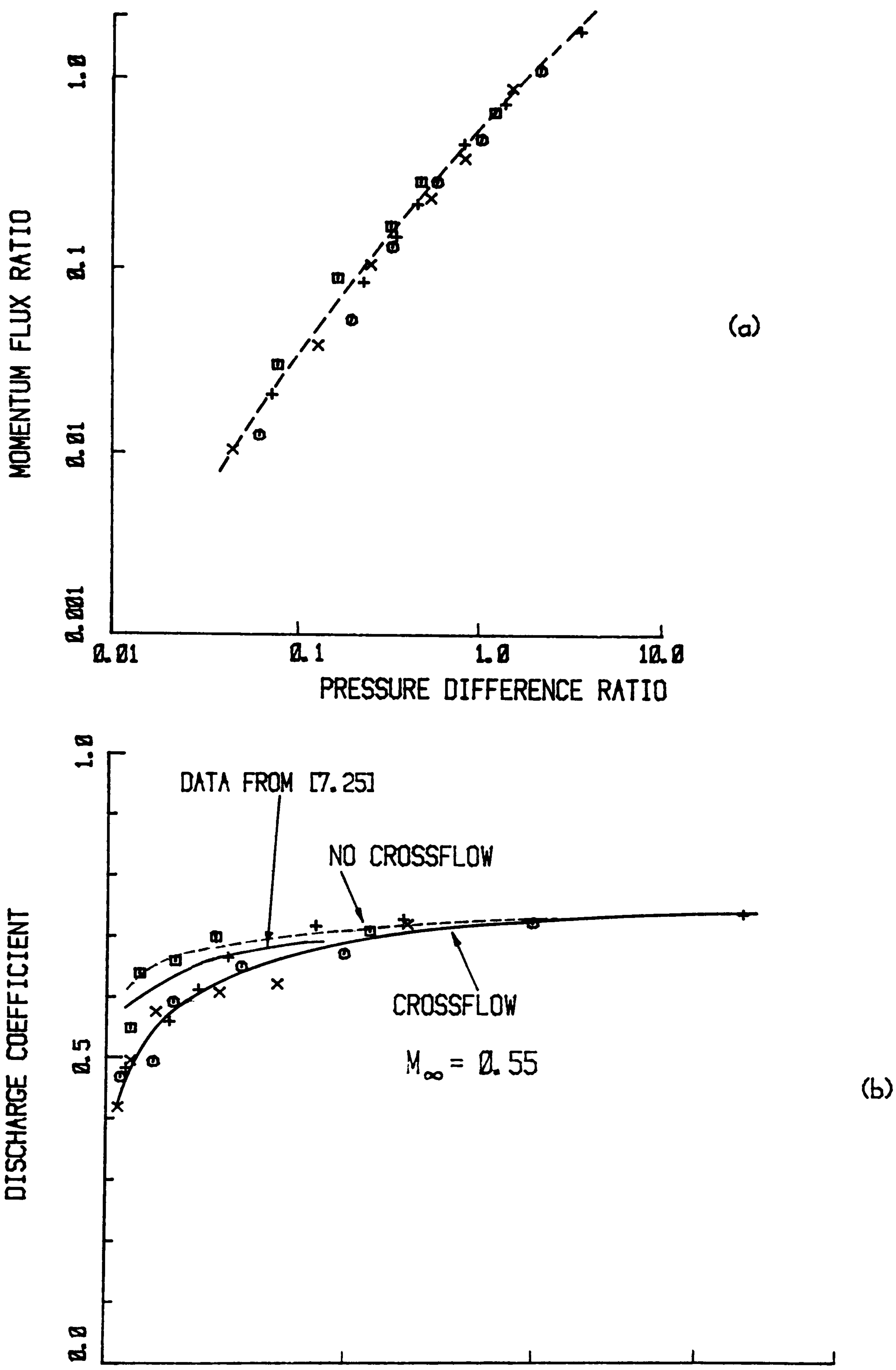

FIG. 7.5 Discharge Characteristics - Single Row of Holes.

Symbols as in Table 8.1

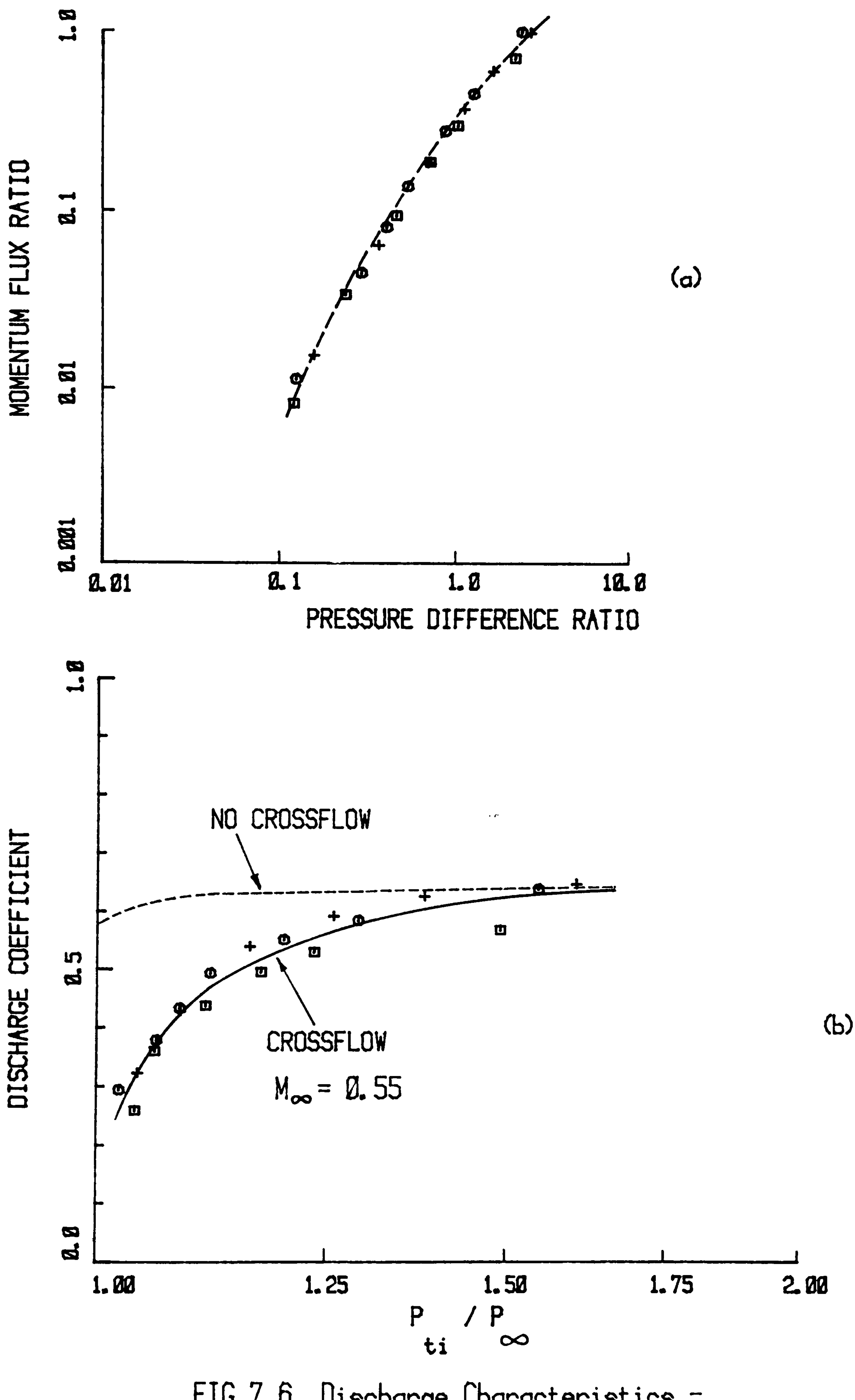

FIG. 7.6 Discharge Characteristics - Slot.
Symbols as in Table 8.2

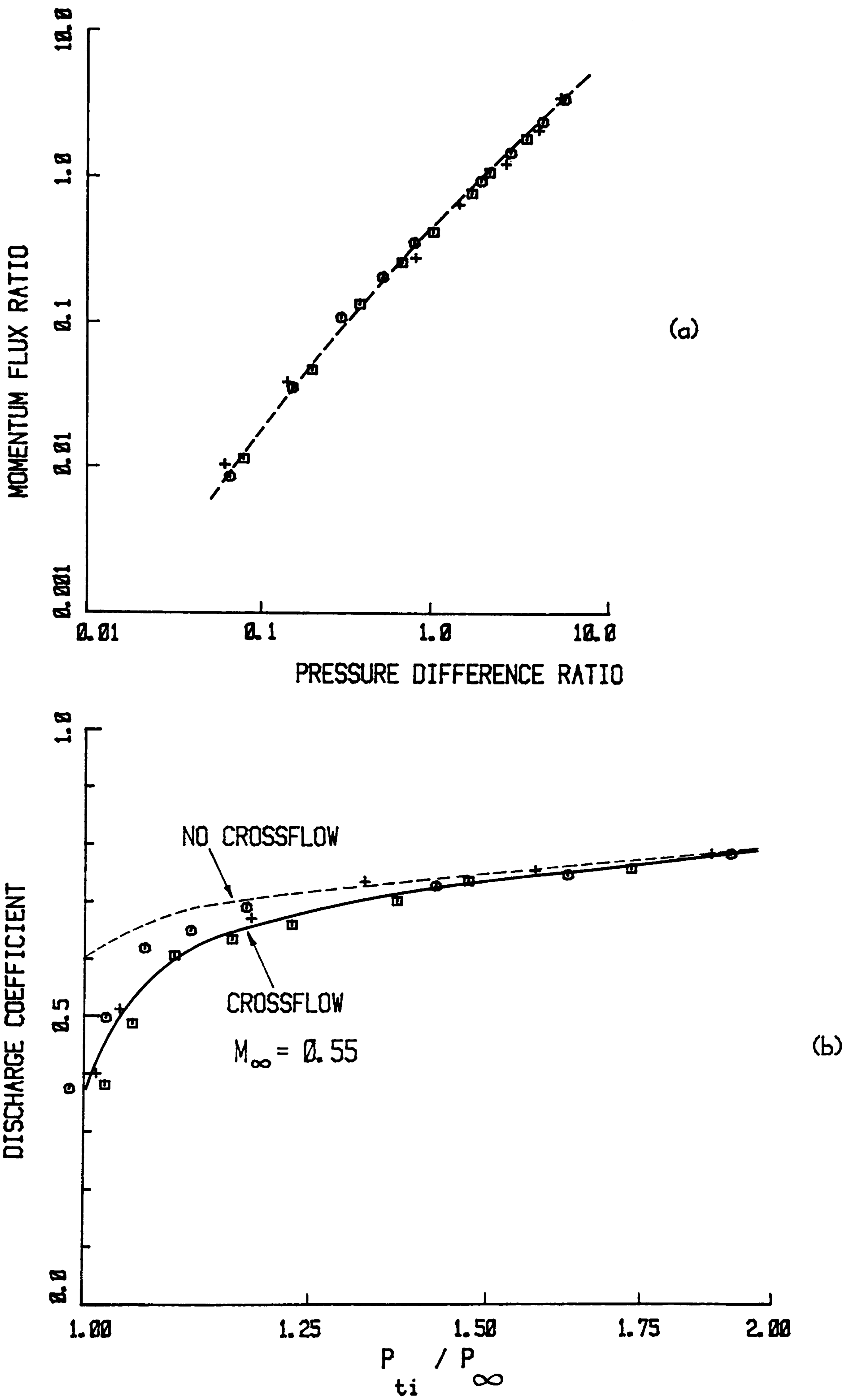

FIG. 7.7 Discharge Characteristics – Double Row of Holes.
Symbols as in Table 8.3

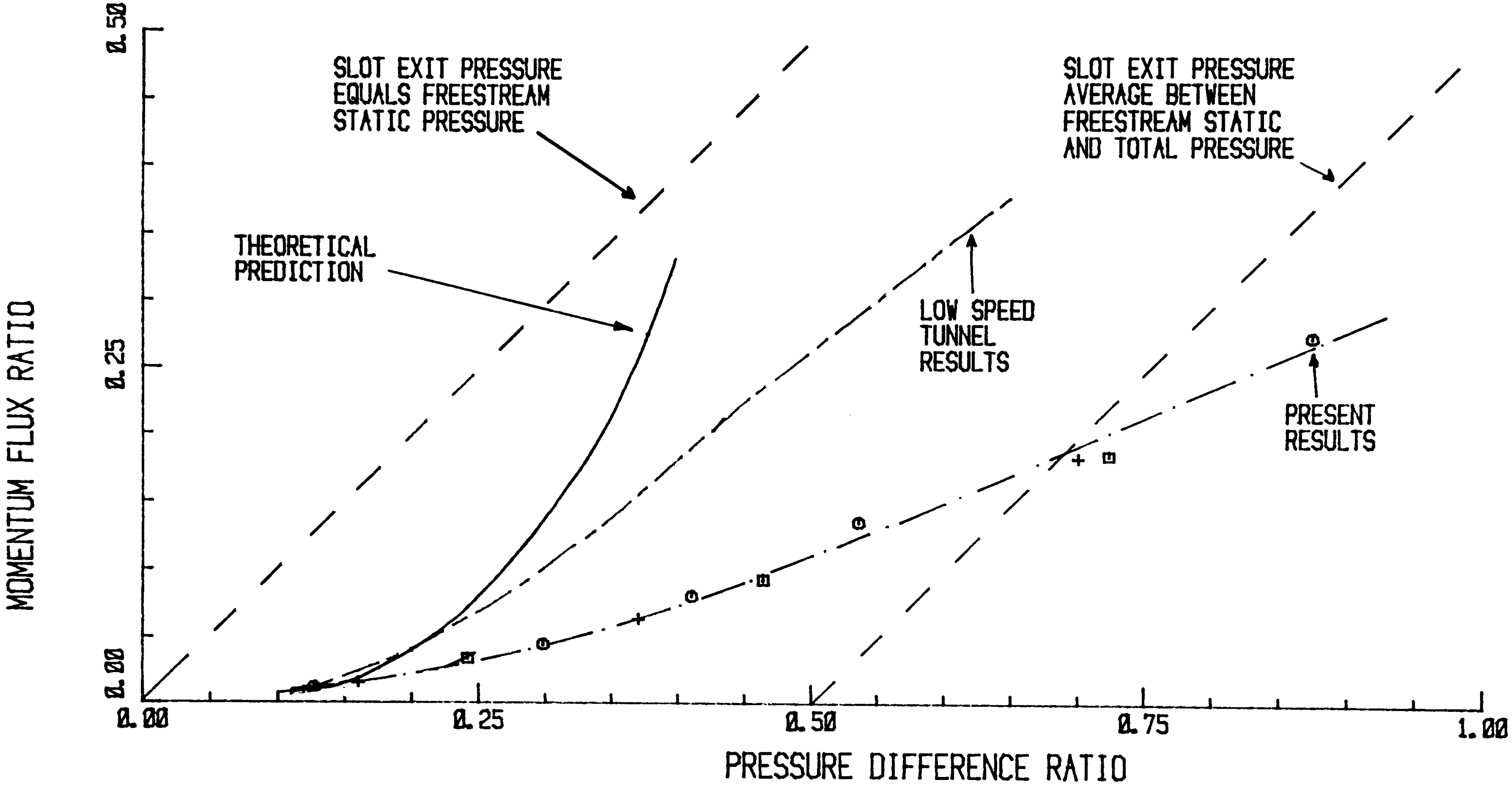

FIG. 7.8 Slot Discharge - Comparison Between Theory and Experiment.

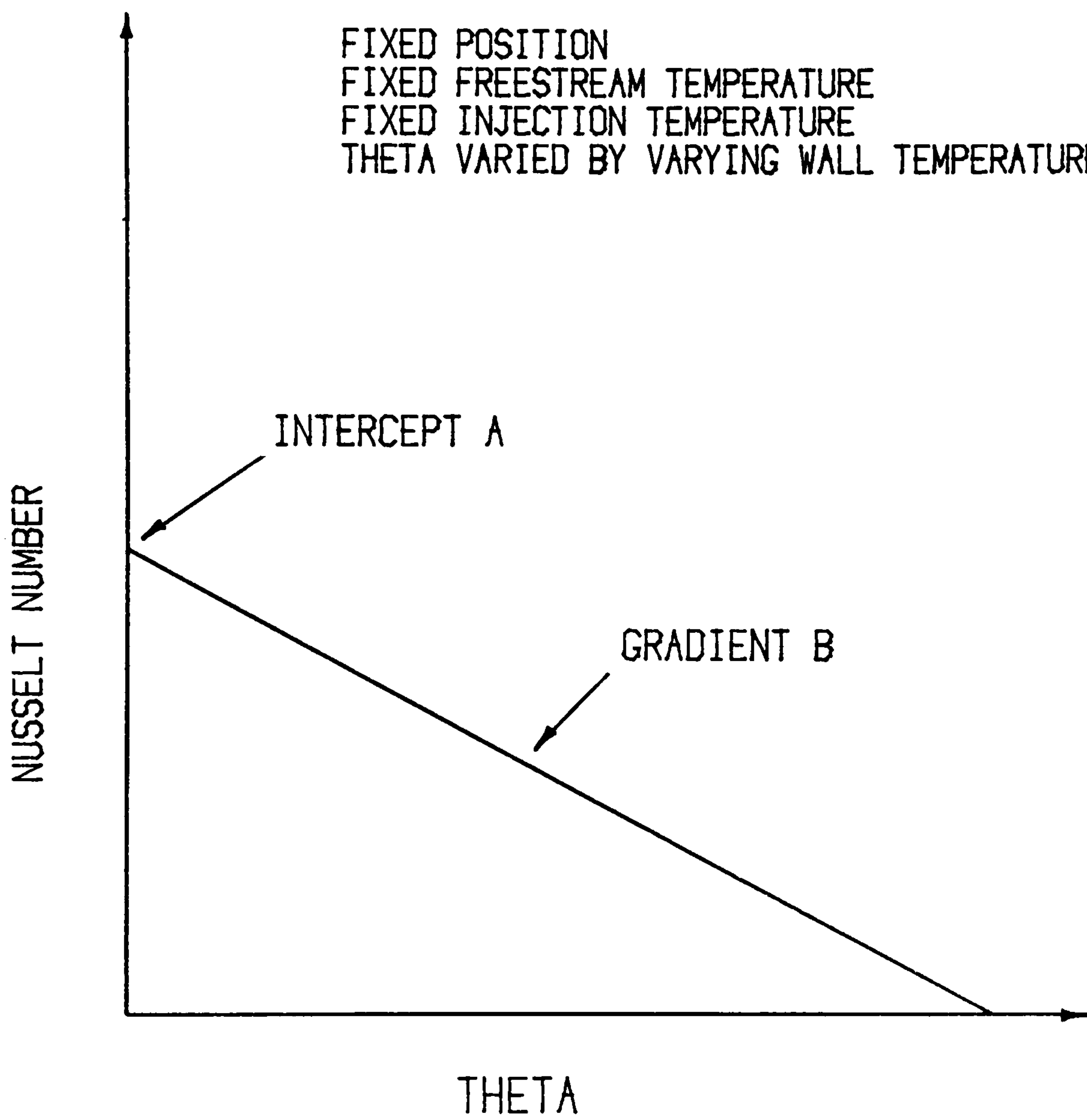

FIG. 8.1 Relationship between Nusselt Number and Theta Predicted by Superposition Model.

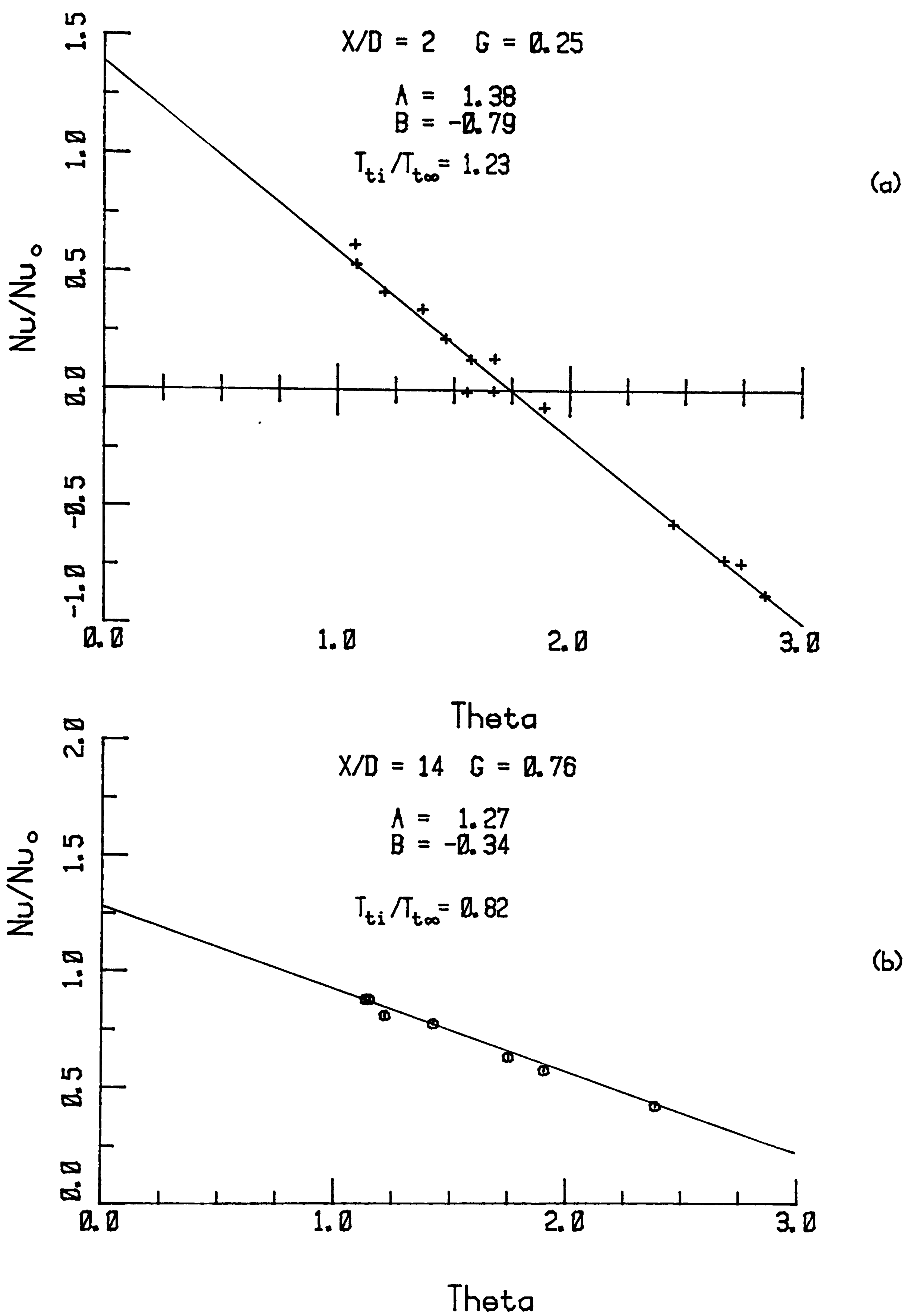

FIG. 8.2 Single row data - Variation of Nusselt Number with Theta as the wall temperature is changed.

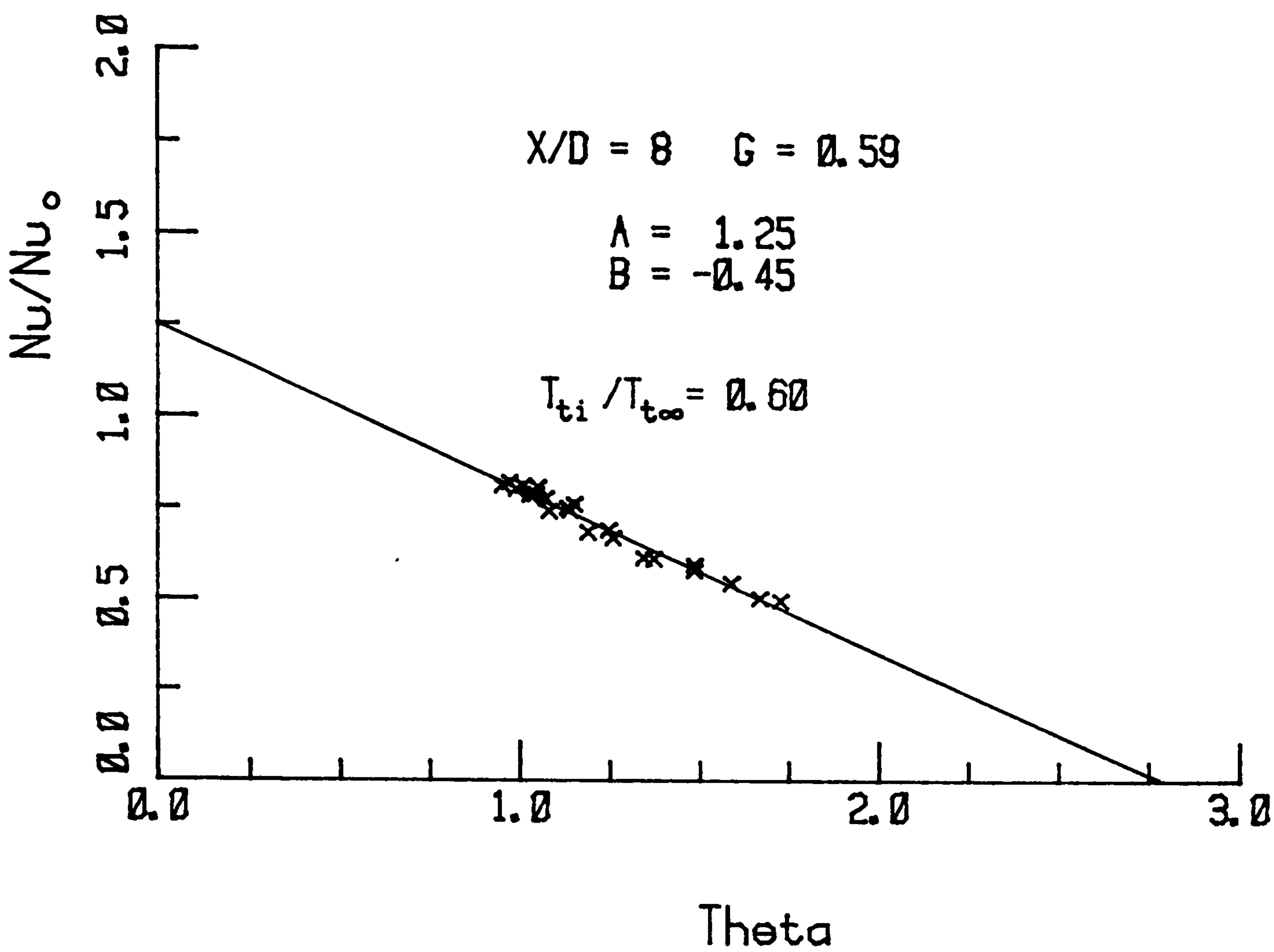

(c)

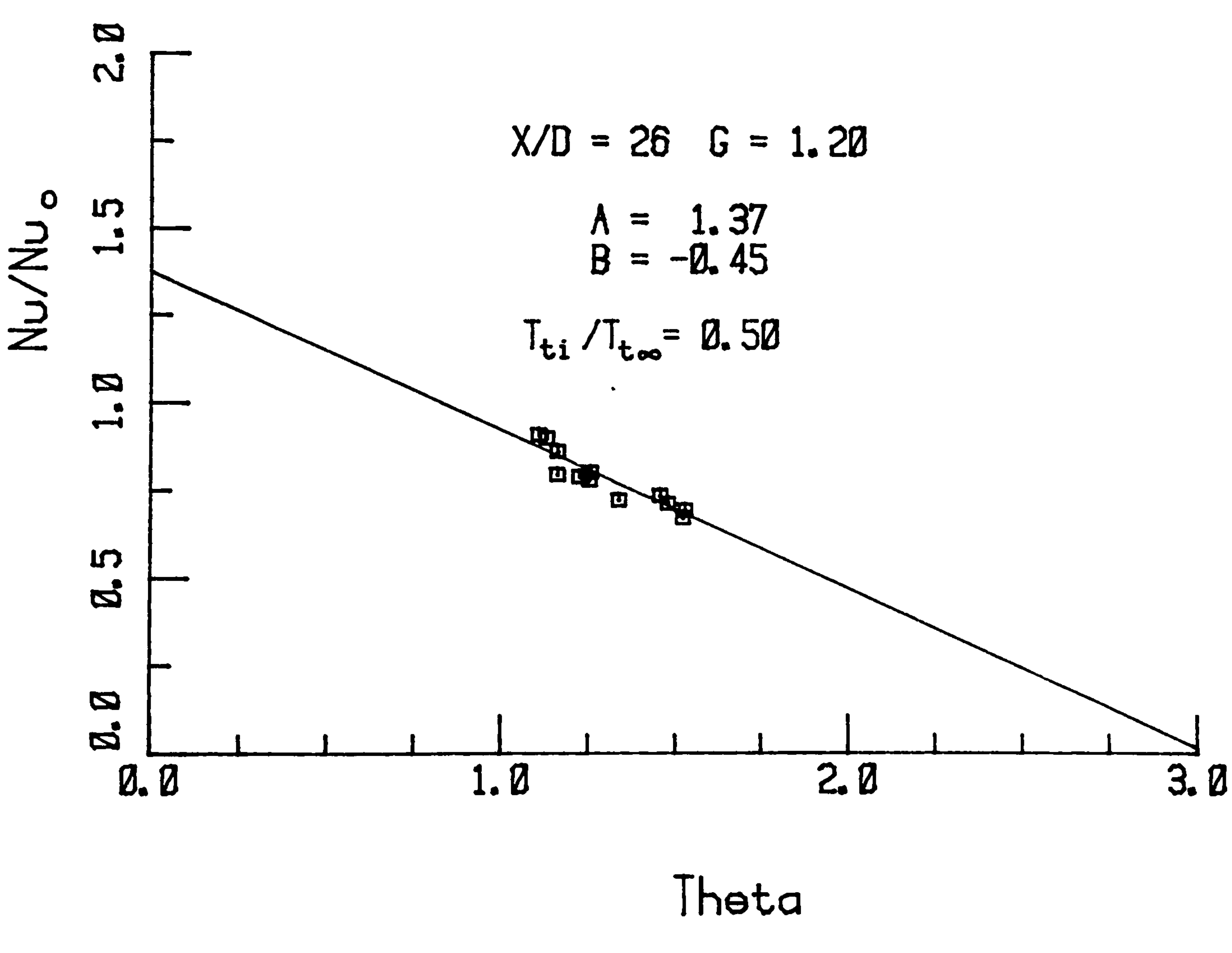

(d)

FIG. 8.2 Single row data - Variation of Nusselt Number with Theta as the wall temperature is changed.

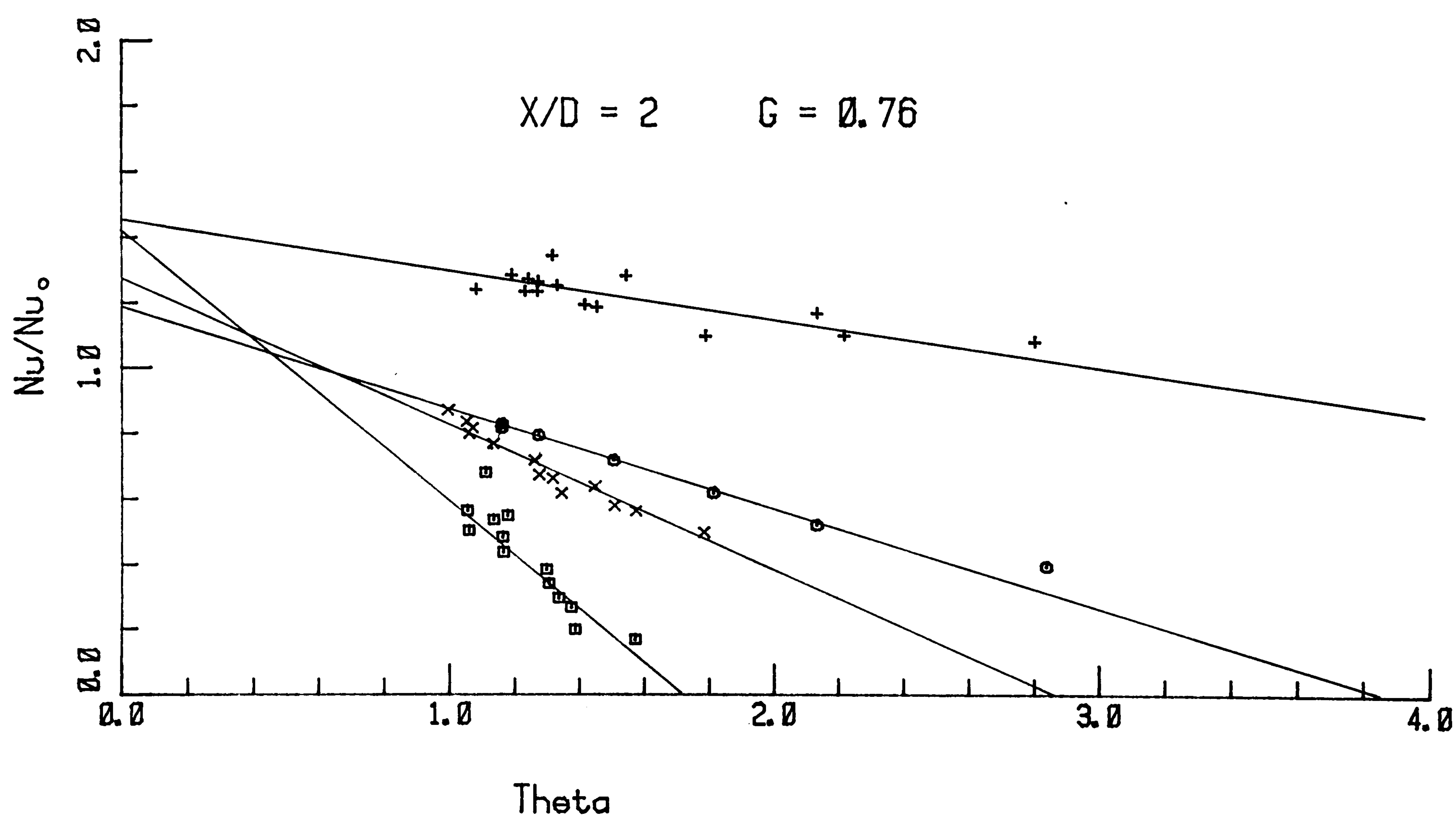

FIG. 8.3 Single row data - Variation of Nusselt Number with Theta for 4 injection-to-freestream total temperature ratios.

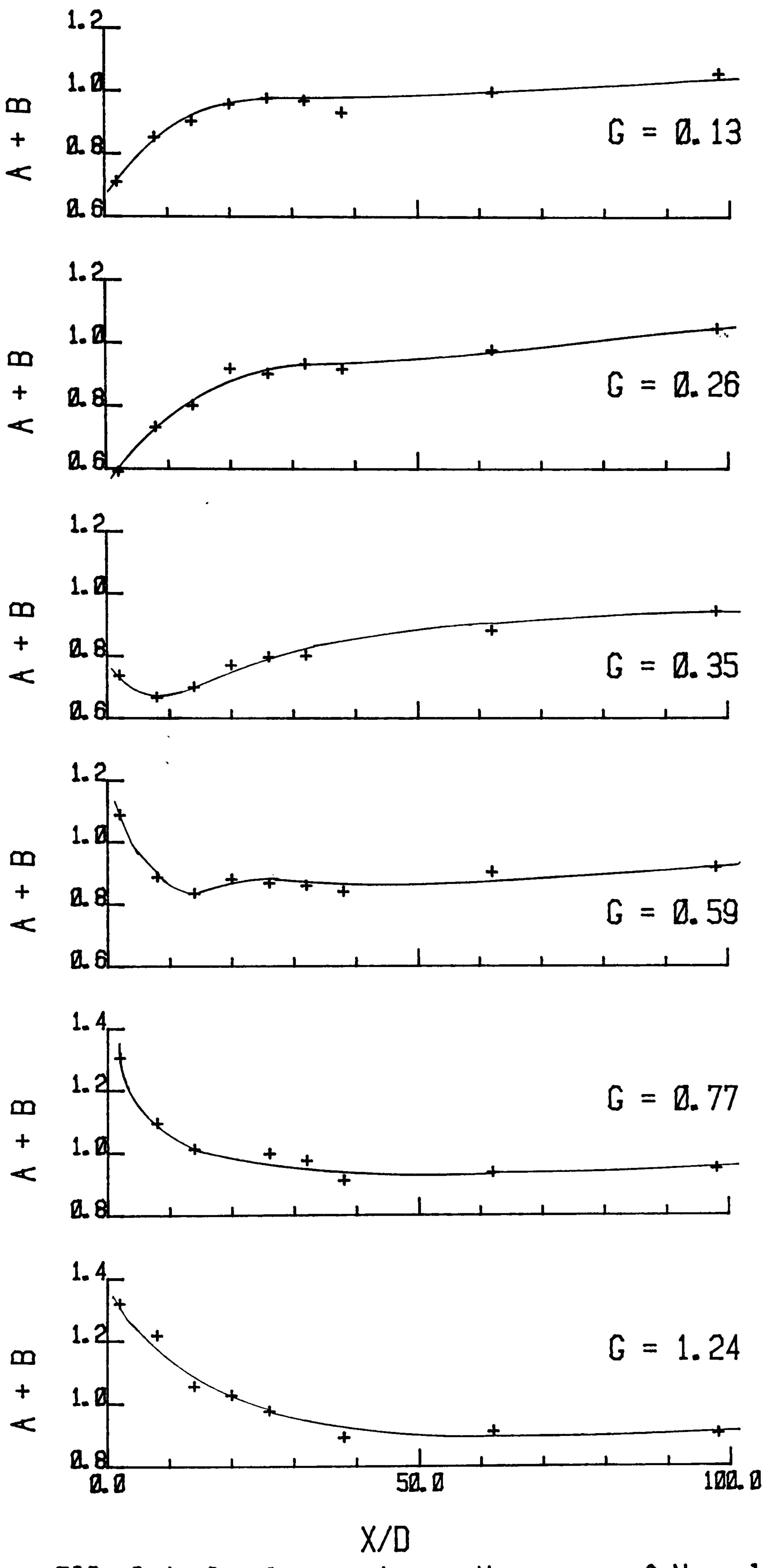

FIG. 8.4 Single row data - Variation of Nusselt Number with distance at Theta = 1.0 $T_{ti}/T_{t\infty}$ = 1.25.

3

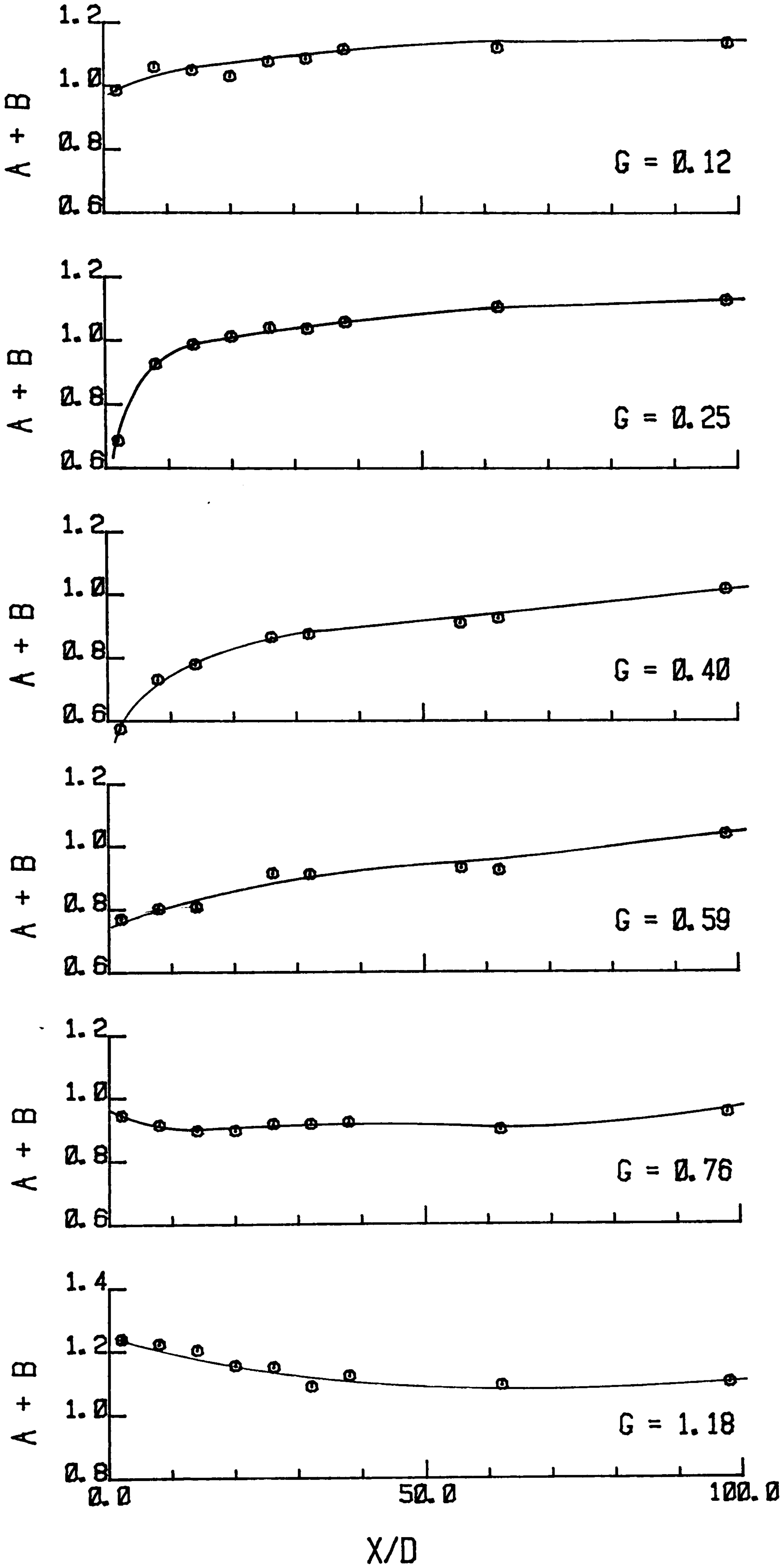

FIG. 8.5 Single row data - Variation of Nusselt Number with distance at Theta = 1.0 $T_{ti}/T_{t\infty} = 0.82$.

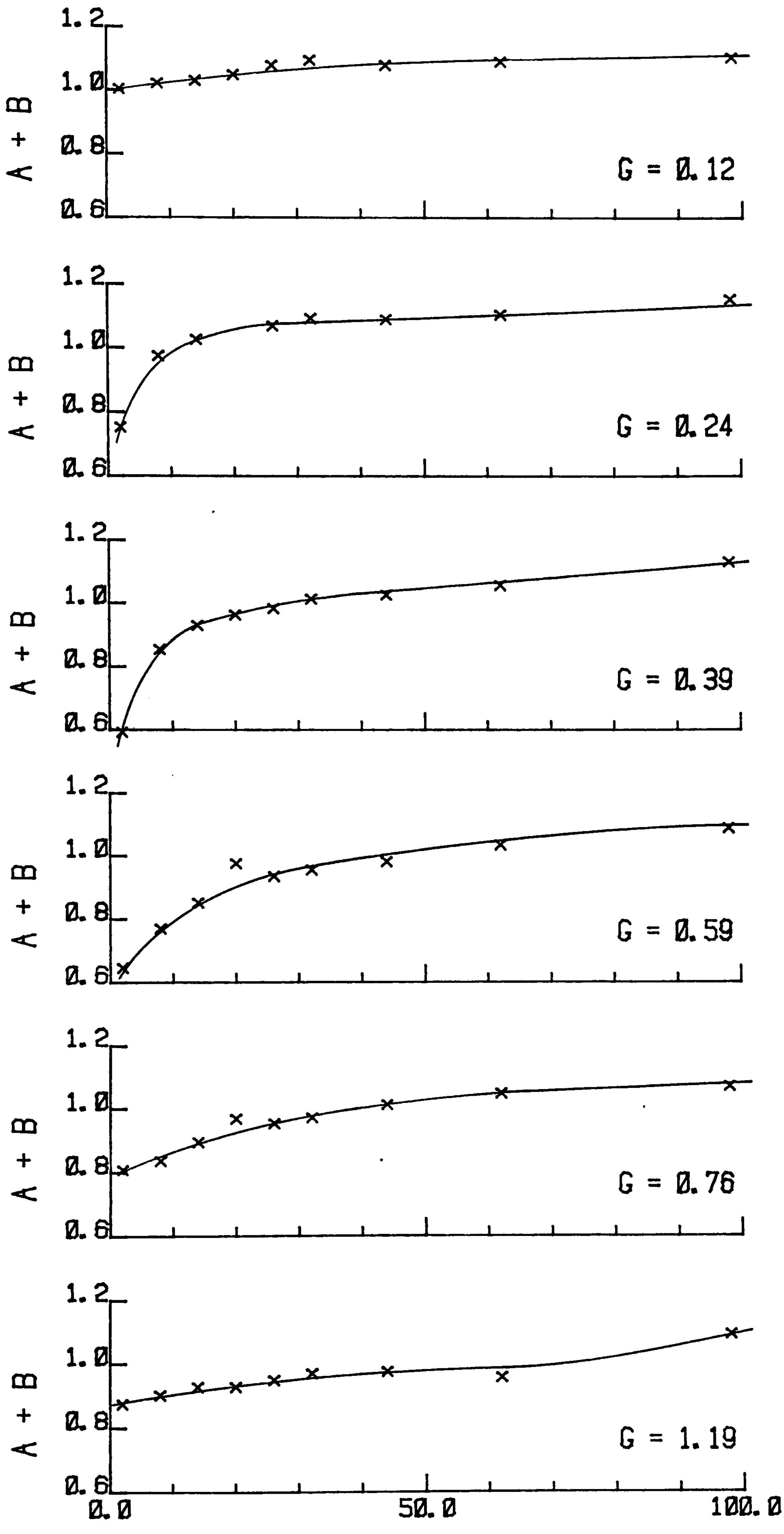

FIG. 8.6 Single row data - Variation of Nusselt Number with distance at Theta = 1.0 $T_{ti}/T_{t\infty} = 0.60$.

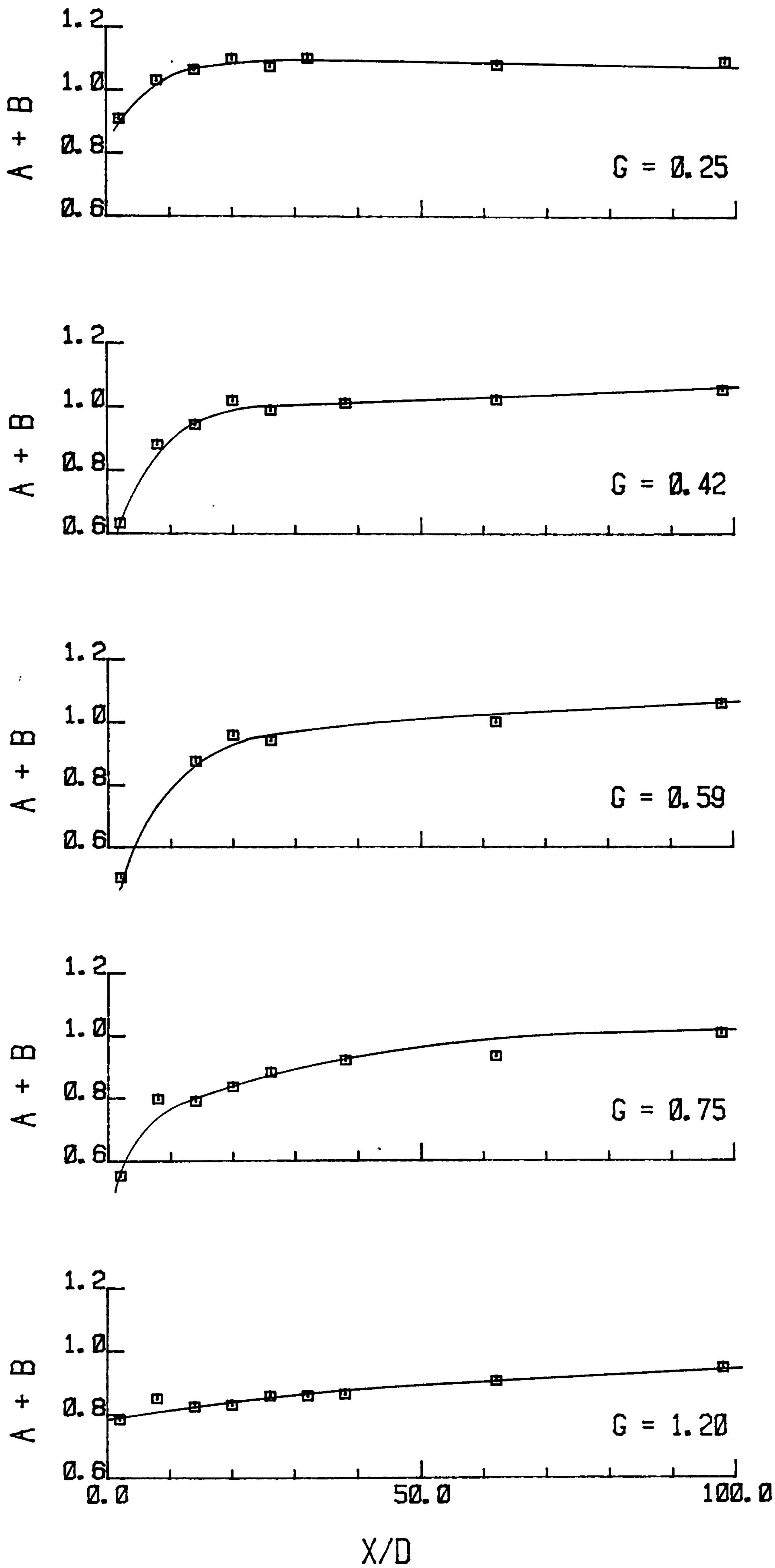

FIG. 8.7 Single row data - Variation of Nusselt Number with distance at Theta = 1.0 $T_{ti}/T_{t\infty}$ = 0.50.

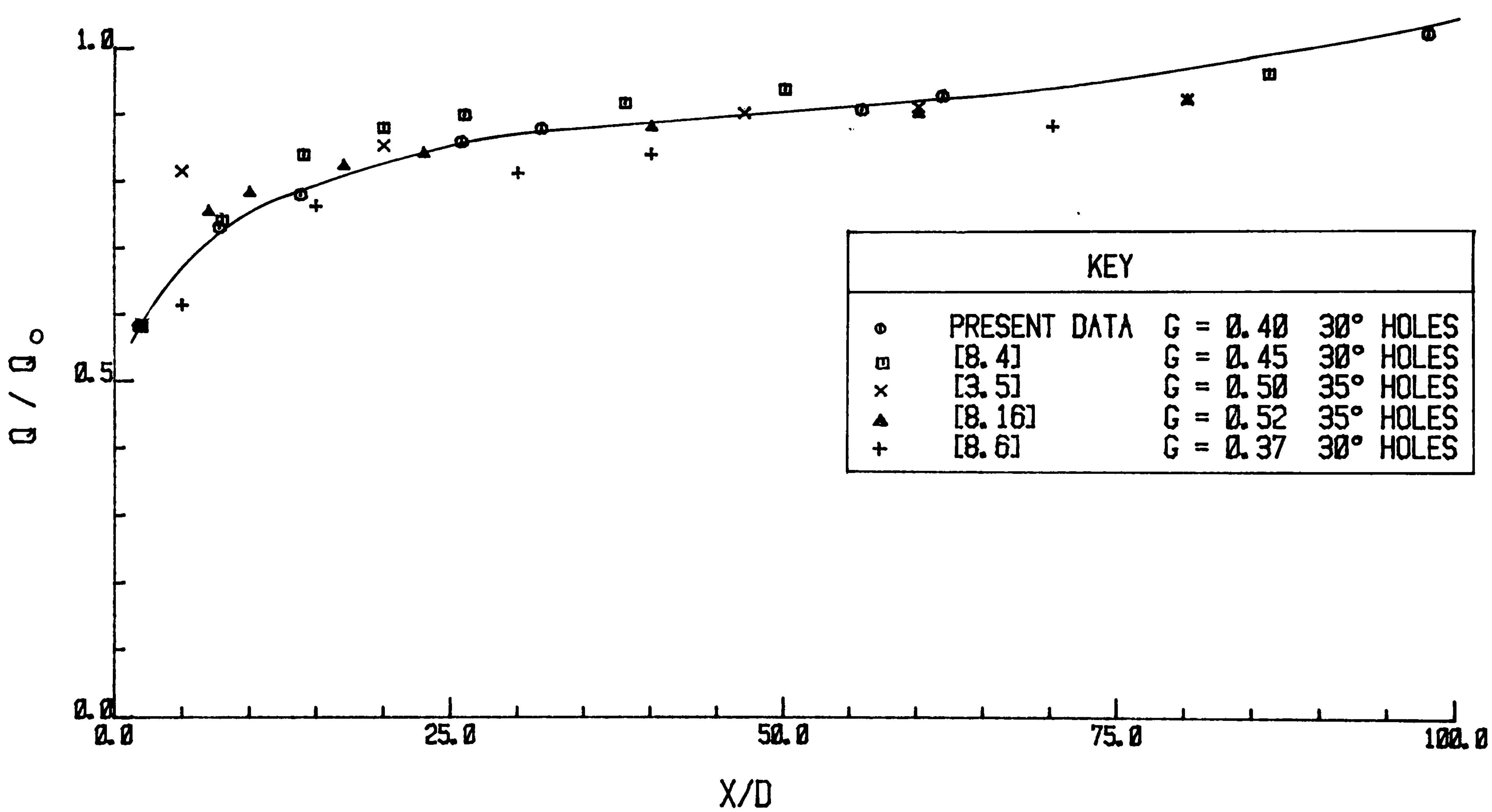

FIG. 8.8 Single row data - Comparison with data in the Literature.

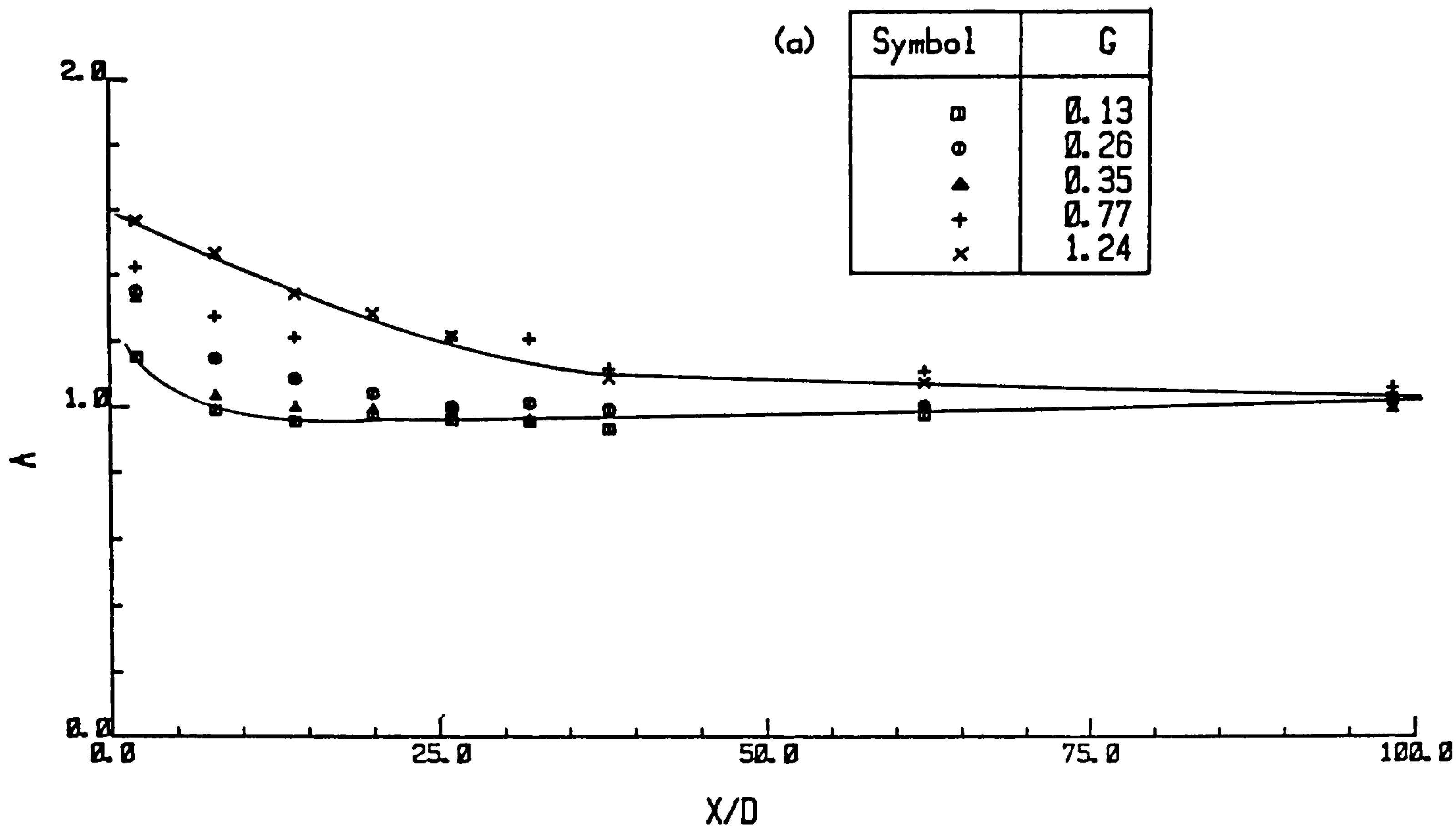

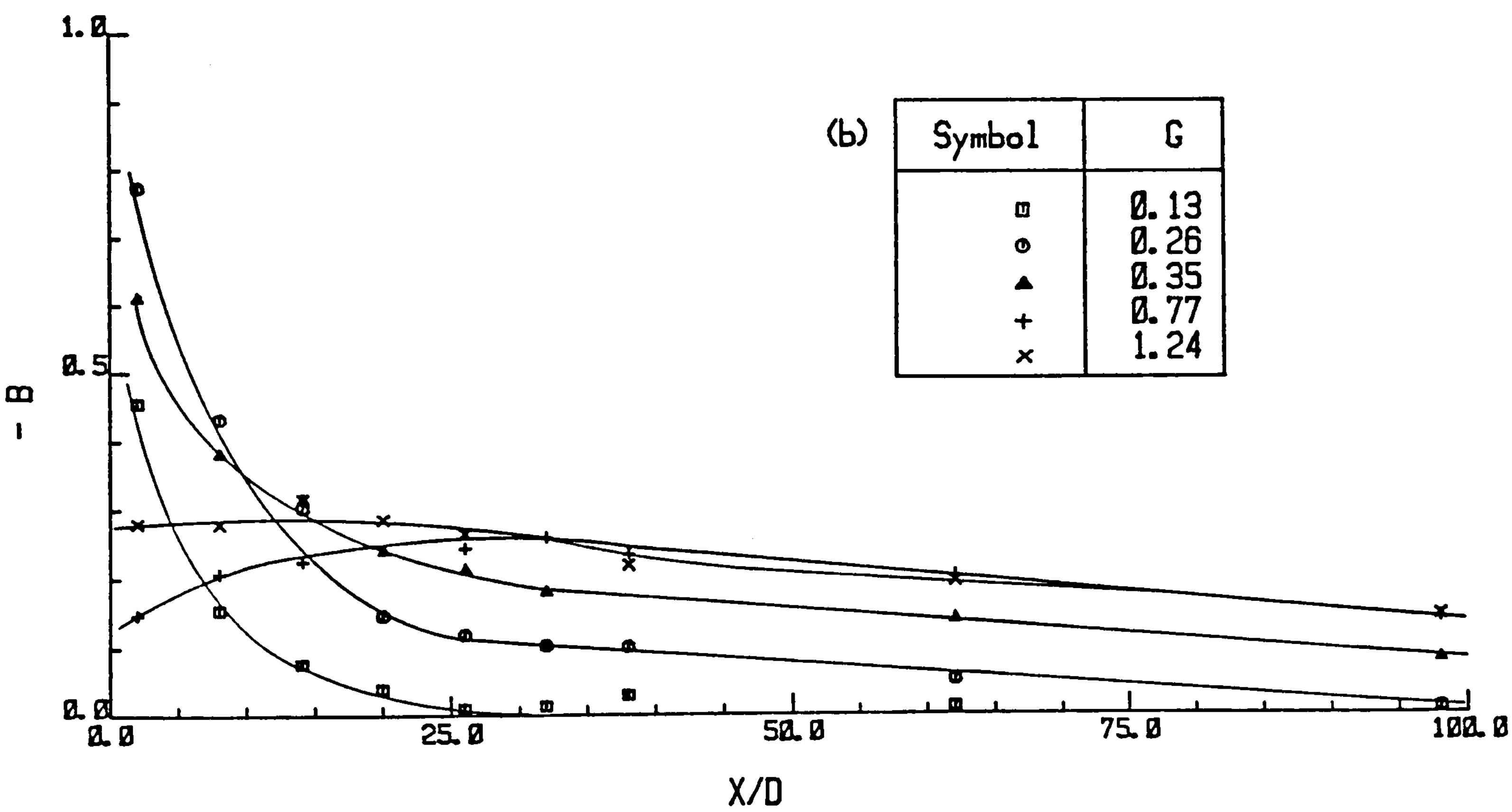

FIG. 8.9 Variation of A and B with distance and blowing rate ; $T_{ti}/T_{t\infty}$ = 1.23

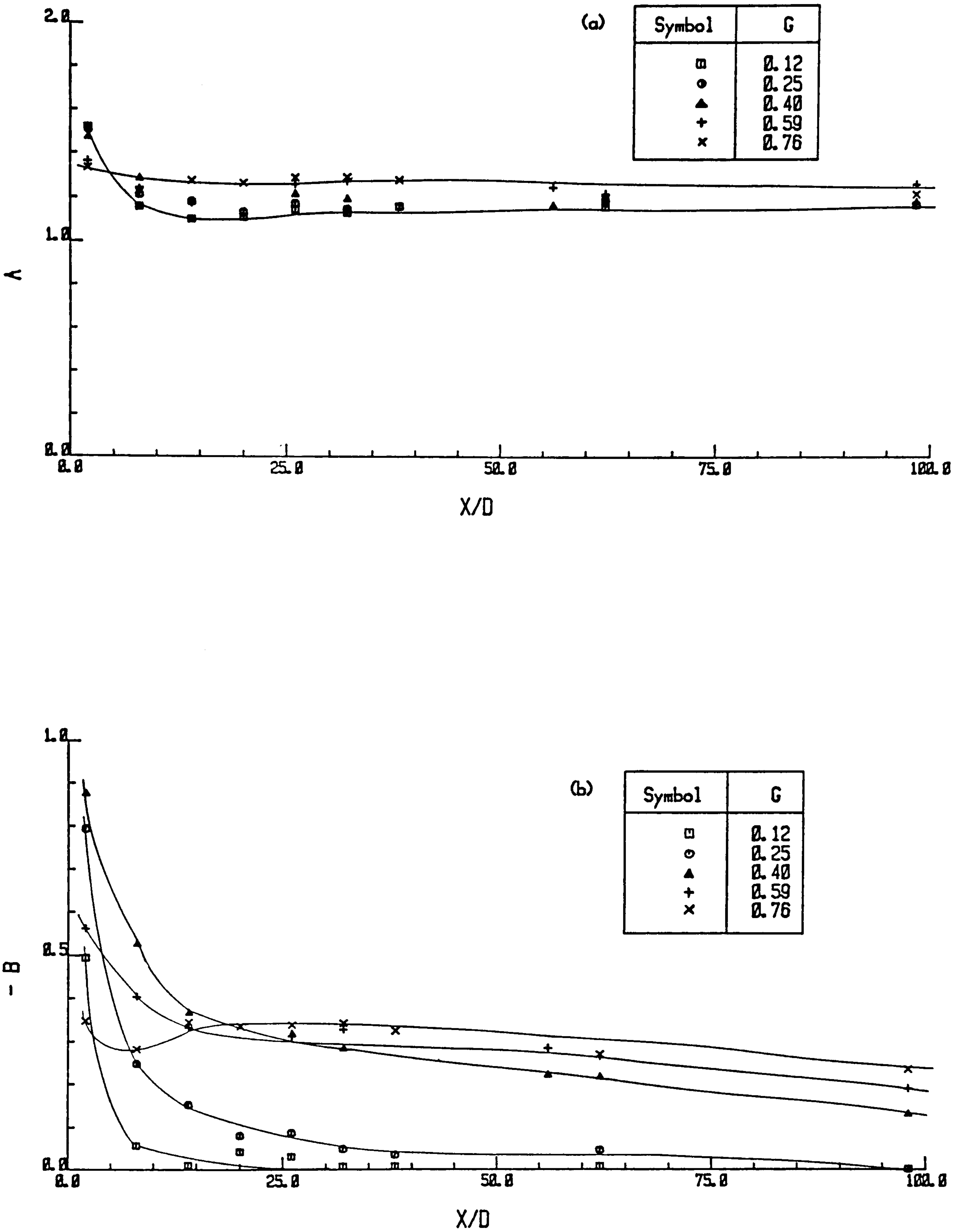

FIG. 8.10 Variation of Λ and B with distance and blowing rate ; $T_{ti}/T_{t\infty} = 0.82$

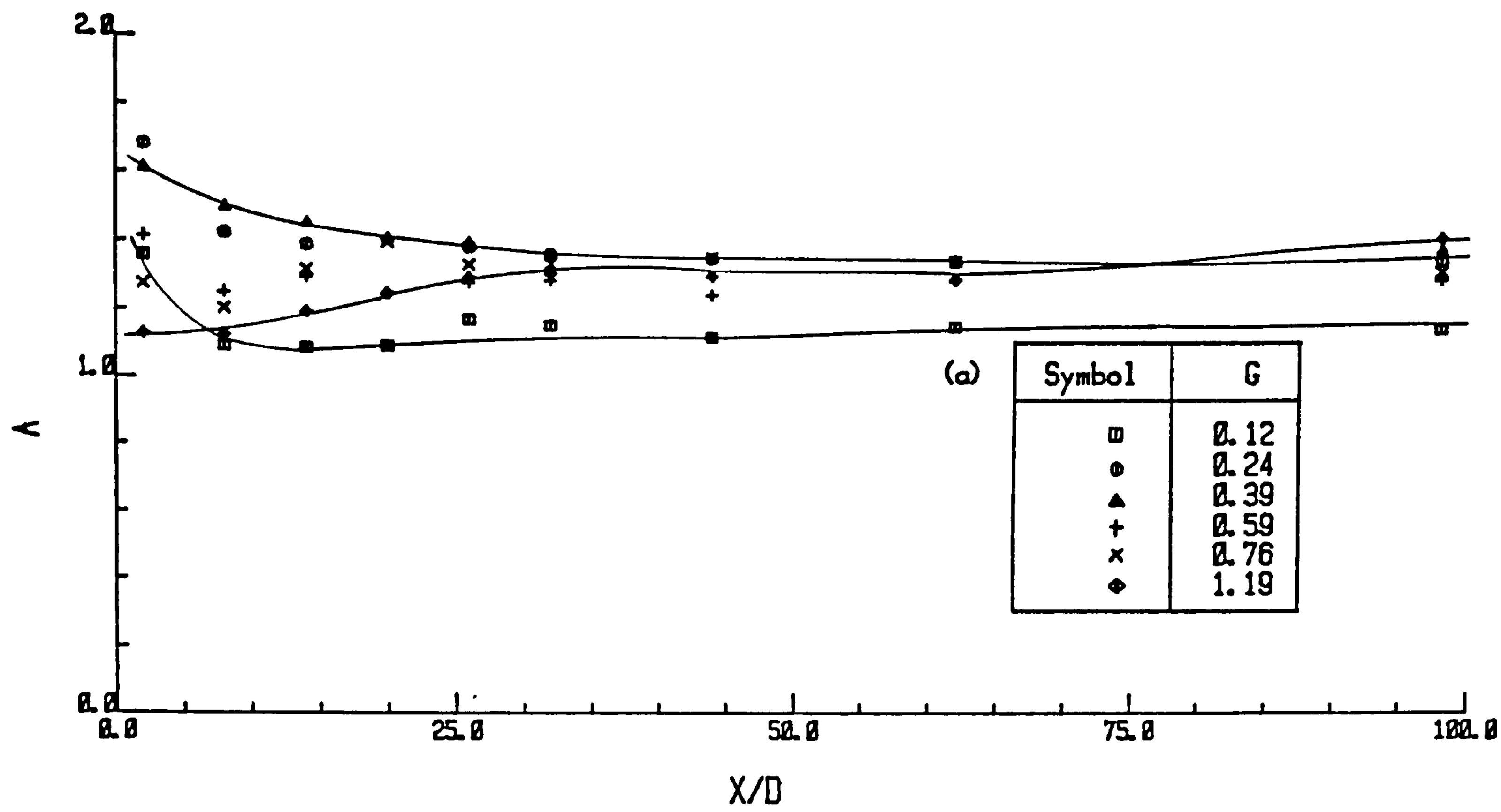

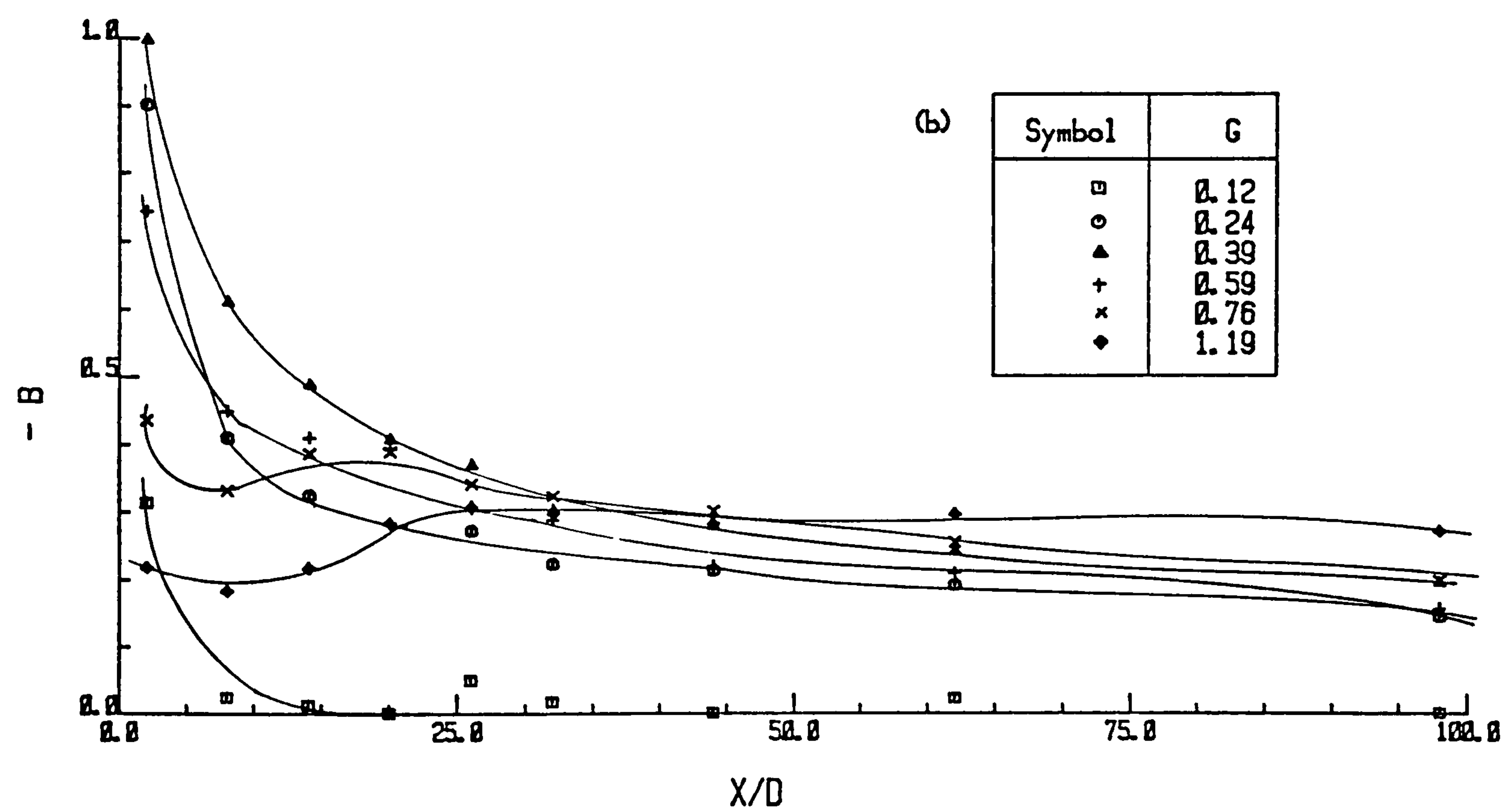

FIG. 8.11 Variation of Λ and B with distance and blowing rate ; $T_{ti}/T_{t\infty} = 0.60$

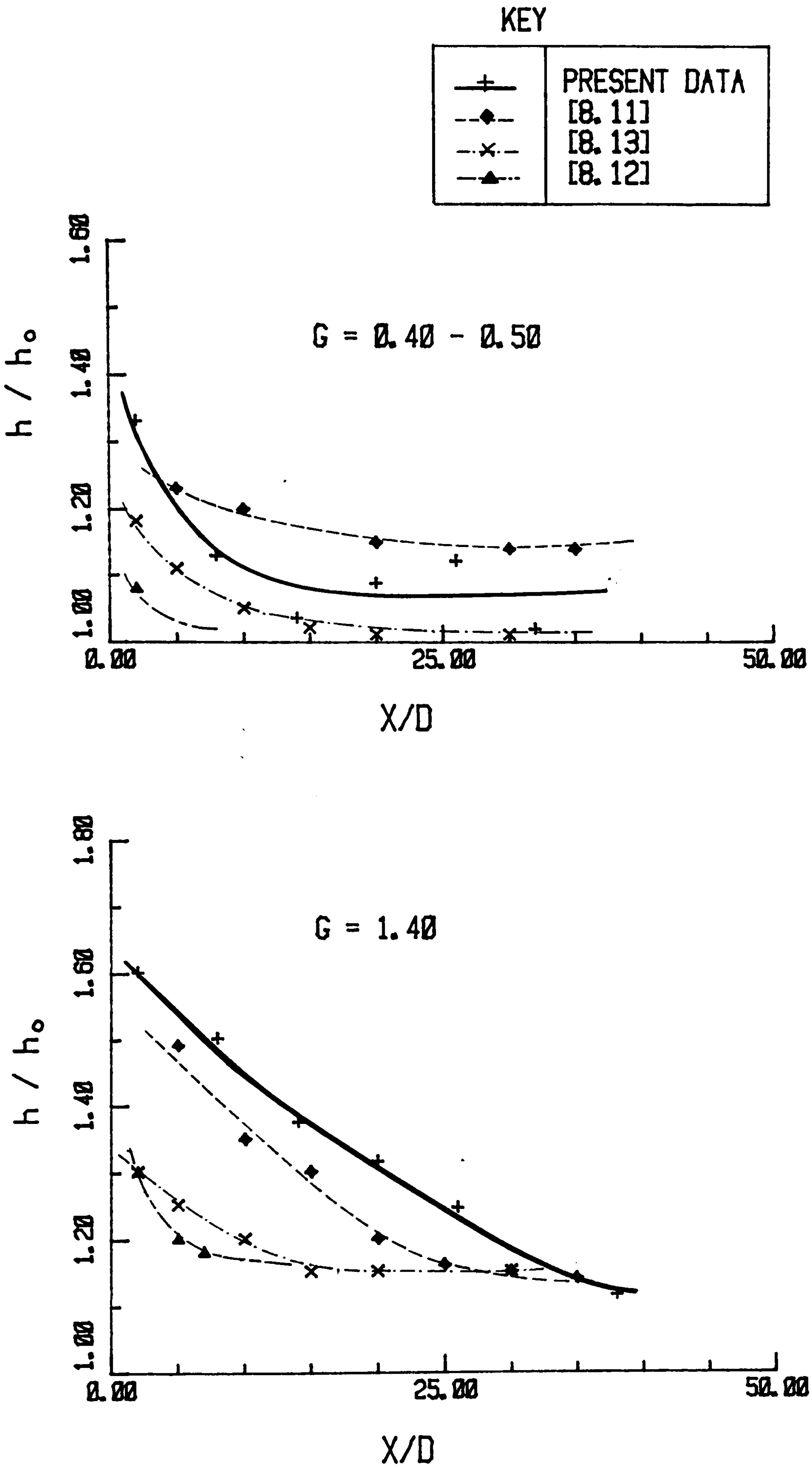

FIG. 8.12 Enhancement of Heat Transfer Coefficient - Comparison with the Literature.

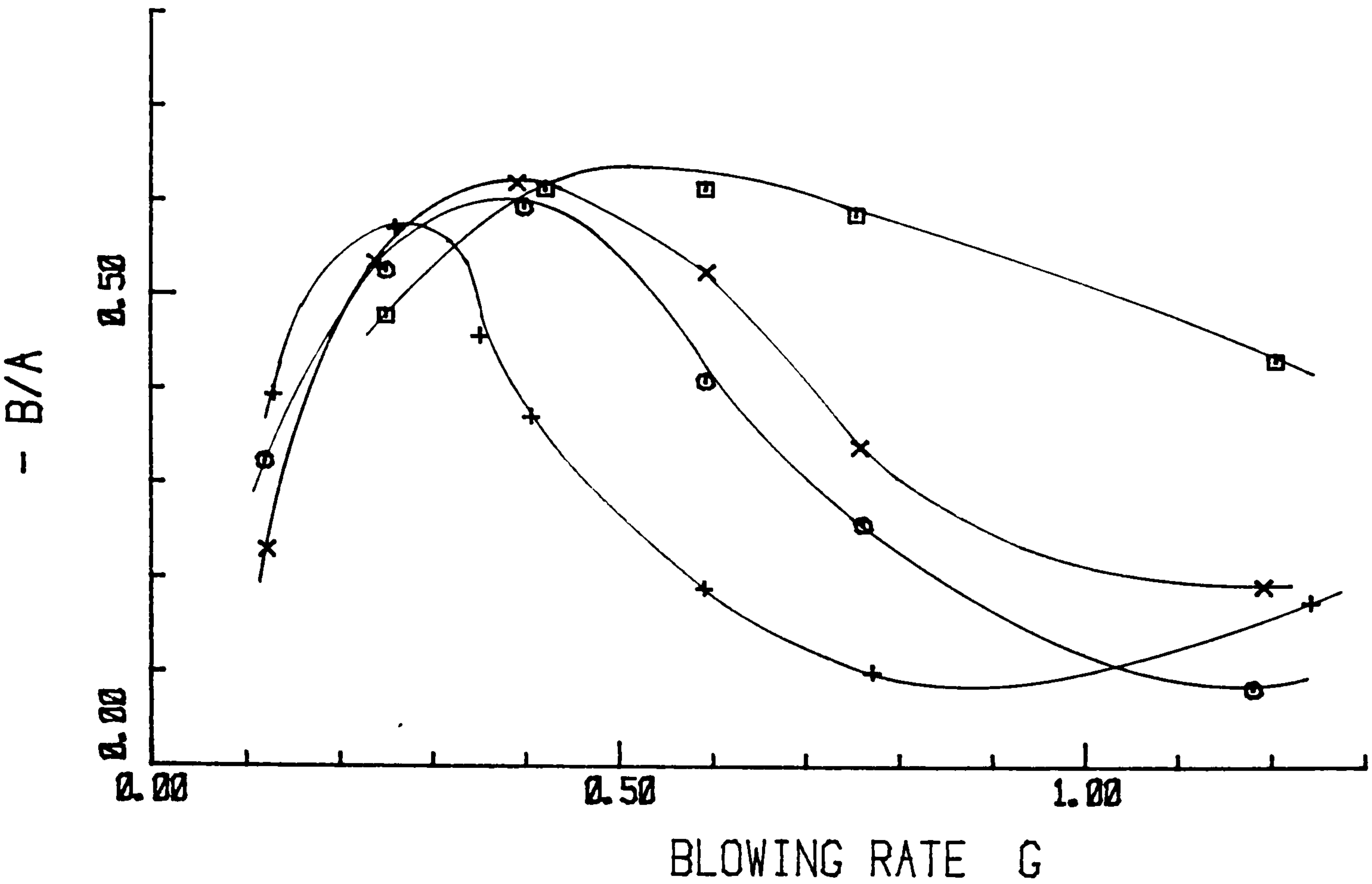

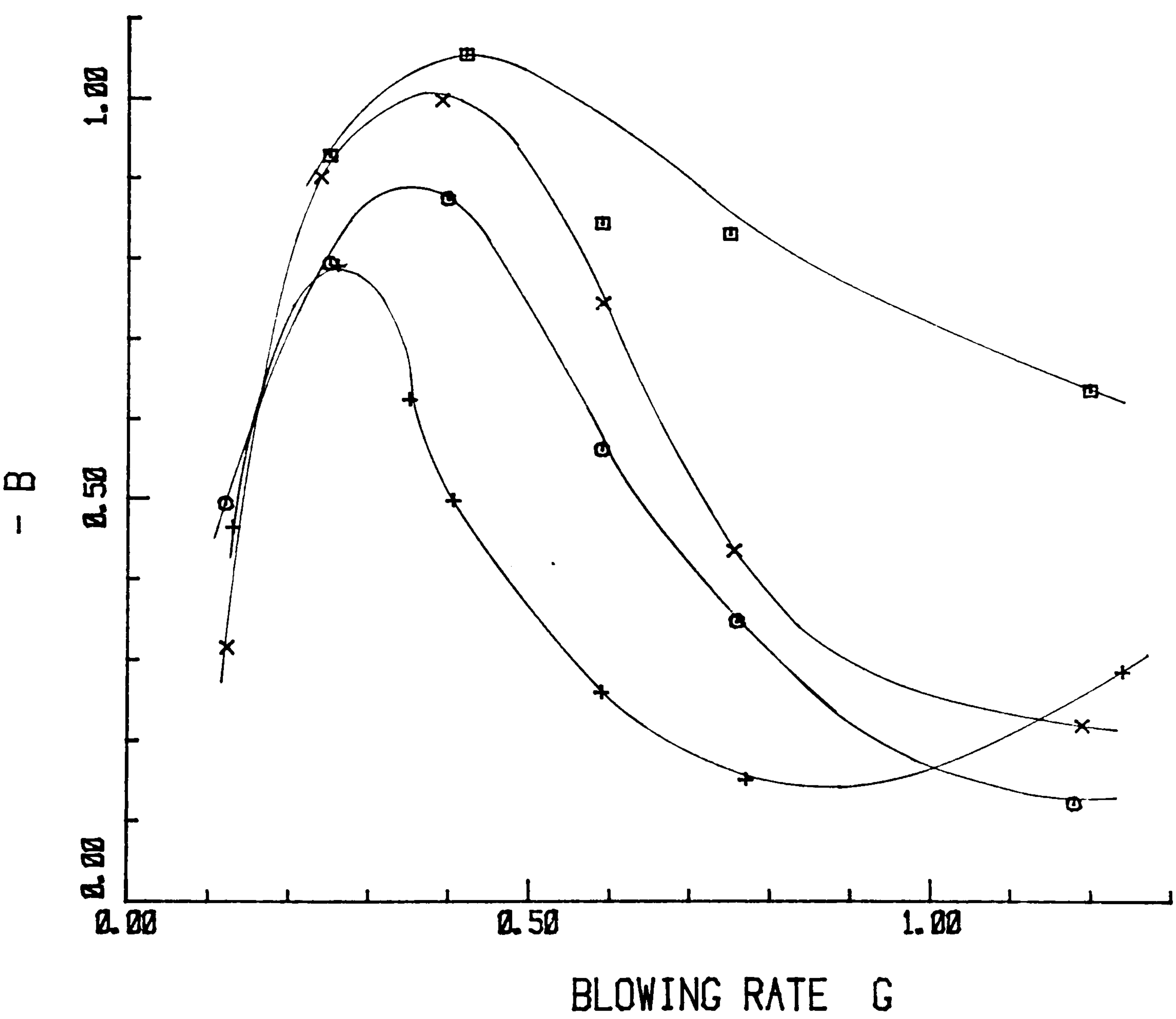

FIG. 8.13 (a) & (b) Variation of Film-Cooling Parameters with Mass Flux Ratio, X/D = 2.
(See Table 8.1 for Symbols).

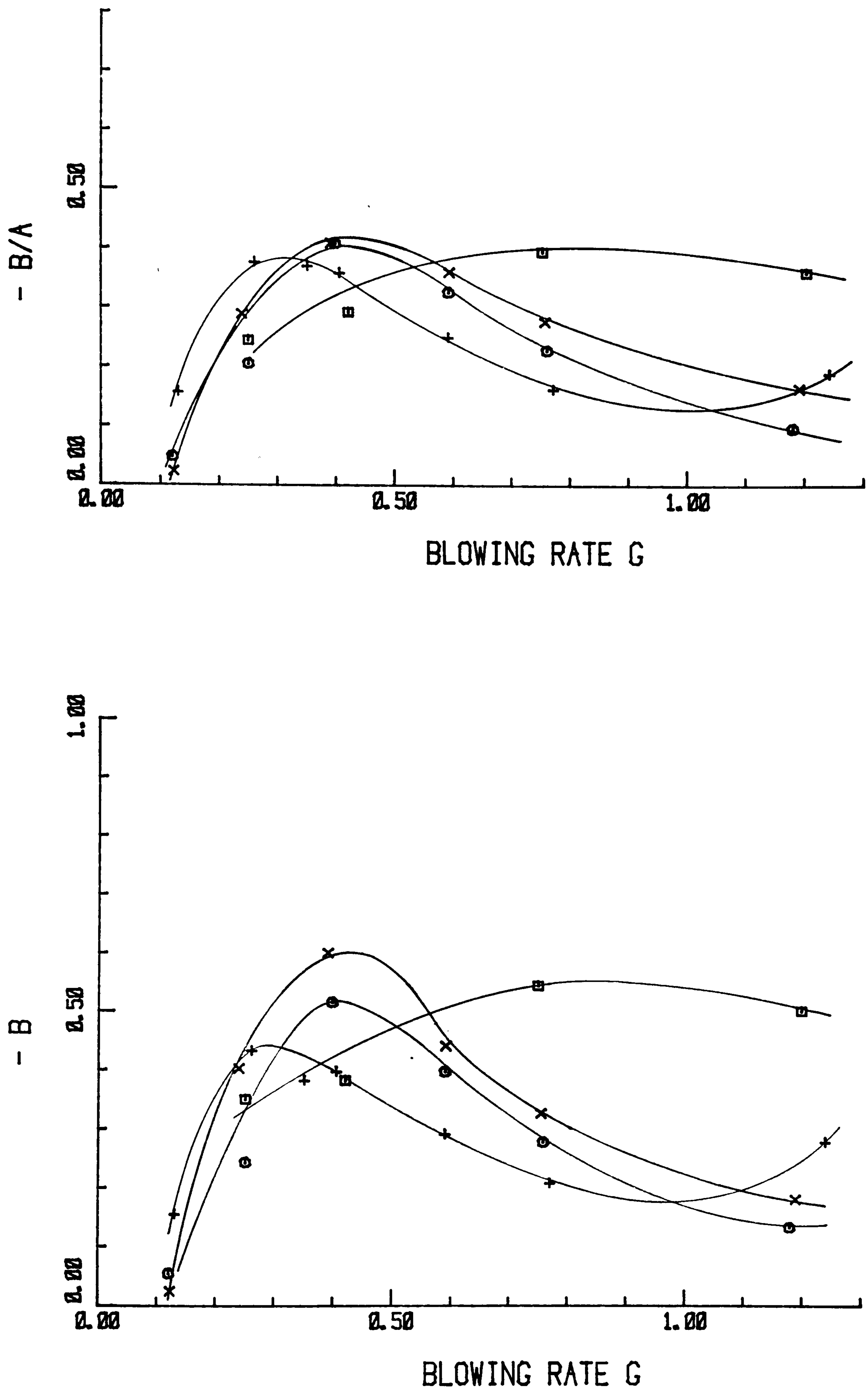

FIG. 8.14 (a) & (b) Variation of Film-Cooling Parameters with Mass Flux Ratio, X/D = 8.

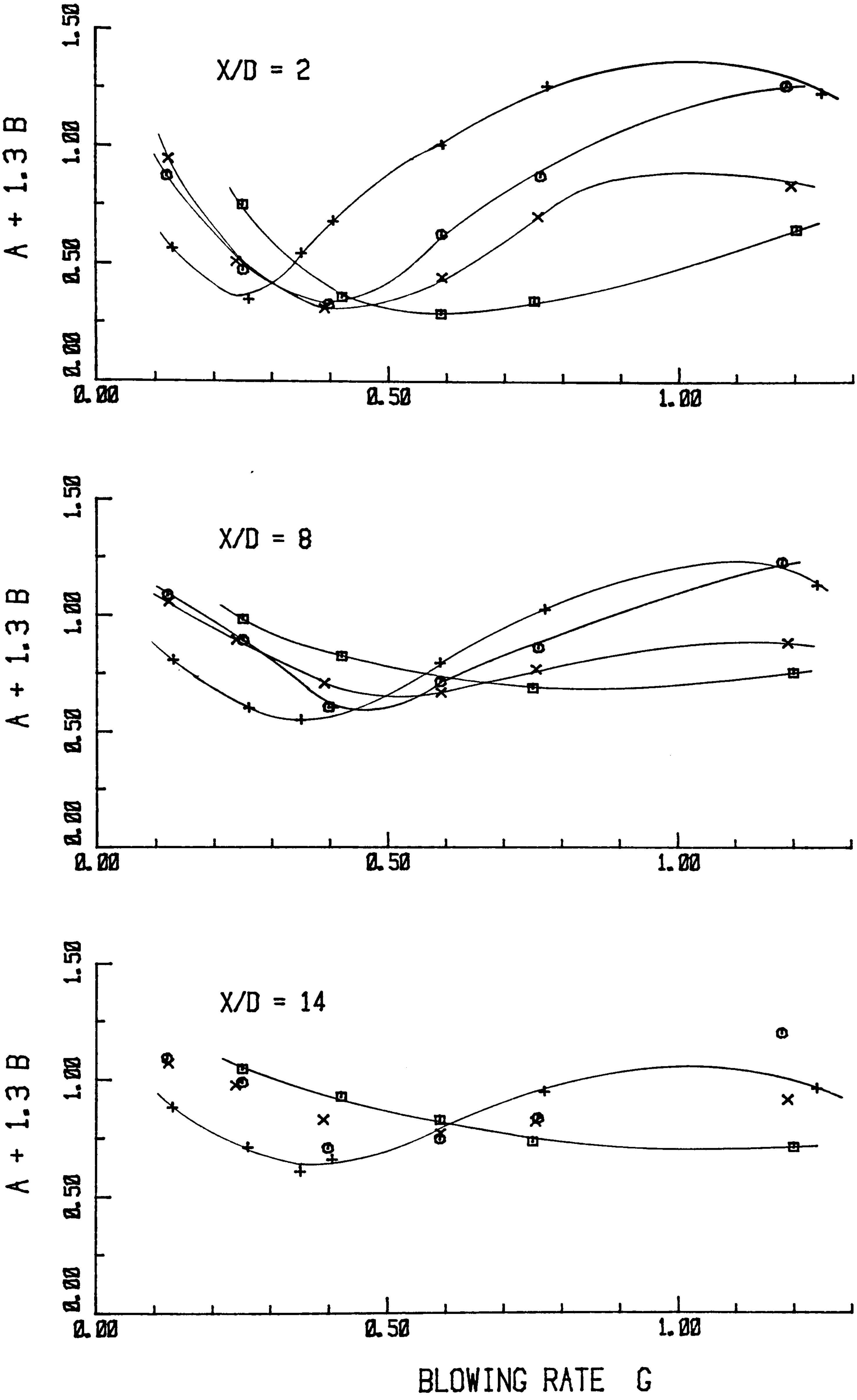

FIG. 8.15 Variation of Nusselt Number with Mass Flux Ratio at Theta = 1.3 for 4 injection-to-freestream temperature ratios.

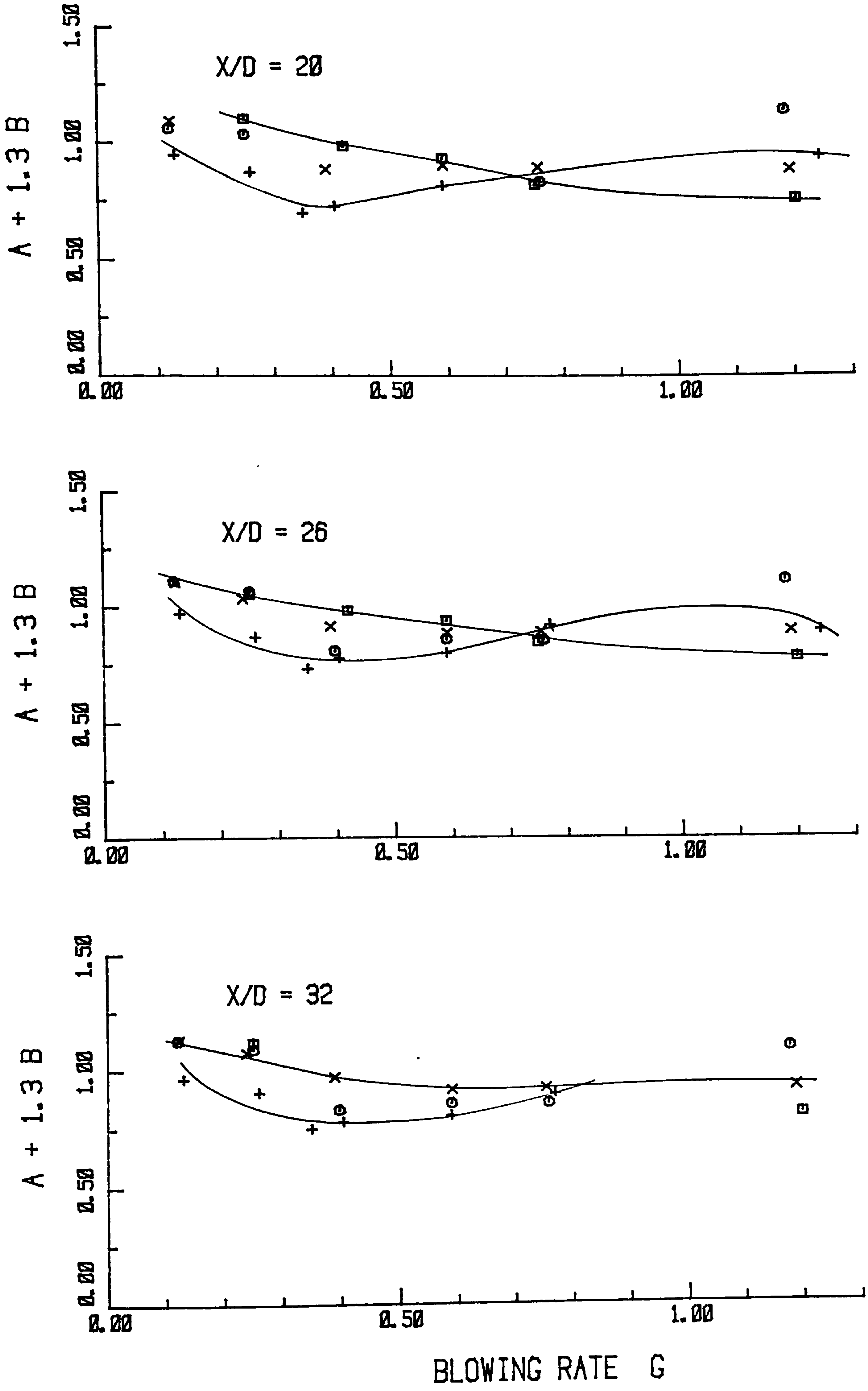

FIG. 8.15 (ctd) Variation of Nusselt Number with Mass Flux Ratio at Theta = 1.3 for 4 injection-to-freestream temperature ratios.

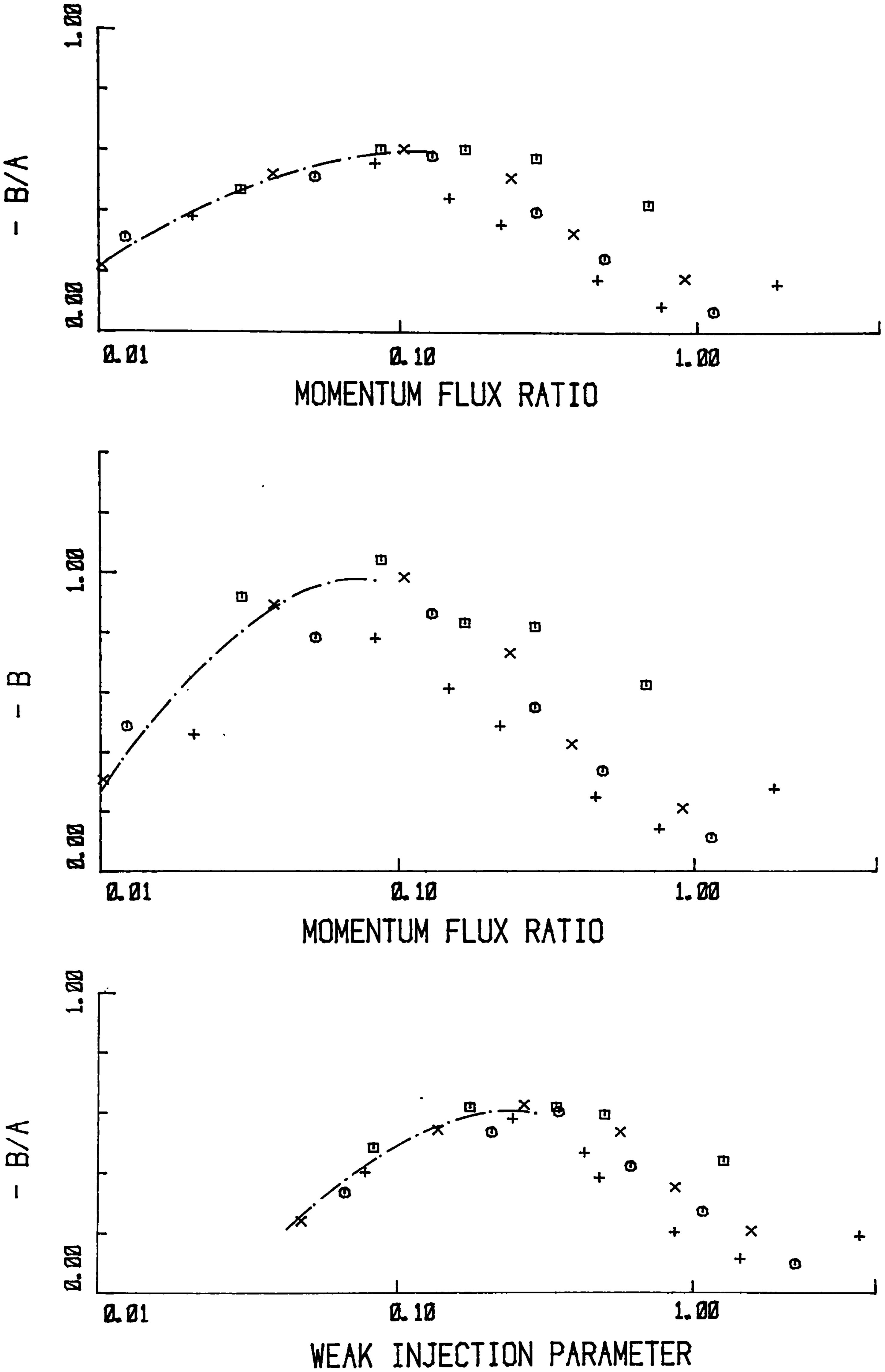

FIG. 8.16 (a)-(c) Correlation of Data with Momentum Flux Ratio and Weak Injection Parameter, X/D = 2.

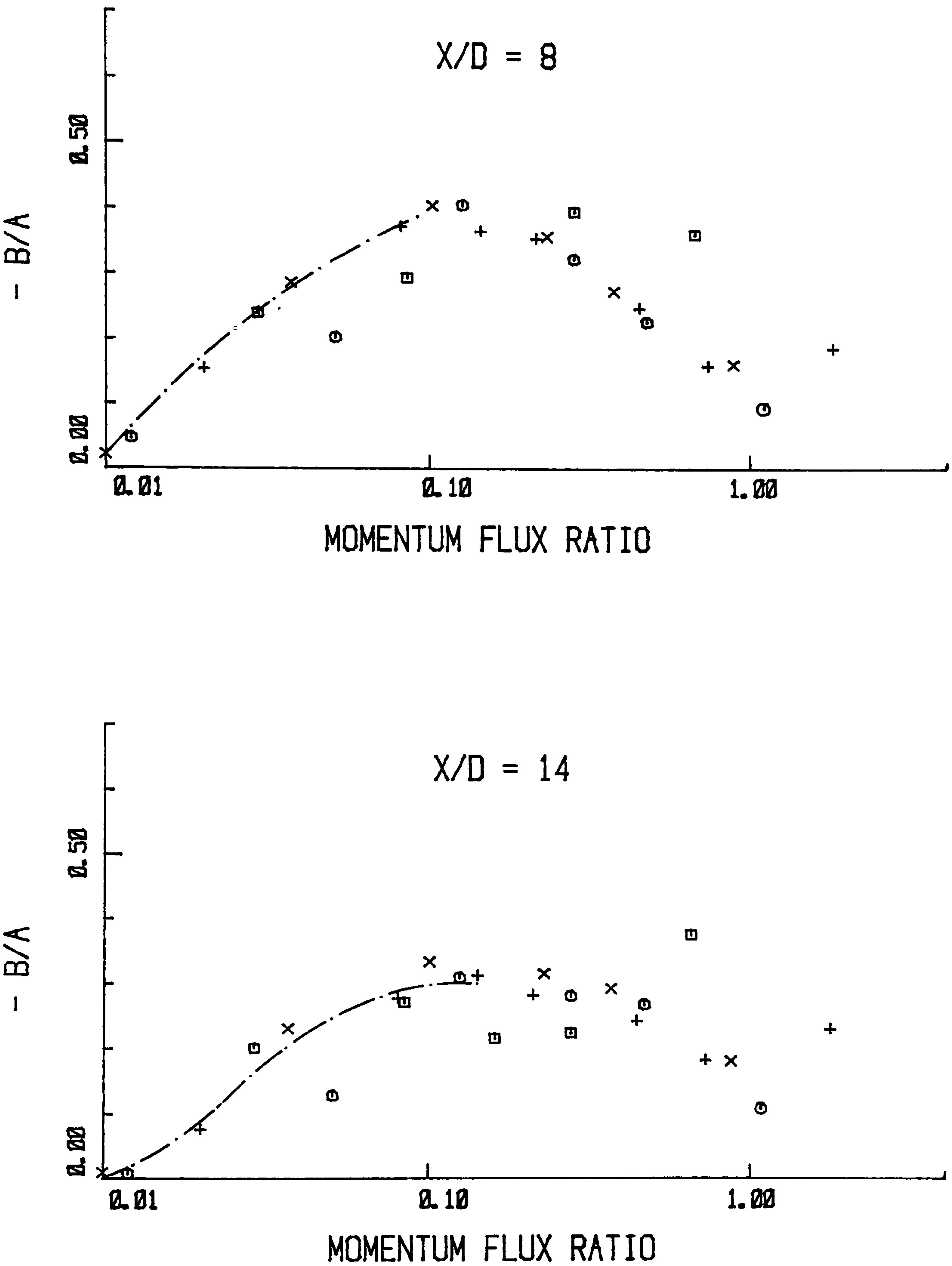

FIG. 8.17 Correlation of Data with Momentum Flux Ratio
X/D = 8 & 14.

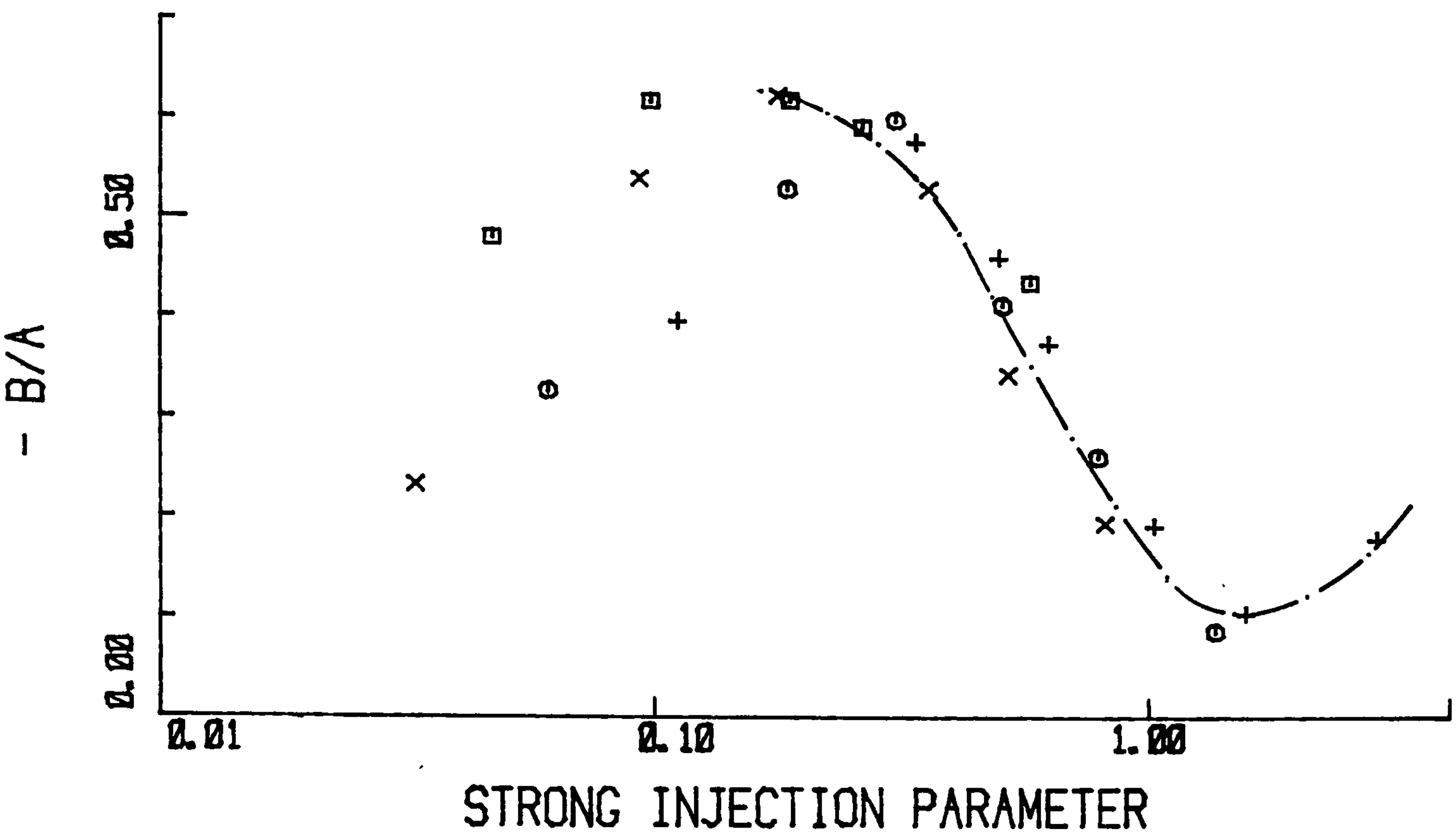

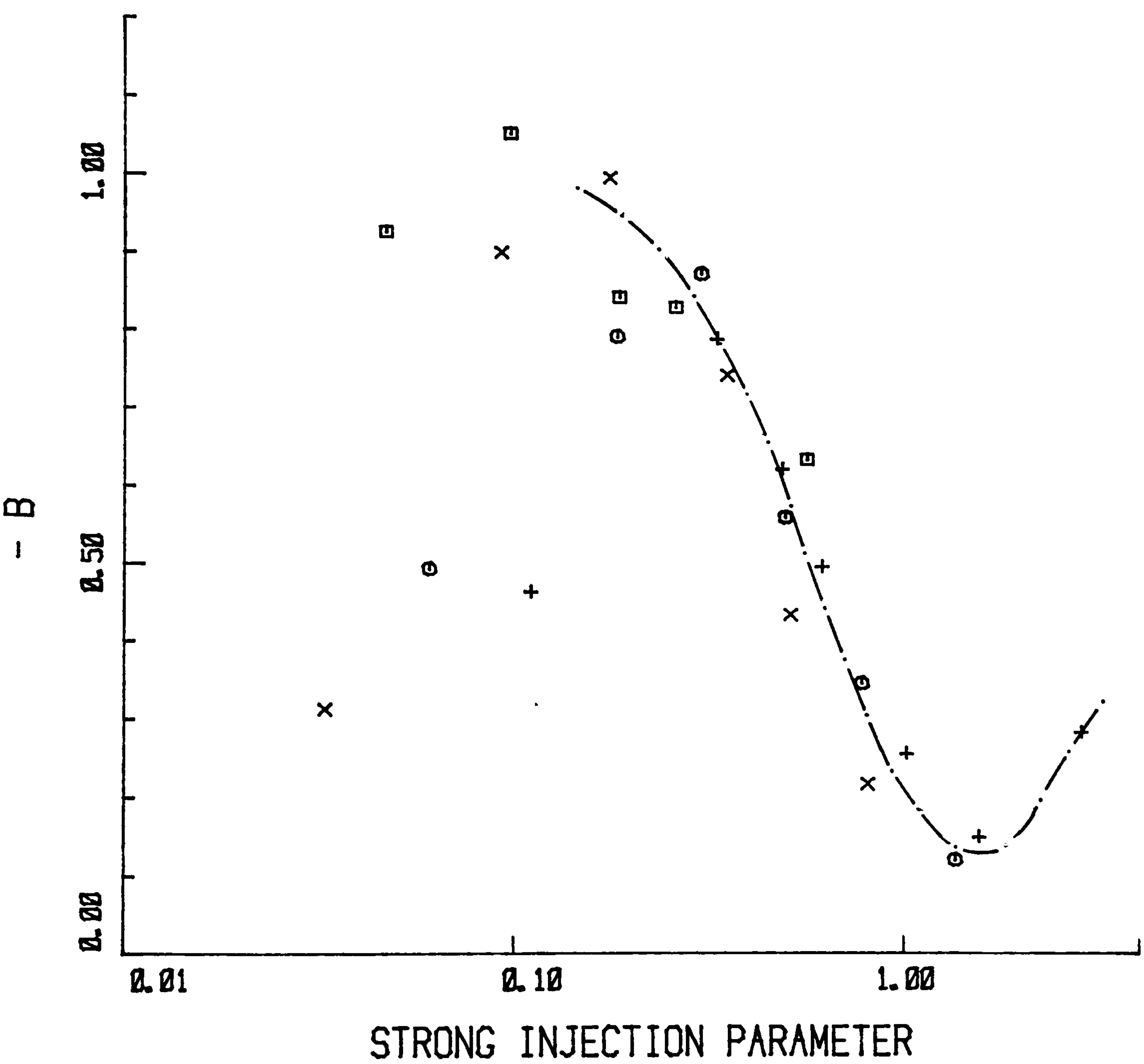

FIG. 8.18 Correlation of Data with Strong Injection Parameter, X/D = 2.

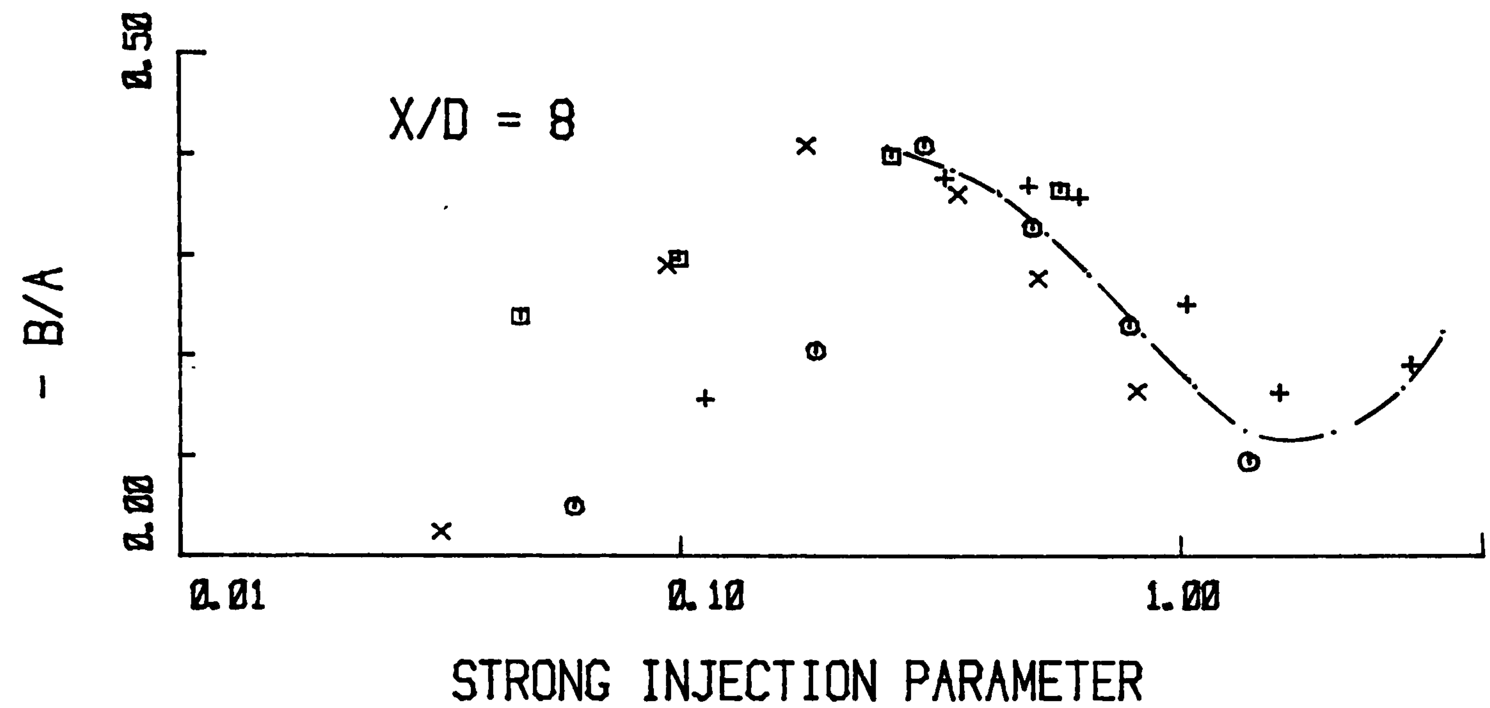

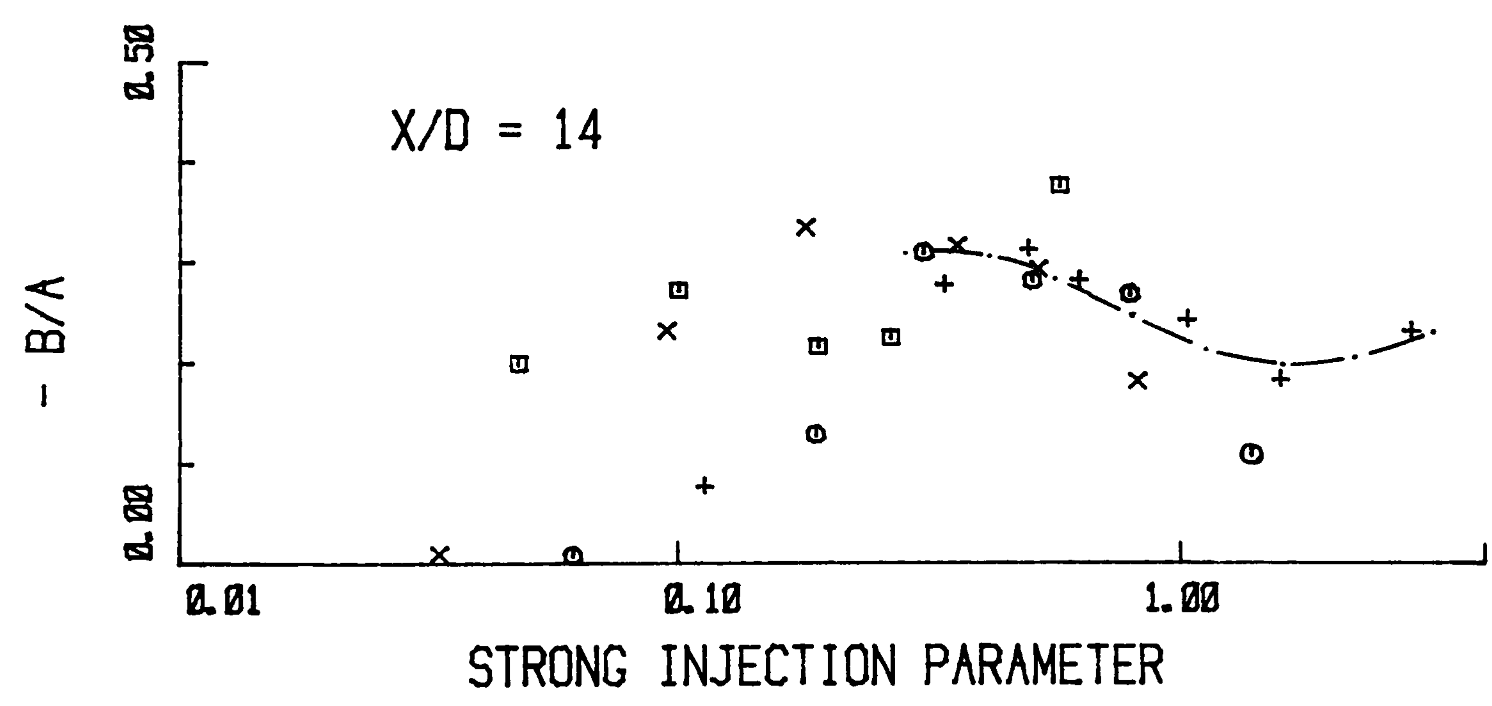

FIG. 8.19 Correlation of Data with Strong Injection Parameter, X/D = 8 & 14.

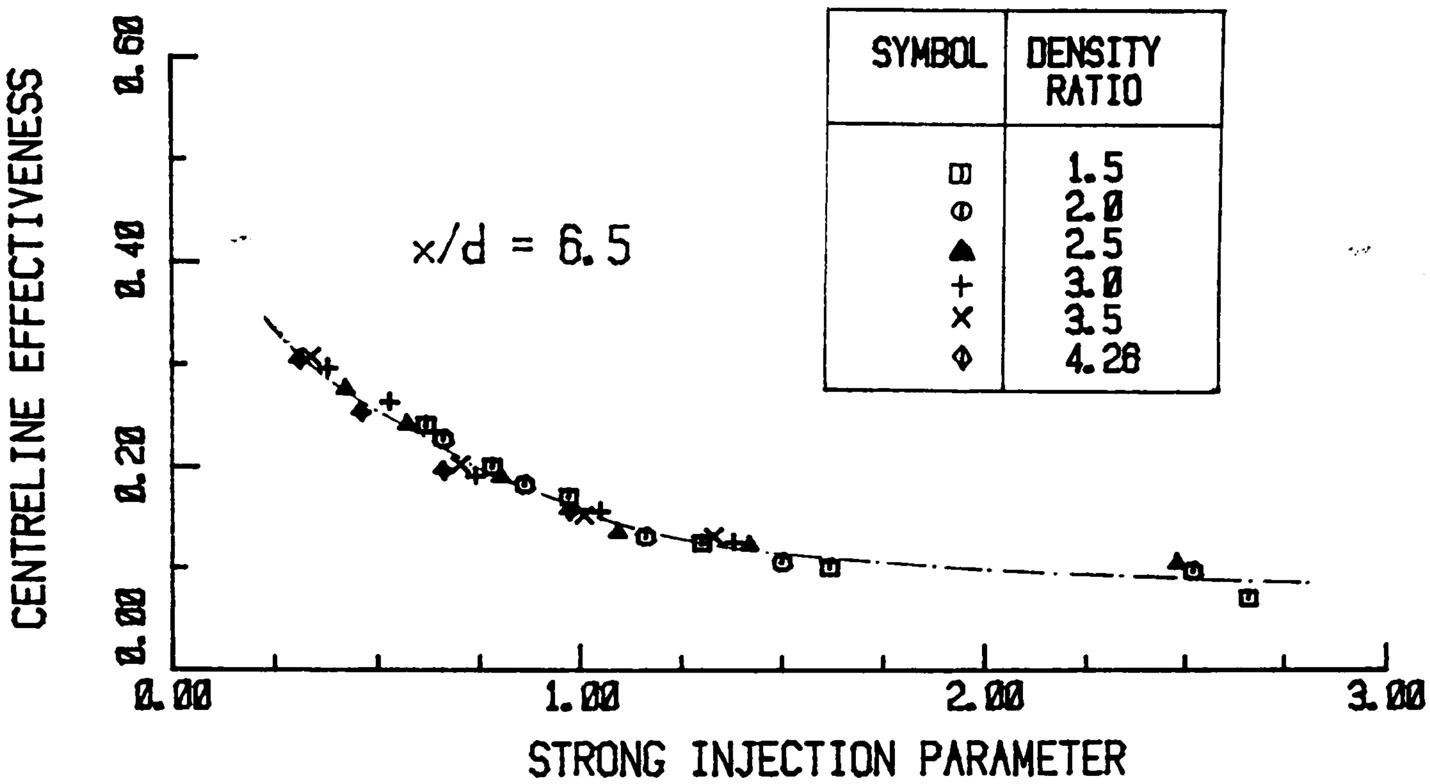

(a) Data from FOSTER & LAMPARD [8.15]

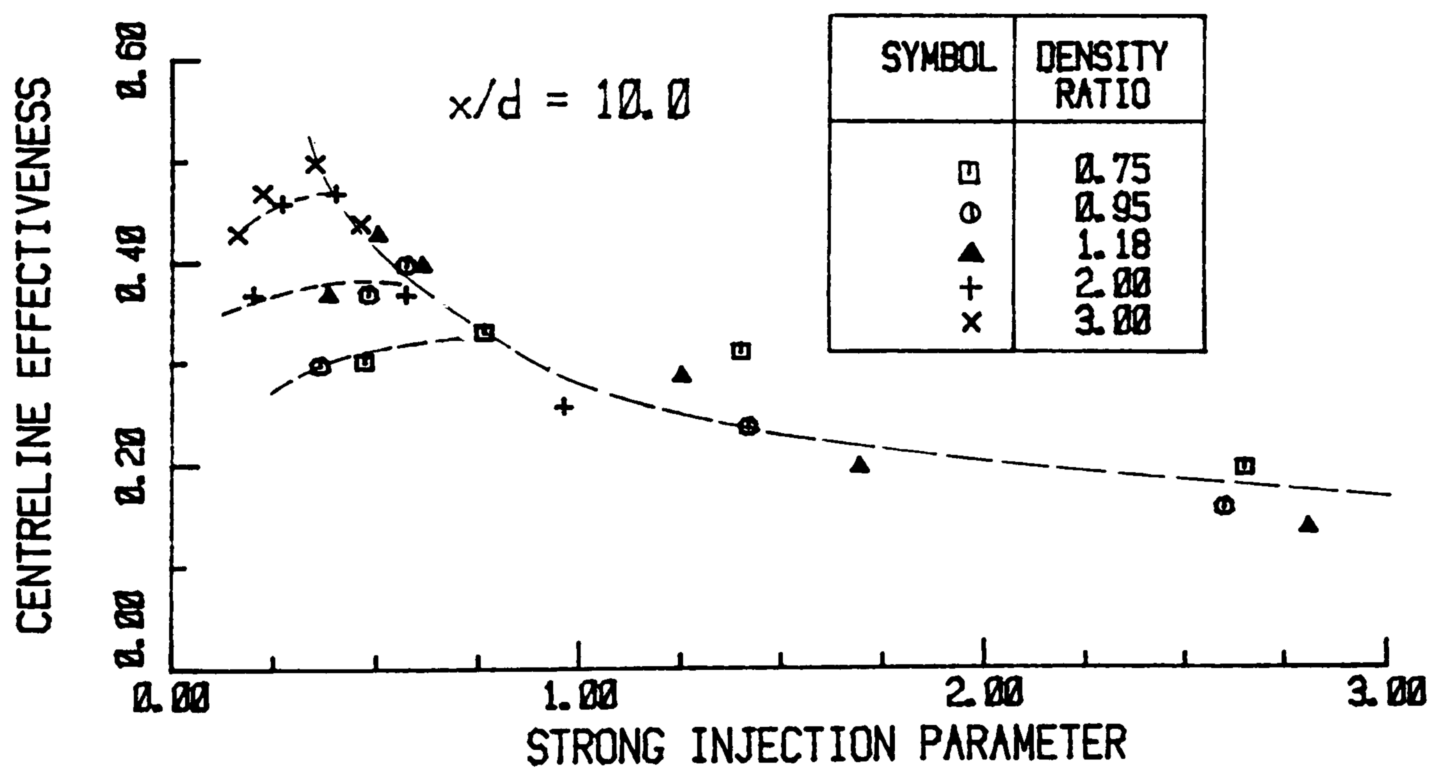

(b) Data from PEDERSEN et al [8.16]

FIG. 8.20 Correlation of Foreign Gas Injection Data with Strong Injection Parameter, after JONES [8.18]. (injection-to-freestream density ratios quoted).

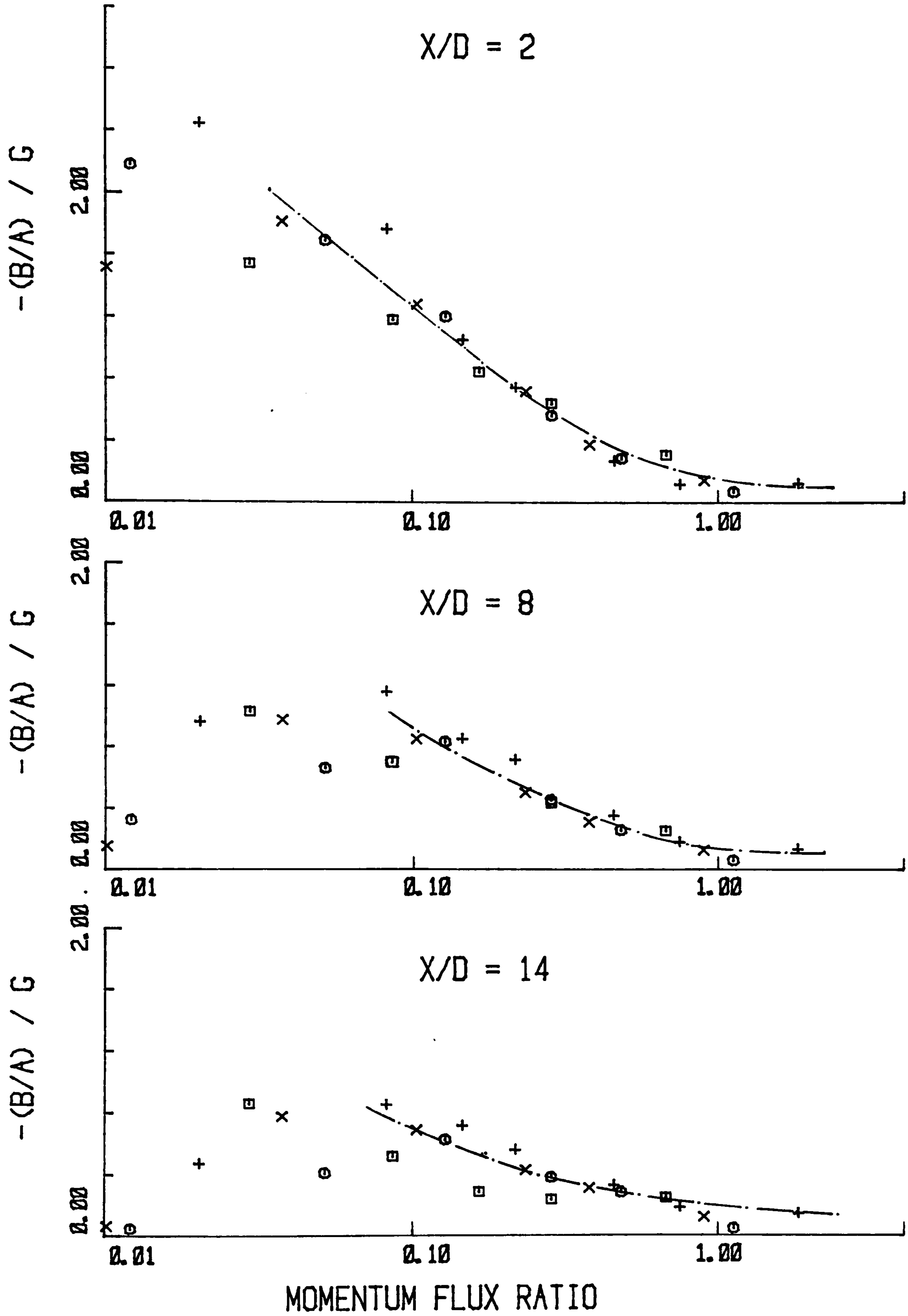

FIG. 8.21 Correlation of Present Data using Parameter from PEDERSEN [8.16].

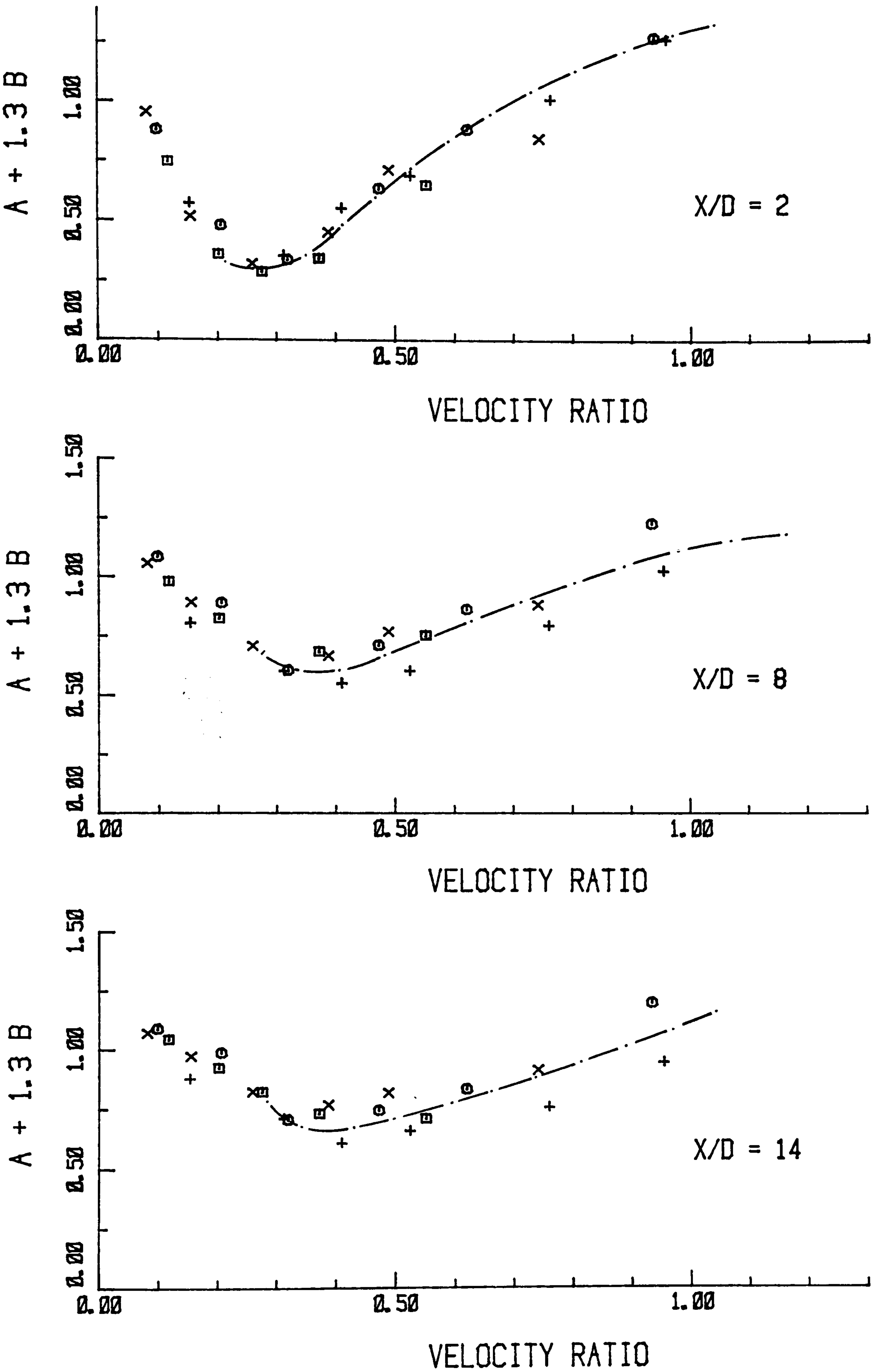

FIG. 8.22 (a) Correlation of Nusselt Number with velocity ratio at Theta = 1.3.

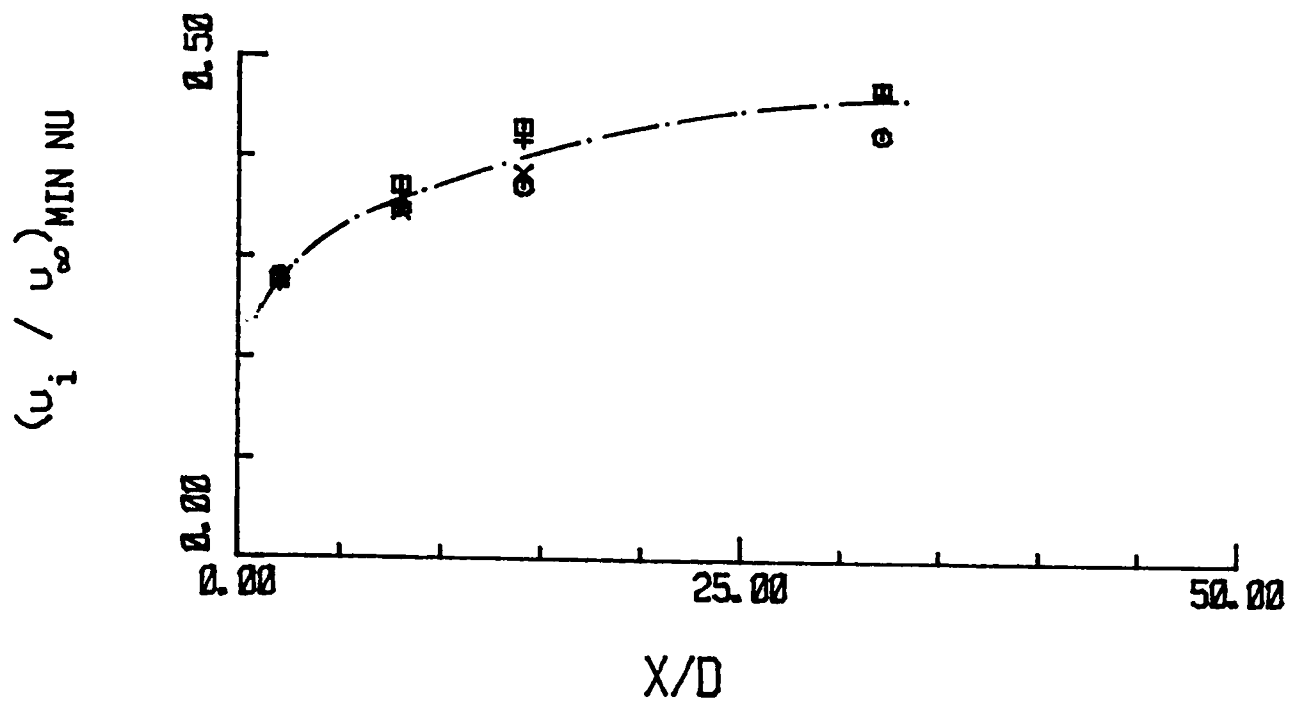

FIG. 8.22 (b) Correlation of Condition of Minimum Nusselt Number at each downstream position with velocity ratio.

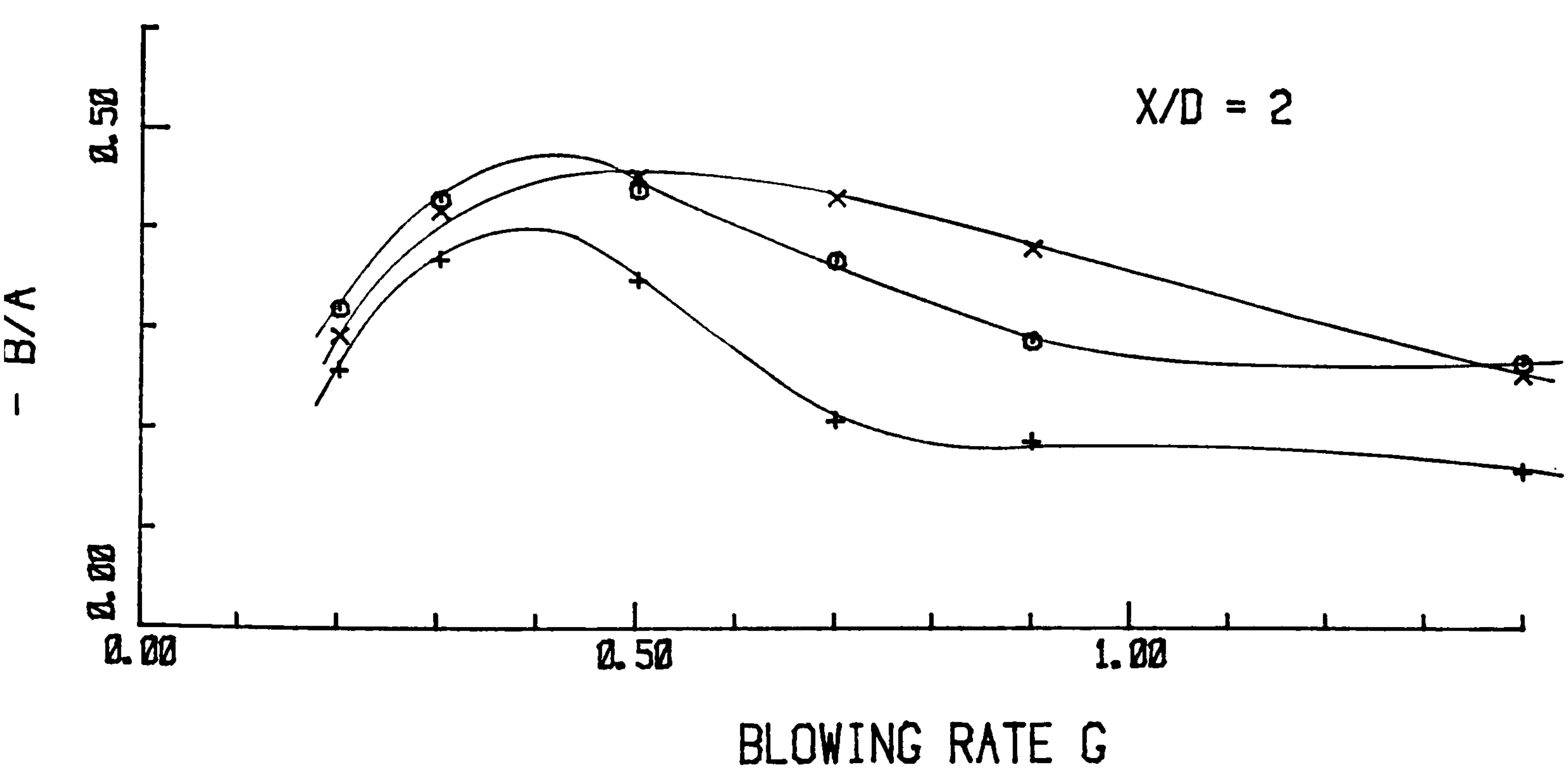

FIG. 8.23 Results from an Industrial Computer Programme based on [8.19] showing the effect of injection-to-freestream density ratio. (Symbols as in Table 8.1)

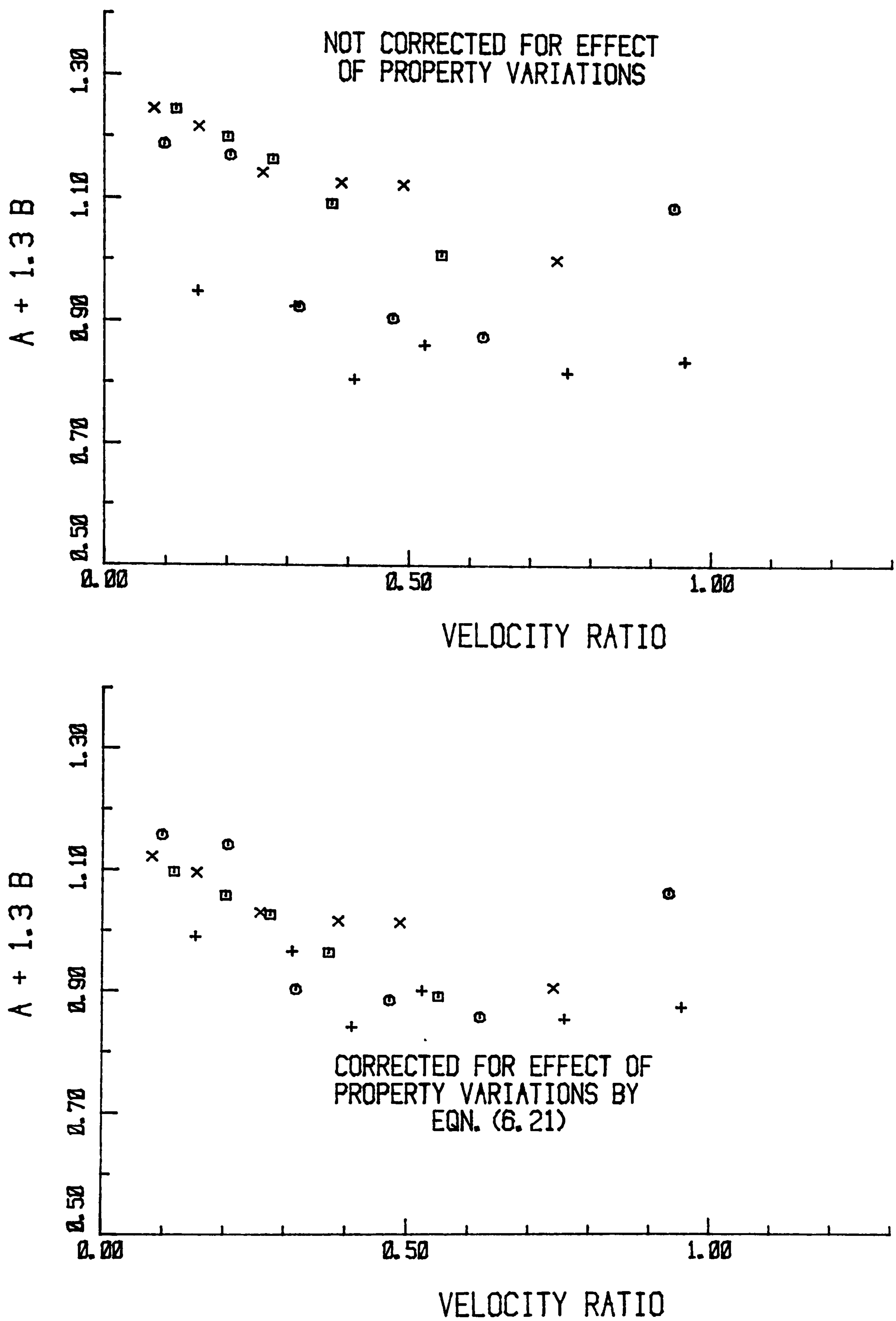

FIG. 8.24 Comparison Between Corrected and Uncorrected data to Illustrate the Effect of Property Variations, X/D = 62.

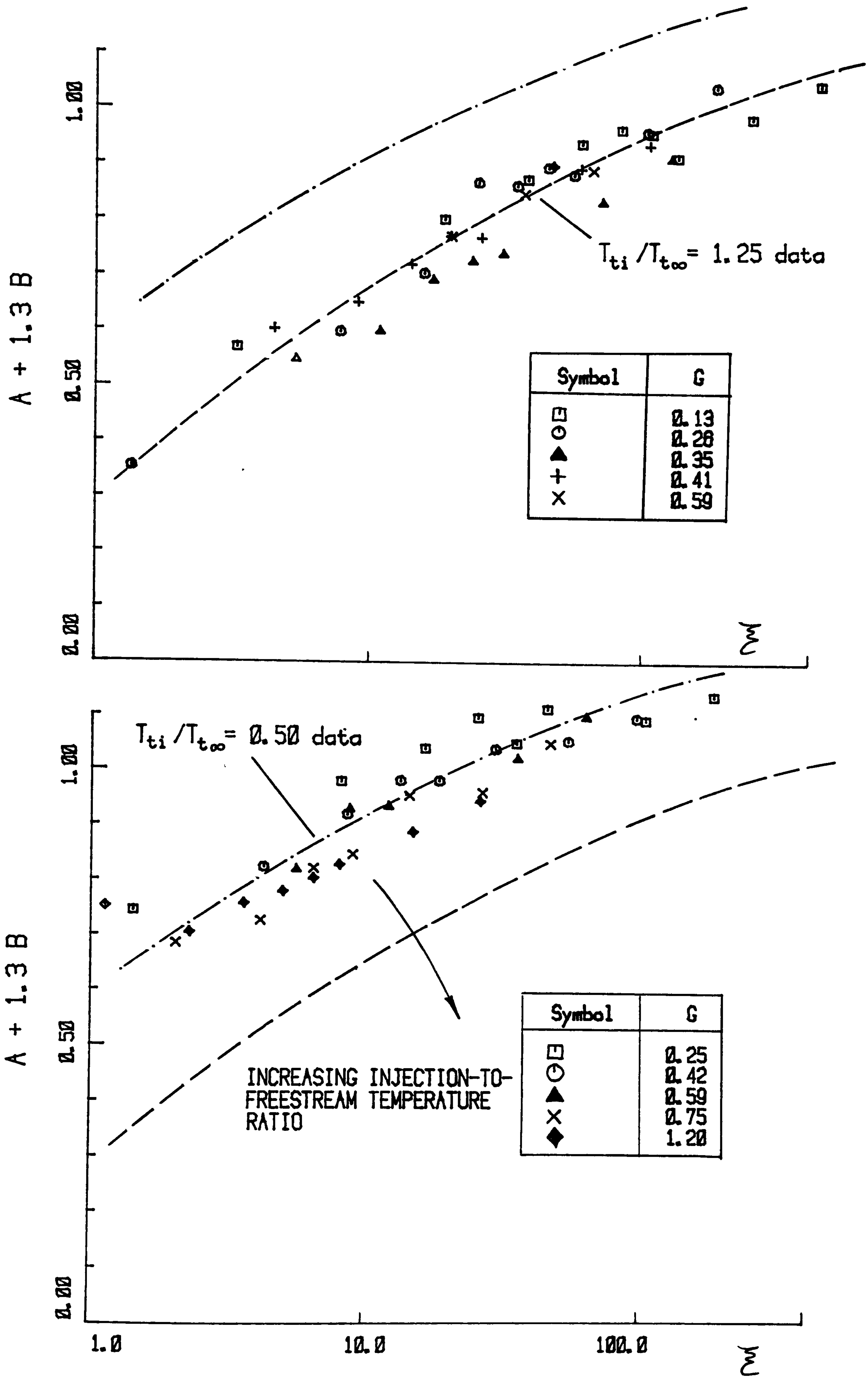

FIG. 8.25 Partial Collapse of Data Resulting from use of the Energy Balance Parameter.

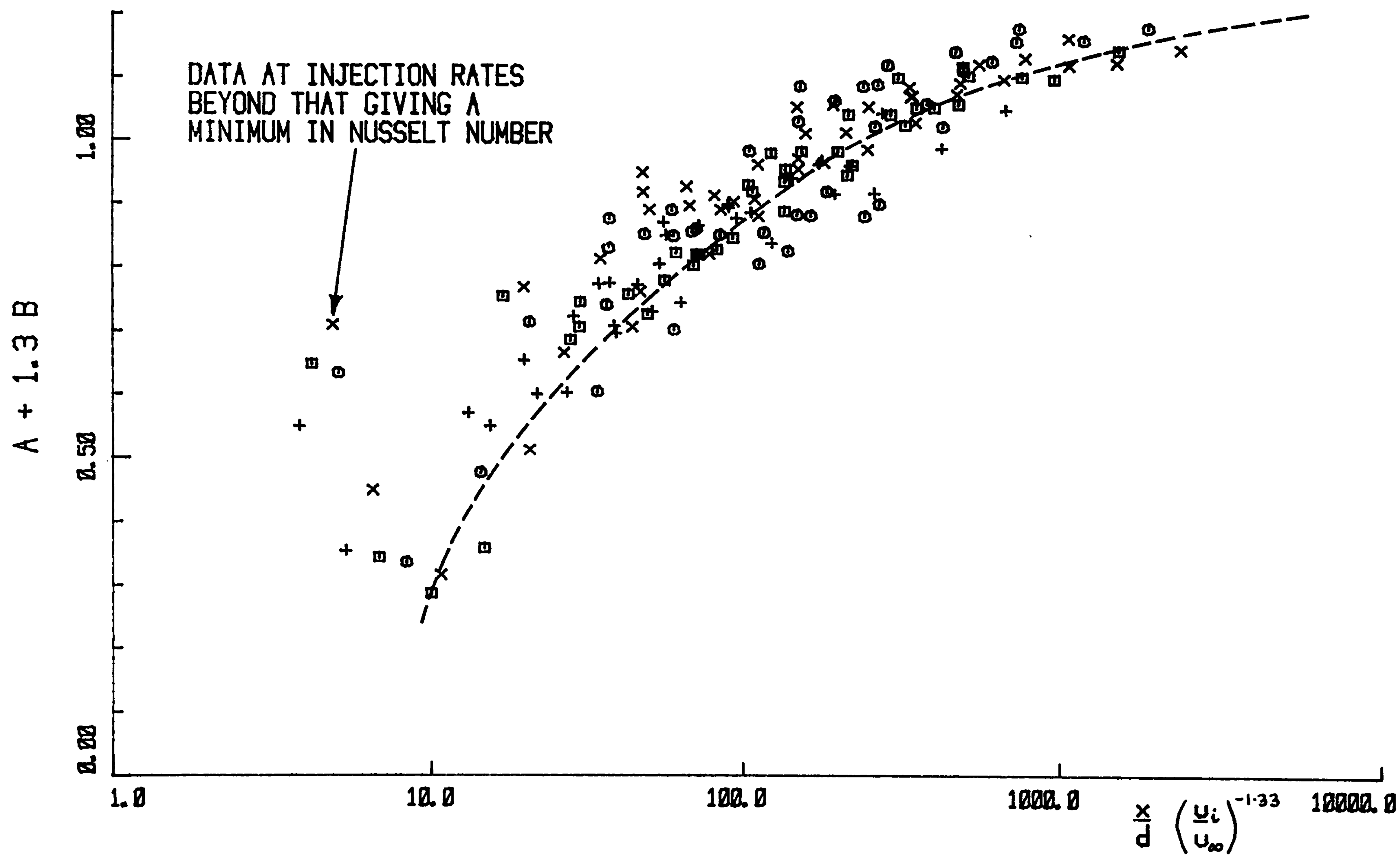

FIG. 8.25(b) Correlation of Single Row Results for four injection-to freestream temperature ratios using slot-wall jet parameter. modified for strong blowing regime.

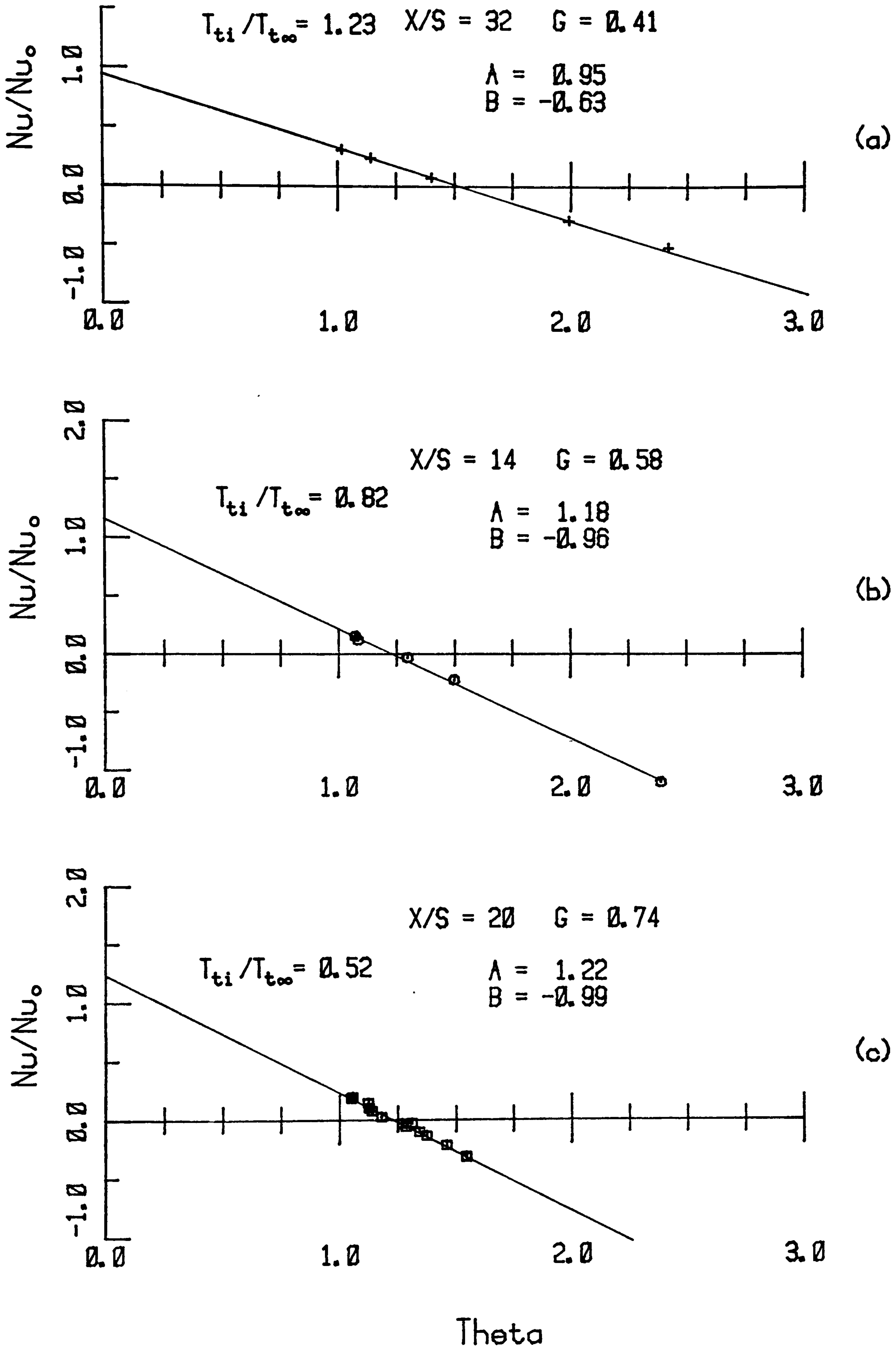

FIG. 8.26 Slot data - Variation of Nusselt Number with Theta as the wall temperature is changed.

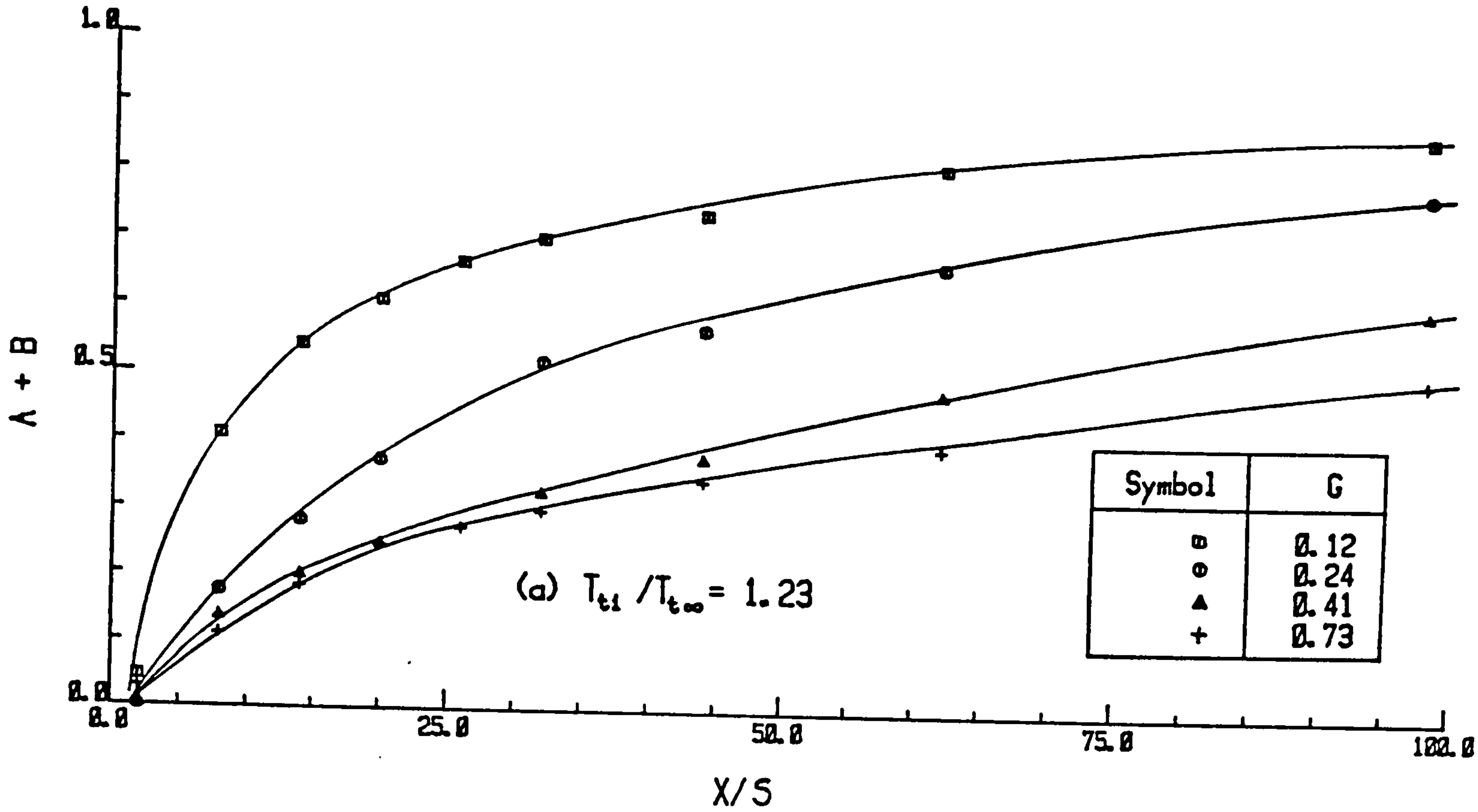

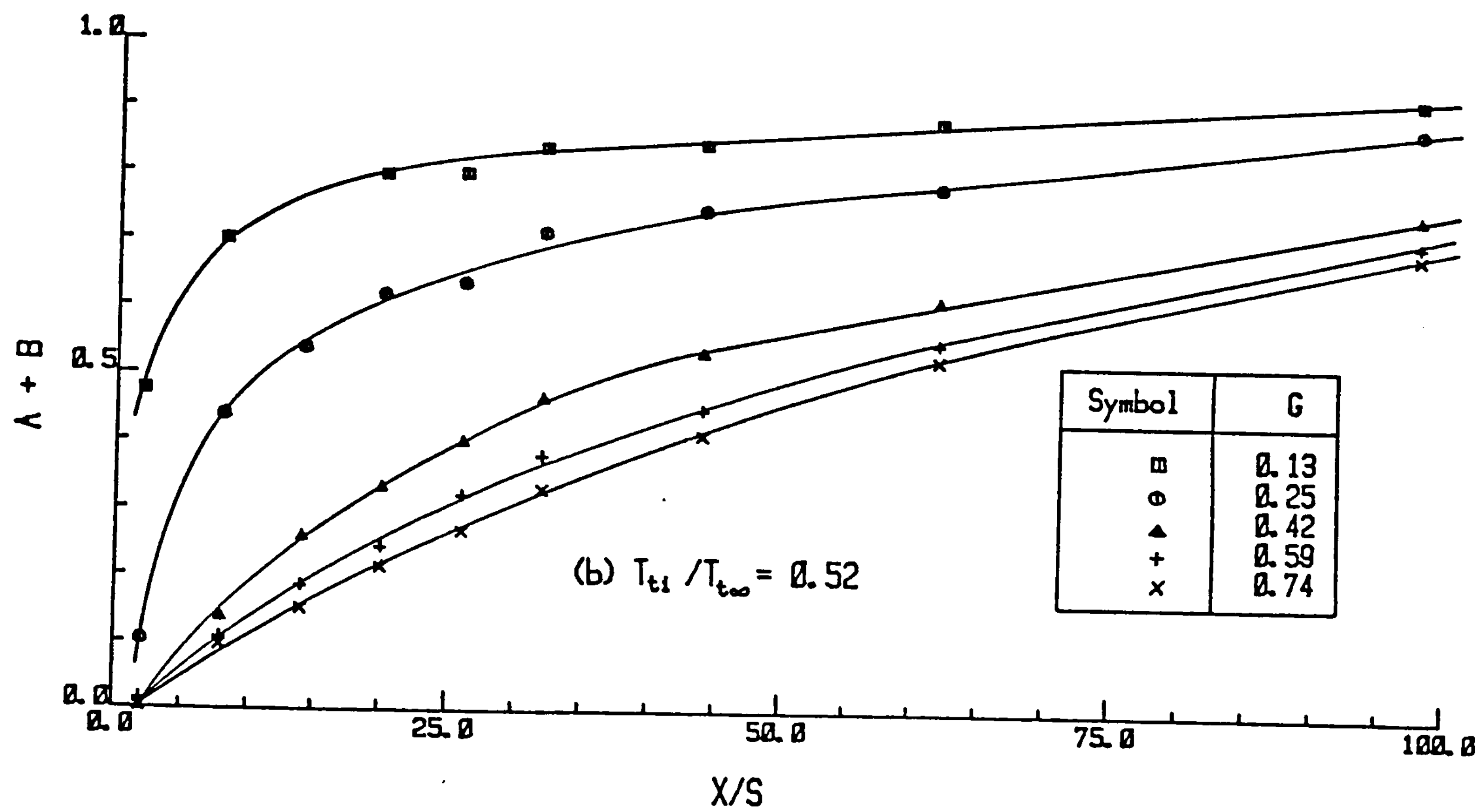

FIG. 8.27 Slot data - Variation of Nusselt Number with distance at Theta = 1.0

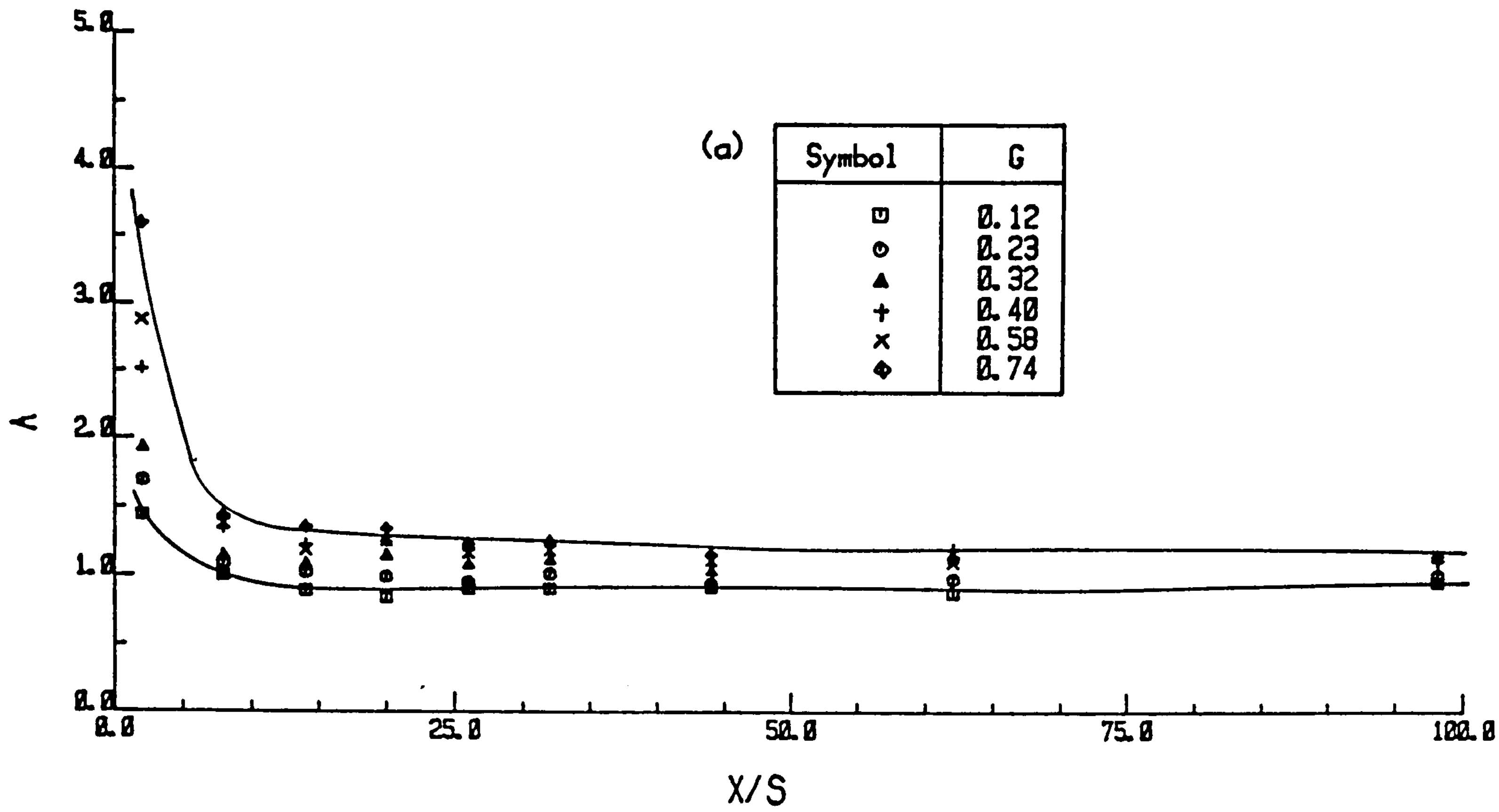

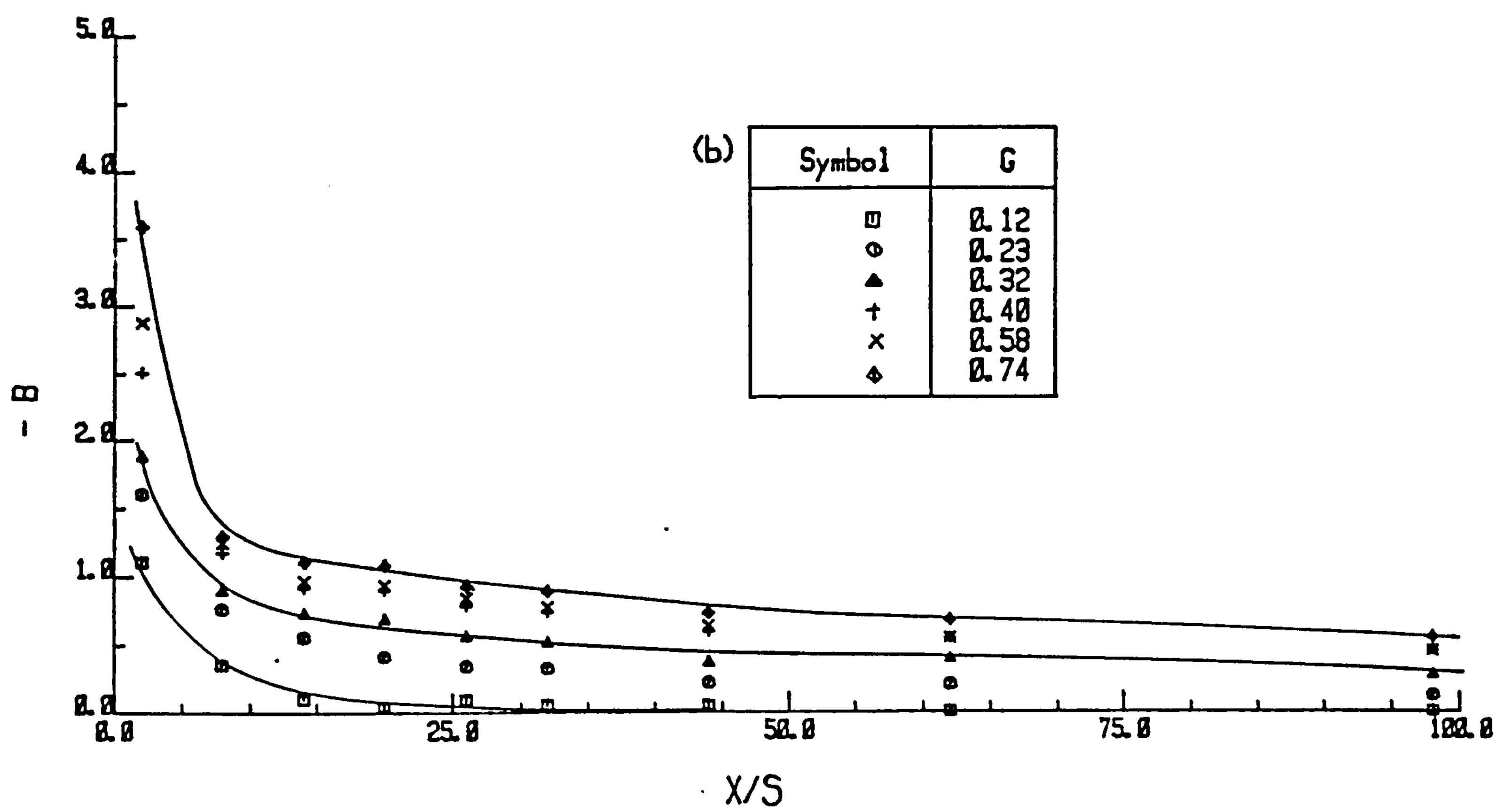

FIG. 8.28 Slot data − Variation of Λ and B with distance and blowing rate ; $T_{ti}/T_{t\infty} = 0.82$

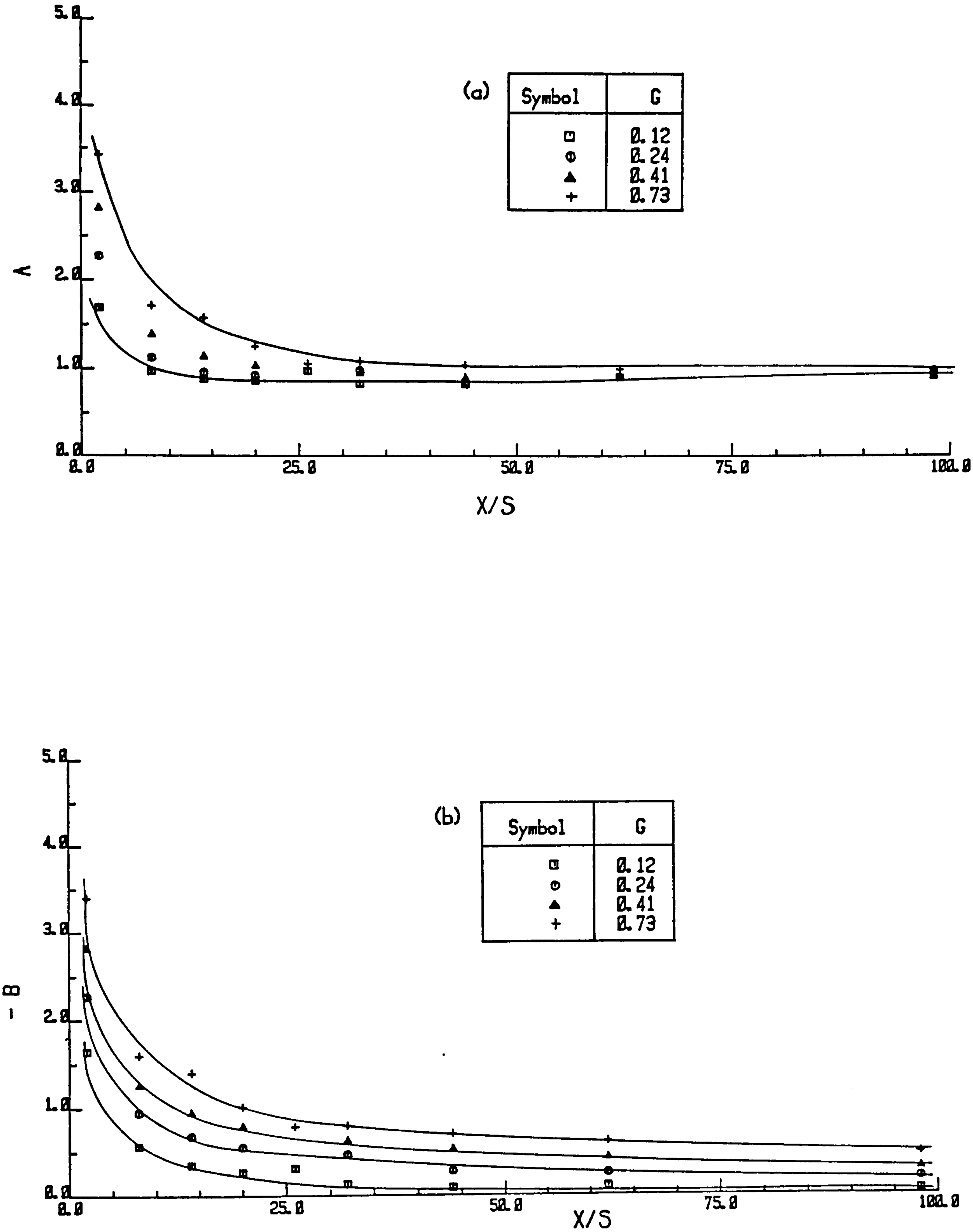

FIG. 8.29 Slot data - Variation of A and B with distance and blowing rate ; $T_{ti}/T_{t\infty} = 1.23$

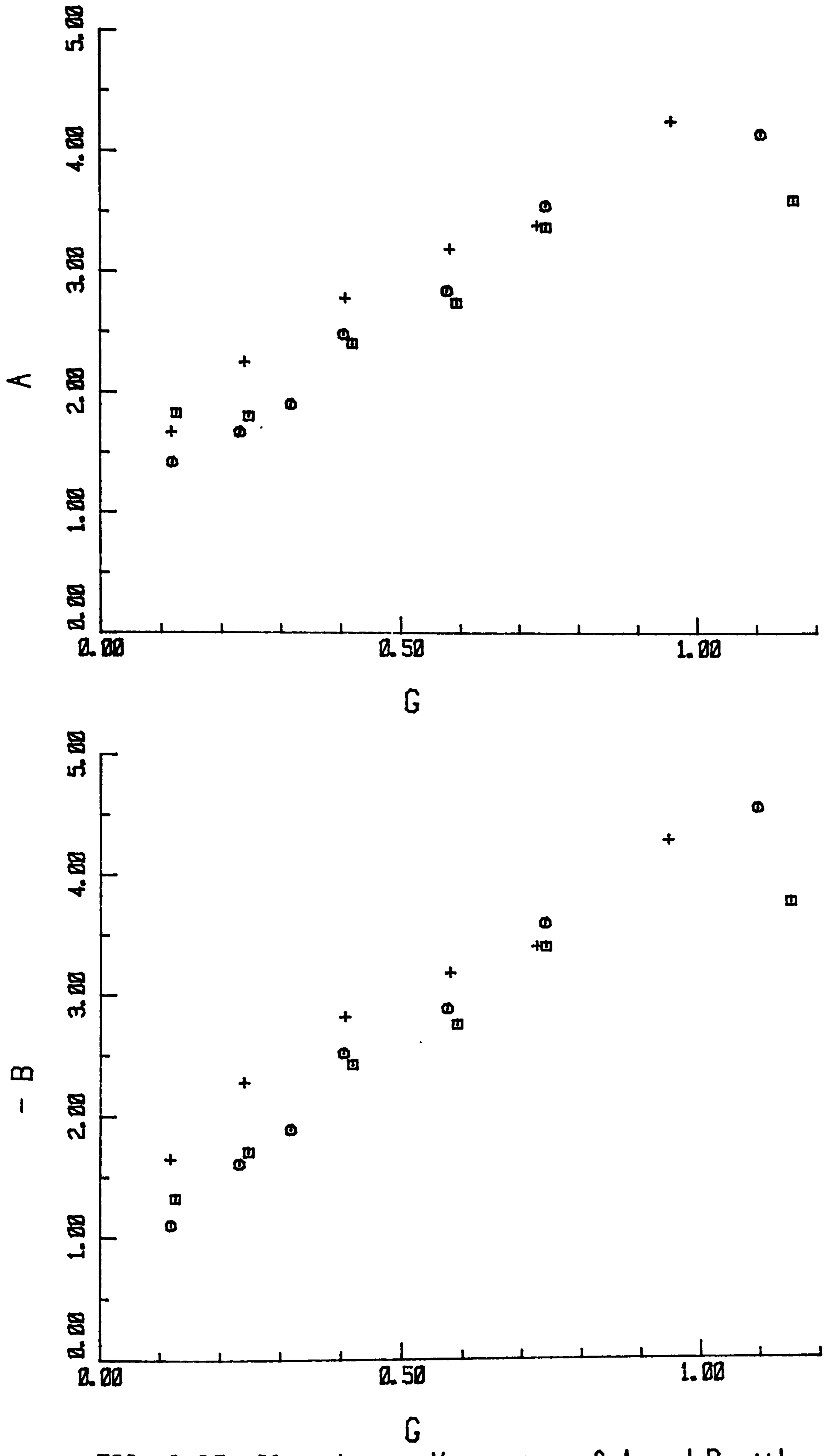

FIG. 8.30 Slot data - Variation of A and B with Mass Flux Ratio - X/S = 2
(See Table 8.2 for symbols)

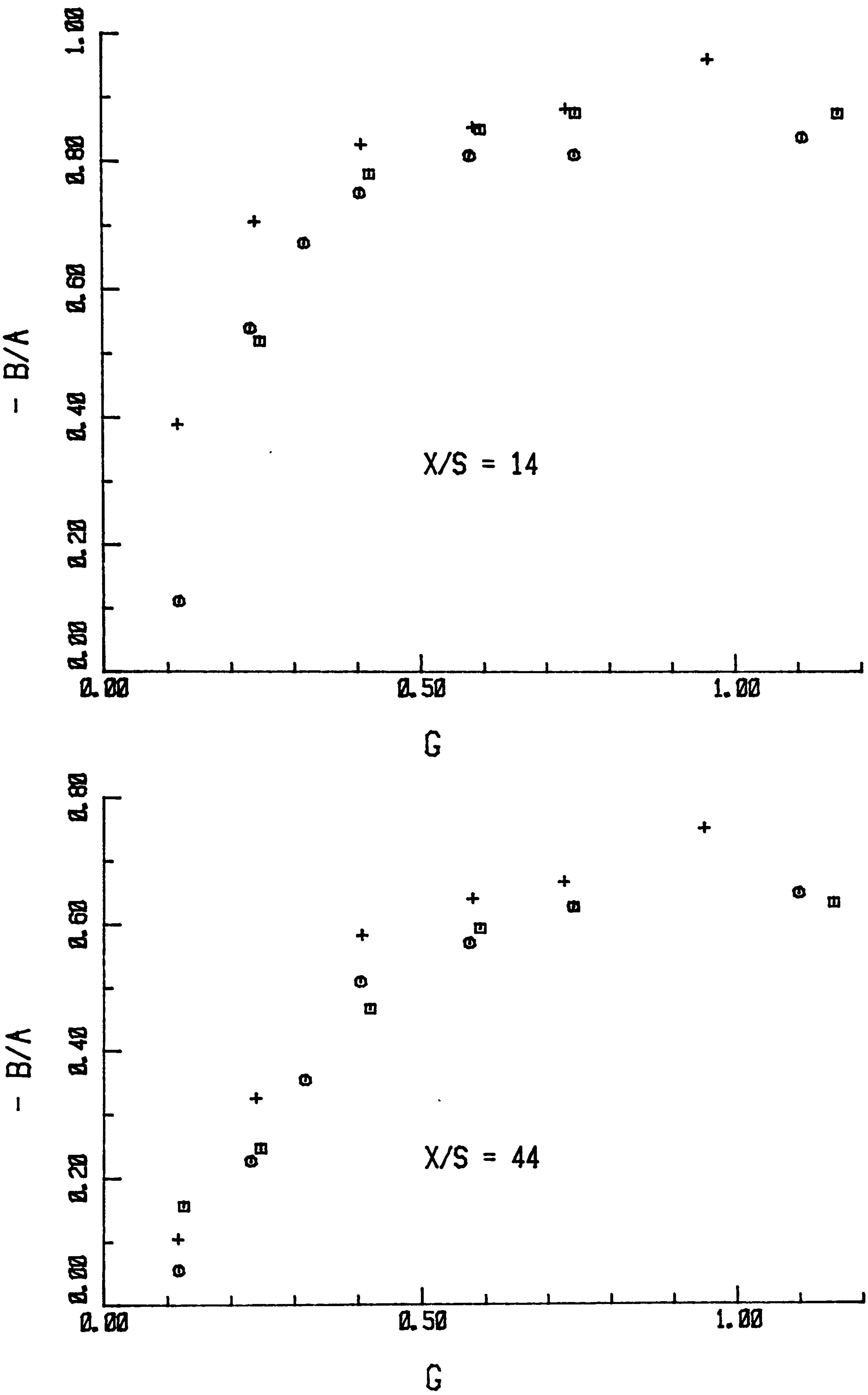

FIG. 8.31 Slot Data - Variation of Film Cooling Parameter - B/A with Mass Flux Ratio.

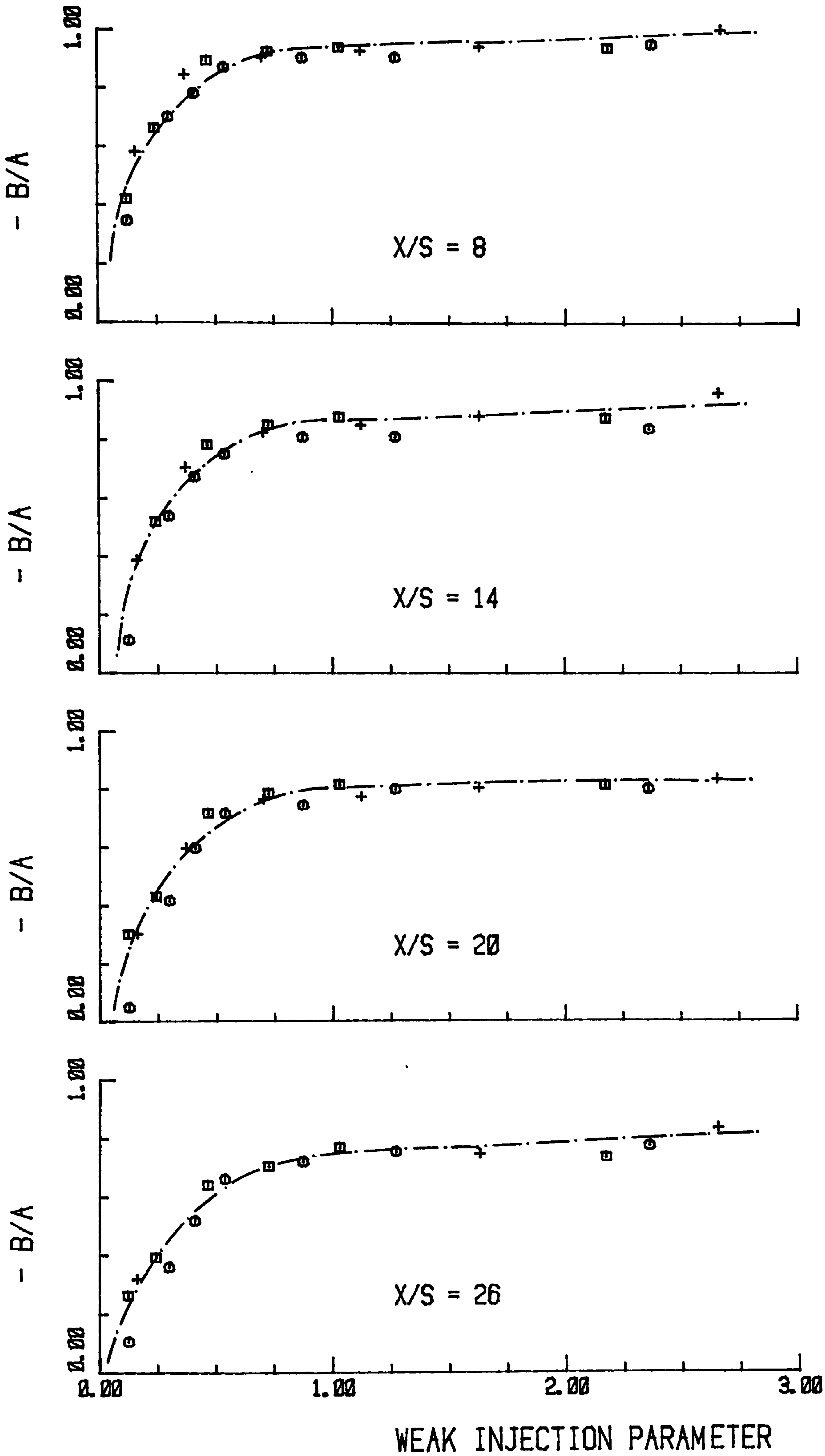

FIG. 8.32 Slot Data - Correlation of Film Cooling Data with Weak Injection Parameter.

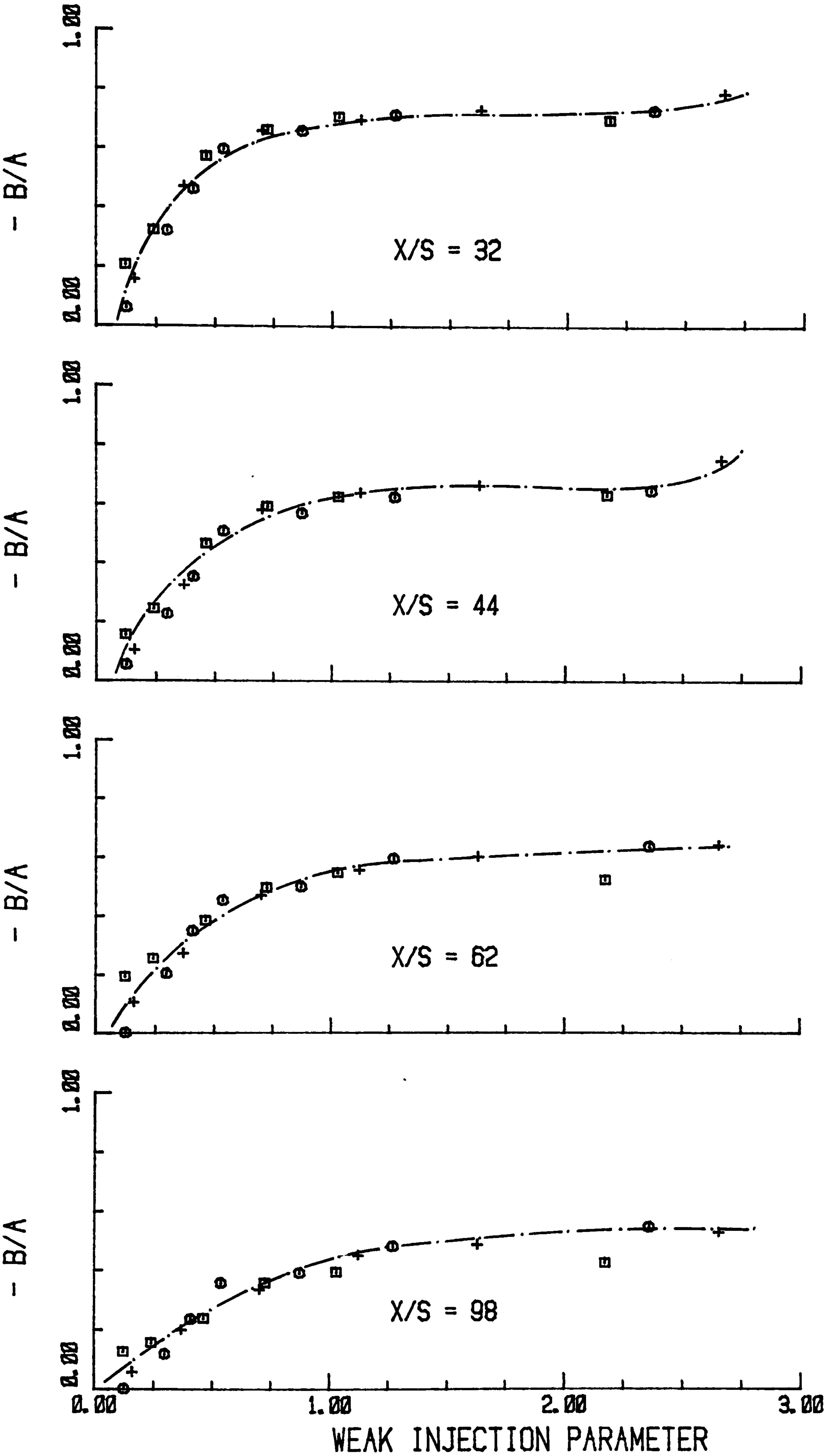

FIG. 8.32 (ctd.) Slot Data - Correlation of Film Cooling Data with Weak Injection Parameter.

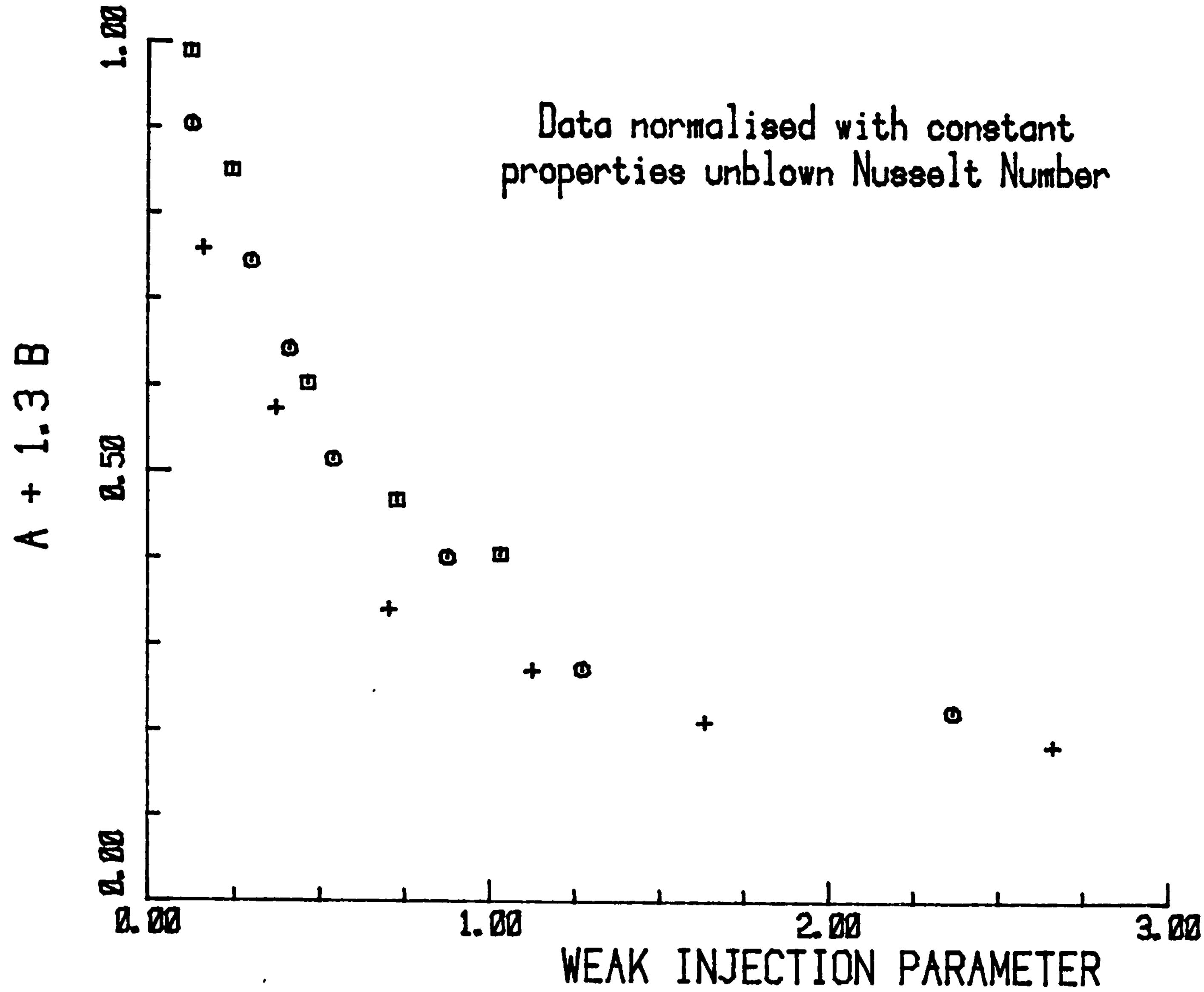

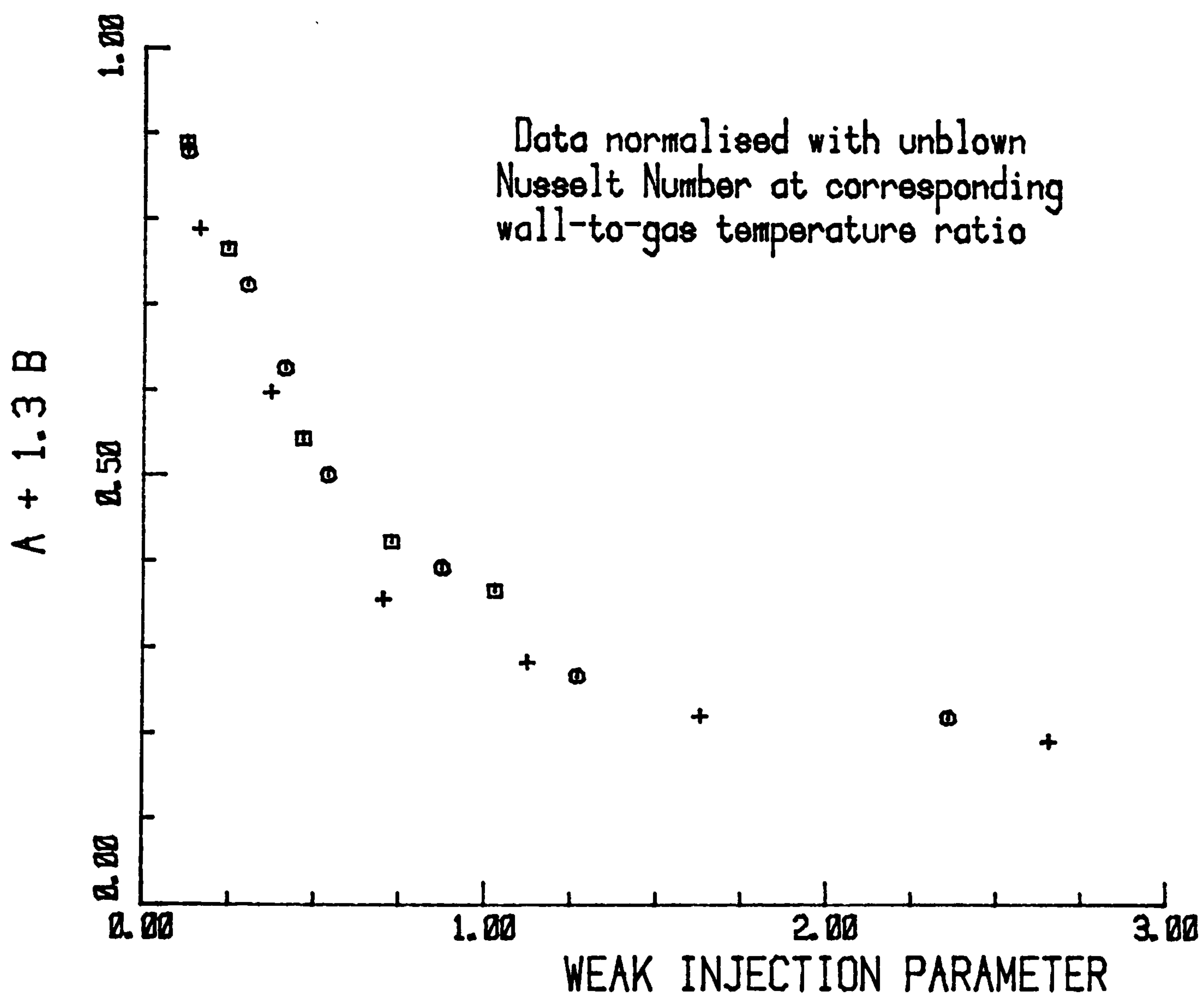

FIG. 8.33 Slot Data – Comparison Between Corrected and Uncorrected Data to Illustrate the Effect of Property Variations – X/S = 62

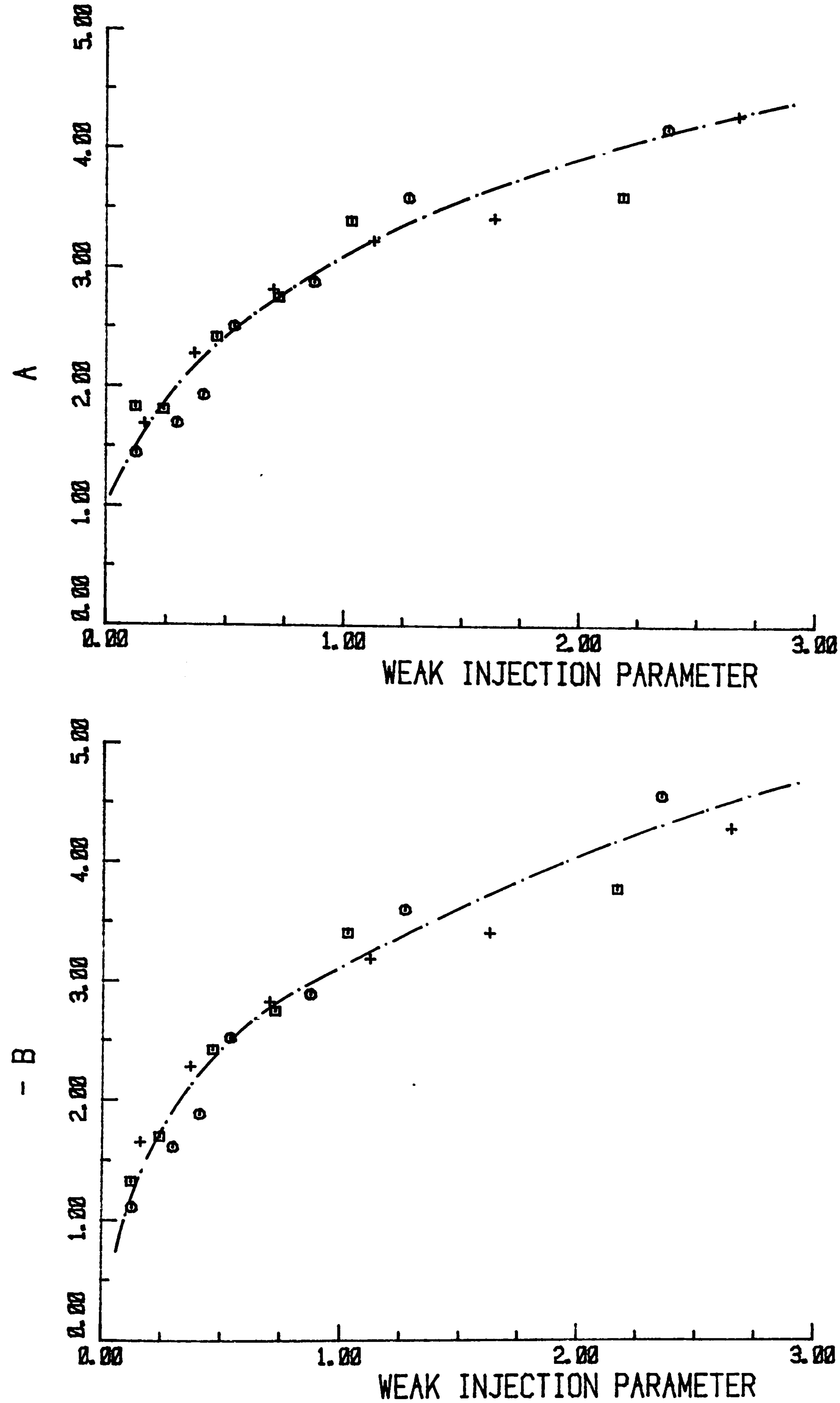

FIG. 8.34 (a) Correlation of A and B with Weak Injection Parameter - X/S = 2

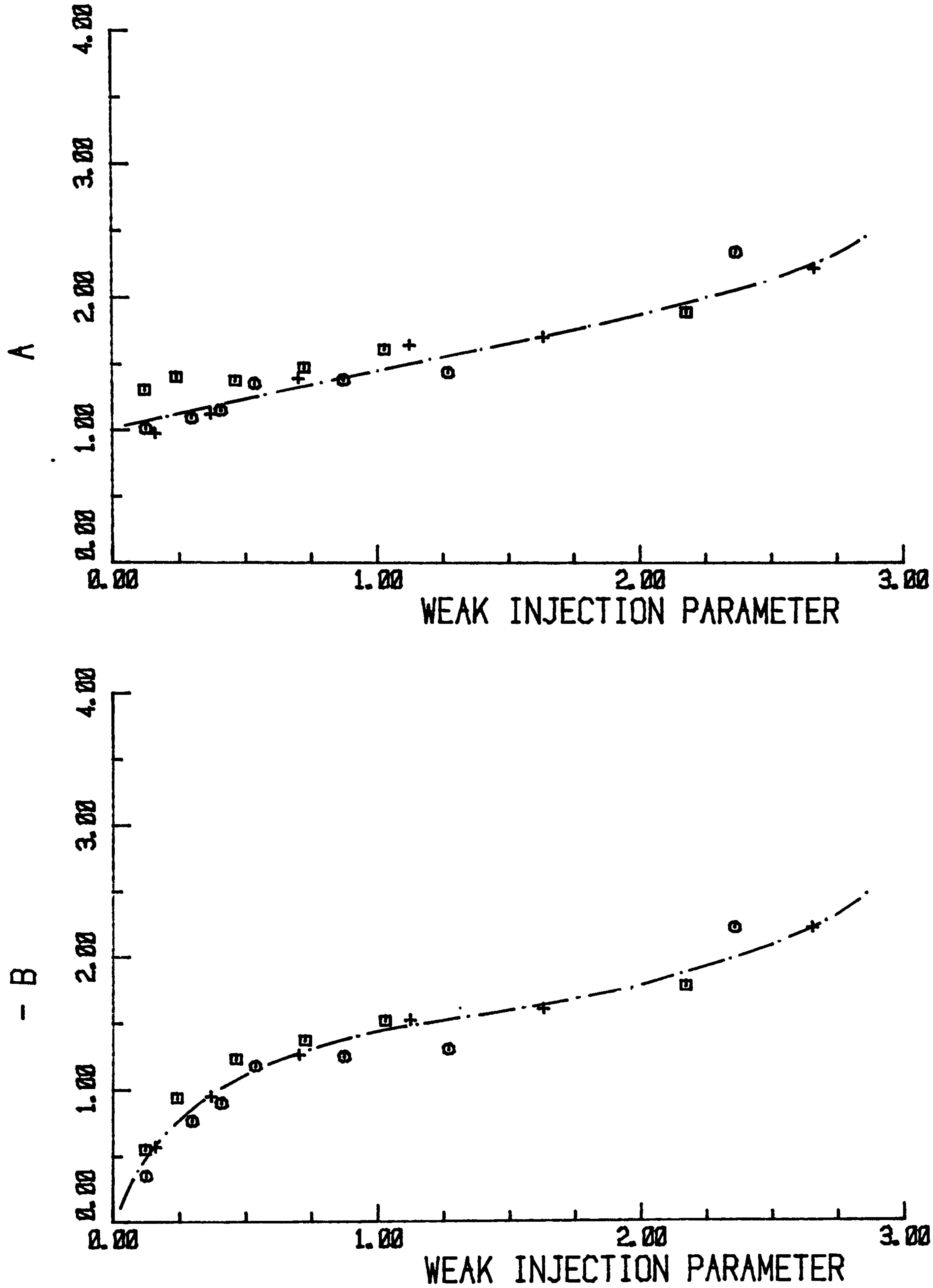

FIG. 8.34 (b) Correlation of A and B with Weak Injection Parameter - X/S = 8

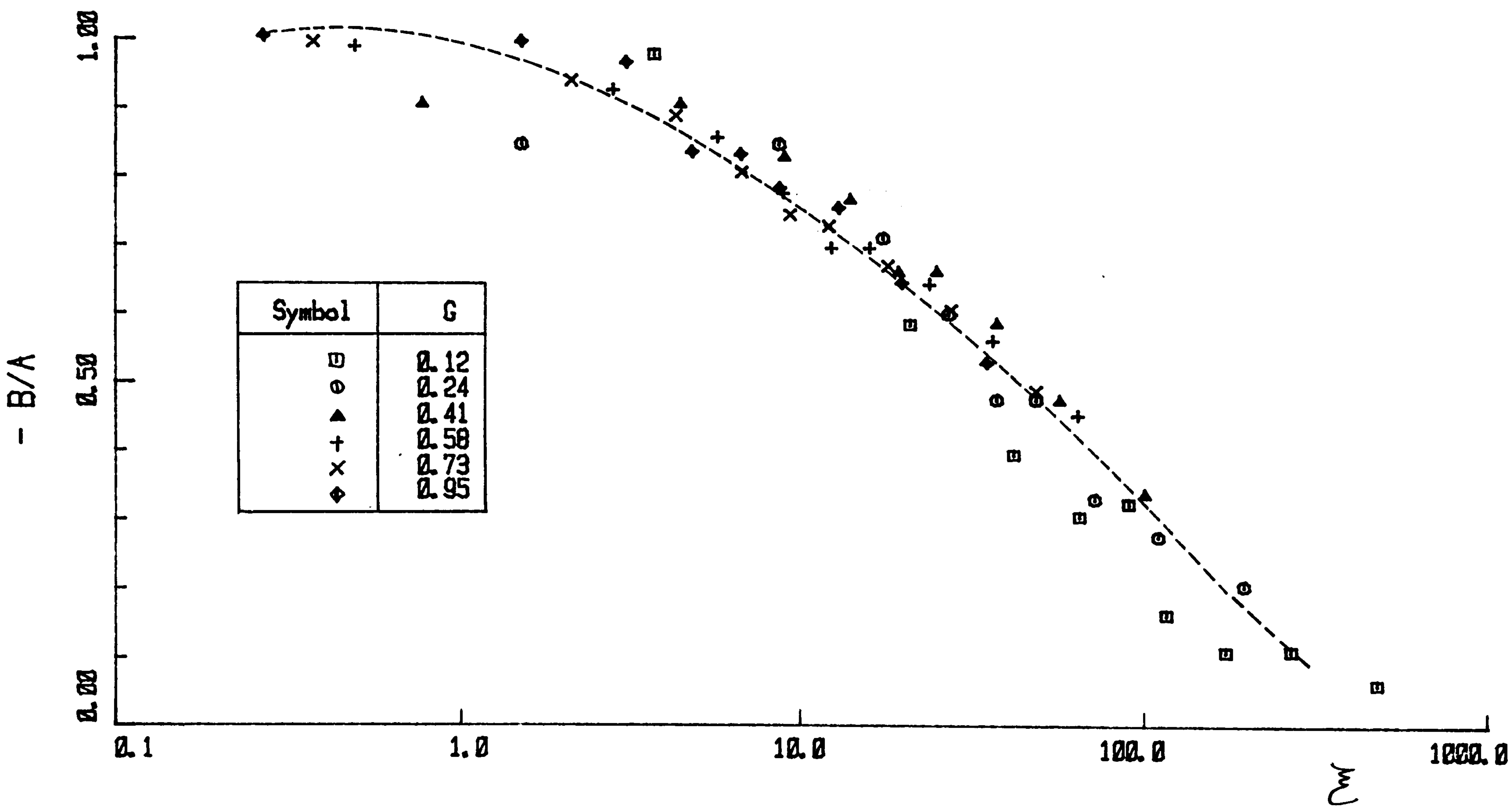

FIG. 8.35 Slot Data - Correlation of Film Cooling Data with Energy Balance Parameter for all Distances and Mass Flux Ratios, $T_{ti}/T_{t\infty} = 1.23$

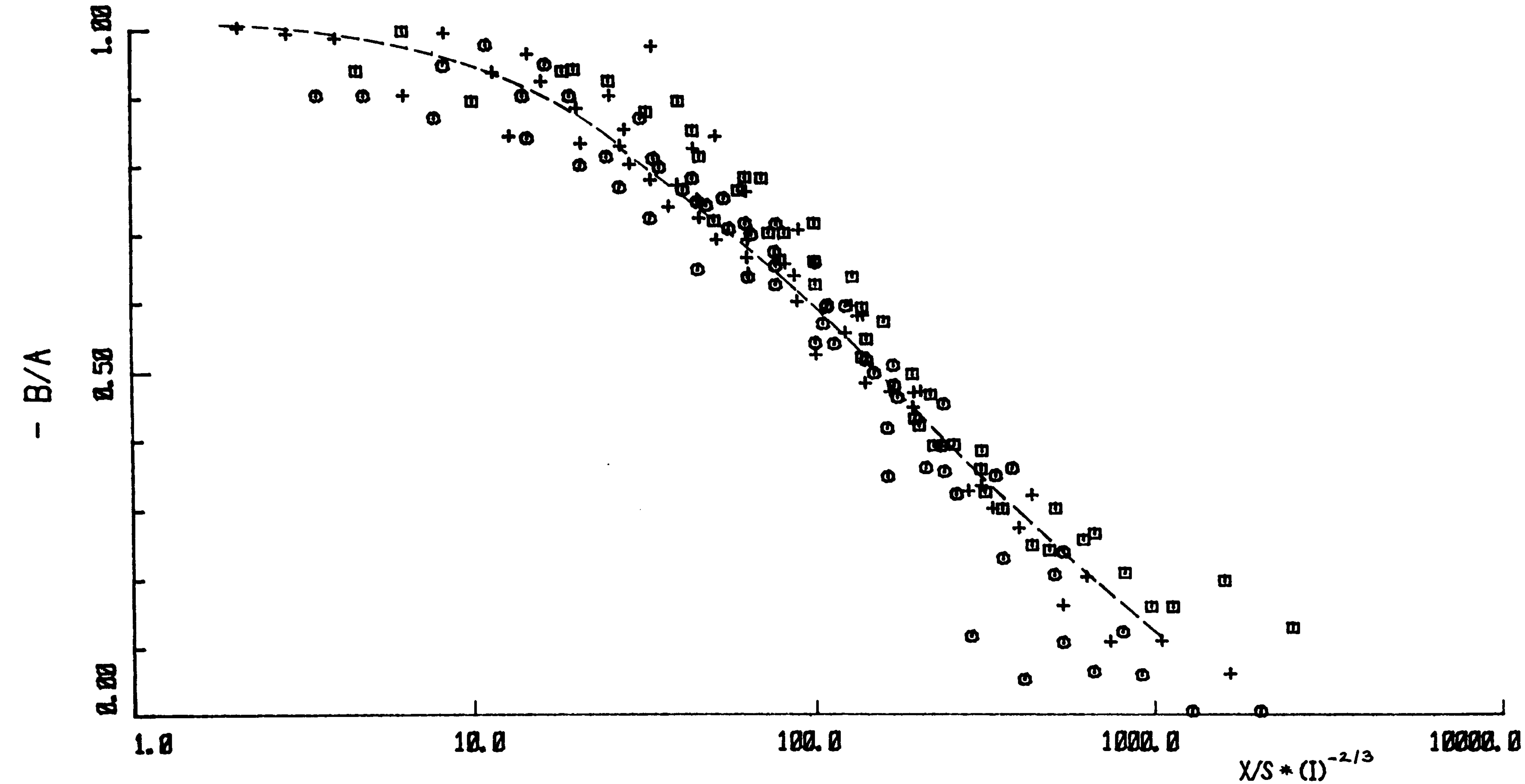

FIG. 8.36 Slot Data - Correlation of Film Cooling Data with Slot-Wall-Jet Parameter for all Distances, Mass Flux Ratios and Injection-to-Freestream Temperature Ratios.

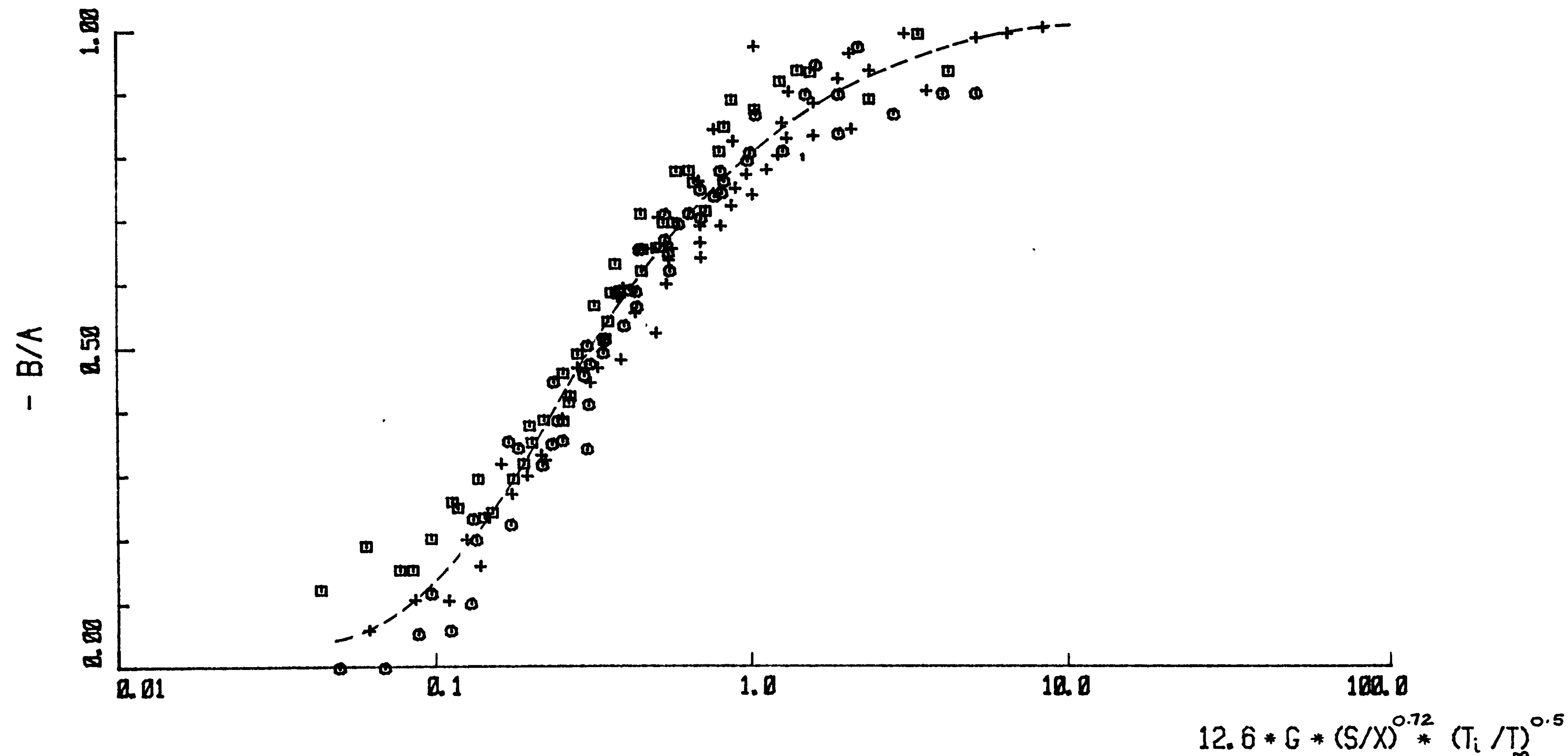

FIG. 8.37 Slot Data - Correlation with Parameter Proposed by PAPELL and TROUT [4.16] for all Distances, Mass Flux Ratios and Injection-to-Freestream Temperature Ratios.

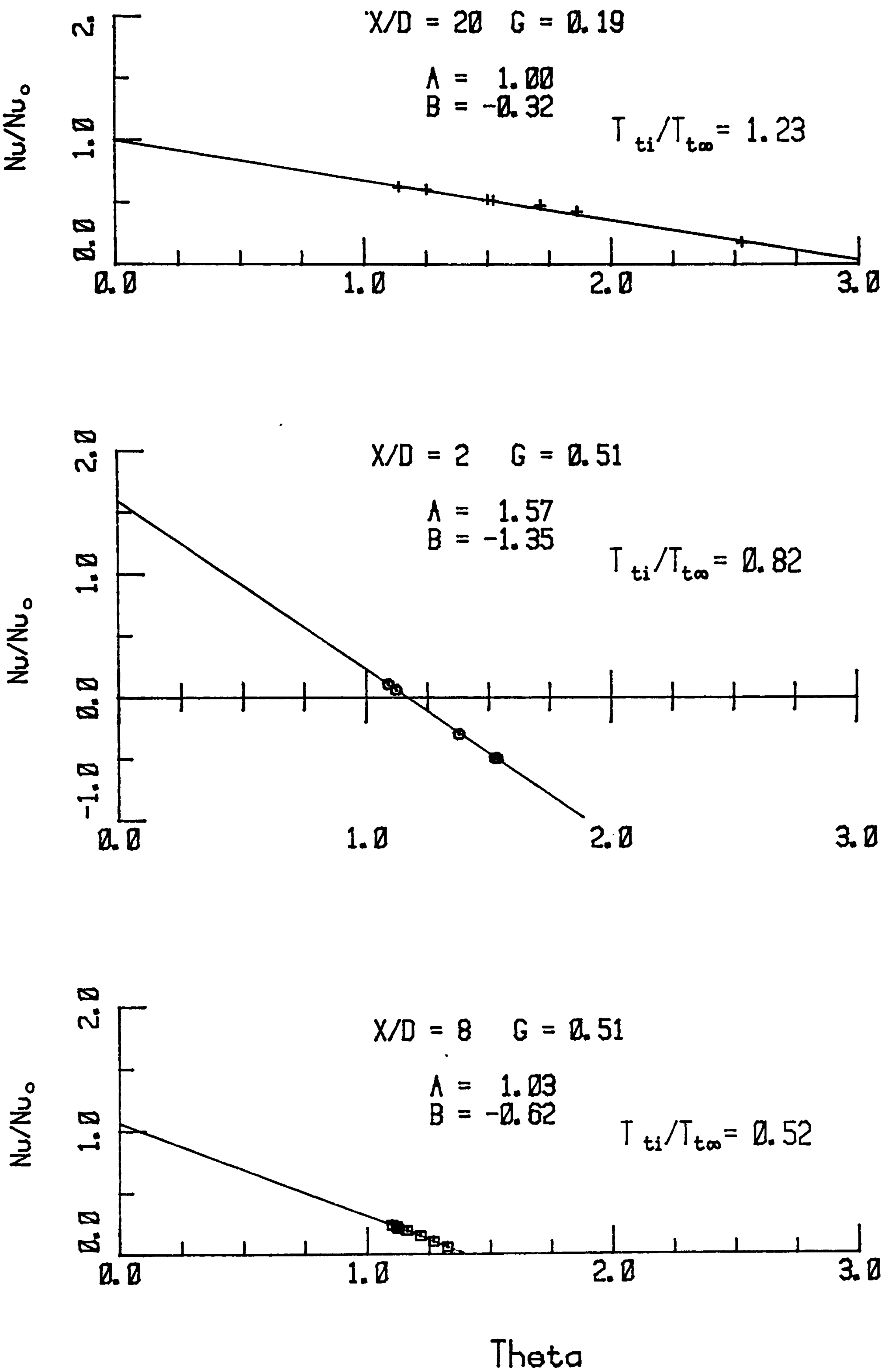

FIG. 8.38 Double Row Data - Variation of Nusselt Number with Theta as the Wall Temperature is Changed.

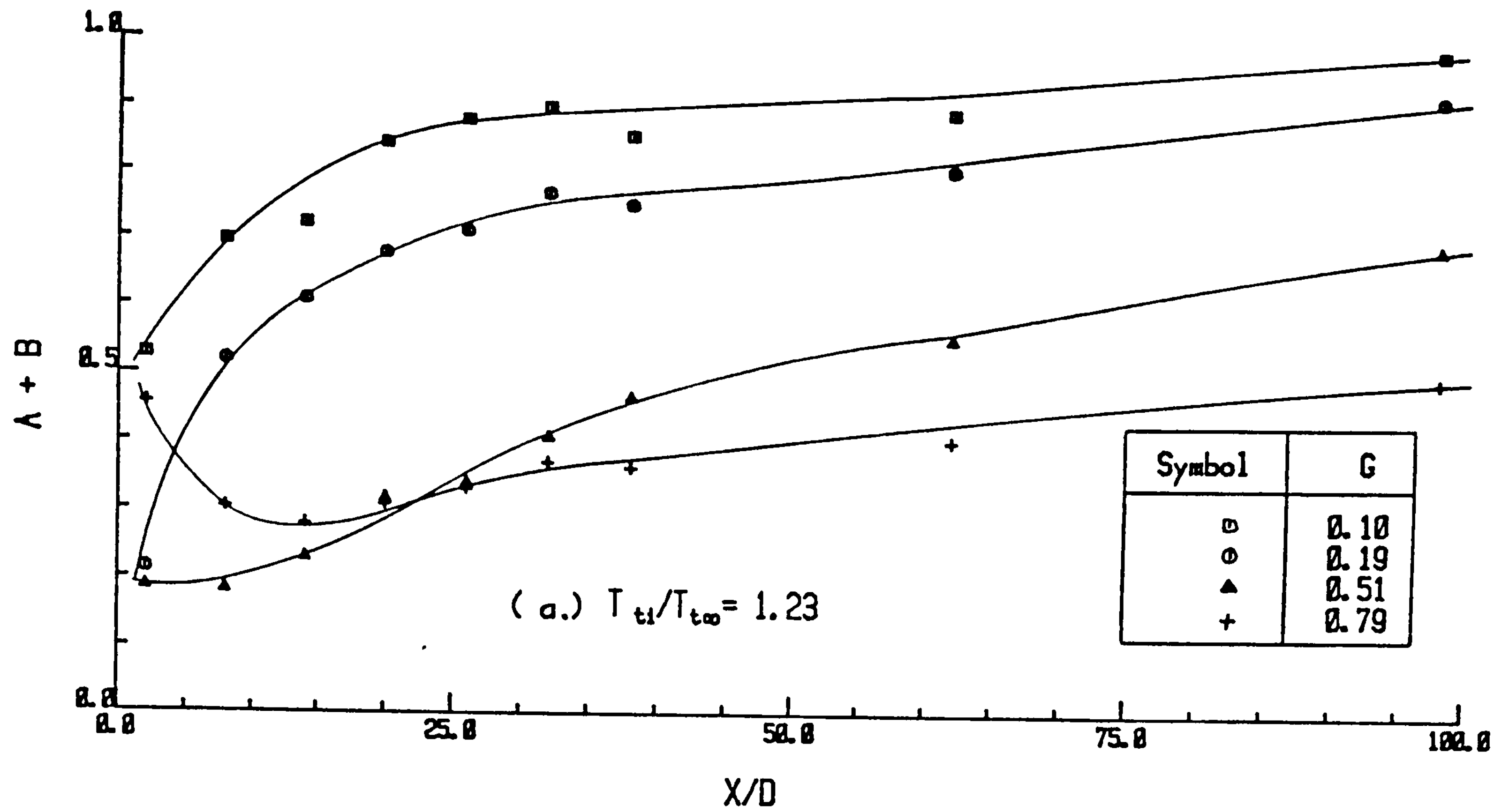

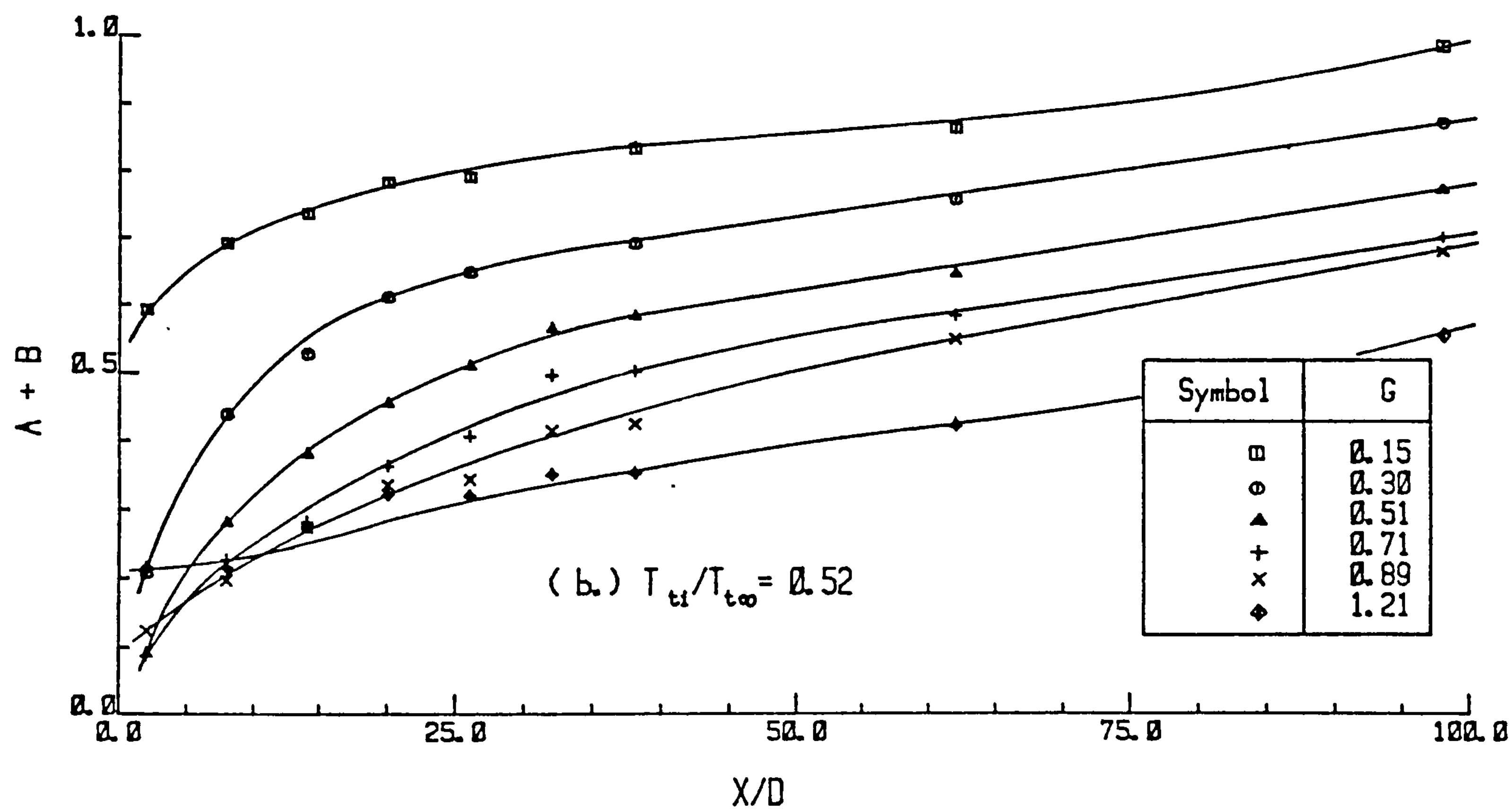

FIG. 8.39 Double Row Data - Variation of Nusselt Number with Distance at Theta = 1.0

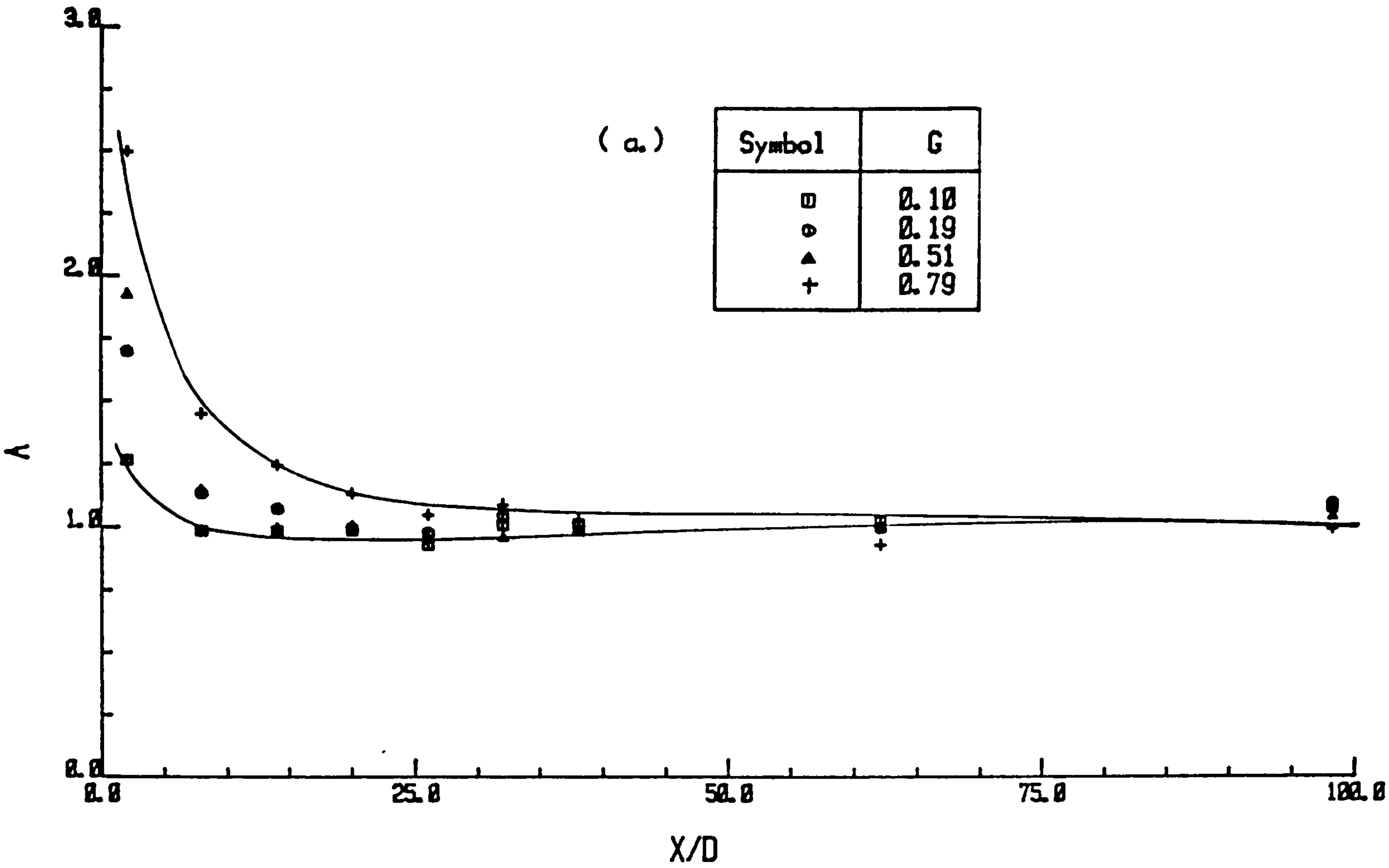

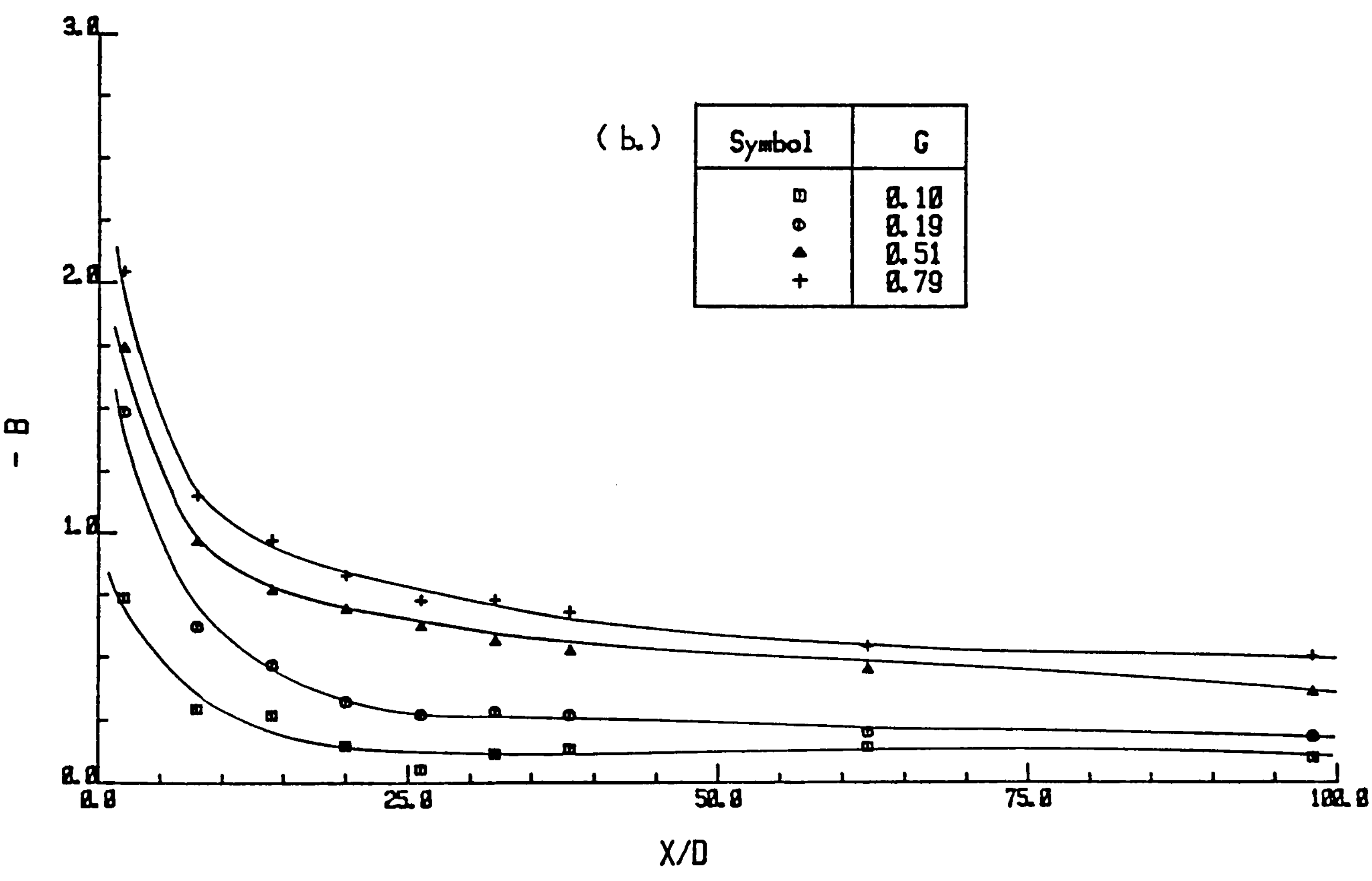

FIG. 8.40 Double Row Data - Variation of Λ and B with Distance and Mass Flux Ratio - $T_{ti}/T_{t\infty}$ = 1.23

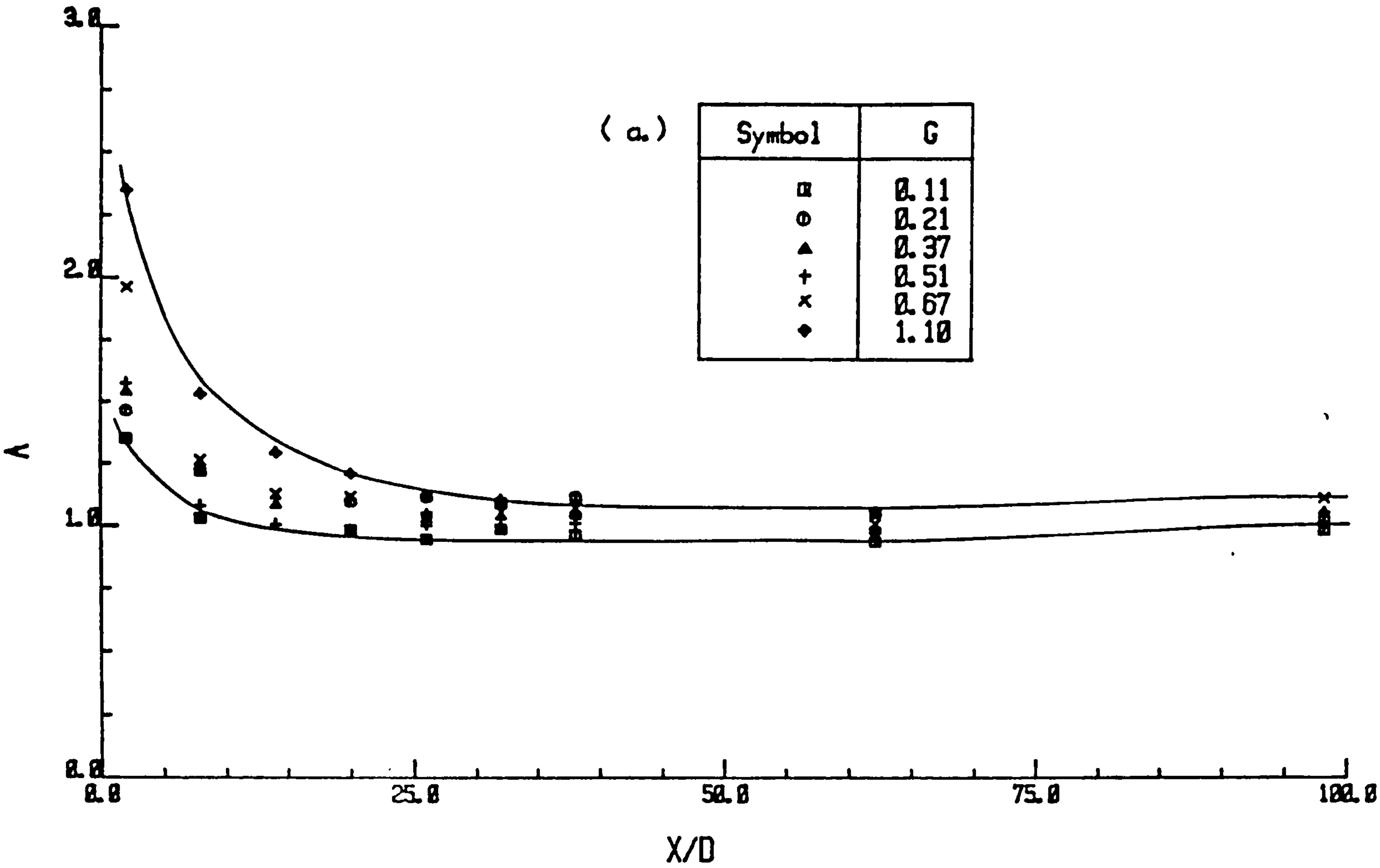

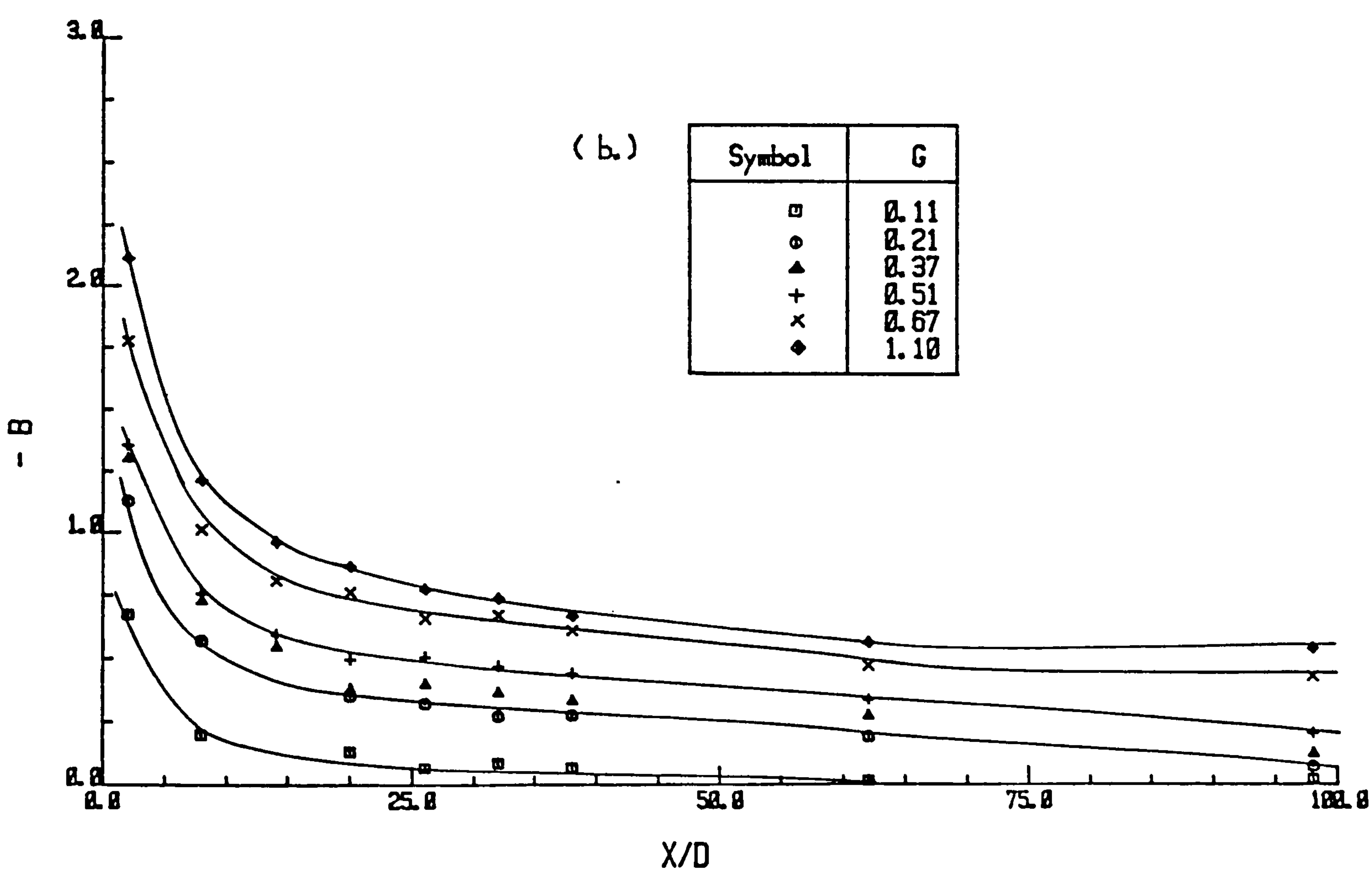

FIG. 8.41 Double Row Data - Variation of A and B with Distance and Mass Flux Ratio - $T_{t1}/T_{t\infty}$ = 0.82

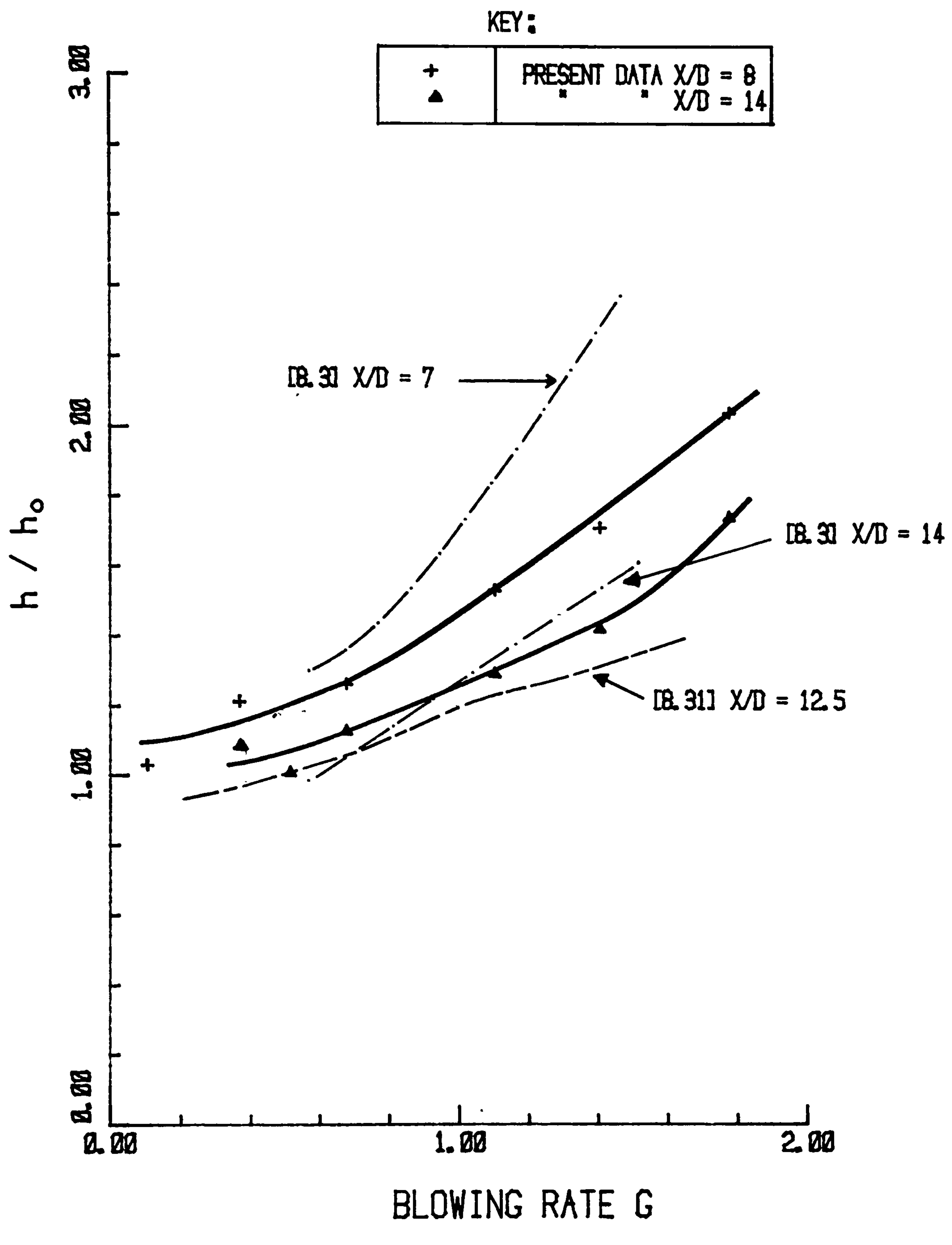

FIG. 8.42 Double Row Data - Enhancement of Heat Transfer Coefficient. Comparison with the Literature.

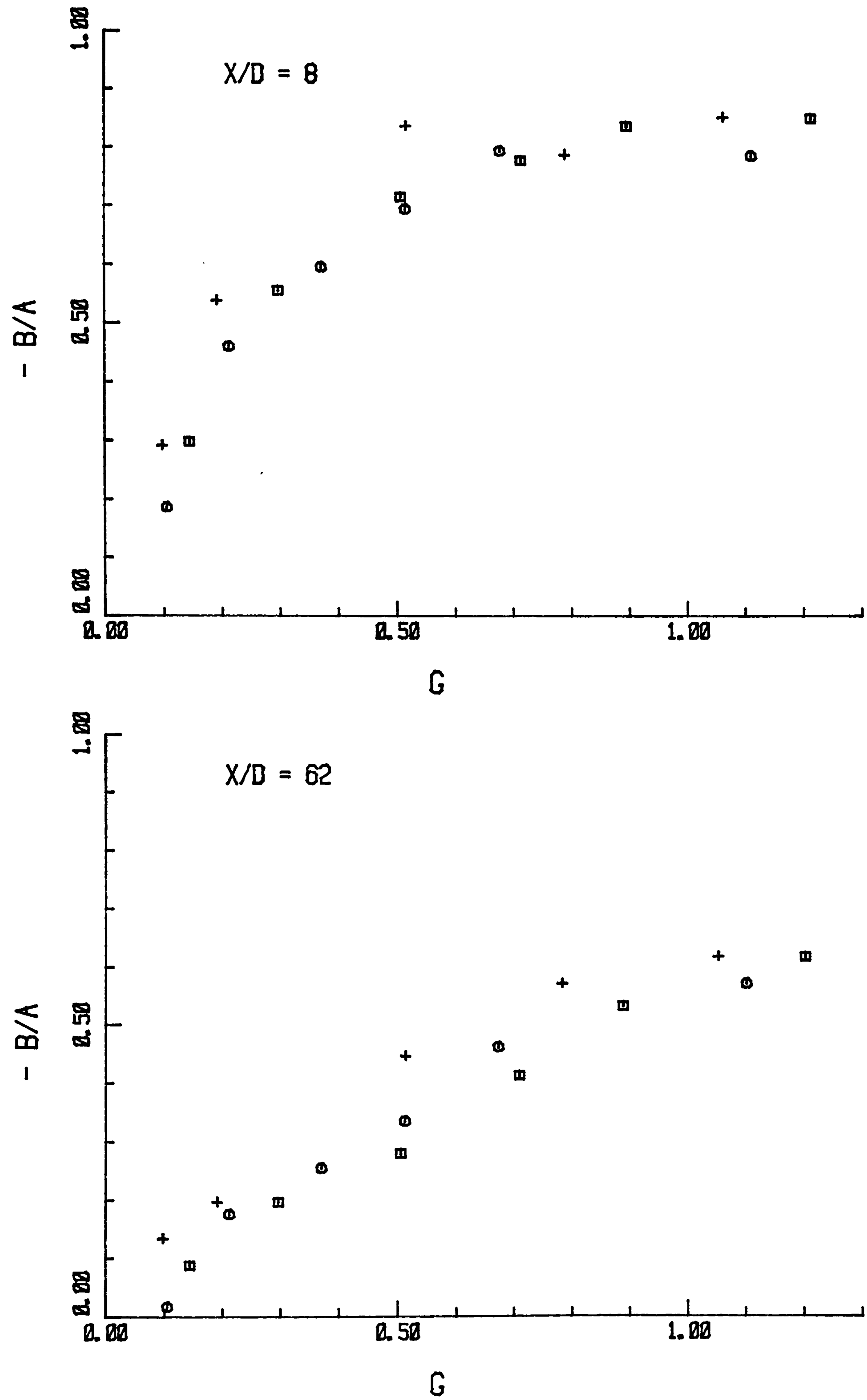

FIG. 8.43 Double Row Data - Variation of -B/A with Mass Flux Ratio. (See table 8.3 for symbols)

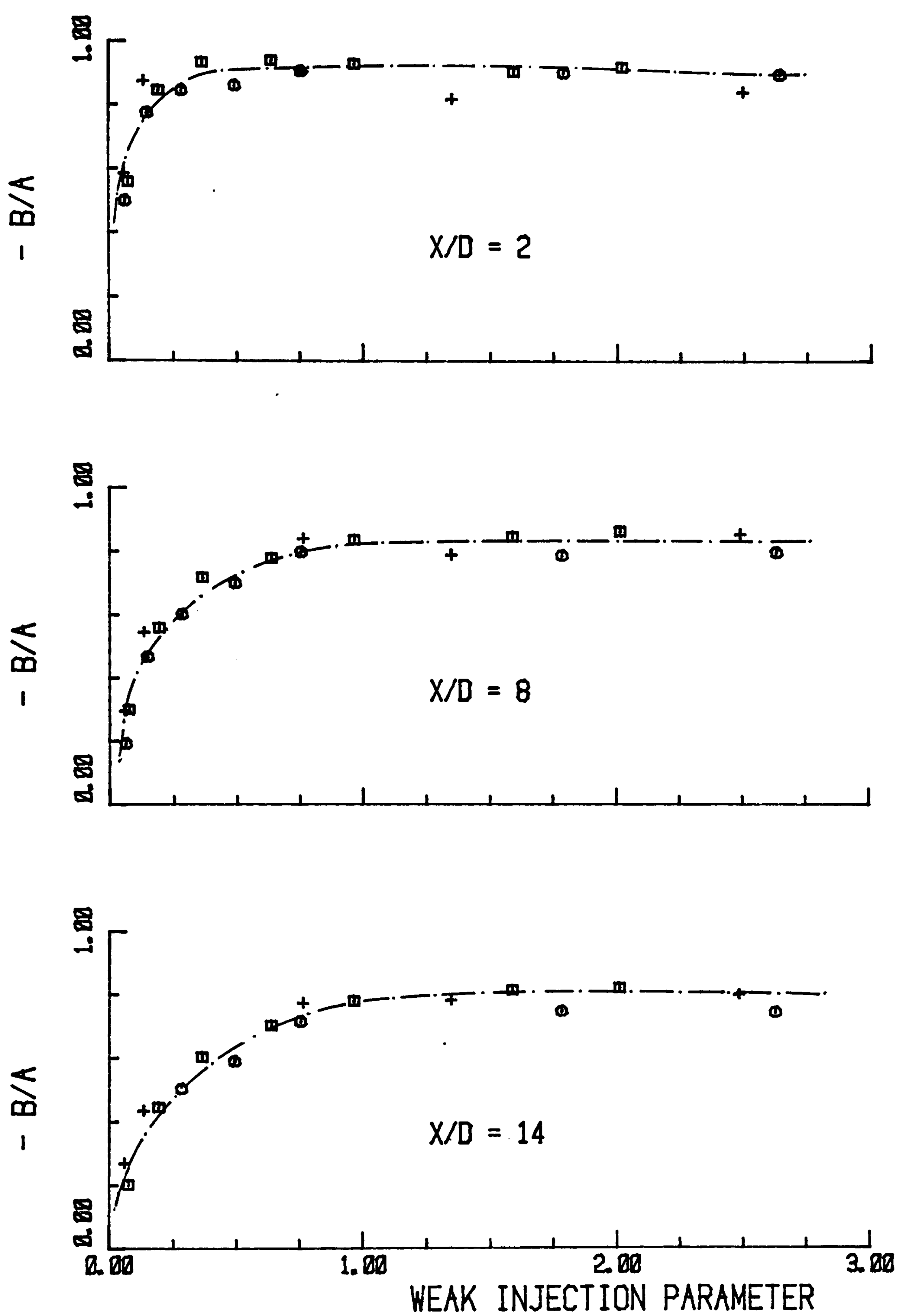

FIG. 8.44 Double Row Data - Correlation of Film Cooling Data with Weak Injection Parameter.

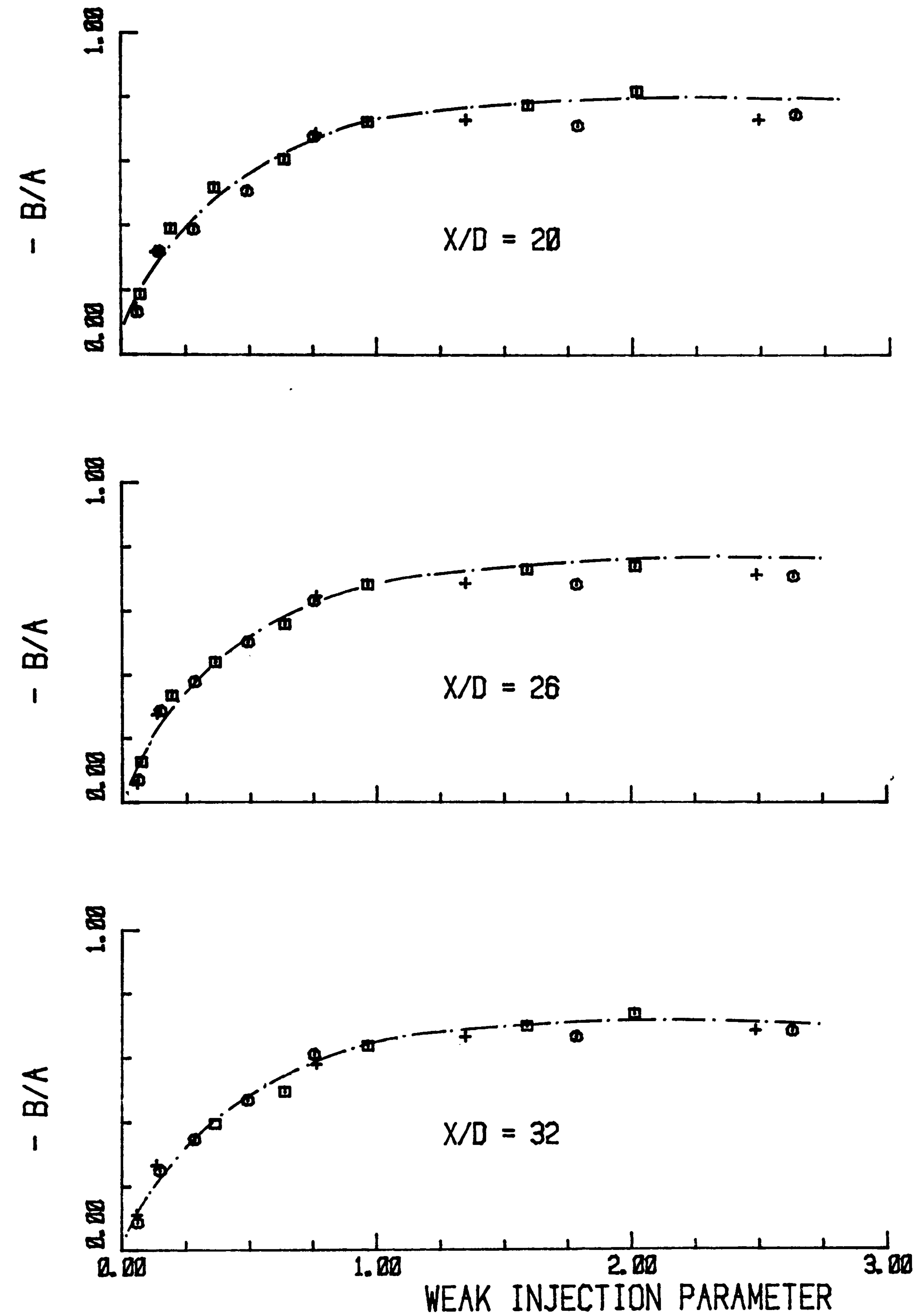

FIG 8.44 (ctd.) Double Row Data - Correlation of Film Cooling Data with Weak Injection Parameter.

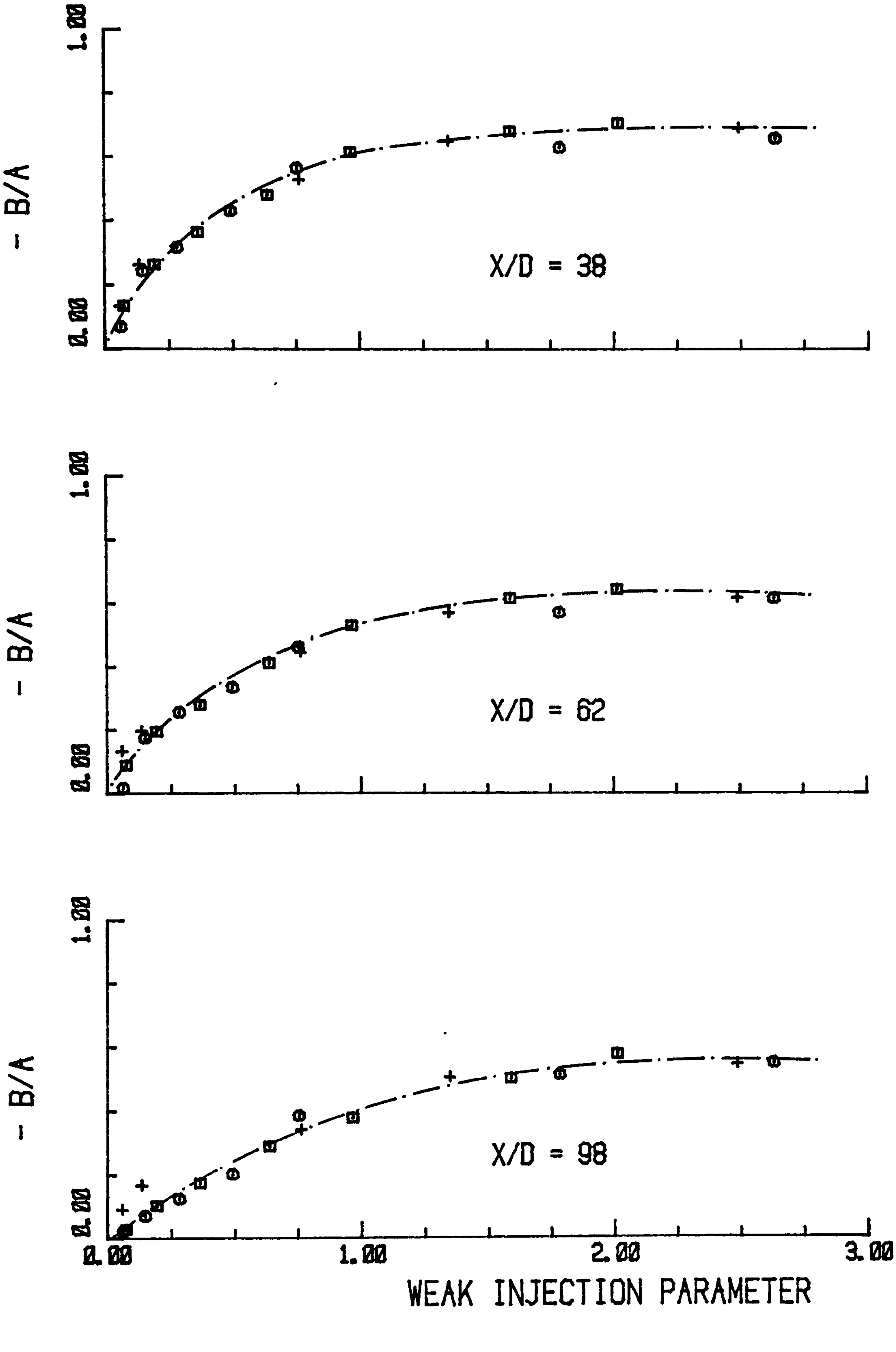

FIG 8.44 (ctd.) Double Row Data - Correlation of Film Cooling Data with Weak Injection Parameter.

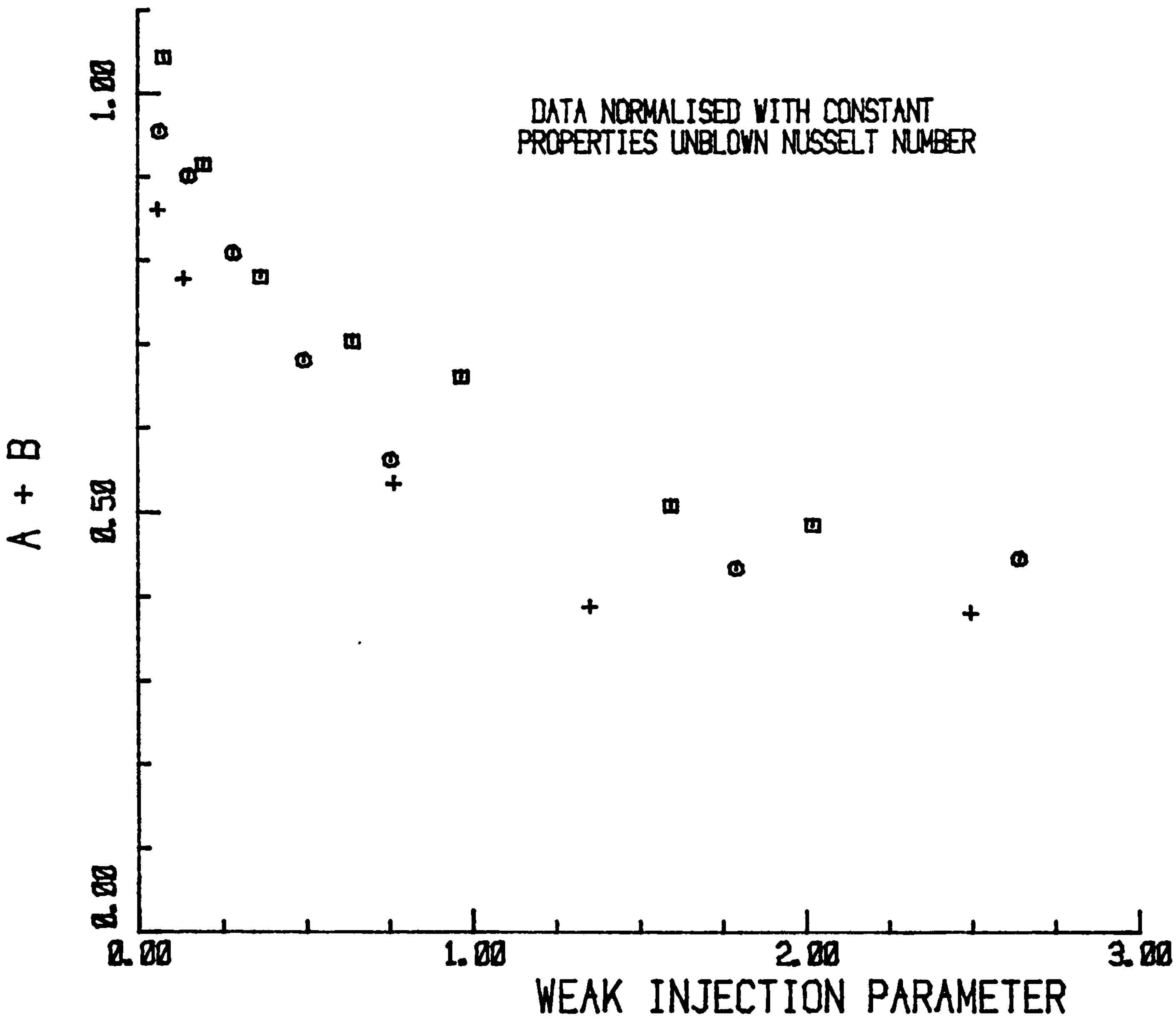

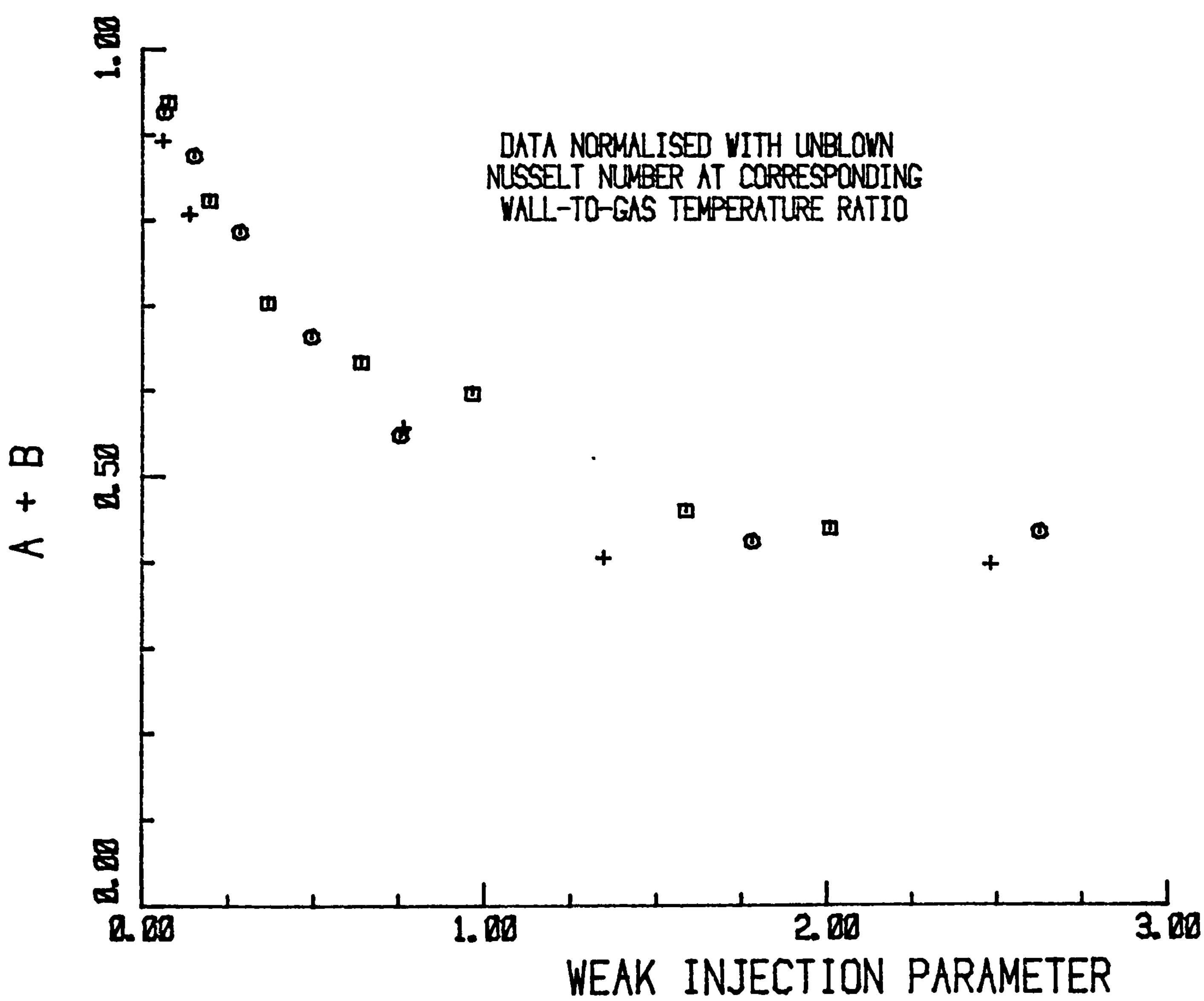

FIG. 8.45 Comparison Between Corrected and Uncorrected Data to Illustrate the Effect of Property Variations - X/D = 62

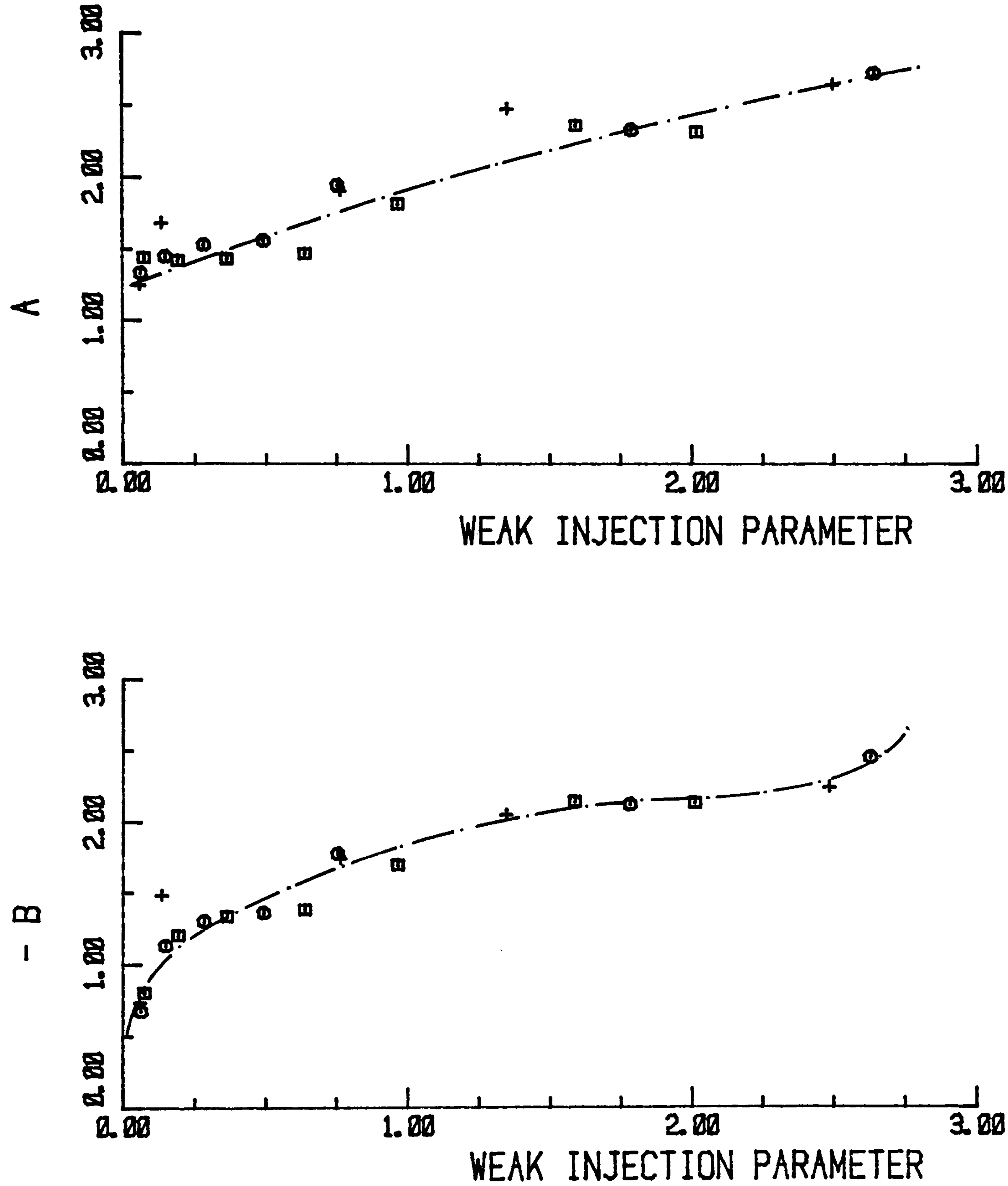

FIG. 8.46 Correlation of A and B with Weak Injection Parameter - X/D = 2

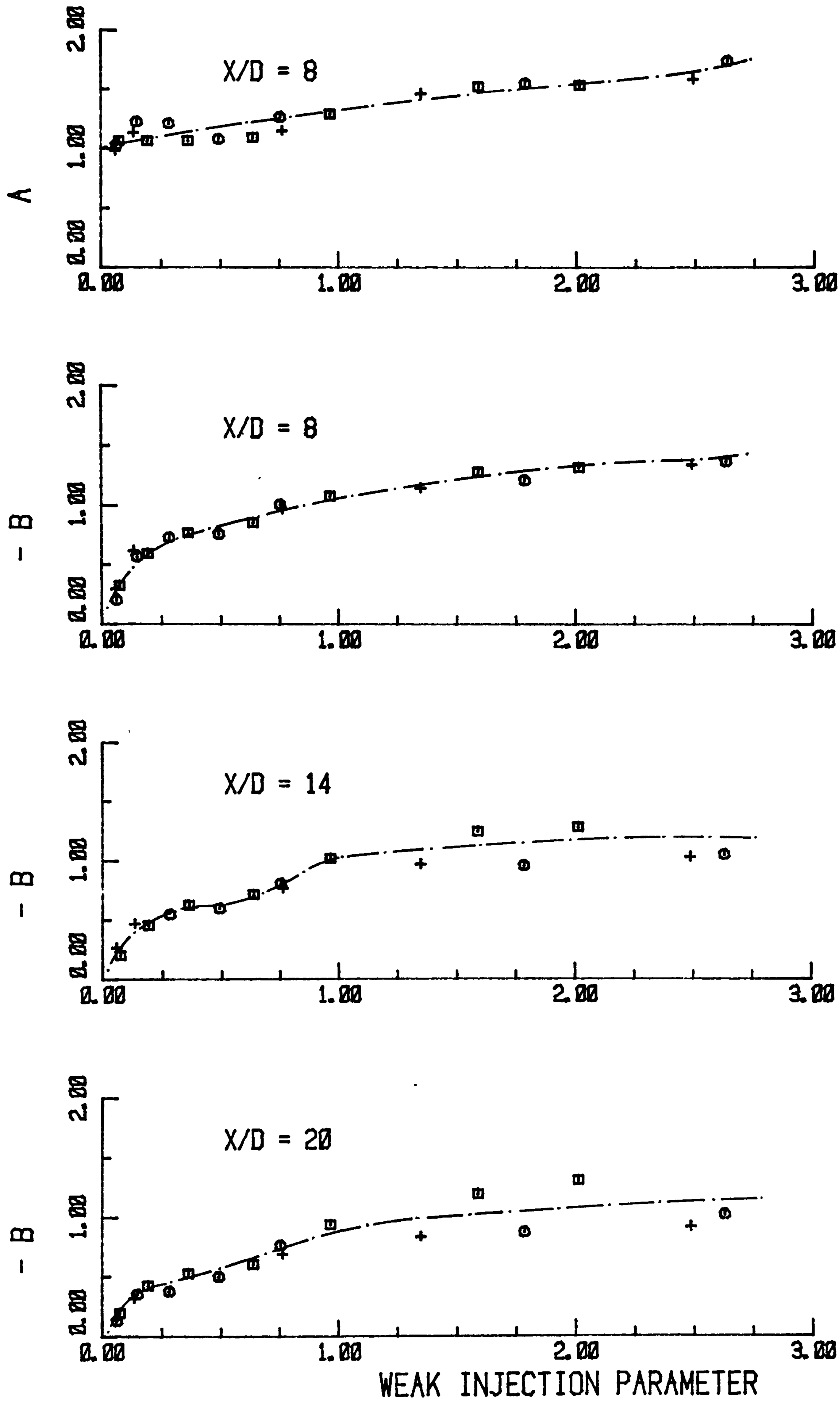

FIG. 8.46 (ctd.) Correlation of A and B with Weak Injection Parameter - X/D varies.

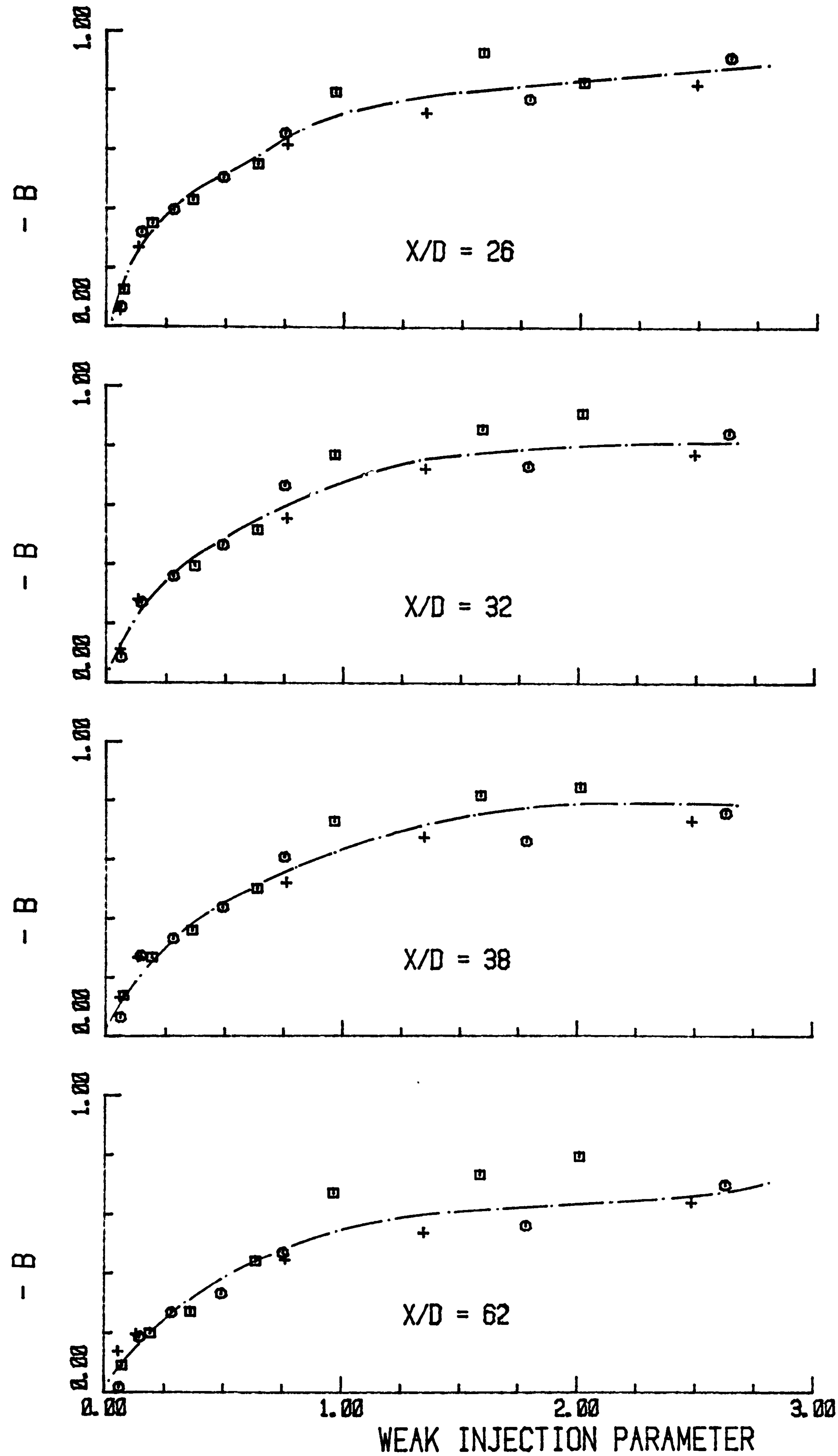

FIG. 8.46 (ctd.) Correlation B with Weak Injection Parameter - X/D varies.

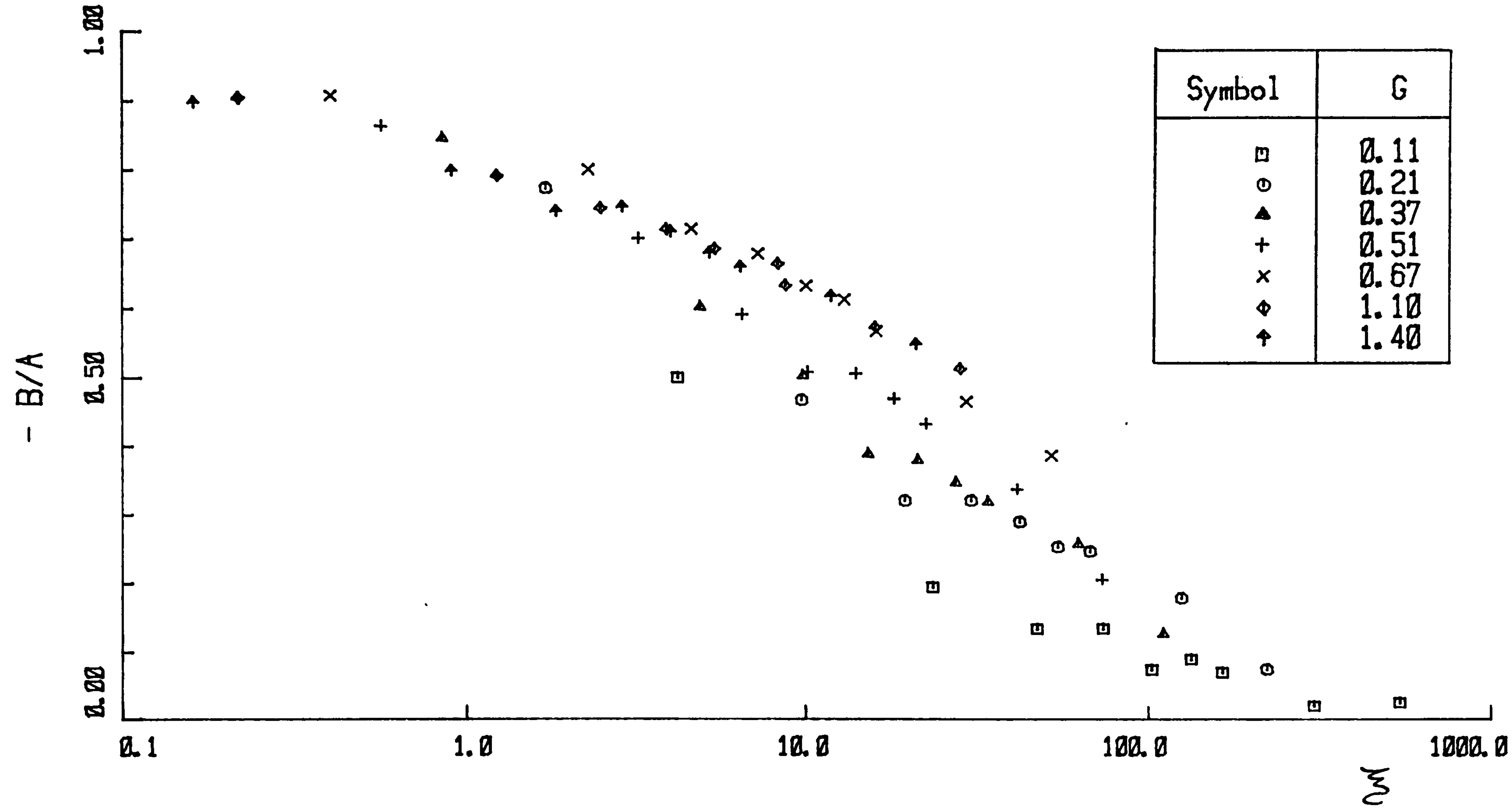

FIG. 8.47 Double Row Data - Correlation of Film Cooling Data with Energy Balance Parameter for all Distances and Mass Flux Ratios $T_{ti}/T_{t\infty} = 0.82$

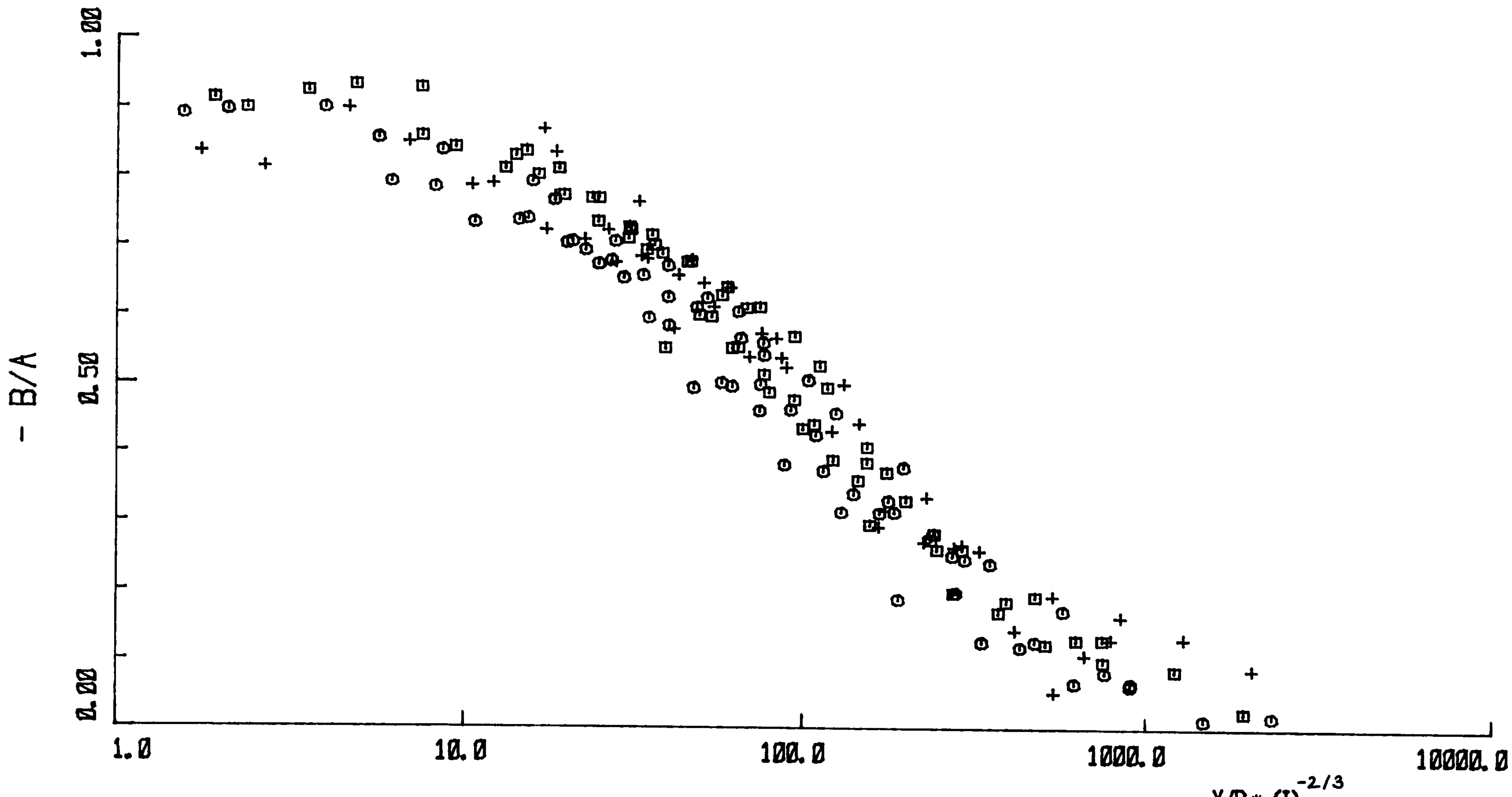

FIG. 8.48 Double Row Data - Correlation of Film Cooling Data with Slot-Wall-Jet Parameter for all Distances, Mass Flux Ratios and Injection-to-Freestream Temperature Ratios.

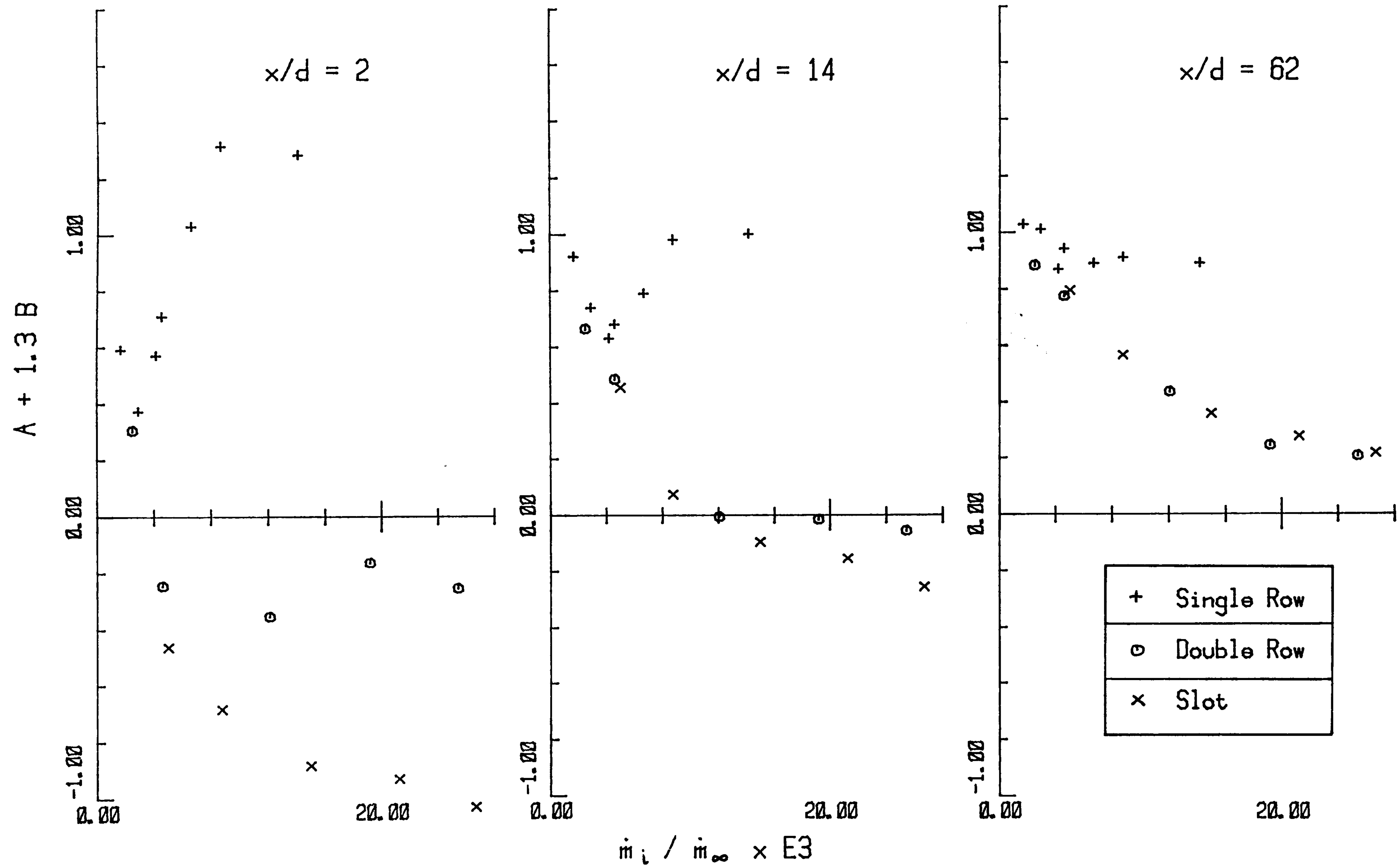

FIG. 8.49 Comparison of the Relative Cooling Effects of the 3 Geometries Tested - $T_{ti}/T_{t\infty} = 1.23$

GIVEN: $T_{t\infty}$

T_{ti}

$p_{t\infty}$, p_{ti} and p_∞ (or injection-to-freestream velocity and density ratios).

and a requirement for T_w.

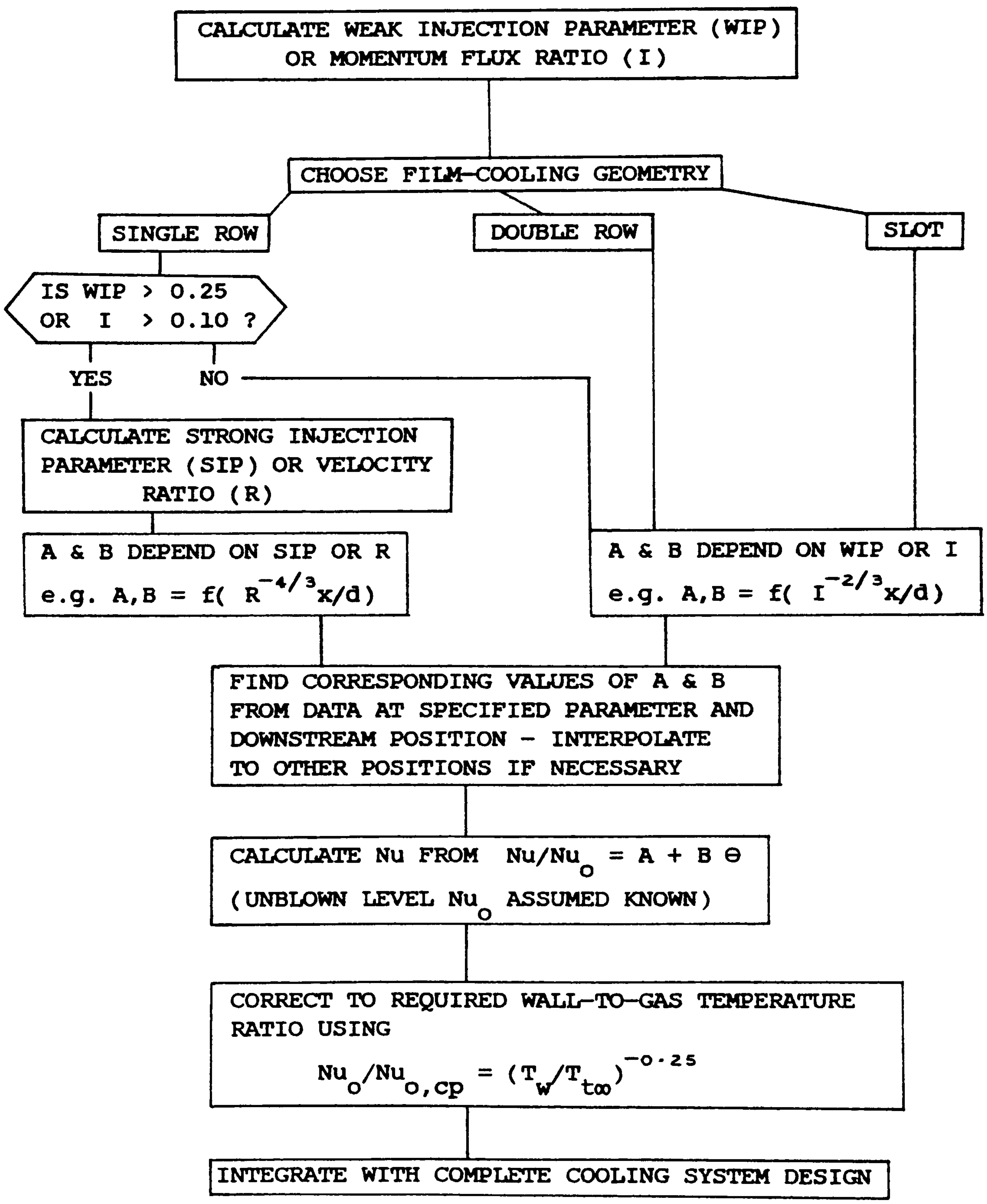

FIG. 9.1 Scheme for Utilising New Correlating Parameters in Cooling Design Procedure.